Analysis of the densification of a biomedical titanium alloy produced by powder metallurgy

Slokar Benić, Ljerka; Komljenović, Luka; Erman, Žiga; Jajčinović, Magdalena

2023

INNOVATIONS

IX INTERNATIONAL SCIENTIFIC CONGRESS

INNOVATIONS 2023

26-29.06.2023 VARNA

PROCEEDINGS

ISSN 2603-3771 (Online)
ISSN 2603-3763 (Print)

SCIENTIFIC-TECHNICAL UNION OF MECHANICAL ENGINEERING - INDUSTRY 4.0
BULGARIA

IX INTERNATIONAL SCIENTIFIC CONGRESS

INNOVATIONS

Year VII **Volume 1(7)** **JUNE 2023**

PROCEEDINGS

"INNOVATION POLICY AND INNOVATION MANAGEMENT"
"INNOVATIVE SOLUTIONS"

26 – 29 JUNE, 2023,
VARNA, BULGARIA

ISSN 2603-3763 (Print)
ISSN 2603-3771 (Online)

INTERNATIONAL EDITORIAL BOARD

C O N T E N T S

“INNOVATION POLICY AND INNOVATION MANAGEMENT”
“INNOVATIVE SOLUTIONS”

Possibilities of using an autoencoder network in the failure state recognition
Ivan Kuric, Daria Fedorova, Vladimir Stenchlák, Michal Bartoš, Martin Bohušík, Andrej Bencel 5

Management of innovation processes in the organization
Naqib Daneshjo, Róbert Rehák, Peter Drábik 9

Risk Driven Design of Technical Product
Josef Dvorak, Stanislav Hosnedl 13

On some aspects of the analysis of urban mobility
доц. д-р Нетов Н, доц. д-р Спасов К., ас. д-р Върбанова Т. 16

Efficiency of formation and development of intrafirm knowledge in a modern market economy
Zoya Gelmanova, Anastassiya Mezentseva 19

Increasing the resilience of critical entities in response to the dynamic spectrum of threats
Valeri Panevski, Lyudmil Nedelchev 23

Choice of cancer treatment as a creative problem
Roman Goot, Vladimir Goot 27

Evaluation of formal education active labor market policy programs in slovenia with propensity score matching
Kavkler Alenka 29

INNOVATIVE SOLUTIONS

Simulation of thick-sheet rolling process in rolls of various design
Evgeniy Panin, Alexandr Arbuz, Almas Yerzhanov, Sergey Lezhnev, Abdrakhman Naizabekov, Dmitry Kuis, Aibol Esbolat 33

Investigation of the microstructure evolution of steel 45 during deformation in strikers of various designs implementing shear strain
Andrey Tolkushkin, Andrey Volokitin, Abdrakhman Naizabekov, Irina Volokitina, Evgeniy Panin, Sergey Lezhnev, Oksana Maldina 36

Extended research on the efficiency of internal crystallization chemical admixtures for cement concrete - mechanical and structural characteristics
Valeriy Naidenov 40

Processing and properties of polymer - mineral compositions
Tomasz Garbacz, Aneta Tor-Swiątek, Lukasz Garbacz 45

CeO2-ZrO2 Multi-layer Cubic Coatings Obtained by Sol-Gel Technology
Vladimir Petkov, Mihaela Aleksandrova, Bojidar Jivov, Marieta Gacheva 49

Investigation of an appropriate marl raw material for the production of innovative ceramic beehives
Todorka Lepkova, Lyuben Lakov, Bojidar Jivov, Gergana Mutafchieva, Marieta Gacheva 51

On Transfer Functions Limitations to Active Vehicle Suspension
Katerina Hyniova 55

Analysis of the influence of internal forces and moments on the nozzle of the main downcomer of a steam boiler drum
Pejo Konjatić, Ana Konjatić, Dajana Bičanić, Ivan Dunđer 60

Stress and stability calculation of the third pass module of the steam boiler during lifting
Pejo Konjatić, Sara Radojičić, Marko Katinić, Meri Rendulić 64

Investigation of the effect of combined thermomechanical processing modes on The microstructure of economy-alloyed steel 5KHV2S
Sergey Lezhnev, Abdrakhman Naizabekov, Dmitry Kuis, Igor Stepankin, Evgeniy Panin, Andrey Tolkushkin 68

A new high-quality dynamic identification structure for im parameters
Daniela Perdukova, Pavol Fedor, Marek Fedor 72

Experimental setup for studying the behavior of sheet blanks during cyclic alternating bending for roller levelling application
Tamila V., Klubovich V., Liaukovich V. 76

Determining the quality of renovation layers using laser technology
Janette Brezinová, Ján Viňáš, Miroslav Džupon, Marek Vojtko, Jakub Brezina 78

Tribological properties of PVD nanocoatings
Janette Brezinová, Miroslav Džupon, Viktor Puchý, Ján Hašuľ, Jakub Brezina 81

Application of innovative procedures for modification of surface topography
Janette Brezinová, Miroslav Džupon, Marek Vojtko, Ján Hašuľ, Jakub Brezina 84

Study of the properties of the metal surface after pre-treatment by phosphating
Dagmar Draganovská, Gabriela Ižaríková, Róbert Moro 89

Analysis of the possibilities of joining thin-walled metallic and composite materials
Nikita Veligotskyi, Anna Guzanová, Erik Janoško 92

Analysis of interference fit joints formed by thermal drilling technology with CNC process control
Erik Janoško, Anna Guzanová, Nikita Veligotskyi 98

Monitoring of changes in the roughness of the metal surface after the application of the conversion layer
Róbert Moro, Dagmar Draganovská 102

Studying the composition and properties of white eco-cement
Lev Chernyak, Nataliia Dorogan, Liubov Melnyk, Petro Varshavets, Victoria Pakhomova 105

Microhardness dependence of Ti-Zr alloys on time and temperature of sintering
Ljerka Slokar Benić, Luka Komljenović, Erman Žiga, Magdalena Jajčinović 109

Analysis of the densification of a biomedical titanium alloy produced by powder metallurgy
Ljerka Slokar Benić, Luka Komljenović, Erman Žiga, Magdalena Jajčinović 113

Peculiarities of sintering of porous sheet blanks from powder of tin-phosphorus bronze
Prof., Dr. Eng., Ilyushchanka A., PhD Eng., Doc. Kusin R., Acad. Adv. Charniak I., Master of Tech. Sciences Kusin A. 117

Possibilities of using an autoencoder network in the failure state recognition

Ivan Kuric[1], Daria Fedorova[1], Vladimir Stenchlák[1], Michal Bartoš[1], Martin Bohušík[1], Andrej Bencel[1]
University of Žilina, Faculty of Mechanical Engineering, Department of Automation and Production Systems[1]
daria.fedorova@fstroj.uniza.sk

Abstract: *Approaches to machine and equipment maintenance based on data analytics and artificial intelligence are trending in modern manufacturing. These methods are used to predict the remaining useful life (RUL) of equipment and thus enable forward maintenance planning. However, for predictive maintenance systems, it is also necessary to detect anomalies in operation and classify the occurring errors. Classical approaches of supervised machine learning are often in this case unusable because those methods require a large amount of run-to-failure data (R2F), which is often not possible to collect due to the undesirable character of failure states in the manufacturing process. The paper presents and tests several methods of detecting device fault states using an autoencoder network, which offers a beneficial solution in the case of the unavailability of R2F data in the system.*
Keywords*: PREDICTIVE MAINTENENCE, AUTOENCODER NETWORK, FAULT DETECTION, DATA RECONSTRUCTION*

1. Introduction

In modern production, with the increase in production capacity, the requirements for manufacturing process productivity are also increasing. However, maintaining the productivity of the production process is only possible with a fault-free operation process of all machines and equipment that are included in the observed production process.

Keeping the operability and the fault-free state of the equipment is the task of maintenance. There are many maintenance strategies, which are divided according to the time of performing (pre-failure or post-failure maintenance), the level of intervention (full repair or partial repair), or also based on the time intervals of execution (systematic, conditional, or planned) [3]. This research is focused on predictive maintenance (PdM) as a modern maintenance trend. The goal of this approach is to increase uptime, reduce maintenance costs, and improve safety by identifying and correcting potential problems before they cause a breakdown or accident.

Using sensors, data analysis, and machine learning algorithms, PdM can provide real-time information about the performance of various components of systems. By collecting and analyzing data on factors such as temperature, vibration, and noise levels, predictive maintenance algorithms can detect early warning signs of equipment failure and alert responsible persons. Also, an important task of PdM is the detection and subsequent classification of abnormal device states and the definition of condition indicators (CIs).

Commonly used machine learning algorithms include NAR and NARX neural networks [4,9], convolutional neural networks [6,7], LSTM networks [1], and hybrid approaches [2]. However, these algorithms belong to the group of supervised learning algorithms, for the training of which a large amount of labeled data, which contains possible faults and errors in the operation of the observed device is required. That could be a problem if the observed system starts to become more complex and contains many possible fault scenarios.

Based on the analysis of existing research for the solution to the given problem, it was investigated the possibility of using an autoencoder for anomaly detection in the operation of the test equipment.

2. Training and experimental data

Training and experimental data were collected using equipment developed for testing prediction models. The scheme of the testing device is shown in Fig. 1 The device essentially consists of a hydraulic circuit with the ability to heat and pump the working fluid. A set of sensors placed on the device allows sensing of the fluid temperature at three points in the hydraulic circuit, the temperature of the heat exchanger, the flow rate and pressure in the system, and the electrical current and voltage in the electrical circuit. The device is also equipped with an ambient temperature and air humidity sensor for the possibility of investigating the influence of external factors on the operating characteristics of the device.

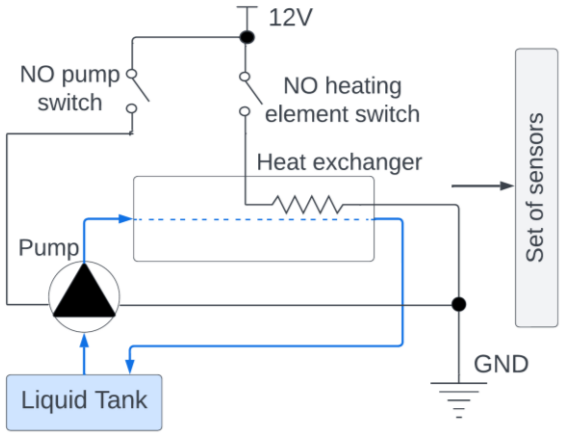

Fig. 1 *Scheme of the testing device*

The control of the working cycle is realized by the Arduino UNO microcontroller. Data acquisition is realized by Arduino MEGA microcontroller with a frequency of 1 measurement every 5 seconds.

Since the proposed neural network should act as an anomalous condition detector in the device operation, the training dataset contains only error-free data. In the context of the present work, error-free data means data while sensing of which there was no abrupt change in the behavior of any of the 10 sensed parameters.

To test the proposed model, it were used two test datasets. Firs dataset contains error-free data and would be applied for testing the ability of the autoencoder to reconstruct the correct waveform of value changes for the new data. The second dataset contains data that are affected by a change in the climatic conditions of the room where the equipment is located. This dataset would be used for evaluating the ability to detect anomalies.

The slight temperature differences at the beginning of the data collection are explained by the 1-2°C differences in ambient temperature at the beginning of the equipment run on each day that the data collection took place.

3. An autoencoder model

Autoencoders (AEs) are the unsupervised learned type of neural network whose primary applications are data compression and dimensionality reduction. However, some studies [5,8] show that AEs can be also implemented as anomaly or fault detectors in machinery.

Autoencoders are trained to learn a compressed representation of input data and then can reconstruct outputs based on only a compressed representation of data. The input to the autoencoder is a fault-free sequence of one or multiple sensor data, and the output is

the same sequence but reconstructed by the decoder. This way during the training process, the autoencoder learns to reconstruct the normal operating conditions of the machinery. During training, the autoencoder learns to reconstruct the normal operating conditions of the machinery.

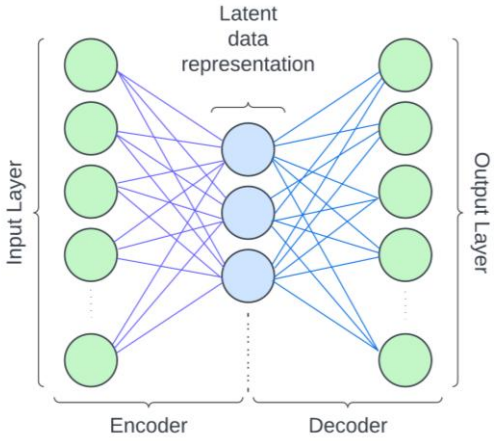

Fig. 2 *Basic autoencoder architecture*

As it is shown in Fig. 2, schematic autoencoder architecture consists of 3 main parts: encoder, decoder, and compressed latent representation. The latent representation or bottleneck forces a neural network not only to copy the input but to learn only the specific features of data which are useful for the next data reconstruction. Once the autoencoder is trained, it can be used to detect anomalies in the sensor data. When new sensor data is fed into the autoencoder, the output of the decoder will be different from the input if the data contains an anomaly.

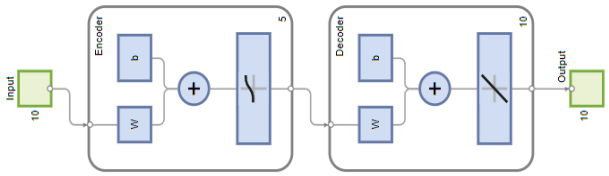

Fig. 3 *Proposed network architecture*

In this paper, we proposed an autoencoder model in MATLAB software. The model is shown in Fig. 3. It consists of 3 layers: 5 neurons bottleneck layer, 10 neurons input layer with a logistic sigmoid transfer function, and 10 neurons output layer with a linear transfer function. The neural network was trained on the fault-free dataset with 10 input features and 5633 samples corresponding to 7,5 hours of real-time measurement.

4. Evaluation of the purposed autoencoder network

After training the neural network, the ability of the autoencoder to reconstruct already-known data was first tested. Some reconstructed features compared to the original data are shown in Fig. 4.

As it can be seen in Fig. 4 (a-c) the neural network can reconstruct the known data with the repeating character of the pattern with good accuracy. For data with a more complex nature of change over time (ambient temperature, Fig. 4d) the reconstruction is a more difficult task since it is difficult to estimate the nature of the change in this parameter. Thus, it is possible to say that the architecture of the autoencoder is adequate and the neural network works correctly.

The next step is to test the ability of the superimposed autoencoder to predict data that was not part of the training. To assess the accuracy of the reconstructed data, it was used the MSE (mean squared error) function.

The next step is to test the ability of the superimposed autoencoder to predict data that was not part of the training. To assess the accuracy of the reconstructed data, the mean squared error (MSE) function was used.

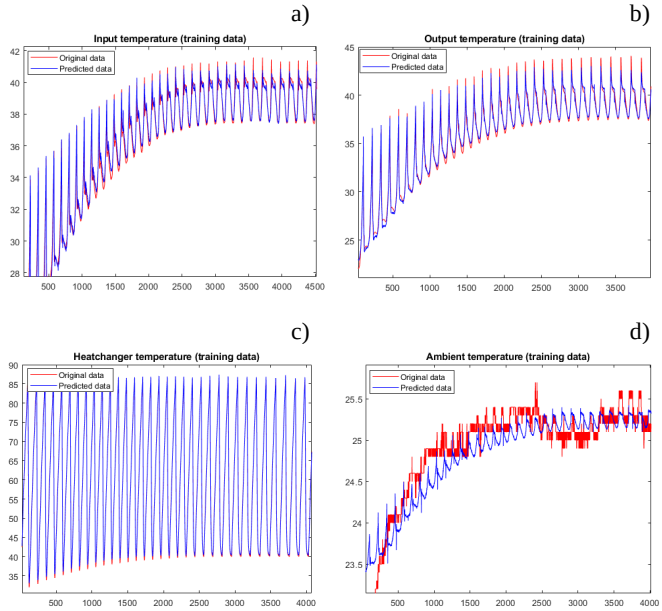

Fig. 4 *Reconstruction of training data features a) Input temperature; b) Output temperature; c) Heat exchanger temperature; d) Ambient temperature*

First, the autoencoder was tested for prediction on the new error-free data. The test error-free dataset contains 5419 samples and 10 features. Reconstruction plots for the same 4 features are shown in Fig. 5.

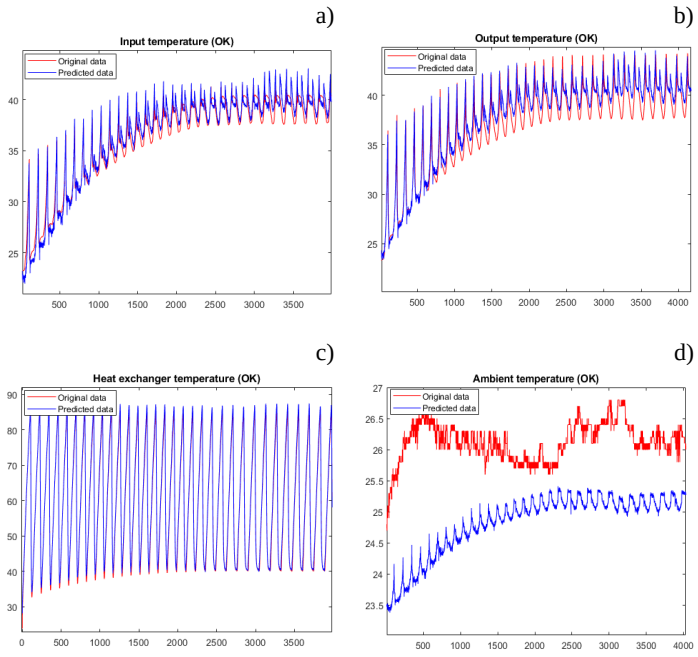

Fig. 5 *Reconstruction of no-error data features a) Input temperature; b) Output temperature; c) Heat exchanger temperature; d) Ambient temperature*

Next, the model input was fed with data that may be perceived as erroneous. In this case, the error appeared in the premature cooling of the working fluid due to the external environment. This error is mainly seen in the variation between the input temperature and the ambient temperature (see Fig. 6). The dataset containing the

anomaly contains 5523 samples. The values showing anomalous behavior are between 3700 and 3800 measurement steps.

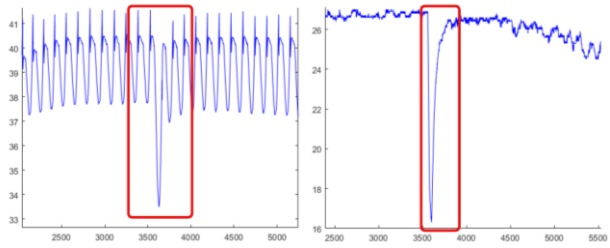

Fig. 6 *Anomaly in feature patterns behavior*

The sphere of interest of the model behavior, in this case, is whether this error is reflected in the sign of the parameter sensing waveform and in the computation of the model accuracy metric. The result plots of the prediction on the error data for inlet and outlet temperature, heat exchanger temperature, and ambient temperature are shown in Fig. 7.

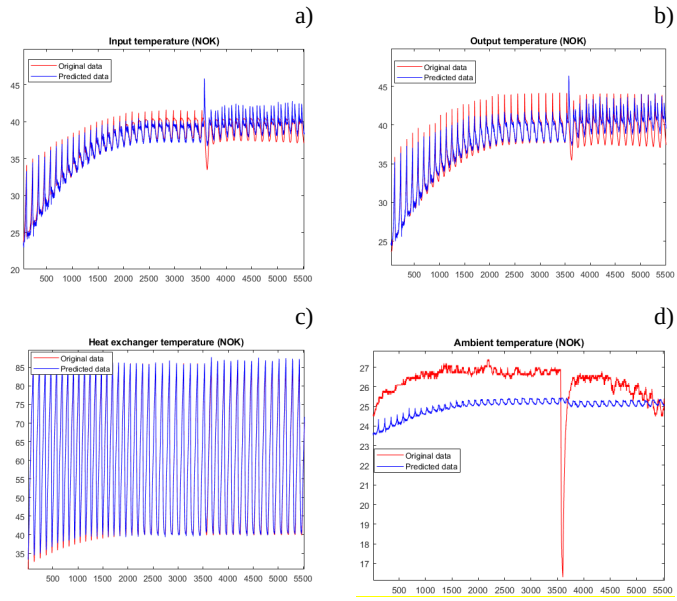

Fig. 7 *Reconstruction of anomaly data features a) Input temperature; b) Output temperature; c) Heat exchanger temperature; d) Ambient temperature*

The calculated MSE metrics for each parameter and dataset are shown in Table 1.

Table 1: *Mean-squared error metrics*

	Input temperature	Output temperature	Heat exchanger temperature	Ambient temperature
Training dataset	0.1755	0.1911	0.1914	0.0779
No-error dataset	0.7863	1.8765	1.0808	1.5030
Anomaly dataset	0.8643	1.3275	0.7792	2.8067

5. Results and discussions

In this paper, 4 parameters of the test equipment were monitored: the temperatures at the input and the output to the heat exchanger, the temperature of the heat exchanger, and the ambient environment temperature.

The superimposed neural network was tested on two test datasets, one of which contained examples of the anomalous behavior of the system. As it can be seen in Fig. 4, Fig. 5 and Fig. 7(a-c) the presented autoencoder model shows good results when reconstructing the dependencies between parameters on the new data. The success of the model is mainly shown when reconstructing a signal with a repeating pattern (inlet, outlet, and heat exchanger temperatures). The performance of the ambient temperature reconstruction is low (see Fig. 5d, Fig. 7d) as this parameter is generally difficult to predict and estimate.

The ability of the model to detect anomalies can be seen in Fig. 7(a,b). If there was an unexpected change in the waveform of the basin data, the waveform of the predicted value also changed its behavior for the parameters on which the anomalous behavior was occurring.

The occurrence of an anomaly is also indicated by an increase in the MSE value compared to the error-free dataset (see Table 1). The decrease of the MSE value in the anomalous dataset for the outlet temperature and heat exchanger temperatures can be explained by external conditions. Each of the datasets used was collected on a different day and the same climatic conditions could not be ensured in the location where the data collection took place.

6. Conclusions

Development and improvement of the proposed model would be possible by training the model on a larger amount of error-free data to cover a larger range of temperature parameters. The accuracy of prediction and detection of anomalies could also be improved by using the ambient temperature as a complementary parameter, increasing the overall accuracy of the model. The exact influence of this parameter on model accuracy is the subject of further research.

The ability to detect anomalies is powerful when R2F data are not available and provides an opportunity to estimate indicators of non-failure operating conditions. With the availability of data on errors and anomalous device states, the purposed model can be combined with classifier layers to classify existing anomalies. These factors show that autoencoders have perspectives for use in predictive maintenance tasks.

Acknowledgments

The outputs of paper was supported by grant VEGA 1/0470/23 "Research of implementation methods and means of artificial intelligence in systems of automated quality control of products with volatile quality parameters".

References

1. Aydin, O., Guldamlasioglu, S. (2017). Using LSTM networks to predict engine condition on large scale data processing framework. 2017 4th International Conference on Electrical and Electronics Engineering, ICEEE 2017 [online]. 2017, s. 281–285. doi:10.1109/ICEEE2.2017.7935834

2. Bampoula, X., Siaterlis, G., Nikolakis, N., Alexopoulos, K. (2021). A Deep Learning Model for Predictive Maintenance in Cyber-Physical Production Systems Using LSTM Autoencoders. Sensors 2021, Vol. 21, P. 972 [online]. ISSN 1424-8220.doi:10.3390/S21030972

3. Červeňan, A., (2015). *Systém údržby* [online]. 70. https://www.sjf.stuba.sk/buxus/docs/docs/edicne/Udrzba_farebna_final.pdf

4. Chan, R., W.K., Jason K.K. Yuen, E., Lee, W.M. a Arashpour, M. (2015). Application of Nonlinear-Autoregressive-Exogenous model to predict the hysteretic behaviour of passive control systems. *Engineering Structures* [online]. ISSN 0141-0296. doi:10.1016/J.ENGSTRUCT.2014.12.007

5. Fathi, K., Van De Venn, H. W., Honegger, M. (2021). Predictive Maintenance: An Autoencoder Anomaly-Based Approach for a 3 DoF Delta Robot. *Sensors 2021, Vol. 21, Page 6979* [online]. 2021, ISSN 1424-8220. doi:10.3390/S21216979

6. Huuhtanen, T., JUNG, A. (2018). Predictive Maintenance of Photovoltaic Panels Via Deep Learning. *2018 IEEE Data Science Workshop, DSW 2018 - Proceedings* [online]. 2018, s. 66–70. doi:10.1109/DSW.2018.8439898

7. Jing, L., Zhao, M., Li, P., Xu., X. (2017). A convolutional neural network based feature learning and fault diagnosis method for the condition monitoring of gearbox. *Measurement: Journal of the International Measurement Confederation* [online]. 2017, roč. 111, s. 1–10. ISSN 02632241. doi:10.1016/J.MEASUREMENT.2017.07.017

8. Kaji, M., Parvizian, J., Van De Venn, H. W. (2020). Constructing a Reliable Health Indicator for Bearings Using Convolutional Autoencoder and Continuous Wavelet Transform. Applied Sciences 2020, Vol. 10, Page 8948 [online]. 2020, roč. 10, č. 24, s. 8948 [cit. 24.1.2023]. ISSN 2076-3417. doi:10.3390/APP10248948

9. Xie, H., Tang, H., Liao, Y. H. (2009). Time series prediction based on narx neural networks: An advanced approach. *Proceedings of the 2009 International Conference on Machine Learning and Cybernetics* [online]. 2009, roč. 3, s. 1275–1279. doi:10.1109/ICMLC.2009.5212326

Management of innovation processes in the organization

Naqib Daneshjo[1], Róbert Rehák[1], Peter Drábik[1]
Ekonomická univerzita v Bratislave, Slovensko[1]
naqibullah.daneshjo@euba.sk, robert.rehak@euba.sk, peter.drabik@euba.sk

Abstract: *In the changing business environment and the global understanding of the market environment, the driving force of which are increasingly demanding customer requirements, the growth of supply and services, higher competition, technological development, globalization of business, innovation is a means for the implementation of constant changes. Nowadays, success is achieved by integrating innovation into business processes, and creativity of human resources in various professions, for example, technologists, designers, economists and optimizers, which is replaced by innovation engineers, business and marketing innovators, thought innovators, innovation managers, etc., is also important for productivity support.*
Strong and agile companies thus gain a leading position on the market. By connecting the knowledge of employees, innovation strategy and business management, a management model of the innovation process was created, which takes into account the diversity of types of organizational structures of enterprises and uses the elements of the innovation climate of the enterprise. An important part of managing the innovation process is determining the elements of the innovation climate, through which innovative ideas from employees are supported and their dissemination and implementation. They must be managed on the basis of the chosen type of organizational structure of the company. By properly setting the elements of the innovation climate and aligning it with the organizational structure, enterprises can manage their processes and get more innovative ideas for implementation, thus increasing their innovation performance and achieving better competitiveness in the market.
Key words: *INNOVATION PROCESS, INNOVATION STRATEGY, COMPETITION, GLOBALIZATION, INNOVATION ENGINEERING*

1. Introduction

The basic premise of a successful company is its constant progress against the competition on the market, it follows that the innovation process in the company is one of its key attributes. The manager is responsible for the innovation process in the company, who must consistently pay attention to which decisions are beneficial for the company and, conversely, which decisions can lead the company to decline and loss of prosperity. The effectiveness of management decisions lies in how intensively and successfully they can respond to the needs of the market and the current state of the company's environment. The preparation and gradual implementation of innovative changes is called the innovation process. Its result is innovation as a realized, used and above all positive change. The task of innovation processes is to purposefully influence the reproduction of all business in accordance with the growing needs and demands of the customer and the market as a whole. The innovation process is the process of creating and spreading innovations. We understand innovation processes in business activities as the implementation of individual innovations or their sets, which ensure quantitative and qualitative changes in products, processes and the structure of the production and technical base with all economic and social contexts. Innovation processes penetrate deeply into the production-technical structure of the business sphere and thus into the process of its reproduction. For example, a new technology of any nature in industry usually affects the relevant branch of engineering and electronics and causes a certain need for raw materials and energy, is associated with investments, movement of labor forces, which further causes a chain of needs. In a broader sense, innovation processes are also large programs and projects of economic development, scientific research activity, significant actions that affect the entire business process and the reproductive process within it. In practice, the main place of innovation processes are companies, where innovations are implemented in products, technologies and other activities. Creation and management of innovation processes are fully subject to business management with all its principles. The innovation process is not random. It is controlled by a specific project or program linked vertically and horizontally in the sphere of implementation.

Improving the management of innovative development in industrial enterprises includes the creation of a new market infrastructure that would stimulate and support this mechanism, as well as perform its direct control. Therefore, the problem of rational and effective use of innovative products is of particular importance in the current socio-economic conditions of our country. It also requires the latest approaches to building a management system for innovative development in companies, improving the quality of the innovation process in companies and increasing their investment and innovation attractiveness.

2. Methodology of creation and management of innovation processes of the organization

The analysis and synthesis of theoretical knowledge serve as the basis for the creation of a general model of the creation and management of innovation processes in the company. The starting model for the creation and management of innovation processes in the company (Fig. 1) is also based on the analysis of other models and practical studies and is a general model that can subsequently be elaborated in more detail on the basis of findings from primary and secondary research. From the analyses of theoretical knowledge so far, it is clear that in each type of business there are specific conditions that must be taken into account when creating and managing innovation processes (Fig. 2) and they often change depending on the sector, type of industry, size of the company and length of time on the market etc.

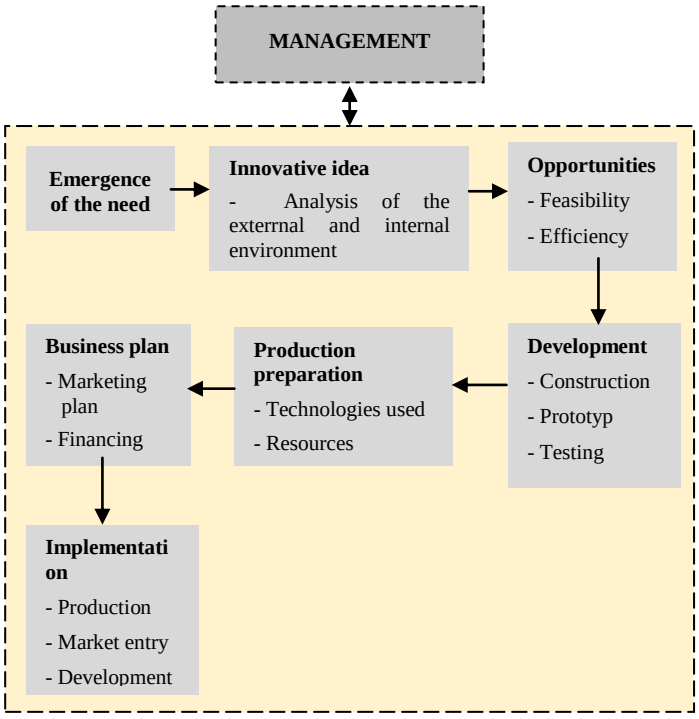

Fig. 1 *Initial model of creation and management of innovation processes in the company*

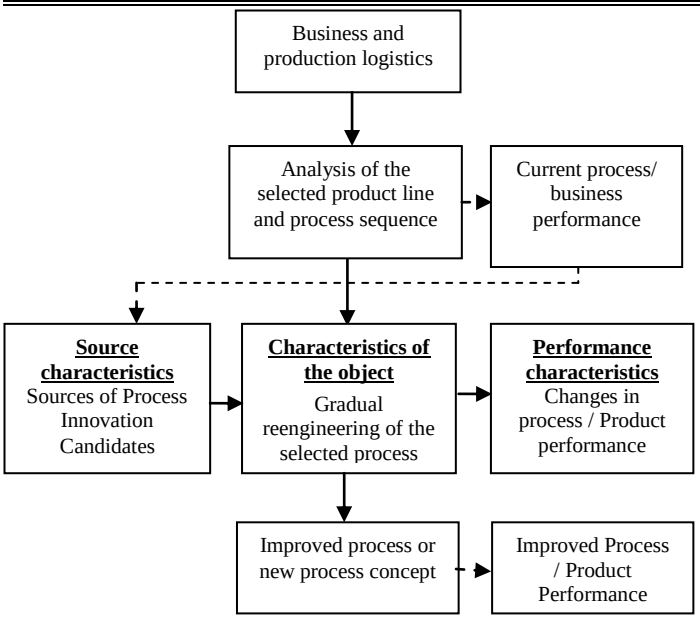

Fig. 2 *Basic model of process innovations*

Innovation is not only the use of high technology, but also a change in the field of managerial decisions. In order to realize most of the tasks faced by the enterprise, it is necessary to reorganize the enterprise management system on the basis of new management technologies. A company that wants to work flexibly inevitably comes to the need to use innovative approaches. Its essence lies in the creation of such a company management structure in which the personnel is embedded in the business process, which ensures the quality production of the product. Project management methodology plays an important role in building such a system. For this, it is necessary to develop a management system, the basis of which is the breakdown of a complex process into simple components based on a project approach and the construction of a kind of "pipeline" of management. This has a significant impact: work becomes more purposeful, requirements for personnel qualifications are reduced, labor productivity rises sharply, and the rate of errors is reduced. When designing a model for the creation and management of innovation processes in the company and based on the analysis of the state of the problem, it is necessary to take into account the following criteria [3]:

1. Openness: Flexible work with innovations that come to the company from an internal or external environment. Unused innovative ideas are registered for their possible future use through the corporate information system.
2. Cooperation: an innovation process enabling cooperation with interested parties, which significantly contribute to the improvement of the innovation process and the emergence of successful innovations. These are, for example, research institutions or universities.
3. Management elements: the course of the innovation process in the company should be effectively managed using basic managerial functions.
4. Learning from innovation: the innovation process should enable continuous improvement of its management based on learning from the implementation of the innovation process over time.
5. Feedback: on the individual stages of the innovation process, from which the company can take lessons.
6. Creative thinking: supporting the generation of innovative ideas. Emphasize creativity and creative thinking already when selecting employees and constantly support the development of creativity, for example through training.
7. Information support of the innovation process: provision of necessary information to responsible persons at the right time in the right place.

The proposed model supports working with innovative ideas, which the company acquires through stakeholders and most often from customers, employees and competitors. The proposed model is divided into three phases: creation of invention, creation of innovation, penetration of innovation and the result is innovation as a realized and used change.

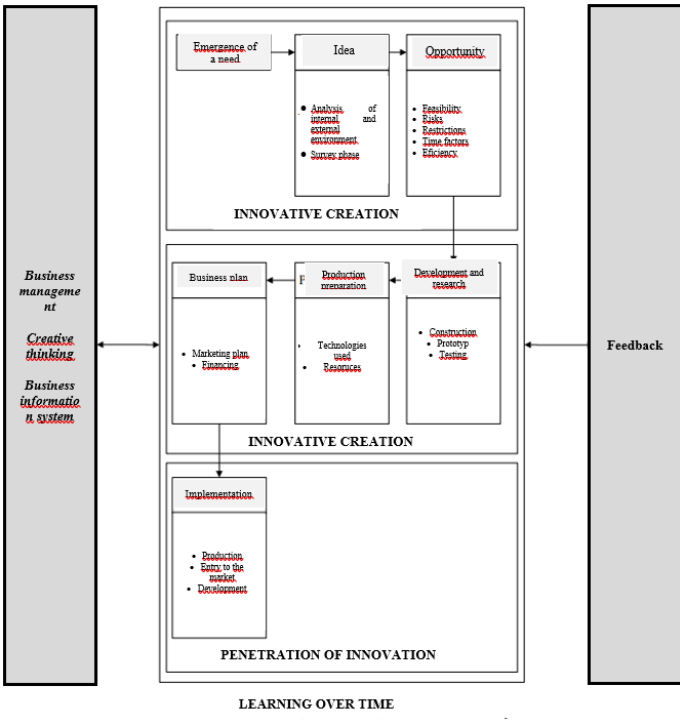

Fig. 3 *Model of creation and management of innovation processes in the company [1] [2]*

The proposed model of creation and management of innovation processes in the company takes into account attributes such as management of the innovation process, openness of the innovation process in relation to interested parties, the ability to learn from the results of the individual phases in which creativity and feedback are applied.

3. Generating ideas during the standard innovation process

Based on the findings, the generation of innovative creativity ideas during the standard innovation process can be described in detail. R&D employees and group managers have the freedom to pursue their own ideas. If e.g. ten ideas, management will decide on the winning idea according to criteria such as exceptionality, feasibility and potential. Some ideas generated within the department may be presented during an appropriate event. Ideas are generated individually or in teams, and teams are usually from the same department and belong to the same work group. The idea generation process contains several stages and milestones and is a traditional stage-gate process (stage-gate process also referred to as stage-gate process or waterfall process is a technique that is initiated by the needs of the project (for example, the development of new products, development software, process improvement ,business exchanges, etc.) that is created either on the basis of new scientific discoveries or on the definition of needs by the market. Process research and development employees generate ideas all the time. If they have an idea, they can promote it only by direct contact with research

and development employees [34, 48]. On the one hand, ideas can come from a specific form of professional training of workers. Efficient and motivated R&D employees thus complete specific training and can work in other departments. These employees are selected by the management. The person concerned from the R&D department will participate of this program and provide feedback about it. On the other hand, management can organize creative meetings with workers and allow R&D workers to have an environment to develop their own ideas. Therefore, ideas and innovations come from three different ways of the standard innovation process:

1. Top-down (top-down) (market pull or science pressure).
2. Expert training.
3. Creative meetings.

Ideas can be implemented into the product development or innovation process. A study may be developed to obtain additional knowledge if the potential of the idea is not clear or if the idea is not directly related to the product. One possibility is to do a feasibility study, which starts with the aim of proving the potential of the idea. Idea generation in the standard innovation process focuses on exploration and exploitation. From top to bottom, ideas are more on the exploitation side because they are based on the customer's wishes or have demonstrated very high scientific potential. On the other hand, research is the goal of a creative meeting and expert training. A standard innovation process is shown in Fig. 4.

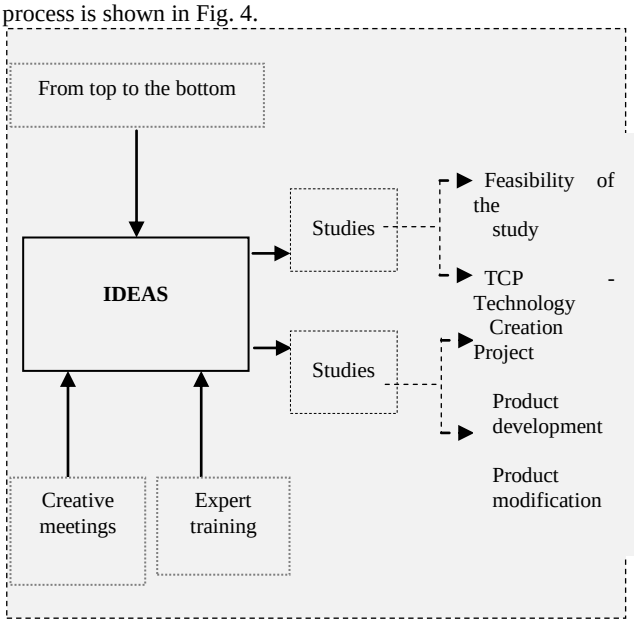

Fig. 4 *Standard innovation process*

Fig. 5 shows the process of spreading ideas and ideas within the framework of innovative creativity and the standard innovation process.

Innovation is an integral part of the development of a modern enterprise. Many new goods and services appear on the world market every day, but the average lifespan of some of them is very short. Buyers don't recognize them and they disappear from the market as quickly as they appeared. This means that they were not considered innovations, although they were new products based on interesting and original ideas. It is well known that goods and technologies have a limited lifespan. Due to its characteristics, innovative activity should be organized separately from the main production processes. In any case, it is necessary to strive to ensure the organizational flexibility of an innovative company.

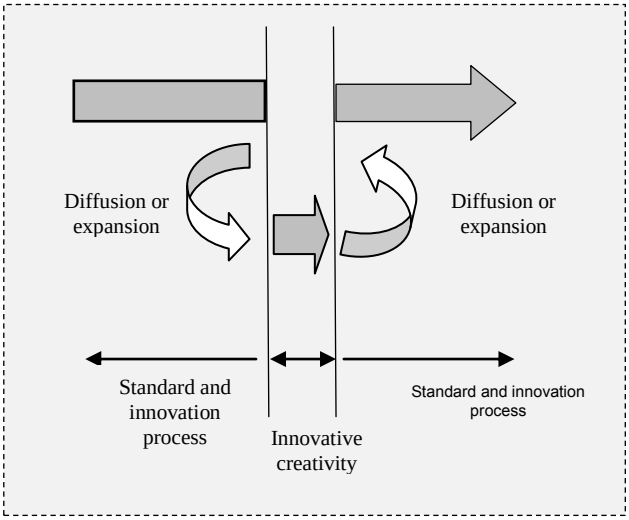

Fig. 5 *Spreading ideas or ideas*

4. Conclusion

The area of creation and management of innovation processes in the company is an increasingly discussed topic in the field of innovation. Innovations contribute to increasing competitiveness, higher sales of products or higher efficiency. If a business is really interested in innovating a product or service, it must first thoroughly examine its own processes, despite the fact that finding new products or services is more exciting. It is a common phenomenon that many parts in organizations need reengineering of company processes. The creation and management of innovation processes is a very important role for the company and its economic and social growth. Business managers are increasingly becoming aware of the importance and importance of innovation.

Product innovations represent shifts in the competitive position, which nowadays can result in a leading position in the market, even in the entire industry. In order for businesses to be successful in the long term, it is essential that they use their innovation potential to the fullest. Problems often arise that companies often encounter, such as insufficient use of innovation opportunities, the absence of a comprehensive model for the creation and management of innovation processes, the absence of a comprehensive systematic methodology for the creation or management of innovation processes. Therefore, the innovative activity of the company is considered a necessary condition for its growth and competitiveness in global markets. Increasingly demanding customer requirements, increasing competition, technological development and globalization in a changing business environment are becoming a driving force for innovation.

Acknowledgements: This work has been supported by the Scientific Grant Agency of the Ministry of Education of the Slovak Republic (KEGA 029EU-4/2022 and Project KEGA 030EU- 4/2022).

5. References

[1] J. Soviar, V. Lendel, M. Kocifaj, E. Čavošová, *Kooperačný manažment*, Žilina: EDIS – vydavateľstvo ŽU, (2013)

[2] V. Lendel, M. Varmus, *The level of utilization of innovative activities of transport businesses in the Slovak Republic*, In: Periodica Polytechnika Social and Management Sciences. Vol. 21, No. 2, (2013), p. 83-90.

[3] B. Bernstein, P. J. Singh, *An integrated innovation process model based on practices of Australian biotechnology firms.* In: Technovation 26, (2006)
[4] M. Kováč, *Tvorba a riadenie inovácií.* Technická univerzita v Košiciach, Edícia EQUAL, 2007
[5] Ch. Palmberg, *The sources and success of innovations – Determinants of commercialisation and break-even times.* In Technovation 26, (2006)
[6] V. Lendel, Š. Hittmár, E. Siantová, *Management of innovation processes in company*. Procedia economics and finance, 23, (2015)
[7] M. B. Bulturbayevich, *Improving the mechanisms of strategic management of innovation processes in enterprises.* In Archive of Conferences, (2021)
[8] J. Sundbo, *Management of innovation in services.* Service Industries Journal, (1997)
[9] S. Ben Mahmoud-Jouini, T. Burger-Helmchen, F. Charue-Duboc, Y. Doz, *Global organization of innovation processes.* Management international, (2015)
[10] I. L. Popa, G. Preda, M. Boldea, *A theoretical approach of the concept of innovation*. Managerial Challenges of the Contemporary Society. Proceedings, (2010)
[11] S. Jirásková, *Inovácie a trvalo udržateľný rozvoj*. Manažment v teórii a praxi-on-line odborný časopis o nových trendoch v manažmente, (2007)
[12] F. Rybár, *Vybrané faktory ovplyvňujúce efektívnosti riadenia manažéra*, Doctoral dissertation, AMBIS vysoká škola, as, Bankovní institut vysoká škola SK, (2009)

Risk Driven Design of Technical Product

Josef Dvorak, Stanislav Hosnedl
University of West Bohemia, Czechia
dvorakj@fst.zcu.cz

Abstract: *Technical Products that companies put on the market must be competitive and must find their way to the customer or the customer must find their way to them. In the vast majority, these are new products or innovated existing products that can offer the customer added value compared to the competition and, above all, induce in him the desire to purchase the product and not just include it in the selection of other competitive products. During the development process of these products, it is necessary to take into account the entire life cycle of the product and not only its operational functions and other operational characteristics, which is quite often neglected. There exist a lot of engineering design methodologies, methods and/or tools implemented in guidelines and standards which help engineering designers to innovate products and to reduce constructional, safety, environmental, etc. risks of Designed (future) Technical Products. Their common feature is especially high dependence on specialized experience of their users, time consuming, and their mutual both conceptual and terminological inconsistency resulting in very difficult compatibility with engineering designing itself.*

Keywords*: RISK, INNOVATION, EDSM, THEORY OF TECHNICAL SYSTEMS*

1. Introduction

The issue of innovation is a current global topic and is one of the key factors for a company's success on the market. It must be remembered that if "we (our business) don't do it, someone else will". Product life cycles are constantly shortening, new products must be introduced more and more often. The previously usual "development push (PUSH)" approach is changing to "market pull (PULL)". PULL innovations are those innovations that should be introduced to the market to gain an edge over the competition. A "PULL" innovation can be created by timely and appropriate prediction of properties on an existing (current) Technical Product, and based on this prediction, a qualitatively better product can then be developed. Practice initiates innovation only in relation to operation. Therefore, traditional innovations are mainly focused on improving operational functions.

The Technical Products that companies put on the market must be competitive and must find their way to the customer or the customer must find their way to them. In the vast majority, these are new Products (or innovated existing Technical Products) that can offer the customer added value compared to the competition and, above all, induce in him the desire to purchase the product and not just include it in the selection of other competitive products. During the development process of these products, it is necessary to take into account the entire TS(s) Life Cycle of the Technical Product and not only its operational functions and other operational characteristics, which is quite often neglected.

2. Problem formulation

At the beginning it was necessary to map and analyze at a basic general level the issue of technical product innovations with the aim of identifying options for increasing their effectiveness and, within the limits of possibilities, effectiveness. In the professional literature, one can find a large number of methods whose goal is higher efficiency and quality of the new product development process and improvement of either the entire innovation process or some of its parts (Fig.1). Some methods can be used for the entire process of technical product innovation (from the initial idea to the launch of the product on the market), some can be used only for a part of this process, e.g. the construction process. There is also problem to avoid risk situation(s) of the Technical Product in their Life Cycle (LC) generally.

In the professional literature[8,9], one can find a large number of methods whose goal is higher efficiency and quality of the new Technical Product development process and improvement of either the entire innovation process or some of its parts. Some methods can be used for the entire process of Technical Product innovation (from the initial idea to the launch of the product on the market), some can be used only for a part of this process, e.g. the Design Engineering Process. The goal of our paper is to present methodology which was created as synthesis between innovation methods and methods for risk analyses and elimination as obligatory procedure in several industrial branches when designing Technical Product. Risk analyses are requested often because of certification process mostly by public authority i.e. Chemical industry, nuclear engineering, automotive, healthcare,...

The above and other well-known innovation methods are mainly based on an instructive ("directive") strategy of using knowledge with a significant use of the intuitive strategy, or and the trial-error/success strategy (Fig. 1) [5]:

The instructional strategy is based on guidelines, rules and recommendations leading to the solution of the innovation assignment. These guidelines are based either on standards, company guidelines or are created in the form of methods or methodologies.

Intuitive strategy is based on the use of (irreplaceable, but in any case limited) expertise and experience of innovation solvers.

The trial-and-error/success strategy is applied without the use of rules, experience or methods and is based only on chance (trials).

By using a theoretically based strategy based on the knowledge "map" of Engineering Design Science (EDS) [5], it is possible to implement a "theoretical base" in all mentioned traditional strategies of knowledge support for innovation and use it to make the relevant innovation methods, which are at most at the instructional level, more effective strategy. All of the above-mentioned strategies (i.e. trial-and-error/success, intuitive, instructive) can be incorporated into the strategy of technical systems theories based on EDS, and based on this, they can be optimally combined during the new product development process, which is highly effective.

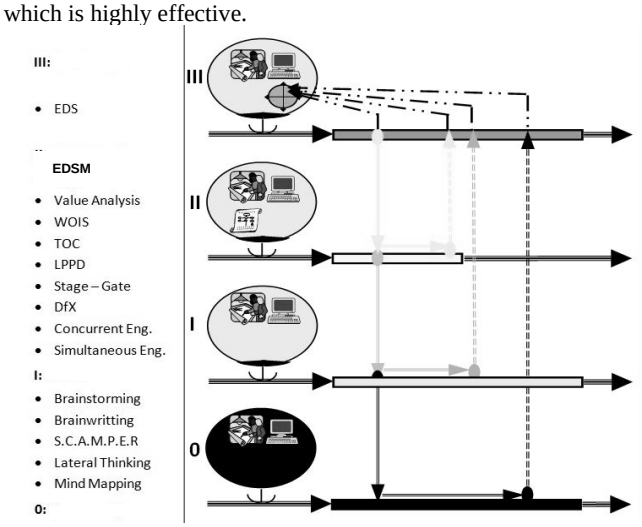

Fig. 1 *Taxonomy of methods suitable for Innovations from the level of its Knowledge support [modified 5 by authors]*

3. Theoretical Background

The basic theoretical structure, which is based on the Theory of Technical Systems to Structures [Hubka & Eder 1988, etc.] is a model of an (artificial) transformation system (TrfS) with a transformation process (TrfP), see Figure 2. This model generally expresses that each activity (e.g. technological operation Tg) is a transformation of a transformed object, marked as OPERAND in a certain input state to OPERAND in a desired state at its output, which is achieved by direct or mediated by the effects of OPERATORS, i.e. the effects of Humans (HuS), Technical Systems (TS), Active and Reactive Environment (AREnv), Information Systems (IS) and Management Systems (MgtS) on the transformed OPERAND.

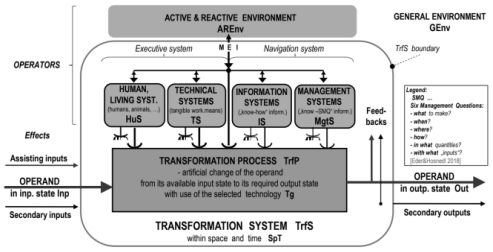

Fig. 2 *General Model of Transformation system with Transformation process* [4]

TS Life Cycle (LC) structuring can be performed according to various aspects (e.g. according to the place of implementation, according to development phases, or cost aspects, sales phases on the market, etc.), but for the needs of designing of TSs their distribution according to dominant transformations - transformation processes (TrfP) [5]. Using the general model of the Transformation system (TrfS) (Fig. 2) with its transformation process (TrfP), a general model of the life cycle of a technical product can be illustrated [2,3,4] The individual stages of the general life cycle of TS are modeled by a serial arrangement of individual stages expressed using these models.

TS life cycle is shown in Fig. 3, is distinguished by index (s) from other technical systems in individual stages. TS (s) is in the initial phase in the form of information (dashed flows), starting with production it is transformed into a material / material form (full flows). TS (s) has mainly the function of an operand, but in the operational /working phase it becomes an operator (with the exception of assisting maintenance and repair processes, when it temporarily becomes an operand). The resulting TS must meet all the requirements for its properties in terms of the entire Technical Product Life Cycle (from planning to disposal) [5].

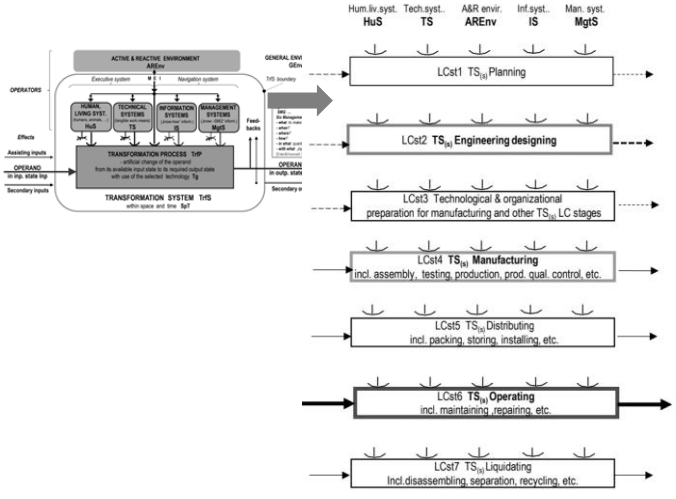

Fig. 3 *TS(s) Life Cycle stages as a sequence of the key transformation processes (TrfP) and respective transformation systems (TrfS) [7] => [2,3,4] => [5,6]*

From analysis of the generalized TS(s) LC model (Fig. 3) with proven systematic structure, it transparently shows that the carrier of R|E/S| in general, could be the following typical Object (sub) systems (ObjS):

- assessed TS (s) (i.e. reliability of TS (s) in its whole LC of TS(s), which is in professional publications, including standards, etc., moreover only with implicit or even explicit focus only on operation TS (s))

- TS (s) & ∑Human/Living Being Systems assessed (i.e. safety of TS (s) for humans and other living beings throughout the LC TS (s)), which is often incorrectly labeled in the professional publications, including standards, "only "as safety against injury / death during the operation of TS (s), moreover only with an implicit or even explicit focus only on the operation of TS (s))

- assessed TS (s) & ∑other TS (i.e. safety of TS (s) for other tangible work equipment in the whole life cycle of TS (s), which is not mentioned in professional publications, etc.)

- assessed TS (s) & ∑Management systems (i.e. safety of TS (s) for management systems in the whole life cycle of TS (s), which is mentioned in professional publications etc., very unsystematically, mostly only with a focus on strategic organization management)

- assessed TS (s) & ∑Environment (i.e. safety of TS (s) for working, natural and space environment in the LC of TS (s), which is mentioned in professional publications, incl. standards, but not systematically)

- assessed TS (s) & ∑Information systems (i.e. security of TS (s) for information systems in LC of TS (s), which is mentioned in professional publications, including standards, very unsystematically, mainly only with a focus on cybersecurity etc.)

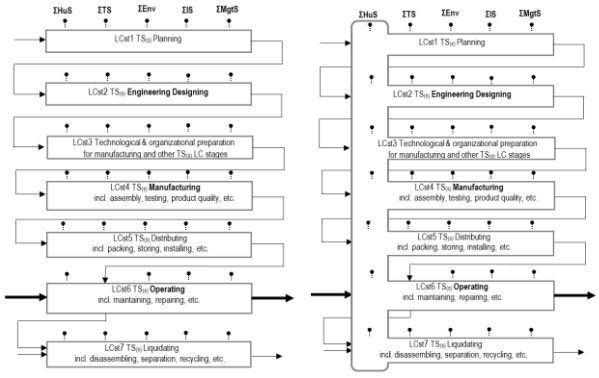

Fig. 4 *EDSM based knowledge "maps" for R|E/S| identification in the LC stages of TS (s) for Object Systems) TS (s) (left), TS (s) & ∑HuS (right) [1]*

4. Conclusion

Technical product innovations are a very current topic, as the success of their solutions determines the success and failure of individual companies. It can be assumed that with the use of knowledge based on the already successfully validated knowledge of Engineering Design Science based on the Theory of Technical Systems (EDSM-TTS) it will be possible to effectively develop and validate improved, possibly and qualitatively new innovative methods for highly creative and at the same time systematic design of innovative technical products with a higher utility value while maintaining optimal proportions: achieved quality - spent costs - spent time.

Further work will mainly be focused on the issue of disruptive innovations, which today represent the current strategy of technical product innovations and their marketing. These innovations focus

on solving current problems of existing technical products. The next expected direction of work will therefore also be focused on the rational initiation of these disruptive innovations. In doing so, the use and development of the aforementioned developed software tool is envisaged to support the specification of requirements and to assess their fulfillment (SP&HA). As mentioned, disruptive innovations are mainly focused on eliminating weak points (functions and other properties) of existing technical products, which can be effectively and efficiently detected, analyzed and evaluated with the help of this SW tool.

To improve them, it will be possible to effectively use the existing knowledge and DfX (Design for X) methods, which today already cover a wide range of knowledge for achieving the required specific properties of technical products during their construction. Above mentioned methodology as a support tool for designers and employees of related engineering professions, who can comprehensively or even partially use it as feedback and control of their design activities and use this knowledge in building their own "knowledge map", which each designer creates during their practice was presented. It brings the opportunity for users use it as an effective tool for innovation and building own portfolio of knowledge, for experienced (so-called senior designers) the methodology can offer a different "perspective" on predicting the risks of technical products and confirming or refuting their routine approaches. The above presented methodology allows to perform risk prediction and analysis for object systems TS (s) & ∑HuS, TS (s) & ∑TS, TS (s) & ∑Env, TS (s) & ∑IS and TS (s) & ∑MgtS in all considered stages of the Life cycle of the designed TS or even existing TS[6].

References

J. Dvořák. Methodological Support for Risk Analysis during the Whole Life Cycle When Designing Technical Products. In: Proceedings of The 30th International Business Information Management Association Conference: Innovation Vision 2020, 2017, pp. 4642 - 4650, ISBN: 978-0-9860419-9-0

2. W. E., Eder, S. Hosnedl. Design Engineering, A Manual for Enhanced Creativity. CRC Press, Taylor & Franciss Group, Boca Raton, Florida USA 2008, 600 s., ISBN 978-1-4200-4765-3 3. W. E., Eder, S. Hosnedl. Introduction to Design Engineering: Systematic Creativity and Management. CRC Press / Balkema, Taylor & Francis Group, Leiden, Netherlands, 2010, ISBN: 978-0-415-55557-9

4. W. E., Eder, S. Hosnedl. Systematic Engineering Design: General Model of Procedures for Systematic and Methodical Engineering Designing. Boca Raton, Florida USA: CRC Press, Taylor & Francis Group, 2018, ISBN: 978-1138050945

5. Hosnedl, S. Systematical Designing of Technical Products. KKS/ZKM. Lectures in Power Pointu. Plzeň: WBU, KKS, 2020 6. Hosnedl, S., Dvořák, J. Complex prediction of risks of Technical Products, UWB, KKS, 2019.

7. V. Hubka, W.E, Eder, W.E: Theory of Technical Systems. Berlin Heidelberg: Springer - Verlag, 1988, ISBN 3-540-17451-6

8. J. Bessant, J. Tidd,. Innovation and Entrepreneurship. New York: 2007, John Wiley & Sons, ISBN 978-0-470-03269-5 9. G.R. Cooper. Winning at New Products: Accelerating the process from idea to launch – third Edition, Basic Books, ISBN 978-0-7382-0463-5

ВЪРХУ НЯКОИ АСПЕКТИ ПРИ АНАЛИЗА НА ГРАДСКАТА МОБИЛНОСТ

ON SOME ASPECTS OF THE ANALYSIS OF URBAN MOBILITY

доц. д-р Нетов Н[1,*], доц. д-р Спасов К.[2], ас. д-р Върбанова Т.[3]
СУ „Св. Кл. Охридски, България[1,2,3]
nnetoff@feb.uni-sofia.bg[1] kspassov@feb.uni-sofia.bg[2] teodorav@feb.uni-sofia.bg[3]

Abstract: *Most of the individual activities, including the daily transport activities of citizens, generally exhibit a combination of changing and common behavioural models. The existing limitations of the models used to design optimal routes and timetables for public transport based on the actual demands and needs of citizens are widely discussed in the scientific literature. The purpose of the article is to consider possible approaches to the analysis of urban mobility in the context of innovations related to the potentials of creating big datasets on the mobility of GSM connected mobile devices by mobile network operators in the context of the requirements for protecting the personal data.*
Keywords*: PUBLIC TRANSPORT, TRAVEL BEHAVIOR*

1. Увод

Бързото развитие на технологиите за облачен компютинг и свързаните с това възможности за създаване и анализ на големи масиви от данни е съпроводено с интензивен процес на иновации в редица икономически и социални сектори. Генерирането на стойност в различните етапи от веригата за създаване на стойност от данните ще бъде в центъра на значителна част от иновациите на нови продукти и решения. Новите и иновативни подходи за генериране на големи масиви от данни и разработването на нови иновативни аналитични подходи за извличане на полезно знание от тях предоставят възможности и предизвикателства както пред бизнеса, така и пред публичните институции които са отговорни за регулаторната рамка в която протичат тези процеси.

В свое съобщение за пресата от 20.01.2023 година Европейската комисия обяви редица набори от данни с висока стойност (1. Геопространствени данни; 2. Наблюдение на Земята и околната среда; 3. Метеорологични данни; 4. Статистика; 5. Дружества и собственост на дружествата; 6. Мобилност), които да се предоставят за повторна употреба. В него се цитира Маргрете Вестегер, изпълнителен заместник-председател с ресор „Европа, подготвена за цифровата ера“, според когото „Предоставянето на набори от данни с висока стойност ще бъде от полза както за икономиката, така и за обществото, например чрез подпомагане на борбата с изменението на климата, намаляване на замърсяването на въздуха в градовете и подобряване на транспортната инфраструктура. Това е практическа стъпка към постигането на успешно цифрово десетилетие и изграждането на по-просперираща цифрово бъдеще.“ В същото съобщение за пресата от 20.01.2023 година Тиери Бретон, комисар по въпросите на вътрешния пазар, подчертава, че „Данните са крайъгълен камък на промишлената конкурентоспособност на ЕС. С новия списък с набори от данни с висока стойност, публикуван днес, ние отключваме голямо количество публични данни в полза на всички. Стартиращите предприятия и МСП ще могат да използват тези данни за разработване на нови продукти и иновативни решения, които подобряват живота на гражданите в ЕС и по света“, [1].

Появата на масиви от големи данни за местоположение на постоянно свързани в интернет устройства създава значителен потенциал за развитието на редица иновативни технологии. Наличието на нови и подробни източници на огромни количества данни за геопозициониране на постоянно свързани в интернет устройства може да доведе до промяна в начина, по който планирането на транспорта и моделирането на търсенето на транспортни услуги ще се извършват в бъдеще.

В своя публикация от 2017 година Николова, Х. подчертава, че технологичните иновации в много голяма степен са доказано ефективни, но сами по себе си не могат да доведат до решаването на съществуващите социални, институционални и политически проблеми. Прилагането на класически подходи за измерване на въздействието на технологичните иновации не позволяват да се изясни в пълна степен тяхното влияне върху устойчивото развитие и това налага използването на по-комплексни подходи. В този контекст нейните изследвания и анализи в голяма степен обхващат всички основни аспекти на устойчивостта на транспортната система и създават възможности за точната оценка на въздействието на информационните технологии върху тях. Авторът установява, че идентифицираните разходи и ползи са ключови елементи по отношение на реализацията на стратегическите инфраструктурни проекти в областта на транспорта и имат важно значение за изграждането на аналитична рамка за комплексен анализ на ефектите от приложението на дигитални технологии и техния принос към устойчивото развитие на транспорта и транспортната инфраструктура. [2]

В своя публикация от 2017 г. Цветкова, С и Минков, Т. подчертават, че във фокуса на изследванията свързани с устойчивото развитие на транспорта и транспортната инфраструктура е необходимо да бъде поставян не само автомобилният транспорт, с неговите все по-нарастващи нужди от пространство и инфраструктура, а и нуждата на гражданите от мобилност, която трябва да бъде задоволена по чист и интелигентен начин, [3].

През 2018 година Национална академия на науките на САЩ публикува свой доклад със заглавие „NCHRP Research Report 868: Cell Phone Location Data for Travel Behavior Analysis“ [4] в който представя насоки за това как:

(1) да се оценява степента, до която данните за местоположението на мобилни телефони и свързаните с тях продукти точно изобразяват пътуванията;

(2) да се идентифицира дали и как тези големи масиви от данни могат да бъдат използвани за подобряване на разбирането на характеристиките на пътуването и способността за по-ефективно моделиране на поведението при пътуване;

(3) да се оценяват силните и слабите страни на анонимизираните данни за местоположения на постоянно свързани в интернет устройства.

Емисиите на парникови газове (ПГ) намаляват във всички основни сектори в Европейския съюз, с изключение на един сектор, който отбеляза значително увеличение на емисиите на ПГ през последното десетилетие – транспортния сектор. Европейският транспортен сектор е изправен пред значително предизвикателство при постигането на целта за декарбонизация, поставена от Европейския зелен пакт, [5].

Интересна нова група от изследвания по темата за устойчивото развитие на транспорта и транспортната инфраструктура са свързани с въвеждането на градски транспорт по заявка, [6], [7], [8]. Авторите оценят влиянието на различни променливи, свързани с местните специфики, като градска инфраструктура и структура на автомобилния парк,

като изследват динамиката в транспортни навици на жителите в контекста на микро специфични фактори свързани с календара на официалните празници, гъстота на трафика, сезонност, метеорологично време и т.н.. Моделирането на ефекта на зависимите променливи служи като шаблон за прогнозиране и за оценка на решенията за влиянието на модела градски транспорт по заявка върху качеството на въздуха.

Изследователският фокус на тази статия е свързан с някои аспекти при анализа на градската мобилност в контекста на използването на гео-пространствени данни на оператори на мобилни мрежи.

2. Градска мобилност

Моделирането на транспортните навици на гражданите е ключово за доброто планиране на градските инфраструктури и свързаните с тях услуги за градска мобилност. Въпреки това, използването на често характеризиращи се с голям обем масиви от гео-пространствени данни е сериозно предизвикателство, както за градските власти, така и за бизнесите предлагащи технологични иновации и нови решения в тази посока.

В актуална публикация на тема “Data-driven public transport routes and timetables based on anonymized telecom data.”, нейните автори правят литературен преглед на значителен брой публикации свързани с анализа на градската мобилност, възможните подходи за интегриране на данни за местоположението на мобилни телефони и свързаните с това предизвикателства, [9]. Основните проблеми при използването на информация за местоположението на мобилни устройства на граждани са свързани с защитата на техните лични данни. За целите на таксуването операторите на мобилни мрежи създават регистри за всяка отделна регистрацията на мобилните устройства на техните клиенти в съответна базова станция при ползване на услуга (т.н. CRD). Тази информация е конфиденциална, съхранява се за кратко време и не може да се използва за други цели. Изискванията за защита на лични данни не позволяват използването ѝ в аналитични масиви от данни чрез които дори и само теоретично да е възможно проследяването на който и да било гражданин. Това налага създаването на аналитични масиви от данни в които се съдържа само анонимизирана и статистически обобщена информация.

Възможен подход за това е предложен в [9]. За целите на анализа на градската мобилност в България този подход може да бъде обобщен в следния алгоритъм:

(1) за всяко мобилно устройство могат да бъдат дефинирани „зони на престой“. Това са клетки на мобилния оператор в които дадено мобилно устройството е престояло за повече от един час.

(2) за всяко денонощие могат да бъдат дефинирани 24 часови слота – от 0:00 до 1:00, 1:00-2:00 …23:00-24:00.

(3) в контекста на така дефинираните часови слотове за всяка двойка клетки на мобилния оператор (n_i) и (n_j) и за всеки пореден часови слот може да бъде дефиниран времеви ред който съдържа статистически обобщена информация за броя мобилни устройства които са били регистрирани за повече от един час в (n_i) и след това са били регистрирани за повече от един час в (n_j). Ако в конкретен часови слот и за конкретна двойка клетки на мобилния оператор броя устройства е по-малко от 5, тази информация няма да се запазва.

Така дефинираните времеви редове няма да съдържат никаква персонална информация за клиентите на мобилния оператор и могат да бъдат използвани за създаване на аналитичен набор от данни за транспортните навици на гражданите.

3. Статистически обобщени данни

Анализираните от нас данни са получени в резултат от споразумение за сътрудничество с един от трите основни мобилни оператора в България, с пазарен дял от 28,6%. Данните съдържат информация за броя пътувания по часови слотове между 609 „точки на престой“ идентифицирани в района на гр. София (виж Фигура 1).

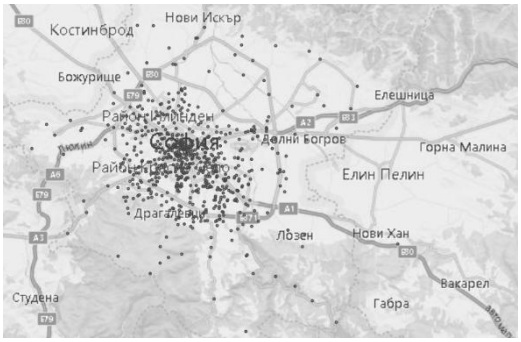

***Фиг. 1** Идентифицирани „точки на престой“ в град София.*

Набора от данни е конструиран по описания от нас алгоритъм и съдържа статистически обобщена информация за транспортните навици на включените в него жителите на гр. София в период от три месеца (януари-март 2023 г.).

4. Получени резултати и дискусия

Конструираните по предложения от нас алгоритъм времеви редове се характеризират с голямо разнообразие. На Фигура 2 е представена информацията за броя пътувания по часови слотове от „точка на престой“ кв. Манастирски ливади“, град София до четири избрани дестинации в град София – кв. Драгалевци, Sofia Ring Mall, Медицинска академия и Горнобански път.

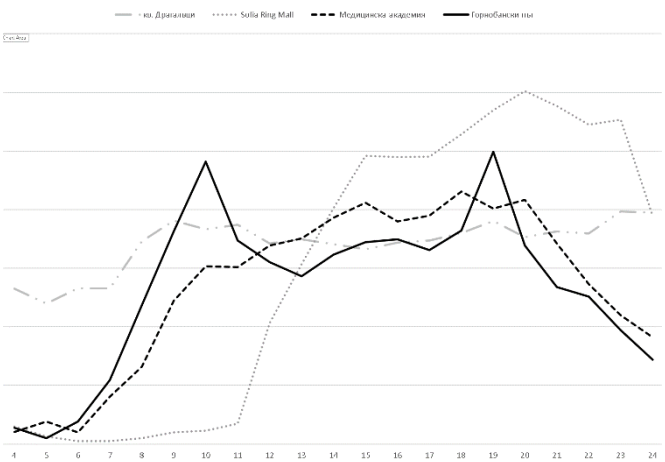

***Фиг. 2** Брой пътувания по часови слотове.*

За да анализираме разпределението на трафика по часови слотове в рамките на работното време на градския транспорт конструираме индикатор T който заема стойност 1, ако в даден часови слот броя на пътуванията от кв. Манастирски ливади“ към съответната дестинация в района на град София е повече от 40% от максималния брой пътувания в който и да е часови слот и стойност 0, във всички останали случай. Така с помощта на индикатора T и класическа K-значна клъстеризация (K-means clustering) бихме могли да класифицираме дестинациите към които пътуват жителите на кв. Манастирски ливади в четири групи, отразяващи динамиката на броя пътуващи граждани в различните части от денонощието. Резултатите от групирането са дадени в Таблица 1 и Таблица 2.

Таблица 1 *Брой дестинации по групи*

Група	Брой дестинации в групата
Група 1	124,000
Група 2	59,000
Група 3	225,000
Група 4	200,000

Таблица 2 *ANOVA*

Часови слот	Cluster		Error		F	Sig.
	Mean Square	df	Mean Square	df		
hs04	0.257	3	0.029	604	8.79	0.000
hs05	0.191	3	0.020	604	9.50	0.000
hs06	0.166	3	0.034	604	4.84	0.002
hs07	0.506	3	0.079	604	6.40	0.000
hs08	6.106	3	0.192	604	31.73	0.000
hs09	25.246	3	0.115	604	219.33	0.000
hs10	27.546	3	0.090	604	305.17	0.000
hs11	27.827	3	0.088	604	314.98	0.000
hs12	27.411	3	0.094	604	290.31	0.000
hs13	27.329	3	0.095	604	288.19	0.000
hs14	24.275	3	0.098	604	247.35	0.000
hs15	26.648	3	0.088	604	302.40	0.000
hs16	25.302	3	0.082	604	308.33	0.000
hs17	27.220	3	0.075	604	361.68	0.000
hs18	17.677	3	0.101	604	175.12	0.000
hs19	15.172	3	0.113	604	134.80	0.000
hs20	21.758	3	0.110	604	197.73	0.000
hs21	22.245	3	0.137	604	161.86	0.000
hs22	24.532	3	0.113	604	216.64	0.000
hs23	24.328	3	0.088	604	275.61	0.000
hs24	14.194	3	0.101	604	141.10	0.000

На Фигура 3 са показани получените средни стойности за индикатора Т във всяка от четирите групи.

Фиг. 3 *Получени средни стойности на индикатора Т по групи*

Най-голям брой дестинации попадат в Група 3 която се характеризира с относително равномерно разпределение на броя пътуващи в часовия интервал между 07:00 часа и 20:00 часа. Втората най-голяма група от дестинации е Група 4, която включва в себе си дестинациите, за които има ясно изразени пикове в трафика, съвпадащи с началото и края на работния ден. Третата по големина Група 1 има много сходни характеристики с тези на Група 3, но в нея се наблюдава запазване на трафика и след 20:00 часа. В най-малката по брой дестинации група попадат дестинации, към които се наблюдава трафик в часовия интервал между 12:00 и 22:00 часа.

Получените резултати за групиране на дестинации могат да бъдат използване за оптимизиране на разписанията на градския транспорт с оглед на обективната нуждата на гражданите от мобилност.

Благодарности

Представянето на резултатите от нашата работа е финансирано по проект 80-10-148/12.05.2023 г.. Дейностите по проекта може да се разглеждат като продължение и популяризация на резултатите от изследванията на Стопански факултет по проект INNOAIR, INDEX: UIA05-202.

Цитирани източници

1] E. Commission, „European Commission website,“ 2023. [Онлайн]. Available: https://digital-strategy.ec.europa.eu/en/news/commission-defines-high-value-datasets-be-made-available-re-use. [Отваряно на 27 4 2023].

2] C. Nikolova, „Deployment of Intelligent Transport Systems for Sustainable Transport Development,“ *Research Papers of UNWE,* том 1, pp. 77-109, 2017.

3] Цветкова, С. Минков, Т. , „Анализ и оценка на вредното въздействие на транспорта върху околната среда в градовете,“ *Икономически и социални алтернативи,* том 3, pp. 48-62, 2017.

4] E. a. M. National Academies of Sciences, „Cell Phone Location Data for Travel Behavior Analysis,“ *National Academies of Sciences, Engineering, and Medicine,* 2018.

5] Kristiāna Dolge, Aiga Barisa, Vladimirs Kirsanovs, Dagnija Blumberga, „The status quo of the EU transport sector: Cross-country indicator-based comparison and policy evaluation,“ *Applied Energy,* том 334, p. 120700, 2023.

6] Marchev, A., Netov, N., Haralampiev, K., Lomev, B., & Spassov, K., „Innovative on-demand public transportation in sofia - an overview of the algorithmic tasks,“ в *10th International Scientific Conference on Computer Science, COMSCI 2022 - Proceedings*, 2022.

7] Netov N., Spassov K., „Intra City Transport On-demand,“ *IFAC-PapersOnLine,* том 55, № 11, pp. 167 - 172, 2022.

8] Marchev A., Jr., Haralampiev K., Lomev B., „Predicting Travel Times for On-demand Public Transport in Sofia,“ *IFAC-PapersOnLine,* том 55, № 11, pp. 161 - 166, 2022.

9] Rizov, R., Netov, N., „Data-Driven Public Transport Routes and Timetables based on Anonymized Telecom Data,“ *Eurasian Studies in Business and Economics,* 2023.

Efficiency of formation and development of intrafirm knowledge in a modern market economy

Zoya Gelmanova, Anastassiya Mezentseva
Karaganda Industrial University, Kazakhstan
zoyakgiu@mail.ru

Abstract. *The set of theoretical and methodological concepts related to the formation, development and knowledge has been studied. Within the framework of the study, approaches are considered that in one form, or another belong to classical theories. The current state and problems of modern organizations in the field of knowledge formation and development are analyzed. Based on the example of Kazakhstani organizations, the main directions are used to improve approaches to knowledge management to improve the quality of labor activity and improve the qualifications of specialists of organizations. The study identified the need to develop a high-quality and flexible in-house training system, which will be relevant in modern conditions. A toolkit has been developed that contributes to the effective formation and development of knowledge of a modern Kazakhstani specialist.*
KEY WORDS: *KNOWLEDGE MANAGEMENT, COMPETENCIES, QUALIFICATIONS, PERSONNEL TRAINING SYSTEMS, COMPETENCY MODELS, ORGANIZATION*

1 Introduction

The Strategic Plan of the Republic of Kazakhstan until 2025 emphasizes the role of human capital as a factor of development in the 21st century: special attention is paid to the role of knowledge and education – training should be aimed not only at knowledge transfer, but also be flexible and systematic, forming in future specialists relevant competencies, ability to respond and adapt to change [1].

2 Methods

The results of this study were obtained by analyzing the data, during the survey of organizations in Kazakhstan. Obtained information was studied and digitized by creating a virtual archive. Respondents were interviewed through a questionnaire survey. A five-point Likert scale was used for responses.

3 Results

There is a growing body of research on the evaluation of existing knowledge management methods, systems and tools, but to date there is no unified system for assessing the results of knowledge creation and management [2].
Approaches to creation and management of learning and competence development systems in organizations can vary significantly depending on the specific area of organizational activity, but there are some common features of staff competence management in organizations of different countries, which can generally be divided into two categories: Eastern (Japanese) and Western (Euro-American) approaches. On the basis of which it is possible to define the directions of these two approaches to the system of capacity building and personnel training as:
- expanding the qualifications of specialists in order to ensure their mobility – the Japanese, horizontal system;
- advanced training of specialists within the framework of a certain professional activity of a specialist – European-American, vertical system.

The system of competence formation in an organization can be divided directly into two main categories – intra-company training of employees (the process of transferring and creating tacit knowledge) and extra-company training – increasing professional level of a specialist outside his/her "working" activity (the process of acquisition of explicit knowledge).Company training is directly connected with the practical part of an expert's activity and allows to better understand his/her position and tasks as an expert in this organization.

One of the main goals of education is to acquire a common set of knowledge, skills and other competencies to achieve the main expression of the subject of study, which in turn is necessary for self-realization and development of society as a whole.
Today there are several priority and actively developing models of education: personalized learning; lifelong learning.
Any changes in today's 21st century education system must be related to free access and the ability to disseminate human ideas and wisdom, and must be consistent with addressing economic, political, and environmental issues. Butles and Stodinger argue that a new model of society must be created in which "collective intelligence" plays an important role in decision-making and human development[3]. When training modern experts, the main task of education is to develop professional competencies and ensure that experts meet professional requirements.
Today, the competences of a modern expert include not only the ability to use "hard", professional skills, but also the so-called "flexible" competences required in forming and developing personal qualities for self-realization and sustainable development of humanity as a whole, which is reflected in the four-level model of competencies (Figure 1) [4]
There are many models of competence formation, but to date there is no universally accepted model that fully reflects all the necessary competences and classifies them. UNESCO also notes the need for a system of quality control of education and the processes associated with it for the formation and continuous improvement of competencies. Each country has its own view on the organizational chart for basic competencies. For example, Singapore considers social, thinking, informational, creative, collaborative, knowledge application, literacy, self-improvement skills, and personal character development as core competencies.
New Zealand has identified several core competencies: use of language skills, self-organization, communication and interpersonal skills, self-organization, and competent use of symbols and symbolic data.
Australia uses a model consisting of ten competencies: mastery, thinking skills, self-improvement, teamwork skills, having social and ethical skills, ability to work and apply information products and communication skills, international understanding, creativity, and quantitative thinking skills.
According to Indonesia, basic competencies can be considered knowledge, intelligence, personality traits, self-education and self-regulation skills.
Harvard Center for Curriculum Redesign (HCR), led by C. Feidl with the support of the OECD, has created a unique model of integrated educational organization, which can identify relevant competencies for the 21st century [5]. The main idea of this model is to create a new space that promotes self-learning and individual decisions about one's future. This model allows to define goals and provides a general framework for redesigning existing educational models, characterized by an increased capacity for transformation,

based on information about the relevance of specific types of knowledge

Type of knowledge and skills	Examples of knowledge and skills	Duration
Contextual	Highly professional competencies that include special physical or social skills.	From a few months to several years
Cross-contextual	Highly professional competencies that include special physical or social skills. Competencies that can be applied in a larger number of areas of socio-economic and individual activity.	
Meta	Methods of operating objects in physical and objective realities. Meta- cognitive competencies include cognitive, logical, emotional and physical, as well as other types of mental abilities.	From several years to decades
Existential	Fundamental competencies that determine the essence of a person's behavior in life, his perception of situations and his character, including competencies that determine willpower, health, emotional self--regulation, abilities for self-knowledge and self-analysis, self--development skills, etc.	From decades to a lifetime

Fig. 1. *Life cycle of types of knowledge and skills [4].*

The model of CPUC reflects the interaction of four facets-dimensions among themselves within the four-dimensional model of education: in addition to traditional skills, knowledge, character a new facet appears – meta-cognition, which is an internal process of comprehension and independent adaptation of an individual's learning. The necessity of singling out meta-cognition as a separate facet is conditioned by its ability to improve the processes of using competences in the spheres beyond the conventional context.

According to D. Hacker and J. Dunlosky, metacognitive processes can be divided into 3 levels of verbalization: transformation of knowledge, transformation of nonverbal knowledge, and transformation of knowledge interpretation. Metacognition develops in the context of the student's current task and can improve the acquisition of knowledge, skills and abilities, regardless of their initial level [6].

The problem of lack of highly qualified personnel with the skills to use the latest technical and social advances constantly arises before the heads of enterprises.

According to the data obtained by Kazakhstani organizations, the distribution of employees of organizations by level of education revealed the difference between holders of a bachelor's degree (total percentage – 65.85%) and holders of secondary general education (30.49%).

The majority of employees have been with the organization for a range of 2 to 7 years. The respondents' average length of employment was 5.98 years, indicating relative stability in employee turnover among administrative and management personnel.

Despite the relative stability among the working staff, the majority of respondents indicated a desire to change jobs or dissatisfaction with the position they held. Factors such as lack of incentives in the form of career advancement or salary increases were cited as reasons. According to a survey of 264 administrative and managerial personnel in 10 organizations, operating in various fields (from industry to commerce), the majority of respondents (53,05%) are not satisfied with the additional, specialized training and professional development.

The data obtained during the survey indicate that the majority of respondents are familiar with such concepts as "knowledge", "qualification", "competence", "personnel management" (about 84.14% of respondents).

According to the survey, about 30.18% of managers are dissatisfied with the qualifications of employees in relation to their positions, 26.34% refrain from commenting, 43.48% to varying degrees are satisfied with the work of their employees.

About 75% of respondents agreed with the statement that various educational activities have a positive impact on the effectiveness of the organization.

According to numerous studies, the obsolescence of knowledge on average is about 20%, with a recommended period of acquisition of new knowledge in the industrial sector (in particular, metallurgy) every 3-4 years, and in business the period is reduced to 2-3 years.

Despite the recognition of training as a factor directly affecting the efficiency and success of the company, most organizations do not invest in the education of specialists. The main reason is that the costs are unprofitable from the economic point of view (according to the top management).

As mentioned earlier, competences are an important element of human resource management. According to M. Hitt and R. Haskisson, competences are a set of resources and capabilities of an enterprise. At the same time, the so-called key competences become a valuable source of competitive and strategic advantages [7].

Competencies can be divided into corporate competencies, which are reflected in the structure and processes of an organization and do not depend on an individual employee, and individual competencies, which belong to the employee himself and reflect the level of knowledge, skills, experience, to perform professional activities effectively.

In the strategic management literature competences are divided into core and unique competences. Core competencies are the organized internal capabilities that underlie a firm's strategy, competitiveness and profitability, while unique competencies are those that enhance an organization's competitiveness [8].

Due to the lack of a clearly articulated system for evaluating the competence of PMS specialists in organizations, we analyzed the requirements for hiring in relation to PMS.

Due to the fact that the representatives of this sphere of activity are the representatives of "mental labor" according to the results of the survey of managers and personnel the following competencies required for a specialist were identified: professional skills, strategic and critical thinking, communication, ICT-skills, result orientation, management skills.

Of course, each profession has its own peculiarities, however, in a general review of the competencies of PMS specialists, all respondent organizations came to this set of competencies.

Since the object of the study is directly administrative and managerial staff, due to the differences in the activities of organizations (from industrial to trade organizations) a general model of competencies, considering managerial, specific and basic competences of economic specialties professionals, was created (Table 1).

Table 1. *Model of key competencies of employees of administrative and managerial personnel of organizations.*

Competencies	Characteristic
1	2
Result orientation	Ability to effectively implement assigned tasks. Availability of skills that ensure the quality of work.
Customer focus	The ability to identify, analyze and provide the customer with the necessary product / service, while focusing both on the interests of the organization and on the needs of the customer. [2]
Strategic and critical thinking	The ability to holistically see the situation, analyze factors, both external and internal, that affect the success and effectiveness of an organization, department or individual, both in the medium and long term, as well as the ability to analyze the data obtained (in particular, information), on their basis, form your own vision, which serves as a guide to further actions and decision-making.
Communication and sociability	Ability to establish effective working relationships, as well as interact in other social, cultural and other contexts
ICT – literacy	Basic knowledge of digital technologies and their products (including knowledge and ability to use a personal computer and its main, as well as specialized programs)
Management skills	Ability to evaluate, plan and make decisions, taking into account all possible factors that can affect the processes in the course of the organization's activities. When holding a managerial position – also be able to analyze and regulate the activities of subordinates for their effective work.
Professional skills	Availability of knowledge, abilities, skills directly related to the performance of official duties [9].

In accordance with this model of competences, a survey was conducted among the employees of the AUP of organizations engaged in the improvement of personnel qualification and competence. Due to the difference in the required competences it was decided to separate the results of the representatives of these two specialties. To evaluate the competences the following gradation was adopted – a 4-point system – basic, average, advanced, professional. The survey took into account the opinions of managers, the employees themselves, their immediate supervisors, and colleagues. The results are presented in Figure 2;3

The analysis of the provided results showed that, on average, all indicators are within the advanced, level 3. At the same time, the data shows that several indicators of competence of employees of the organization coincide with the necessary ones. Among employees in the accounting department, these are competencies related to customer focus, communication, and management skills.
Among managers – indicators of professional skills and ICT competencies coincide with the required level. Deviations were revealed – for the indicator "customer orientation", as well as critical and strategic thinking.
The greatest deviation from the required skills was shown by ICT literacy – in all organizations. The main reasons were such factors as lack of awareness and lack of opportunities for professional development, the employees themselves either do not have the motivation or the financial capacity. Nowadays it is the development of this type of competence that should be paid special attention.

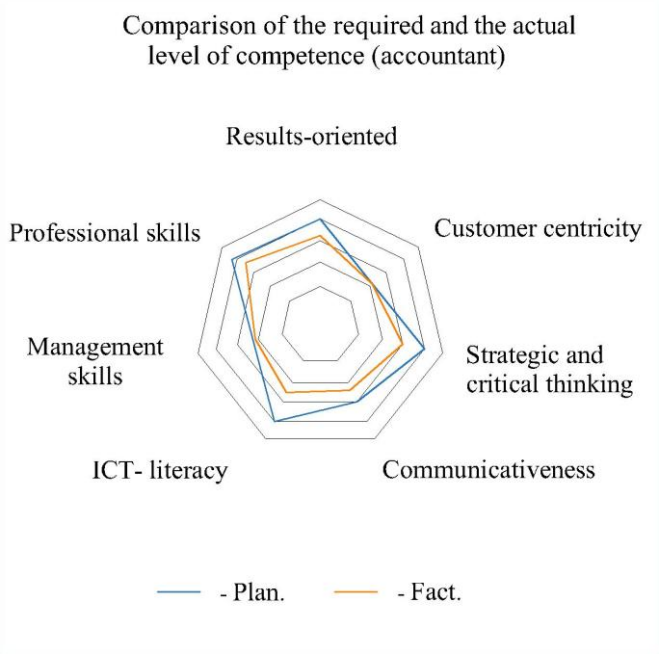

Fig. 2. *Comparative characteristics of the required and actual level of competence of specialists in the administrative and managerial personnel of the organization (accountant)*

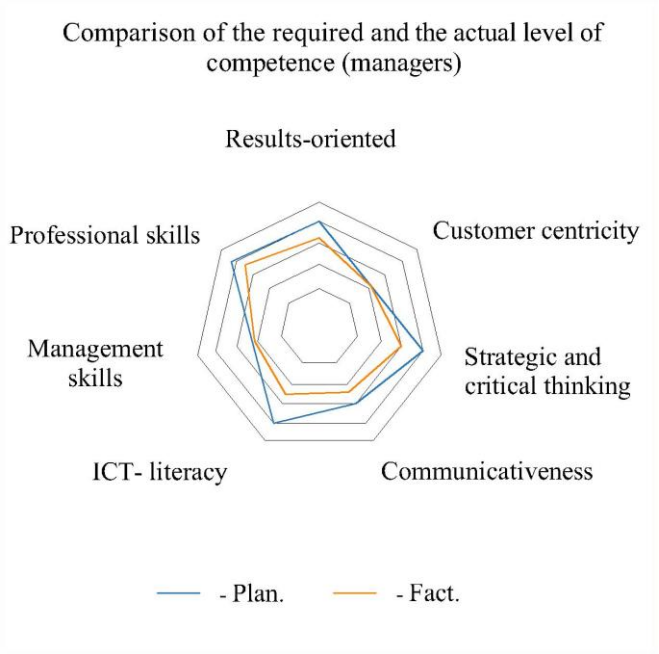

Fig. 3. *Comparative characteristics of the required and actual level of competence of specialists in the administrative and managerial personnel of the organization(managers)*

4 Discussion

A large-scale study of American companies showed that a 10% increase in spending on personnel training led to an 8.5% increase in productivity, while the same increase in capital investment led to productivity growth of only 3.8%. However, in-house professional training of personnel provides an increase in revenue along with an increase in productivity. Studies have shown that extending staff training by one year can increase GDP by another 3%. Training systems in countries such as Japan, USA, France and Korea are considered to be the most developed in-house training systems.
The adoption of the described approach by educational institutions and organizations in the development of training programs for

specialists at all levels of education will ensure that competencies meet modern requirements of employers and the labor market, will contribute to the formation of personnel with modern interdisciplinary competencies, which in turn will help to reduce the deficit.

5 Conclusion

Knowledge is becoming the center of transformation of Kazakhstan's economy and is the most important source of welfare and the key to maintaining the competitiveness of socio-economic
Knowledge becomes the center of transformation of the economy of Kazakhstan and is the most important source of welfare and the key to maintaining the competitiveness of the socio-economic development of the individual, organization and country [9].
Given the data obtained in the analysis, organizations need to develop a clear intra-company training system, which will be relevant in today's environment.
The system of intra-company training in the company should take into account everything – from increasing professionalism, experience and skills to the formation of personal qualities. The means of staff professional development can be image training in higher educational institutions, attendance of professional courses, acquisition of additional specialties, retraining courses, participation in seminars and self-education.
Lack of clearly defined model of competence prevents managers from objective assessment of specialists' competence, which is especially reflected in the system of remuneration and bonus payment. This, in turn, reduces the efficiency and effectiveness of their work and directly affects the atmosphere in the team and the activity of the organization as a whole.
Most organizations note the lack of some competences of their employees – both professional and general, but do not themselves contribute to their development and training.
For effective human resource management, the organization must also consider specific elements of knowledge management, including attention to the training and learning process of its employees, which means: creating and using an organizational culture that pays equal attention to the training and evaluation of its employees; cooperating with various educational institutions to train their professionals in the educational process with respect to the development of professional skills and professional careers. Organizations should pay attention to the training process of their professional employees, particularly the training programs and their cost, because it not only contributes to their professional development, but also helps to maintain and improve the motivation of professional employees and maintain their emotional, physical, mental, and cognitive well-being.

References

1.Resolution of the Government of the Republic of Kazakhstan Strategic Development Plan of the Republic of Kazakhstan until 2025, (2017).
2.Gelmanova Z.S. Assessment of key competences of metallurgical production workers// International Journal of Applied and Fundamental Research. – 2014. – №9 – 2. – P.101-105
3. Baltes P.B., Staudinger U.M.//AP, №55 – 1. – P. 22-36 (2000)
4.Luksha P., Afanasiev D. The future of education: a global agenda. (2014)
5.Feidle C. Four-dimensional education,240(2018).
6.Hacker D., Dunlosky J. New Directions for Teaching and Learning, P.73-79 (2003)
7. M.A. Hitt, R.D. Ireland, R.E. Hoskisson. Strategic Management: Concepts: Competitiveness and Globalization, 480p. (2016).
8.Mikkelsen, J.O. Riis. Project Management: A Multi-Perspective Leadership Framework, 848p. (2017).
9.Gelmanova Z.S. Organization of vocational training in production // International Journal of Experimental Education. – 2016. – No.8. – P.17-21

Increasing the resilience of critical entities in response to the dynamic spectrum of threats

Valeri Panevski[1*], Lyudmil Nedelchev[2]
Institute of Metal Science Equipment and Technologies with Hydro- and Aerodynamics Centre "Acad. A Balevski" at the Bulgarian Academy of Sciences, 67 Shipchenski Prohod Street, 1574 Sofia, Bulgaria[1]
panevski@ims.bas.bg
Institute for Nuclear Research and Nuclear Energy, Bulgarian Academy of Sciences[2]
lnnedelchev@npp.bg

Abstract: *Achieving a comprehensive approach to the issue of resilience of entities that are critical to the proper functioning of the national economy requires the creation of a comprehensive framework addressing the resilience of critical entities to all hazards, whether natural or anthropogenic, accidental or intentional. For this purpose, good practice implies the use of European and international standards and technical specifications that are relevant for both security measures and resilience measures applicable to critical infrastructure.*

Precisely, the presentation of updated information on a possible approach that requires innovation in the field of security and protection of critical infrastructure is the content of this publication.

Key words: *CRITICAL INFRASTRUCTURES, PREPAREDNESS*

1. Introduction

The most significant challenges to the functioning of vital critical infrastructure (CI) systems are natural and human-caused risk impacts, which cause an increased number of events with greater intensity, scale and impacts, leading to loss of life and a greater volume of damage. The implications for existing CI vulnerabilities are greatly exacerbated. With the predicted consequences of the changing security environment, the pressure on the readiness of CI systems will be higher, leading to loss and destruction, damage and disruption, and service interruptions.

Therefore, the change in the security environment is included as a risk to the resilience of CIs, although its impact cannot be precisely predicted, but its potential to significantly affect the resilience of states, societies and communities is identified as a common security threat. For example, in European countries, the changing security environment poses escalating risks to CI stability and security, with potentially far-reaching consequences.

Achieving a comprehensive approach to the issue of resilience of CIs, which are critical to the proper functioning of the national economy, requires a comprehensive framework creation addressing the resilience of CIs to all hazards, whether natural or anthropogenic, accidental or intentional. To this end, good practice implies the use of European and international standards and technical specifications relevant to both security and resilience measures applicable to CIs.

In this regard, leading scientists from the Institute of Metallurgical Engineering and Technologies with the Center for Hydro- and Aerodynamics "Acad. A. Balevski" at the BAS, apply modern standardized approaches to determine the goals and requirements for the development of physical protection systems, tailored to the specifics of the CI and aimed at preventing any level of potential threats both to the CI and to the population in adjacent urbanized areas **[1, 2, 3, 4, 5]**.

That's why, the presentation of updated information on a possible approach requiring innovation in the field of security and CI protection through the application of modern standards is the content of this publication. Possible interruptions, due to technical reasons and carrying out ongoing maintenance activities, are not taken into account, as they are included in the design and technological documentation of the CI systems.

2. Standardization

The basic purpose of standardization is the definition of voluntary technical or quality specifications to which current or future products, production processes or services can conform. Standardization can cover various aspects, such as standardization of different classes or sizes of a product or technical specifications in the area of product or service markets where technical and interoperability with other products or systems is essential for the security and protection of CI.

Standards can contribute to supporting national policy to address significant societal challenges such as climate change, sustainable resource use, innovation, security and resilience, risk management, consumer protection and health and safety in the workplace. Targeting the development of commodity and technology standards (national, European and international) towards expanding markets could create a competitive advantage for manufacturers of CI security and protection products and systems and facilitate trade.

Also, standards are important tools for the competitiveness of enterprises and especially for small and medium-sized enterprises (SMEs), whose participation in the standardization process is important for national and European technological progress. It is therefore necessary for the standardization framework to encourage SMEs to actively participate and include their innovative technological solutions in the field of CI security in standardization efforts. This includes improving their participation at the national level, where they can be more effective due to lower costs and the absence of language barriers.

Last but not least, standards can have a wide-ranging impact on society, and in particular on the safety and well-being of citizens, network efficiency, environmental protection, accessibility and other areas of public policy. It is therefore necessary to ensure the strengthening of the role and contribution of interested organizations in the development of standards through increased support for developers and manufacturers of CI security products and system.

2.1 Definitions

According to the definitions in Article 2, point 1 and point 4 of Regulation (EU) No. 1025/2012 of the European Parliament and of the Council **[6]**:

➢ ‘standard’ means a technical specification, adopted by a recognised standardisation body, for repeated or continuous application, with which compliance is not compulsory, and which is one of the following: **[6]**

– ‘international standard’ means a standard adopted by an international standardisation body;

– ‘European standard’ means a standard adopted by a European standardisation organisation;

– ‘harmonised standard’ means a European standard adopted on the basis of a request made by the Commission for the application of Union harmonisation legislation;

– ‘national standard’ means a standard adopted by a national standardisation body.

➢ ‘technical specification’ means a document that prescribes technical requirements to be fulfilled by a product, process, service or system and which lays down one or more of the following: **[6]**

(a) the characteristics required of a product including levels of quality, performance, interoperability, environmental protection, health, safety or dimensions, and including the requirements applicable to the product as regards the name under which the product is sold, terminology, symbols, testing and test methods, packaging, marking or labelling and conformity assessment procedures;

(b) production methods and processes used in respect of agricultural products as defined in Article 38(1) TFEU, products intended for human and animal consumption, and medicinal products, as well as production methods and processes relating to other products, where these have an effect on their characteristics;EN 14.11.2012 Official Journal of the European Union L 316/19

(c) the characteristics required of a service including levels of quality, performance, interoperability, environmental protection, health or safety, and including the requirements applicable to the provider as regards the information to be made available to the recipient, as specified in Article 22(1) to (3) of Directive 2006/123/EC;

(d) the methods and the criteria for assessing the performance of construction products, as defined in point 1 of Article 2 of Regulation (EU) No 305/2011 of the European Parliament and of the Council of 9 March 2011 laying down harmonised conditions for the marketing of construction products (1), in relation to their essential characteristics.

2.2 Some basic standards of the International Organization for Standardization and the Bulgarian Institute for Standardization in support of CI security and resilience

The main international standardization structure developing standards in the field of CI security policy is the technical committee of the International Organization for Standardization (ISO) - ISO/TC 292 “Security and resilience”. At the moment, within the scope of his activity and responsibility are 67 standards and projects of standards.

The key security and resilience standards of CI are as follows:

➢ ISO 22300:2021- Security and resilience — Vocabulary;

➢ ISO 22301:2019 - Security and resilience — Business continuity management systems — Requirements;

➢ ISO 22313:2020 Security and resilience — Business continuity management systems — Guidance on the use of ISO 22301;

➢ ISO 22316:2017 - Security and resilience — Organizational resilience — Principles and attributes;

➢ ISO/TS 22317:2021 Security and resilience — Business continuity management systems — Guidelines for business impact analysis;

➢ ISO 22326:2018 Security and resilience — Emergency management — Guidelines for monitoring facilities with identified hazards.

The Bulgarian Institute for Standardization has introduced the following standards for national implementation:

➢ BDS EN ISO 22300:2021 Security and resilience. Vocabulary (ISO 22300:2021);

➢ BDS EN ISO 22301:2020 Security and resilience. Business continuity management systems. Requirements (ISO 22301:2019);

➢ BDS EN ISO 22313:2020 Security and resilience - Business continuity management systems - Guidance on the use of ISO 22301 (ISO 22313:2020);

➢ BDS ISO 22316:2021 Security and resilience — Organizational resilience — Principles and attributes (ISO 22316:2017);

➢ BDS ISO 22326:2020 Security and resilience — Emergency management — Guidelines for monitoring facilities with identified hazards (ISO 22326:2018).

It is also important to highlight the direct link between ISO/TC 292 Security and resilience and ISO/TC 262 “Risk management”, implemented by coordinating the development and reference of the following:

➢ ISO 31000:2018; Risk management — Guidelines

➢ IEC 31010:2019; Risk management — Risk assessment techniques

The Bulgarian Institute for Standardization has introduced the following standards for national implementation:

➢ BDS ISO 31000:2018 Risk management — Guidelines;

➢ BDS EN IEC 31010:2019 Risk management-Risk assessment techniques (IEC 31010:2019).

3. Spectrum of threats

The contemporary security environment (natural and man-made risks), characterized by an expanded range of threats (Figure 1) with greater intensity, scale and impacts, causes an increased volume of human and material losses. Hydrometeorological hazards dominate the profile of the security environment. In addition, a number of technical and technological disasters threaten the sustainability of the various national CIs and their elements.

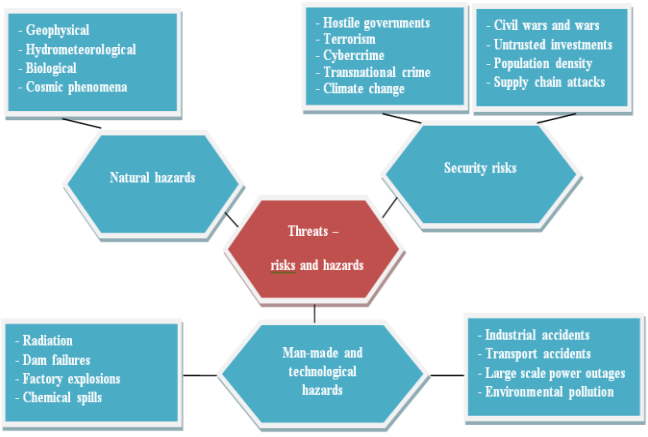

Figure 1: *Threats to critical infrastructure - risks and hazards*

Furthermore, an anthropogenic threat to CI resilience is emerging, arising from mismanagement, improper operation, negligence, organizational failures, and poor maintenance or insufficient investment in rehabilitation and modernization of aging CIs and assets.

We face an uncertain future with more and more pandemics, cyberattacks and high-impact events making up the "Future Risk Menu" **[7]**. Climate change is expected to cause local changes in average and extreme temperatures, as well as changes in rainfall patterns, disrupting roads, railways and airports nationally and internationally.

Potential cybersecurity threats, pandemics, biohazards, and other events, mostly of high consequence and low probability, are likely to affect CI resilience globally. Among these, one threat clearly stands out, located between current and future areas of risk and heavily exploiting existing vulnerabilities, with its impacts being felt across sectors. These are the cyberattacks against CI systems that are increasing in frequency, the number of targeted sectors with a lot of data being stolen or misused, and potentially outpacing the functioning and development of the entire infrastructure system.

Finally, the crisis of the COVID-19 pandemic has affected European countries in an unprecedented way. Furthermore, it is important to emphasize that the existence of pandemic-induced disruptions related to the basic and day-to-day functioning of CIs has resulted in the inability to provide services or the absence of beneficiaries for some services, due to daily mass blockades.

4. Some approaches to enhancing CI readiness through resilience building

Our country, as a member of the European Union, actively participates in the work on updating the policy to achieve a higher general level of resilience and protection of CIs, especially taking into account the changed dynamics of threats that can have an impact on CIs from several member states simultaneously.

4.1. Policy and regulatory frameworks

Resilience policy and legislative frameworks are a prerequisite for integrating CI resilience into disaster risk management and vice versa. This principle means that the member states of the European Union must have a unified approach for creating these frameworks, in order to start the process of integrating CI sustainability building across sectors in accordance with their national contexts and priorities. At present, CI legislation or its integration into other laws is insufficient for various reasons, i.e. lack of clearly defined CI policy concepts, weak integration into strategic documents and a primary focus on the *protection of assets and facilities*. It is therefore essential to rethink the approach, *shifting from CI protection to building overall resilience*.

This will lead to a set of actions enabling the following measures:

- review of existing and adoption of new strategic and policy documents or their adoption;
- amendment of existing legislation or the adoption of new CI laws and regulations;
- ensuring the integration of comprehensive CI sustainability principles into legislation relating to other sectors;
- designing and adopting new standards for building resilience and ensuring their implementation across all relevant sectors throughout the CI lifecycle.

A good example of up-to-date policies and regulatory frameworks of the European Union are the documents, namely:

- DIRECTIVE (EU) 2022/2557 OF THE EUROPEAN PARLIAMENT AND OF THE COUNCIL, of 14 December 2022, on the resilience of critical entities and repealing Council Directive 2008/114/EC;
- DIRECTIVE (EU) 2022/2555 OF THE EUROPEAN PARLIAMENT AND OF THE COUNCIL, of 14 December 2022, on measures for a high common level of cybersecurity across the Union, amending Regulation (EU) No 910/2014 and Directive (EU) 2018/1972, and repealing Directive (EU) 2016 /1148 (NIS 2 Directive).

4.2. Governance and institutional framework

The overall governance and institutional framework are crucial to building CI sustainability both in our country and in the European Union. Across the region, diversity is found in approaches to risk reduction and CI management in a situation where there are no dedicated entities to protect CI. This is mainly due to the existing reactive approach that focuses on protection without considering the sustainability of CI as a whole and the complexity and interdependence of the sectors. A good approach requires that management be seen as an extended area of interaction and responsibilities between emergency management and civil protection services.

Following a whole-of-government and whole-of-society approach to resilience building, the prevailing view of viewing the security of each CI as an isolated process must be overcome and ensure that institution-building takes place within the framework of partnerships established between governments and the private sector. This ensures that all key stakeholders are on board this venture of building resilience.

In particular, it is essential to appoint coordination units, systematize roles, responsibilities and design, and implement adequate measures and actions to build resilience. In this regard, national disaster risk reduction platforms, such as multi-institutional and multi-sectoral mechanisms to advance disaster risk management and build resilience of societies and communities, can significantly contribute through a range of supporting activities and services.

In addition, building cross-border resilience should be included in the promotion of regional or sub-regional partnerships, cooperation and coordination of CIs. Therefore, the building of CI resilience should be provided as a complete, integrated package, thereby ensuring the sustainable development of EU member states.

4.3. Coverage of all CI systems

Building resilience is the responsibility of both CI owners and operators as well as other important actors at national and local levels. The traditional CI security approach only addresses physical parameters such as assets and facilities, operation/maintenance, without considering the full range of functions and services provided, including resources, limited cooperation and coordination, or fragmented resilience. In most countries, apart from public authorities, actors from traditional CI sectors are most active in mitigation and protection activities (eg energy, water, food, transport, telecommunications, health care and banking and finance). Modern disaster risk management is guided by the principle that disaster risk reduction is not the exclusive competence of a national organization, such as a government, but the responsibility of all stakeholders, including society as a whole.

In this way, building resilience is the result of their interactions and the underlying risk management will be achieved by integrating all critical sectors, by involving all relevant key stakeholders and by providing CI-related services. Different key stakeholders have different roles and responsibilities during the phases of the CI resilience building cycle.

4.4. Availability of resources

For the functioning and viability of CIs, adequate resources must be planned and established that are imperative to support their needs before, during and after disasters. The term "resources" must be understood in its complexity, uniting various aspects, ranging from financial resources, through material and technical means, to human and professional. During the COVID-19 pandemic, the importance of human resources for CIs has proven to be significant and vital to their operations and the services they provide. This principle of building CI resilience should be considered in conjunction with private sector involvement, both in the roles of system owners and operators, or the expertise of external actors.

Here's why, CI investments should be proactive and anticipatory, enabling building resilience and transforming CIs into responsive systems rather than reactive structures. After disasters, funding must be provided for efforts to sustainably rebuild affected infrastructure. These investments should be scaled up by both the public and private sectors after assessing critical needs and priorities. Capacity building is one of the key pillars for having a sustainable CI.

The capacity of all stakeholders in CI sectors, along with disaster risk management systems, must be developed to address all risks, hazards and threats, as well as complex disasters that have low probability and high impact . A complex task must be carried out continuously, addressing different roles and responsibilities of actors in the CI security and resilience process – from sensitizing resilience building among policy-makers and decision-makers to providing professional training and specialized training professionals and emergency responders by disseminating knowledge to other key stakeholders and increasing general public awareness.

Consequently, the capacity building portfolio should be based on the life cycle of all potential hazards, an inclusive and systematically organized approach. This capacity building process should be systemic, involving all relevant stakeholders and placed at the heart of CI resilience building.

4.5. Technology and innovation

Technologies and innovations are among the main features of the modern approach to building CI sustainability. Although they are often used to reduce risk, they are not yet fully incorporated into practices, given the financial costs and the need for specialized resources and knowledge. Therefore, their application should be the starting point for designing sustainable policies, norms, codes and standards while using new and emerging technologies and smart solutions.

In addition, CI resilience building should include measuring/determining the reliability of future infrastructure systems, addressing anticipatory resilience as a future-oriented knowledge system that addresses new extreme risk events, such as changing climate conditions and emerging risks for security. Accordingly, CI design must be more innovative, intuitive and secure, ensuring sustainability beyond existing frameworks. In this regard, partnerships should be established to advance the research and development agenda with relevant partners, such as academia and the private sector. In addition, innovative solutions are sometimes linked to the implementation of effective solutions, such as nature-based solutions, which are approaches that weave natural features or processes into the CI built environment to promote adaptation and resilience.

5. Conclusion

As complex, interconnected and interdependent systems and networks, CIs provide vital support for daily life and activities, providing services and making a crucial contribution to the sustainable development of society in the face of current and emerging future risks and threats. To achieve resilience, the paradigm needs to shift from risk to resilience, adopt and implement a standardized approach for all hazards, for all society and for the life cycle of CIs, and ensure policies that are future-oriented. Thus, CI resilience can be understood as the ability to anticipate, withstand or absorb shocks and stresses while CI adapts to new conditions, which would lead to rapid recovery and transformation to better cope with stresses and shocks in the future.

ACKNOWLEDGMENTS

This paper is the result of the implementation of tasks in the field of intelligent and mechatronic security systems from the Plan of the Research Plan of IMSETHC-BAS for the period 2023-2025.

References:

[1] Dimitrov, D., "Possible approaches to ensure security of information for nuclear facilities", International Scientific Journal "Security & Future", 6, 2, STUME, 2022, ISSN:2535-0668 (print); 2535-082X (online), pp. 68÷71;

[2] Dimitrov, D., "Engineering solutions to ensure protection of nuclear power plants against sabotage", International Scientific Journal "Security&Future", 6, 1, STUME, 2022, ISSN:(PRINT) 2535-0668, (ONLINE) 2535-082X, pp. 18÷21;

[3] Dimitrov D., „Examples of nuclear security measures for nuclear facilities", Technics. Technologies. Education. Safety. 2021, Military sciences and national securityy, Proceedings 3, 3(13), Scientific Technical Union of Mechanical Engineering "Industry - 4.0", 2021, ISSN:ISSN 2535-0315 (Print), 2535-0323 (Online), pp. 212÷215;

[4] Dimitrov D., „Basic regulations and associated administrative measures providing nuclear security", Proceedings of the Annual University Scientific Conference, 5, Publishing House of Vasil Levski National University, 2021, ISSN:ISSN 2367-7481, pp. 73÷80;

[5] Kolarov A.P., "TRENDS IN THE DEVELOPMENT OF MARINE MINE PROTECTION SYSTEMS", VI INTERNATIONAL SCIENTIFIC CONFERENCE CONFSEC, 05-08. DECEMBER 2022 BOROVBETS, BULGARIA, YEAR 6, ISSUE 1 (8), Scientific technical union of mechanical engineering "Industry - 4.0", 2022, ISSN:ISSN PRINT 2603-2945, ISSN ONLINE 2603-2953, pp. 78-81;

[6] REGULATION (EU) No 1025/2012 OF THE EUROPEAN PARLIAMENT AND OF THE COUNCIL of 25 October 2012 on European standardisation, amending Council Directives 89/686/EEC and 93/15/EEC and Directives 94/9/EC, 94/25/EC, 95/16/EC, 97/23/EC, 98/34/EC, 2004/22/EC, 2007/23/EC, 2009/23/EC and 2009/105/EC of the European Parliament and of the Council and repealing Council Decision 87/95/EEC and Decision No 1673/2006/EC of the European Parliament and of the Council;

[7] UNDP 2022, United Nations Development Programme (UNDP), "Guidance notes on building critical infrastructure resilience in Europe and Central Asia", One United Nations Plaza New York, NY, 10017, USA,

https://www.undp.org/eurasia/publications/guidance-notes-building-critical-infrastructure-resilience-europe-and-central-asia.

Choice of cancer treatment as a creative problem

Roman Goot, Vladimir Goot
gootrom@gmail.com

Abstract: *The choice of a treatment method, like any other innovative process, is a two-stage process: generation and formation of an idea and its realization – implementation. Unlike most works on innovation topics, the focus here is on the first stage of the innovation process, when the methodology for the choice is only for creation, making problems, containing contradictions, arise.*

1. Introduction

1.1 Innovation as a two-stage process.

The concepts creation and innovation were separated for a rather long time. It was considered, that creation is only generation and formation of new ideas, while innovation is their realization. In works on innovation, the ideas were usually described to the extent necessary for understanding, and the main attention was paid to the realization of ideas. As for creation, usually some vague general ideas were brought without any real relation to the subject matter. However, by now the quite general opinion has become that innovation activity is inseparable from creativity, since it provides the generation of new ideas, without which innovation is impossible. Thus, the innovative process turns out to be a single process consisting of two-stages. At the first stage the new idea is generated and designed; at the second stage includes its implementation. In this article, in contrast to the generally accepted, we focus precisely on the first stage, the creative part of the innovation process.

1.2. A Creative problem

In the works [1],[2] the definition of a creative problem was given, as a problem containing a contradiction in its conditions, so that the problem appears as unsolvable. However, as it was shown, such a problem could be resolved by introduction of an additional factor allowing to resolve this contradiction.

2. Cancer treatment choice

2.1 First stage. Creative problem

Since we are dealing with a creative problem, first, the goal should be defined, the conditions should be formed and the contradictions, that prevent us from achieving the goal, should be identified. However, the significance of the choice becomes known only at the end of the patient's life, but the choice of the methods of treatment must be made at the beginning of the treatment.

2.1.1. First contradiction

At present times, clinical practice is greatly drawn to standardization since in this way it is far easier to ensure the quality and reliability of therapeutic measures. On the other hand, the natural desire to increase effectiveness and reliability of the therapy stimulates the desire to use an individual approach that potentially possesses higher effectiveness.

Thus, the first contradiction is revealed: it is necessary to prosue both: standardization and individualization.

Overcoming the contradiction

In order to find the necessary factor, the technique separation is used [2]: several *standard* methods of treatment are developed and an *individual* choice is made of the best method for a given case.

Let $X=(x_n)_{n=1}^{N}$ be a vector that constitutes individual characteristics of the patient, and $Y=(y_m)_{m=1}^{M}$ be set of the treatment methods. To make the choice, you must first clarify how the term "best" should be interpreted in this case.

It is s quite obvious that in our case the best method will be the one that provides the most effective treatment. For an oncological disease the natural indicator for effectiveness of the treatment is survival time (1), which depends on the selected treatment method y_m and the individual vector *X*.

(1) $T_m(X)=T(y_m,X),$

The indicator *T* stands for the length of time the patient lives after the completion of the treatment. Also, it is assumed, the history of the application for each method and each treated patient (2), stored in the database of the treatment centre and accessible for use.

(2) $H_m(X)=\{Y,X,T_m\},\ m=1,\ldots,M,$

The problem of cancer treatment choice is discussed in detail in [3],[4]. Here we present only the method of solution and the results.

2.1.2. Second contradiction

As it was stated above, the effectiveness of the treatment is represented by the indicator *T*. However its' value naturally could become known only at the end patient's life, but the decision over the treatment method should be made at the beginning of treatment process. Thus, a serious contradiction arises: it is necessary to make a decision and it is impossible to make it. This contradiction is resolved by using, as a required additional factor, data from the database, representing the experience of the already existing treatment.

2.1.3. *Overcoming the contradiction - Choice of a treatment method*

Briefly, the choice procedure is as follows.

Survival time *T* is considered as a random value characterized by a conditional survival function.

(3) $S_m(t\mid X)=\Pr(T>t\mid X,y_m)=\Pr(T_m>t\mid X),\quad m=1,\ldots,M.$

Thus, the best choice comes down to the comparison of the conditional survival functions (3). To perform this, it is necessary to have a formular representation of the conditional survival function. A group of regression models is used, this group widely used in the analysis of survivality and reliability. One of the simplest models from this group is the Cox model [5].

(4) $S(t\mid X)=\exp\left[-\exp(Z,X)\int_0^t\lambda_0(\tau)\,d\tau\right],$

This model could be found in (4), where $Z=(z_1,..,z_M)$ is the vector of regression coefficients, (Z,X) is the scalar product of vectors *Z* and *X*, and λ_0 is a so-called base function of failure rate. The values *Z* and λ_0 are parameters of function (4). The determination of *Z* and λ_0 values is performed using the of data from $H_m(X)$, $\varphi(t)\equiv 1$, by the methods of statistical estimation. This represents the usage of the the past experience mentioned above. The survivals comparison is described in detail in [6].

That term presume two types of problems, not coinciding in the general case. The first type is qualitative comparison by the "best-

worst" principle and is realized by the introduction of an order relation in the set of survival functions (3). The second type requires a quantitative characterization of the difference between these functions and is solved by metrization of these sets [5]. At the same time it would be useful to have a characteristic that would make the solution of both types of these problems possible.
Such an object was introduced in [6] and called "directed semimetrics". The details could be seen in [2]. In (5) could found a typical example
of a linear directed semimetrics, where $\varphi(t)$ is a bounded nonnegative function.

(5) $$\rho(S_1, S_2) = \int_0^\infty \varphi(t)[S_1(t) - S_2(t)]\, dt$$

If $\varphi(t) \equiv 1$, that (6) is the the difference in mean time lengths of patient lives after treatment.

(6) $$\rho(S_1, S_2) = \overline{T}_1 - \overline{T}_2$$

Now we can formulate the decision rule for choice of the treatment method.

Method y_m is the best for patient *X*, if (7).

(7) $\rho(S_m(X), S_k(X)) > 0,$
$\forall k = m,\ldots M,\ k \neq m$

2.2 Second stage. The innovation proces.

2.2.1 Testing the decision rule

Now when the decision rule is constructed, it could be accepted or rejected according to whether or not it provides a real gain in cancer efficacy treatment. This raises the necessity of testing the rule on a basis of real clinical data.
Medical practice which is followed in testing of new treatment procedure, requires clinical trials. Such trials usually last for extremely long period and are extremely labor-costy.
In addition, ethical problems may arise here if a certain group of subjects will have to be assigned to a method that is significantly different from the recommended one. Thus, we face a contradiction: we have to perform the trial, meanwhile it is impossible to do it. Once again, we face a creative problem, and in order to resolve the contradiction, we have to involve an additional external factor. Such factor might be the results of earlier made treatment decisions existing in the database and the known results of their implementation (2). Thus, the treatment results for this "alternative procedure" group consists in evaluation the potential usefulness of a particular rule retrospectively, using the data already available.
The algorithm for the testing is presented in [3]. Here we restrict ourselves to a short description.

3. Algorithm and results of testing [3],[4]

3.1 *The algorithm*

1. All elements H_m, *m =1,...M,* belonging to the set (2), randomly divided into two non-overlapping subsets of equal numbers of elements, H_{m1} and H_{m2}, called "training" and "control".

2. The elements from the training subset H_{m1} are used for th determination of parameters Z and λ_0 of the survival functions $S_m(t \mid X)$, (3),(4).

3. For each element *X* from the control subset H_{m2}, the optimal therapy *m0* is obtained by the method described above.

Thus, each element obtains the labels of two methods of treatment, optimal and actually used, which are either the same or different. It relates to each element *X* from H_{m2}, *m2=1,...,M.* Consequently, for each element of the united set $H = \bigcup_{m2=1}^{M} H_{m2}$ it is revealed whether its treatment was optimal or not.
We citate here shortly our articles.[3], [4] .
The procedure was applied to the clinical data of a group of more then 1000 patients. The set of treatment alternatives consisted of methods **A** and **B** By using of a random number generator, a training sample and control sample were created.

3.2 *Results*

The results are shown in Fig 1. Four survival curves are represented: the initial $S_A(t)$ and $S_B(t)$ for methods A**,** B, and for $S_{opt}(t)$, $S_{non}(t)$ after determination "optimal" and "non-optimal' methods.
Elementary conclusions can be drawn by simply observing the graphs, the "optimal" treatment method demonstrates a higher survival rate over time. For a more in-depth medical analysis, please see [3],[4]. We avoid doing it here because the purpose of the article, as the title suggests, is a bit different.

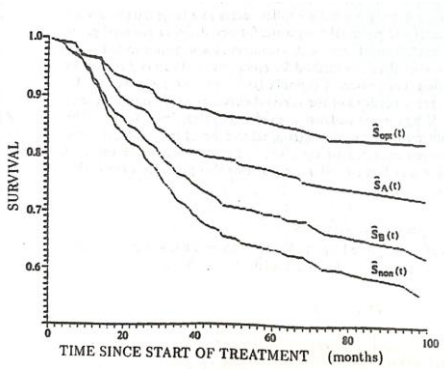

Fig 1 *– Survival over time*

4. Conclusions

In conclusion, it should be noted that the described technique and results could be interpreted as a step towards building Artificial-Intelligence based systems to be used for diagnosis and decision making in the process of determination of a treatment methos.

Additionally, the described method could have a very wide range of additional applications, in particular, the reduction healing time for patients suffering from severe diseases and body injuries.

References

1. Goot R.E., Goot V.M., Creation in science and technique – a general approach,
Intrnational Scientific Journal Scientific Innovation, Year V, Issue 3/2017, Sofia,
p. 107-110
2. Goot R.E., On creation in science and technique, "Voprosy psychology" (Problems of psychology), No.2, 2007.
3. Yakovlev A.Yu., Goot R.E., Osipova T.,T., The choice of cancer treatment based on covariate information, Statistic in medicine, vol.13, 1994, p.1575-1581
4. Goot R.E., Mallaev L, E.Yakubov, E.,H., Selection of the treatment method for oncological disease, Automatic control and computer science,Vol.38, No.6,2004,
p. 42-48.
5. Cox D.R. Regression models and life table., 'J.Royal Statistics, vol.34 p.220, 1977.
6. Goot R.E. and Osipova T.T.,A possible approach to comparison of survival functions, "Biometrical Journal", vol.33. p.291-297. 19

Evaluation of formal education active labor market policy programs in slovenia with propensity score matching

Kavkler Alenka
Faculty of Economics and Business, University of Maribor, Razlagova 14, Maribor, Slovenia
EIPF – Economic Institute, Einspielerjeva 6, Ljubljana, Slovenia

Abstract: *In this paper, we evaluate the formal education active labor market policy programs in Slovenia during the great recession. The quasi-experimental method of propensity score matching is applied. Performance of active labor market policy programs is typically measured with the average treatment effect on the treated. In the short term, the programs do not reduce unemployment and are characterized by a high dropout rate or a high percentage of unsuccessful completions due to some problematic target groups.*
Keywords: *ACTIVE LABOR MARKET POLICY, UNEMPLOYMENT, PROPENSITY SCORE MATCHING.*

1. Introduction

The aim of this study is to evaluate an important active labor market policy (ALMP) program in Slovenia, namely Formal education. The main question that should be answered by analyzing the efficiency of active labor market policy is whether ALMP measures reduce unemployment. Unemployment is the result of imbalances in the labor market, namely the differences between the supply of labor, which is determined by demographic and social trends, and demand for labor that stems from economic activity. The unemployment rate is, at least in the short term, determined by fluctuations in economic activity, since the labor supply is rather stable. ALMP measures that would effectively reduce unemployment should affect labor supply and/or demand.

The rest of this study is structured as follows. Section 2 describes the data and variables used in the study. Section 3 explains the methodological approach of propensity score matching. In Section 4, the results of evaluating the formal education programs are explained in detail. The implications of the empirical analysis are examined in the Section 5, Conclusion. The Data and Methodological approach sections are summarized from [6] and from [7].

2. Data

The data for the empirical investigation were obtained from the Employment Service of Slovenia (ESS). The first database (called US as abbreviation for unemployment spells) consists of all unemployment spells that ended between 1st January 2007 and 31st December 2010, as well as all of the ongoing spells on 31st December 2010. For each of the unemployment spells, the start and end date and the variables gender, age, level of education, occupation and statistical region were made available. Because ESS is not allowed to disclose personal data about the unemployed, only a personal ID number was added to enable identification of repeated spells. 411,338 unemployment spells with positive durations are included in this database.

The second database stores data about ALMP program participants in Slovenia in the period from 2007 to 2010. This database is called AL. In addition to the variables from the US database, AL also contains information about the type of ALMP program attended by the individual, source of financing and success of the individual at completing the program. From the initial 189,924 periods, the ALMP program ended in 166,166 cases. Since the ALMP program classification changed in 2007, the study only considers the 158,546 periods according to this classification. ALMP programs were successfully completed in 122,492 cases.

When estimating the models, the study used the following variables: employment status, age, gender, level of education, region, occupation and whether this is the first job. It is important to mention other variables that are often statistically significant in similar studies of other authors, for example health status, income, marital status and number of children. Unfortunately, we were not able to obtain the data on these variables for Slovenia.

3. Methodological Approach

A statistical method of matching is used to measure effectiveness of a treatment in a population. A subset of non-treated individuals is called the control group, whereas the set of treated individuals is called the experimental group (or treatment group). For applications of matching to the labor market, population is made up of all the unemployed in a given period of time, while the treatment group consists of all individuals participating in a specific ALMP program.

Performance of ALMP programs is typically measured with the average treatment effect on the treated (ATT) that is defined below. ATT simply put represents the difference between the expected probability of employment for the experimental group and the probability in the case that given individuals from experimental group would not have participated in ALMP. The second probability can only be approximately estimated. The first step involves logit or probit models with relevant explanatory variables to calculate the propensity for participation in the observed ALMP measure. In the second step, for each individual in the experimental group, one finds one or more persons in the control group with the same or at least a similar enough propensity for participation. With this subgroup of the control group the study estimated the probability needed for ATT.

4. Results

Table 1: *description of the Formal education ALMP programs (based on the Catalogue of Measures of Active Employment Policy, Employment Service of Slovenia [4])*

GOAL AND OBJECTIVE:
Increase employability and flexibility of unemployed individuals in the labor market, reduce structural mismatch in the labor market, and raise the educational and qualification levels of unemployed individuals
IMPLEMENTATION PROCEDURE:
Inclusion is carried out based on an employment plan. Formal education includes publicly recognized educational programs that run throughout the vertical from primary school to undergraduate education. Participants who successfully complete the program obtain a publicly recognized formal education.

TARGET GROUP:	
• Unemployed individuals who received education under an employment plan according to Article 53b of the Employment Relationship Act in the school year 2009/2010; • Unemployed individuals without professional or vocational education; • Unemployed individuals with health limitations; • Individuals whose employment relationship ended as redundant workers due to business reasons, bankruptcy, liquidation of the employer, or compulsory settlement and had a contract with the employer for education (in this case, the remaining costs of the education program are covered); • Unemployed individuals with professional or vocational education in fields in which they cannot find employment that have been registered with the Employment Service of Slovenia for more than one month, with an emphasis on eliminating regional structural mismatches in the labor market. • Unemployed individuals over 45 years of age.	
DURATION OF INCLUSION:	The duration of education or inclusion of an individual depends on the type of education in which the individual is enrolled and their prior knowledge, abilities, and skills.

As the effects of formal education often manifest in the long term, we selected 1,348 formal education programs that started in 2007 as the basis. The histogram for the length of these programs, shown in Figure 1, shows that most of them (909) last up to 1 year, and the longest program was supposed to last more than 4 years and end in 2011, but it is unfortunately not in our database. We selected 519 out of a total of 909 education programs lasting up to 1 year for the experimental group, in which unemployment also began in 2007. The control group consists of individuals enrolled in vocational education in 2007 who did not participate in any of the active employment policy programs. The control group, as defined, includes 37,082 individuals.

When studying the experimental group, we noticed an unusually high percentage of unsuccessful completions. As shown in Table 1, only 56.8% of the participants successfully completed the programs, approximately 9% interrupted the education, and slightly over 32% completed it unsuccessfully (11.95% for justifiable reasons, and 20.42% for unjustifiable reasons). We suspect that the reason for such a high percentage of unsuccessful completions is due to certain problematic target groups, such as unemployed persons with health limitations and unemployed persons over the age of 45 who probably have not received any education for at least 20 years. Unsuccessful completions due to justifiable reasons are probably a result of medical certificates, so we assume that the percentage of people with health limitations in the experimental group is significant. Figure 2 shows the success rate for completions for the entire ALMP database (top figure) as well as for formal education programs (bottom figure). The ALMP database shows a 65% success rate for completions, taking into account that approximately 12% of programs were still ongoing at the beginning of the study, so there were no data on their success rate. For formal education programs as a whole, the success rate for completions is 42%, with approximately 20% unsuccessful. Some programs were not yet completed when our study ended.

The results of calculations at the end of the years 2008, 2009, and 2010 are presented in Table 3 below. The calculations were performed with R software [11]. The values for ATT are negative and statistically significant in all three cases. In the short term, negative results can be expected from education because this program has a pronounced "locking-in" effect. In the long term, some foreign studies show positive results, but the target group is usually selected from all unemployed individuals. At the end of 2010, 67.24% of individuals in the experimental group were removed from the US database, and there were 9.53% more such individuals among those paired in the matching process (because ATT is -0.0953), or 76.77%. At the end of 2009, 65.13% of the experimental group were not among the registered unemployed, and at the end of 2008, this proportion was the same at 67.24%. The corresponding proportions for the matched control group are obtained by subtracting ATT from the proportion for the experimental group.

It should be noted that the calculation of ATT is biased because we do not have data on the health status of the experimental and control groups. To ensure unbiased calculation in the matching method, all variables that affect both enrollment in the ALMP program and the success of the program (i.e., removal from registered unemployment) must be controlled. Unbiased calculation could be achieved with data on some indicators of health status, such as the number of visits to a doctor by an individual in the observation period or expenditures from the health insurance fund. Currently, the obtained ATT values are too low because in the matching process, individuals with health limitations in the control group should be paired with those who also have health limitations. In any case, it would be good to reconsider the rationale for some target groups, which contribute to the high proportion of unsuccessful completions.

Figure 1: *histogram for the length of formal education programs that began in 2007 (in years)*

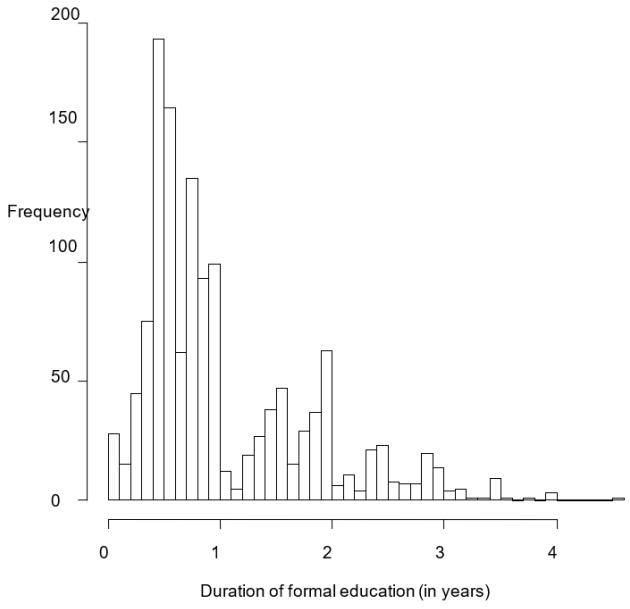

Table 2: *Rate of completion of education for the experimental group (in %)*

No data	0.77
Successfully completed activity	56.84
Interruption of activity - justifiable reasons	6.94
Interruption of activity - unjustifiable reasons	2.31
Unsuccessfully completed - justifiable reasons	11.95
Unsuccessfully completed - unjustifiable reasons	20.42
No entry for success rate	0.77

Figure 2: *Rate of completion for the entire ALMP database (upper image) and for formal education programs (lower image)*

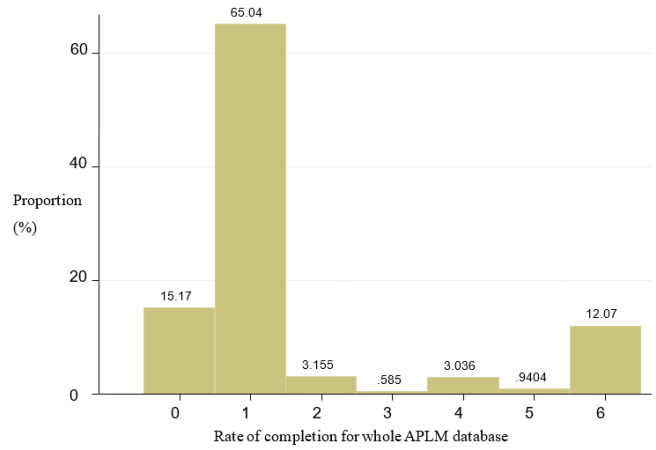

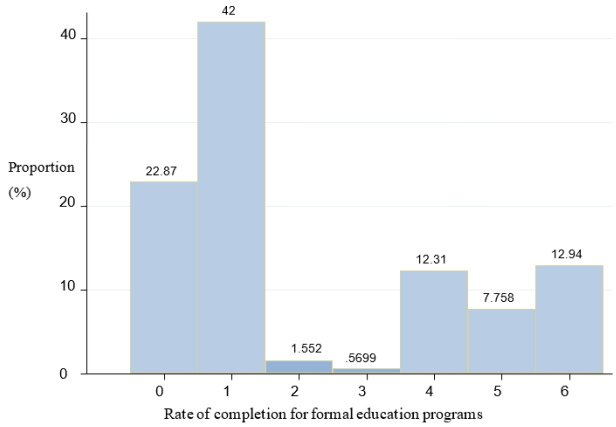

Legend: 0: No data, 1: Successfully completed activity, 2: Interruption of activity - justifiable reasons, 3: Interruption of activity - unjustifiable reasons, 4: Unsuccessfully completed activity - justifiable reasons, 5: Unsuccessfully completed activity - unjustifiable reasons, 6: No entry for success rate.

Table 3: *ATT calculations*

	At the end of 2008	**At the end of 2009**	**At the end of 2010**
ATT	-0,1089	-0,11247	-0,0953
AI SE	0,0234	0,022817	0,0224
t-stat	-4,6618	-4,9294	-4,2486
p-value	0,0000	0,0000	0,0000

Note: AI SE represents the standard error using the method developed by Abadie and Imbens [1].

Formal education as an active labor market policy program has been studied by other authors. Domadenik and Pastore [3] analyze youth unemployment in two former transition economies, Slovenia and Poland. The authors apply the multinomial logit model and argue that tertiary education lowers the probability of unemployment, especially for the young adults.

Južnik-Rotar ([5], summarized from Martin and Grubb, [10]) claims that empirical research that has investigated the effectiveness of education active labor market policy programs using a microeconometric approach has shown that such programs have a very low positive impact on the likelihood of further employment and potential earnings of program participants. Therefore, state interventions must be appropriately designed if we want to achieve greater employment opportunities for program participants and greater cost-effectiveness. Klužer [9], on the other hand, estimates the effectiveness of active labor market policy programs with a macroeconometric approach, namely with an augmented matching function.

Caliendo and Schmidl [2] examine youth unemployment in European countries that spend significant resources on active labor market policy programs for the young unemployed. According to the authors, a smaller part of training active labor market policy programs are »preparatory programs that promote the take-up of regular formal education, such as the continuation of general schooling, or participation in apprenticeship-based vocational education.«

5. Conclusion

Educational active labor market policy programs consist of Formal education programs and Project-based learning for young adults. These are typical attempts to reduce structural unemployment, increase employability, and flexibility on the supply side of the labor market. In the short term, the programs do not reduce unemployment; the first program is characterized by a high dropout rate or a high percentage of unsuccessful completions enrolled in formal education, and reducing unemployment is not the only goal of the project-based learning program for young adults. We assume that the reason for such a

high percentage of unsuccessful completions of formal education is in some problematic target groups, such as unemployed persons with health limitations and unemployed persons over 45 years of age who have probably not been in education for at least 20 years. Unsuccessful completions due to justifiable reasons are likely a result of medical certificates, so we conclude that the percentage of persons with health limitations in the experimental group is not negligible. It would be wise to reconsider the relevance of certain target groups, which is why this program has such a high percentage of unsuccessful completions.

References

1. Abadie, A., Imbens, G. (2006). Large Sample Properties of Matching Estimators for Average Treatment Effects. *Econometrica* Vol. 47: 235-267.
2. Caliendo, M., Schmidl, R. Youth unemployment and active labor market policies in Europe. *IZA J Labor Policy* **5**, 1 (2016).
3. Domadenik P., Pastore, F. (2006). The impact of education and training systems on the labour market participation of young people in CEE economies: A comparison of Poland and Slovenia. *International Review of Entrepreneurship & Small Business*, **3**(1): 640-666.
4. Employment Service of Slovenia (ESS) (2010). Catalogue of Active Labour Market Policy Measures.
5. Južnik-Rotar, L. (2008). Vključevanje mladih brezposelnih oseb v aktivne politike zaposlovanja. *Naše Gospodarstvo*, **54**(1-2): 112-119.
6. Kavkler, A. (2019). Evaluation of work trial programs, verification and validation of national vocational qualification in Slovenia during the great recession with propensity score matching approach. In: Schaefer, T. M. (ed.). Innovations in the modern world: monograph SEPIKE. Poitiers (etc.): Association 1901 "SEPIKE", p. 70-79.
7. Kavkler, A., Volčjak, R. (2020). Effectiveness of active employment policy programs in European countries before the great recession. IOSR journal of economics and finance: IOSR-JEF. Vol. 2020 (1): 13-18.
8. Kluve, J. (2006). The Effectiveness of European Active Labor Market Policy. *IZA Discussion Paper*, No. 2018.
9. Klužer, F. (2008). Ocena učinkovitosti aktivne politike zaposlovanja z združevalno funkcijo. *IB Revija*, **42**(2): 17-27.
10. Martin, J., Grubb, D. (2001). What Works and for Whom: A Review of OECD Countries' Experiences with Active Labour Market Policies. *Swedish Economic Review* 8: 9–56.
11. Sekhon, J.S. (2011). Multivariate and Propensity Score Matching Software with Automated Balance Optimization: The Matching package for R. Journal of Statistical Software Vol. 42 (7).

МОДЕЛИРОВАНИЕ ПРОЦЕССА ПРОКАТКИ ТОЛСТОГО ЛИСТА В ВАЛКАХ РАЗЛИЧНОЙ КОНСТРУКЦИИ

SIMULATION OF THICK-SHEET ROLLING PROCESS IN ROLLS OF VARIOUS DESIGN

Evgeniy Panin[1], Alexandr Arbuz[2], Almas Yerzhanov[1], Sergey Lezhnev[3], Abdrakhman Naizabekov[3], Dmitry Kuis[4], Aibol Esbolat[1]

[1] Karaganda Industrial University, 30 Republic ave., Temirtau, 101400, Kazakhstan
[2] Nazarbayev University, 53 Kabanbay Batyr ave., Astana, 010000, Kazakhstan
[3] Rudny industrial Institute, 38 50 let Oktyabrya str., Rudny, 115000, Kazakhstan
[4] Belarusian State Technological University, 13a Sverdlova str., Minsk, 220006, Belarus
e-mail: cooper802@mail.ru

Abstract: *This paper presents finite element modeling of thick-sheet rolling process in rolls of various design. Key feature of rolls was their relief barrel design. Models of with different roll rotation speeds, different roll diameters, and different friction coefficients of the rolls were considered. During comparative analysis, the shape change in the longitudinal and transverse directions and equivalent strain were considered. The simulation results showed that asymmetry factor is the effective way to increase the metal processing. And relief barrel design allows to avoid the workpiece bending in the vertical direction.*
Keywords: *ROLLING, RELIEF ROLLS, ASYMMETRY, SIMULATION, STRAIN STATE.*

1. Введение

Повышение качества металлопродукции в процессе обработки давлением была и остается одной из наиболее актуальных задач современной инженерии. Среди многочисленных способов улучшения качества металлоизделий особое место занимают способы ОМД, реализующие интенсивную пластическую деформацию. Эти способы обработки давлением не просто улучшают исходную литую структуру металла – они способны измельчить исходный размер зерна до мелкозернистого состояния, что в итоге придает металлу значительный рост механических характеристик. Все это требует поиска новых технологий и способов реализации и внедрения в современное производство металлопродукции.

Перспективным направлением является ассиметричная прокатка, получившая свое распространение в начале 2000-х годов. Толчком к этому явилось введение в эксплуатацию рабочих клетей с индивидуальным приводом валков. Практика исследования и применения процессов АП при горячей и холодной прокатке листов свидетельствует о возможности управления при этом практически всем спектром параметров прокатки и служебных свойств листов и полос. [1].

Асимметричная прокатка позволяет понизить усилие прокатки и энергозатраты на процесс деформации, уменьшить продольную и поперечную разнотолщинность, улучшить плоскостность и форму полосы, дает возможность оперативно управлять качеством поверхности, физико-механическими свойствами проката.

Анализ факторов, которые влияют на уширение, и способов асимметричной прокатки показал, что наиболее рациональным способом для исследования влияния рассогласования скоростей валков на уширение со стороны ведущего и ведомого валков является скоростная асимметрия. Применение скоростной асимметрии дает возможность регулировать рассогласование скоростей валков в широком диапазоне непосредственно в процессе прокатки, а также позволяет использовать системы автоматического регулирования. [2]

Разделение процессов прокатки на симметричные и асимметричные имеет условный характер. Например, если процесс прокатки не имеет признаков намеренно вносимой асимметрии, а влияние асимметрии на условия прокатки незначительно и определено допусками технологии, то такой процесс прокатки относят к симметричным. Если же асимметрия задается такими специальными технологическими приемами, как вращение рабочих валков с различными окружными скоростями, применение рабочих валков с неодинаковыми диаметрами, нанесение различной шероховатости на поверхности верхнего и нижнего рабочих валков и т.д., то в этих случаях процесс прокатки относят к асимметричным [3]. Авторы работы [4] считают, что прокатка всегда асимметрична, а случай симметричного процесса прокатки есть идеализация реальных условий. Асимметрия может быть целенаправленно введена для улучшения условия протекания процесса прокатки - это позволит управлять формой раската, уменьшить усилия прокатки, получить более высокие механические свойства и снизить затраты энергии на производстве.

В работах [5-6] повышение качества металла толстолистовой стали при незначительном изменении размеров исходной заготовки достигается тем, что прокатка толстых листов осуществляется в валках, включающие верхний и нижний валки с рельефной поверхностью в виде кольцевых проточек, образующих выступы и впадины трапециевидной формы, чередующиеся друг за другом по всей длине бочки валка с шириной трапециевидных выступов меньше ширины трапециевидных впадин. Основная идея данного изобретения заключается в способности осуществить деформацию сдвига и возможности выравнивать прокатанную заготовку в гладких валках при незначительном обжатии.

Необходимо учитывать, что кроме положительных свойств, в процессе прокатки асимметричным способом, имеются также отрицательные явления, заключающиеся в изгибе полосы вне очага деформации, возможность существования скольжения в очаге деформации. а так же повышенная нагрузка на приводы прокатных станов. Исходя из этого прокатку ассиметричным способом, необходимо проводить при таких параметрах, при которых возможно минимизировать отрицательные эффекты, авторы [7-9] в своих работах описывали данные технологии.

2. Экспериментальная часть

Для оценки влияния предлагаемой схемы деформирования на уровень проработки металла было решено использовать компьютерное моделирование методом конечных элементов (МКЭ). Моделирование проводилось в программе Deform v.12, построение трехмерных геометрических моделей осуществлялось в программе Компас-3D v.16.

Диаметр валков с рельефной поверхностью по буртам составляет 200 мм, длина бочки 500 мм. Скос проточки на выступах и впадинах составляет 45°. Заготовка представляет собой лист прямоугольной формы сечением 10 х 400 мм и длиной 350 мм. При этом было решено смоделировать прокатку с плоскостью симметрии по ширине, т.е. в модели

ширина заготовка была равна 200 мм, которая зеркально отражалась. В качестве материала для заготовки была выбрана латунь Л63, при этом ранее было установлено, что данная технология прокатки в рельефных валках вполне пригодна и для прокатки сравнительно мягких сталей типа Ст3. При компьютерном моделировании процесса использовались следующие технологические параметры:

- материал заготовки был полностью изотропным;
- прокатка проводилась при температуре окружающей среды 20°С;
- температура нагрева заготовки перед прокаткой была равна 600°С;
- коэффициент теплообмена заготовки с инструментом составлял 5000 Вт/(м2•°С);
- коэффициент теплообмена заготовки с окружающей средой составлял 0,002 Вт/(м2•°С);
- для создания максимально жестких условий захвата коэффициент трения на контакте металла с валками был принят 0,5 (что соответствует загрубленной поверхности с высоким уровнем шероховатости);
- скорость вращения верхнего валка 60 рад/с.

Для определения оптимальной скорости вращения нижнего валка было решено смоделировать 2 варианта асимметрии: со скоростью вращения 80 рад/с (где коэффициент асимметрии равен 1,3) и со скоростью вращения 90 рад/с (где коэффициент асимметрии равен 1,5). Также для сравнительного анализа были построены дополнительные модели прокатки в рельефные валках, где асимметрия отсутствует и две модели прокатки в гладких валках с указанными коэффициентами асимметрии.

3. Результаты и обсуждение

Обычно при рассмотрении деформированного состояния используют показатель интенсивности деформации, или так называемую эквивалентную деформацию.

На рисунках 1-2 представлены результаты моделирования прокатки в гладких валках с различными коэффициентами асимметрии и относительным обжатием 10%.

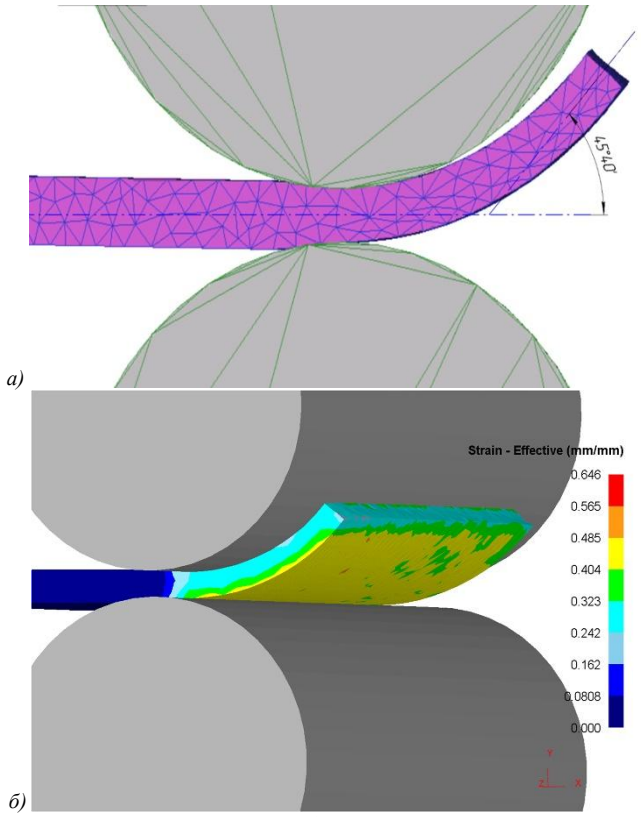

а)

б)

Рис. 1. *Общий вид прокатки (а) и распределение эквивалентной деформации (б) в гладких валках с коэффициентом асимметрии 1,3*

При прокатке с высоким уровнем асимметрии 1,3 и 1,5 заготовка изгибается в вертикальной плоскости, причем угол изгиба увеличивается с повышением коэффициента асимметрии. При этом распределение эквивалентной деформации носит неравномерный характер – в зоне контакта с верхним валком ее величина равна примерно 0,2; а на контакте с более быстрым нижним валком ее величина равна примерно 0,4 (при коэффициенте асимметрии 1,3) и 0,52 (при коэффициенте асимметрии 1,5)

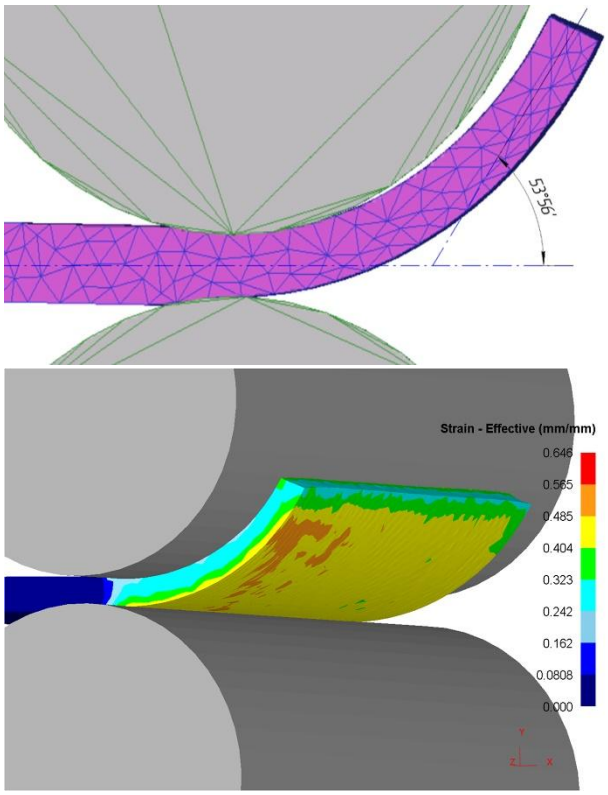

а)

б)

Рис. 2. *Общий вид прокатки (а) и распределение эквивалентной деформации (б) в гладких валках с коэффициентом асимметрии 1,5*

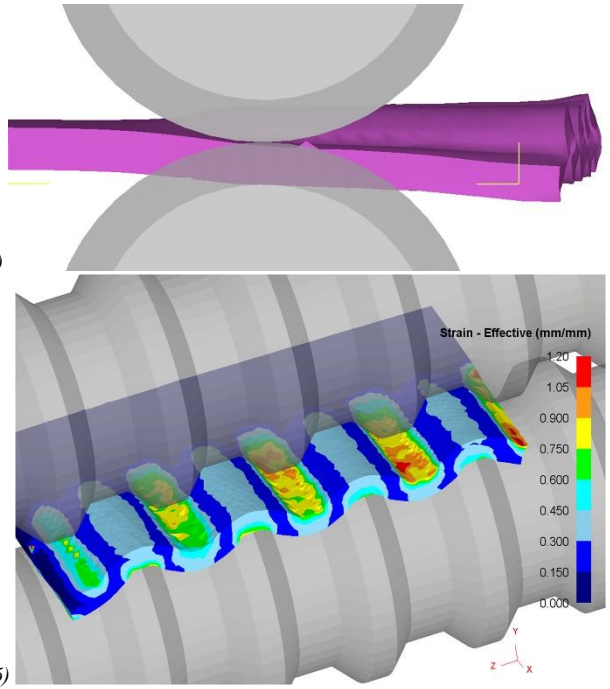

а)

б)

Рис. 3. *Общий вид прокатки (а) и распределение эквивалентной деформации (б) в рельефных валках без асимметрии*

Результаты моделирования прокатки в рельефных валках без асимметрии (рисунок 3) показали существенный рост

уровня эквивалентной деформации до 1,15-1,2 в зонах контакта металла с кольцевыми проточками и до 0,45 на противоположных зонах. На наклонных участках уровень деформации находится в пределах 0,3. Заготовка в данном случае выходит из валков без искривления, поскольку фактор асимметрии отсутствует.

При включении в данную схему фактора асимметрии (рисунки 7-8) было отмечена одна ключевая особенность. Несмотря на достаточно высокий уровень асимметрии, заготовка после выхода из очага деформации рельефных валков практически не изгибалась, сохраняя свою горизонтальную траекторию движения. Такой эффект достигался за счет получаемого рельефного сечения заготовки, в которой образуемые выступы и впадины выполняли своеобразную роль ребер жесткости.

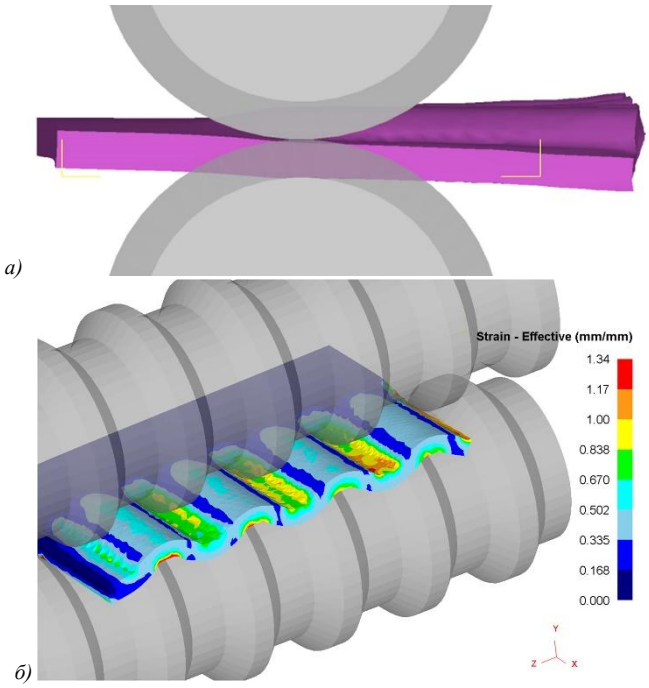

Рис. 4. *Общий вид прокатки (а) и распределение эквивалентной деформации (б) в рельефных валках с коэффициентом асимметрии 1,3*

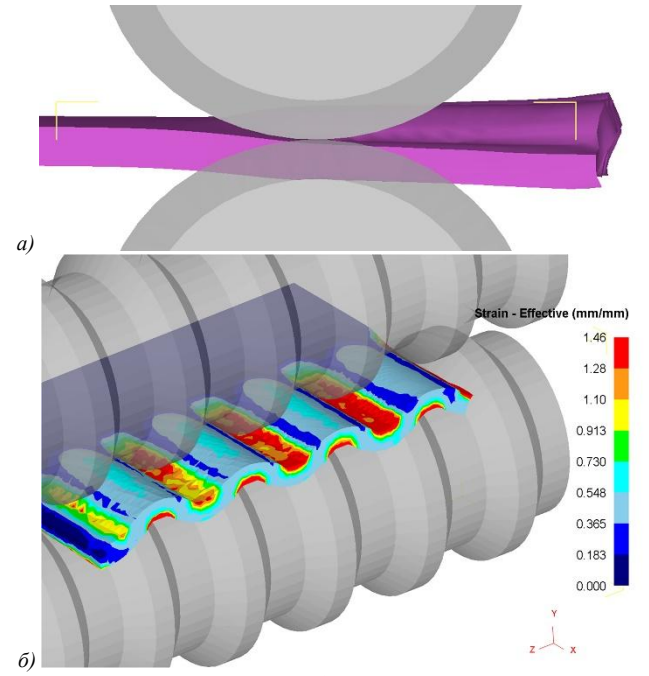

Рис. 5. *Общий вид прокатки (а) и распределение эквивалентной деформации (б) в рельефных валках с коэффициентом асимметрии 1,5*

При этом было установлено, что повышение коэффициента асимметрии приводит к росту уровня эквивалентной деформации по всему сечению заготовки. Так, при коэффициенте асимметрии 1,3 максимальный уровень деформации составил 1,3-1,34 на контакте с кольцевыми проточками, в противоположных зонах уровень деформации вырос до 0,65. При этом на наклонных участках зоны падения деформации до 0,3-0,35 стали существенно меньше.

При коэффициенте асимметрии 1,5 максимальный уровень деформации составил 1,4-1,46 на контакте с кольцевыми проточками, в противоположных зонах уровень деформации вырос до 0,7. При этом на наклонных участках зоны падения деформации до 0,3-0,35 практически отсутствуют.

Таким образом было установлено, что введение фактора асимметрии в стадию прокатки в рельефных валках благоприятно влияет на уровень проработки деформируемого металла. Вследствие чего было решено в дальнейшем рассматривать модель с коэффициентом асимметрии 1,5.

Выводы

Проведенные исследования показали эффективность реализации кинематической асимметрии при прокатке в рельефных валках. Путем моделирования в среде Deform было выявлено, что даже при высоком уровне асимметрии заготовка после выхода из рельефных валков практически не изгибается, сохраняя свою горизонтальную траекторию движения. Такой эффект достигается за счет рельефного сечения заготовки, где образуемые выступы и впадины выполняют роль ребер жесткости. Уровень деформации при этом возрастает примерно на 20% по сравнению с симметрично прокаткой в рельефных валках.

Данное исследование финансировалось Комитетом науки Министерства науки и высшего образования Республики Казахстан (Грант № AP14869080).

Литература

1. A.M. Pesin, D.O. Pustovoitov, O.D. Biryukova. The effect of speed asymmetry on the strain state in aluminium bimetals during accumulative rolling. IOP Conference Series: Materials Science and Engineering. 2018. Vol. 447. Iss. 1, № 012066.

2. А.А. Перогив, Е.Н. Смирнов, А.П. Митьев, Исследование влияния процесса асимметричной прокатки на поперечную деформацию толстых полос. Металлургия XXI столетия глазами молодых. Материалы всеукраинской научно-практической конференции студентов физико-металлургического факультета ДонНТУ. - Донецк: ДонНТУ, 2011, с. 79-80.

3. В.Н. Выдрин. Расчет давлений и натяжений при прокатке с различным соотношением окружных скоростей валков. В кн.: Тонколистовая прокатка. - Воронеж: изд-во ВПИ, 1979, с. 38-42.

4. К.С. Горбунов, К.В. Бахаев. Асимметричный процесс прокатки. Металлургия XXI столетия глазами молодых. 2019, С.193-196.

5. Патент РК № 14791. Валки для прокатки толстых листов. А.Б. Найзабеков, С.Н. Лежнев, 2007.

6. A. Naizabekov, S. Lezhnev, E. Panin, I. Mazur. Alternating sign rolling technology in grooved rolls for nonferrous metal plate billets. Metallurgist, 2017, Vol. 61, Iss. 5–6, P. 406-413.

7. H. Dyja, W.M. Salganik, A.M. Piesin, A. Kawalek, Asymetryczne walcowanie blach cienkich: teoria, technologia i nowe rozwiazania. Seria: Monografie nr 137. Wydawnictwo Politechniki Czestochowskiej. Czestochowa, 2008, 345 p.

8. A.M. Pesin, V.M. Salganik, H. Dyja, D.N. Chikishev, D.O. Pustovoitov, A. Kawałek. Asymmetric rolling. Theory and technology. Hutnik Wiadomości Hutnicze. 2012, № 5, P. 358-362.

9. J.-S. Lu, O.-K. Harrer, W. Schwenzfeirer, F.D. Fisher. Analysis of the bending of the rolling materials in asymmetrical sheet rolling. International Journal of Mechanical Sciences. 2000. Vol.42. Iss. 1, P. 49-61.

ИССЛЕДОВАНИЕ ЭВОЛЮЦИИ МИКРОСТРУКТУРЫ СТАЛИ 45 ПРИ ДЕФОРМИРОВАНИИ В БОЙКАХ РАЗЛИЧНЫХ КОНСТРУКЦИЙ, РЕАЛИЗУЮЩИХ СДВИГОВУЮ ДЕФОРМАЦИЮ

INVESTIGATION OF THE MICROSTRUCTURE EVOLUTION OF STEEL 45 DURING DEFORMATION IN STRIKERS OF VARIOUS DESIGNS IMPLEMENTING SHEAR STRAIN

Andrey Tolkushkin[1], Andrey Volokitin[1], Abdrakhman Naizabekov[1], Irina Volokitina[1], Evgeniy Panin[2], Sergey Lezhnev[1], Oksana Maldina[1]

[1]Rudny Industrial Institute, Rudny, Kazakhstan
[2]Karaganda Industrial University, Temirtau, Kazakhstan
sergey_legnev@mail.ru

Abstract: *In this paper, a forging tool of a new design is proposed, which allows to implement shear and alternating strain in the entire volume of the deformable workpiece with a smaller change in its initial dimensions. In order to confirm the effectiveness of the proposed new forging tool in obtaining plate type blanks of the required quality, a laboratory experiment was conducted. During the laboratory experiment, the forging of blanks of 45 steel was carried out in such forging tools as step-wedge-shaped strikers of two different variants (proposed and previously known) and in step strikers. Analysis of the shape change of workpieces after forging and the microstructure evolution of steel after two deformation cycles showed that the use of stepped wedge-shaped strikers with a wedge on the upper striker and a wedge-shaped depression on the lower striker is more promising, since it allows to obtain a fine-grained structure in the metal with a smaller change in the initial dimensions of the workpiece.*
Keywords: *SHEAR STRAIN, FORGING, STEP-WEDGE STRIKERS, STEP STRIKERS, MICROSTRUCTURE.*

1. Введение

При выборе кузнечного инструмента для проведения операции деформирования заготовок целесообразно использовать такую конструкцию бойков, которая позволит реализовывать достаточно хорошую проработку литой структуры металла при сниженных энергозатратах или меньшем количестве циклов деформирования. Это позволит существенно увеличить срок службы инструмента, снизит расход необходимой энергии, что в итоге даст ощутимый экономический эффект. Классические плоские бойки, несмотря на все еще широкое распространение на многих металлургических предприятиях, уже давно потеряли свою актуальность, так как деформирование в таких бойках является крайне энергозатратным, поскольку в данном случае в деформируемом металле развиваются в основном нормальные напряжения и практически отсутствует деформация сдвига. Поэтому разработка новых технологий ковки, и в частности протяжки, которые бы позволили увеличить долю сдвиговых деформаций, является актуальным направлением развития кузнечного производства.

На данный момент известно множество инструментов для ковки [2-7], позволяющих в процессе деформирования реализовывать, как сдвиговые, так и знакопеременные деформации. Они имеют, как свои преимущества, так и недостатки. Но на данный момент до сих пор нет совершенного или хотя бы универсального инструмента для ковки, реализующего в процессе деформирования сдвиговые и/или знакопеременные деформации.

Так, например, известен инструмент для изготовления поковок, содержащий бойки со ступенчатыми и наклонными участками, выполненные с углом наклона к горизонтальной плоскости участка между ступенями не более 45° и шириной ступени большей протяженности не менее 1,5 суммарной протяженности меньшей ступени и наклонного участка [8]. Но недостатком данного известного инструмента является то, что при протяжке заготовок в ступенчатых бойках для получения мелкозернистой структуры поковок, обеспечивающей необходимый уровень механических свойств данных поковок, необходимо осуществлять несколько проходов протяжки в ступенчатых бойках, что снижает производительность данного процесса.

Так же известен инструмент для изготовления поковок, содержащий бойки со ступенчатыми и наклонными участками, выполненные с углом наклона к горизонтальной плоскости участка между ступенями не более 45° и шириной ступени большей протяженности не менее 1,5 суммарной протяженности меньшей ступени и наклонного участка, при этом наклонный участок и меньшая ступень в поперечном сечение выполнены в виде клина [9]. Но данный инструмент так же имеет недостаток, который заключается в том, что при протяжке заготовок в данном инструменте обеспечивается получение мелкозернистой структуры и необходимый уровень механических свойств поковок за меньшее количество проходов, но при большем изменении исходных размеров заготовки по сравнению со ступенчатыми бойками.

Перед нами же стояла задача повышения качества металла заготовки при меньшем количестве проходов и меньшем изменении исходных размеров заготовки путем реализации интенсивных пластических деформаций во всем объеме деформируемого тела.

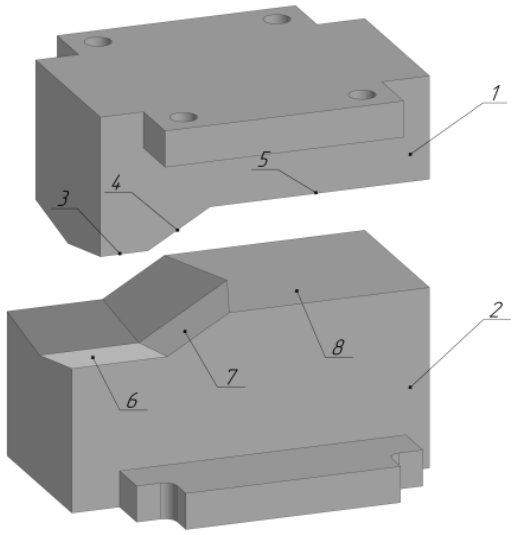

Рис. 1 *Ступенчато-клиновидные бойки новой конструкции: 1 – верхний боек; 2 – нижний боек; 3 – меньшая ступень с клином верхнего бойка, 4 – наклонный участок с клином верхнего бойка; 5 – большая плоская ступень верхнего бойка; 6 – меньшая ступень с клиновидной впадиной нижнего бойка; 7 – наклонный участок с клиновидной впадиной нижнего бойка; 8 – большая плоская ступень нижнего бойка*

Данная задача может быть решена за счет реализации в материале заготовки интенсивной пластической деформации

по схеме простой сдвиг одновременно в продольном и в поперечном направлениях. Это достигается тем, что инструмент для изготовления поковок, содержит бойки со ступенчатыми и наклонными участками, выполненные с углом наклона к горизонтальной плоскости участка между ступенями не более 45° и шириной ступени большей протяженности не менее 1,5 суммарной протяженности меньшей ступени и наклонного участка, при этом наклонный участок и меньшая ступень верхнего бойка в поперечном сечение выполнены в виде клина, а нижнего бойка в виде аналогичной клиновидной впадины [10] (рис. 1).

2. Методика проведения эксперимента и исследований микроструктуры

Для проведения лабораторного эксперимента по изучению влияния новой технологии ковки поковок в ступенчато-клиновидных бойках новой конструкции на эволюцию микроструктуры были подготовлены заготовки из углеродистой стали 45 размерами h×b×l = 30×40×200 мм. Для восстановления начальной структуры заготовок из стали 45 их перед деформированием подвергали неполному отжигу при температуре 820°С с выдержкой 2 часа [11] в трубчатой печи сопротивления.

Для проведения эксперимента были подготовлены в ступенчато-клиновые бойки новой конструкции с углом наклона 30° и с углом клина верхнего бойка и клиновидной впадины нижнего бойка равным 160°, ступенчато-клиновые бойки старой конструкции так же с углом наклона 30° и с углом клина верхнего и нижнего бойков равным 160°, ступенчатые бойки с углом наклона 30°.

Деформирование заготовок в лабораторных условиях производили на гидравлическом прессе ПГМ – 1500МГ4. Деформирование заготовок осуществляли следующим образом. Заготовки нагревали до температуры начала ковки 1200°С, а затем их подавали в ступенчато-клиновые бойки новой конструкции [14] на первую ступень с клином на верхнем бойке и клиновидной впадиной на нижнем бойке. После обжатия заготовки на первой ступени осуществляли подачу заготовки на наклонный участок и так же производили обжатие. После чего заготовку уже подавали на вторую плоскую ступень, на которой производили выпрямление данной заготовки. Таким образом заготовку подвергали обжатию по всей длине.

Рис. 2 *Деформирование заготовки в ступенчато-клиновидных бойках новой конструкции*

Размеры продеформированных заготовок после их протяжки по всей длине составили $b \times h \times l$=24,9×42,4×227,3 мм, уков при этом равен 1,14.

Вторую партию заготовок подвергли двум проходам деформирования без кантовки по схеме деформирования представленной выше. Уков после 2-х проходов составил - 1,22.

Заготовки такого же типоразмера были продеформированы в ступенчато-клиновидных бойках старой конструкции [10] и в ступенчатых бойках [9] с аналогичным количеством проходов, что и в ступенчато-клиновых бойках новой конструкции.

При этом размеры продеформированных заготовок после их протяжки по всей длине в ступенчато-клиновидных бойках старой конструкции составили $b \times h \times l$=24,1×42,7×233,2 мм, уков при этом равен 1,17. Уков после 2-х проходов составил – 1,28.

Размеры продеформированных заготовок после их протяжки по всей длине в ступенчатых бойках составили $b \times h \times l$=25,2×42,2×225,7 мм, уков при этом равен 1,13. Уков после 2-х проходов составил - 1,2.

Из всех продеформированных заготовок были вырезаны темплеты в поперечном и продольном направлениях. Исследование микроструктуры выполнялось на специально подготовленных микрошлифах. Изучение микроструктуры осуществлялось с помощью оптической микроскопии.

3. Обработка экспериментальных данных

Данные, полученные при изучении микроструктуры стали 45, приведены на рисунке 3.

В исходном состоянии доэвтектоидная сталь перед деформированием имеет феррито-перлитную структуру состоящую из сравнительно крупных для стали зерен размером 55,2 мкм (рис. 3а).

а)

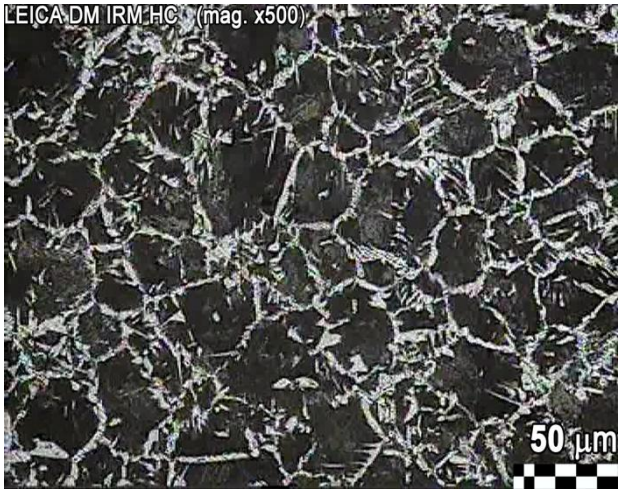

б)

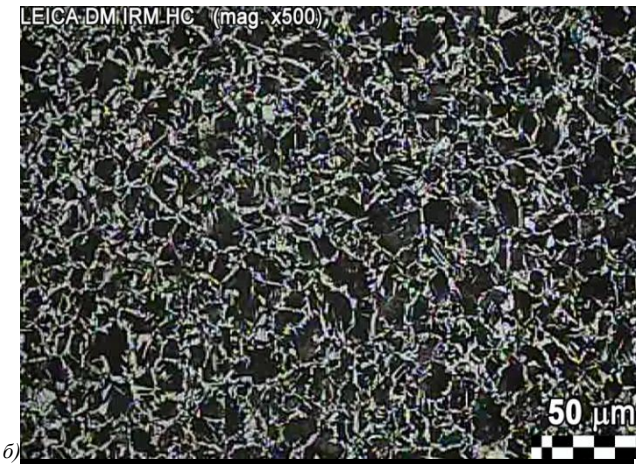

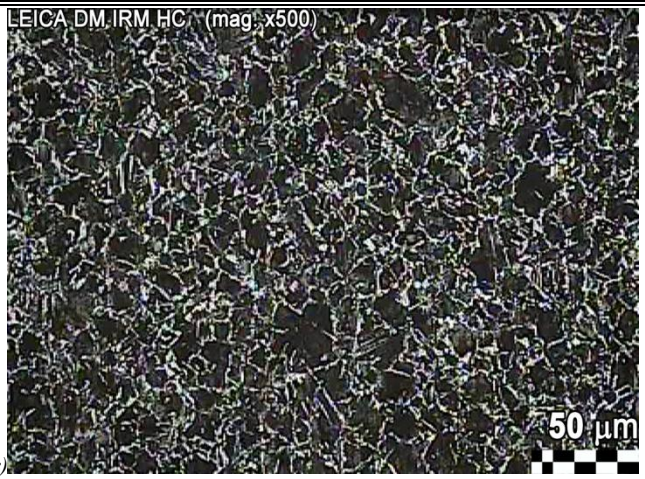

в)

ж)

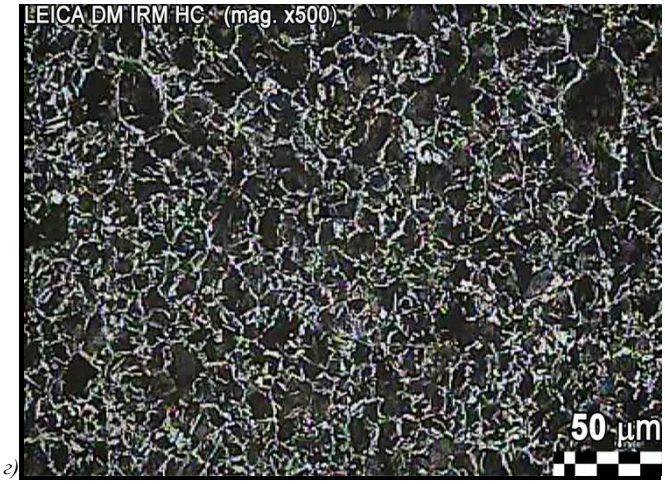

г)

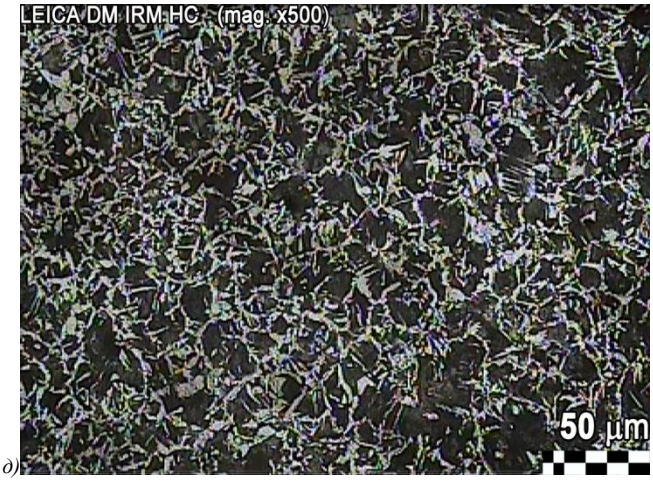

д)

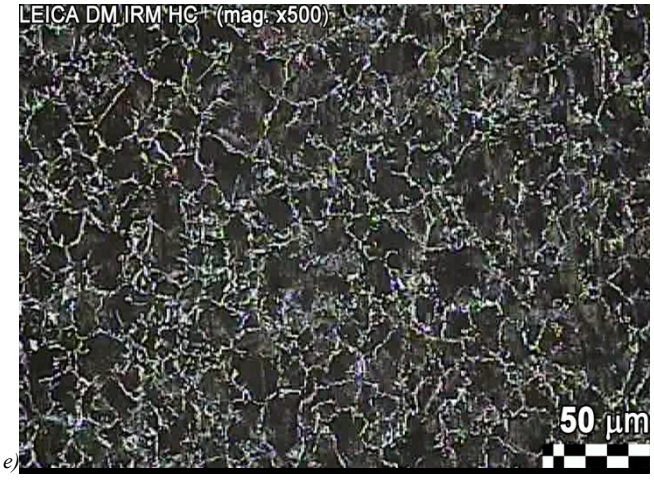

е)

Рис 3 *Микроструктура стали марки 45: а – исходная структура; б,в – после деформирования в ступенчато-клиновых бойках новой конструкции; г,д - после деформирования в ступенчато-клиновых бойках старой конструкции; е, ж – после деформирования в ступенчатых бойках; (б, г, е - в продольном направлении; в, д, ж - в поперечном направлении)*

Анализ микроструктуры продеформированных образцов показал, что ковка в ступенчато-клиновых бойках старой конструкции приводит к значительному измельчению зерна, структура равномерна, как в продольном, так и поперечном сечениях, средний размер зерен после двух проходов составляет 17,3-17,6 мкм (рис. 3 г, д). Микроструктура характеризуется наличием как рекристаллизованных, так и деформированных зерен. После ковки в ступенчато-клиновых бойках новой конструкции полученная структура является также мелкозернистой и однородной, как в продольном, так и поперечном сечениях. Средний размер зерен после двух проходов составляет 18,1-18,3 мкм (рис. 3 б, в). При деформировании в ступенчатых бойках наблюдается самое слабое измельчение структуры, микроструктура состоит из большого количества рекристаллизованных зерен размером 27,3-27,6 мкм. После деформирования в бойках всех трех модификаций получена феррито-перлитная структура, практически все зерна феррита фрагментированы, что отличает их от феррита в структуре стали в исходном состоянии.

4. Выводы

В данной работе была разработана новая технология ковки и инструмент для ее реализации, в частности, ступенчато-клиновидные бойки новой конструкции, имеющие клин на наклонном участке и меньшей ступени верхнего бойка, и аналогичную клиновидную впадину на нижнем бойке. Из проведенного сравнительного анализа результатов исследования микроструктуры при деформировании заготовок в ступенчатых и ступенчато-клиновых бойках (новой и старой конструкции) можно сделать вывод, что при использовании всех трех конструкций бойков наблюдается равномерная проработка исходной структуры металла по всему объему деформируемой заготовки. При этом использование для ковки заготовок и поковок типа плит и пластин ступенчато-клиновых бойков в обоих случаях обеспечивает все-таки более интенсивную проработку исходной структуры металла за один цикл. А с учетом того, что при использовании ступенчато-клиновых бойков с клином на верхнем бойке и клиновидной впадиной на нижнем бойке происходит меньшее изменение исходных размеров заготовки по сравнению с использованием ступенчато-клиновидных бойков с клином на верхнем и нижнем бойке и практически равном изменению исходных размеров при ковке в ступенчатых бойках, использование ступенчатых клиновидных бойков новой конструкции более перспективно для получения необходимого качества поковок с заданным уровнем механических свойств при меньшем укове.

Данное исследование финансировалось Комитетом науки Министерства науки и высшего образования Республики Казахстан (Грант № AP09057965).

Список использованной литературы

1. Найзабеков, А.Б. Условия развития сдвиговых деформаций при ковке, Алматы, Гылым, 1997.

2. Markov O.E. (2012) Forging of large pieces by tapered faces. Steel in Translation 42(12). 2012.- pp. 808–810.

3. Naizabekov A.B., Lezhnev S.N., Panin E.A. Research of the deformation process of blanks in the dies with elastic elements. Journal of Chemical Technology and Metallurgy, 52, 2, 2017. – pp. 205-212.

4. Андреященко, В.А., Ю.Б. Ичева, Особенности деформационного поведения конструкционной стали при ковке, Вестник Пермского национального исследовательского политехнического университета. Механика, 2018, № 4, С. 7-19.

5. Banaszek G, Bajor T., Kawałek A., Garstka T. Analysis of the Open Die Forging Process of the AZ91 Magnesium Alloy. Materials (Basel). 2020 Sep; 13(17): 3873.

6. A.A. Bogatov, D.Sh. Nukhov Forging of strip by alternating deformation, with unchanged size and shape, Steel in Translation, 45, 6, 2015, 412-417.

7. Машеков С.А., Биякаева Н.Т., Нуртазаев А.Е. Технология ковки в инструменте с изменяющейся формой. - Павлодар: Издательство «Кереку», 2008. - 485 с.

8. А.с. СССР №1409394 Способ изготовления поковок и инструмент для его осуществления. Воронцов В.К., Котелкин А.В., Найзабеков А.Б. и др. 1988.

9. Инновационный патент РК №30420. Инструмент для изготовления поковок. Найзабеков А.Б., Лежнев С.Н., Панин Е.А., Толкушкин А.О., 2015.

10. Патент РК №33694. Инструмент для изготовления поковок. Найзабеков А.Б., Лежнев С.Н., Панин Е.А., Богатов А.А., Толкушкин А.О., 2019.

11. Бернштейн М.Л., Рахштадт А.Г. Металловедение и термическая обработка стали. Справочник в 3 томах. Том 2 - Основы термической обработки. - М.: Машиностроение, 1983. – 368 с.

Extended research on the efficiency of internal crystallization chemical admixtures for cement concrete - mechanical and structural characteristics

Valeriy Naidenov
Institute of Mechanics[1], Bulgarian Academy of Sciences & Val technology Ltd, Sofia, Bulgaria
valna53@mail.bg

Abstract: *In recent years, the use of internal crystallization chemical admixtures for concrete and mortar to increase their water-tightness and other physical and mechanical characteristics has been of increasing importance in modern construction. These types of chemical modifiers allow for the effective replacement of conventionally performed waterproofing works (membranes, rolls, brushed or sprayed coatings, etc.) by purposefully improving the physical-mechanical characteristics of structural concretes, rendering them, to one degree or another, impermeable to water or/and aggressive agents from different origins. In the specialized world market for such products there are several leading competing companies - producers of internal-crystallization chemical admixtures, which have different activity in Bulgaria. The new extended research on such several new types of those admixtures were reported and discussed. The complex mechanical and structural tests are conducted and respective results are compared to predict the admixture's efficiency of their ability to limit the ingress of water into concrete and reinforced concrete sections, as well as their ability to increase the durability of concrete as the main structural material.*

Keywords*: PORTLAND CEMENT CONCRETE AND MORTAR, INTERNAL CRYSTALLIZATION CHEMICAL ADMIXTURES, CONCRETE WATERPROOFING, DTA, SEM, BET STRUCTURAL INVESTIGATIONS*

1. Introduction

In recent years, the use of internal crystallization chemical admixtures for concrete and mortar to increase their water-tightness and other physical and mechanical characteristics has been of increasing importance in modern construction. These types of chemical modifiers allow for the effective replacement of conventionally performed waterproofing works (membranes, rolls, brushed or sprayed coatings, etc.) by purposefully improving the physical-mechanical characteristics of structural concretes, rendering them, to one degree or another, impermeable to water or/and aggressive agents from different origins [1].

In the specialized world market for such products there are several leading competing companies-producers of internal-crystallization chemical admixtures, which have different activity in Bulgaria.

Since 2017 and at the moment, a part of the author's scientific interests are directed towards conducting specialized research for the comprehensive characterization of many such admixtures, more or less known on the Bulgarian market.

The admixtures, previously tested and compared are KRYSTALINE Add1, KRYSTALINE Plus 2.5, PENETRON Admix, XYPEX C1000 NF and BETOCRETE-CP-360-WP [2,3].

The present research is devoted to full-range testing and comparing of couple of different crystallization admixtures - KRYSTALINE Add1, Krystol Internal Membrane (KIM®), SIKA WT-200P, MAPEI Indrocrete KR1000 and ADING Hydrofob Crystal.

The purpose of the investigation is to assist all participants in the construction investment process in understanding the nature, specific characteristics and differences in the performance (effectiveness) of different products in terms of their ability to limit the ingress of water into concrete and reinforced concrete sections, as well as their ability to increase the durability of concrete as a main structural material.

2. Tests methods and comparative characteristics

The tests method used and all comparative characteristics are equal to previous already published ones [2,3]. The mix design of ordinary reference concrete (Table 1) was used to perform the studies, with the mineral composition of the cement being presented in Table 2.

For the purpose of comparative studies to the mix of reference concrete (Table 1), the appropriate crystallization chemical admixtures are incorporated in the dosage and according to the technology prescribed by their manufacturer.

The homogenization of the fresh concrete is accomplished by adding a metered amount of mixing water to obtain the same workability as assessed by the slump measure. The chosen method of comparison on the basis of **"equal workability"** of the concrete mixture is directly related to the actual production conditions at the construction site, where the **"workability"** factor is the key one to the quality of the concrete works performance.

The following physical-mechanical and structural characteristics have been selected to compare the same age of the fresh concrete and the hardened concrete:

- **fresh concrete** - water-cement ratio, consistency by slump test (cm), change of consistency in time after homogenization, air content (%);
- **hardened concrete** - compressive strength (MPa), splitting tensile strength (MPa), the static modulus of elasticity deformation (GPa), the depth of penetration of water under pressure (mm), frost resistance under an accelerated method (loss of mass change and the speed of ultrasound propagation) - cycles, structural studies (low-temperature gas absorption (BET method), differential thermal analysis (DTA), X-ray phase analysis (RFA) and scanning electron microscopy (SEM);
- **cement-sand mortar** - capillary absorption.

Table 1: *Concrete mix design.*

№	Materials	Quantity, kg/m^3
1.	Portland cement CEM II 42,5 A-LL, Devnya Cement Plant, Bulgaria	330
2.	River sand, fraction 0-4 mm, Quarry "Chepinzi"	810
3.	Crushed stone, fraction 4-11,2 mm, Quarry "Studena"	1060
4.	Mixing water for fresh concrete slump 13 cm (S3)	≈250 (for reference concrete)

Table 2 *Mineral composition of the Portland cement used*

Cement type	**Specific surface, cm^2/g**	**Mineral composition, % by mass**			
		C_3A	**C_3S**	**C_2S**	**C_4AF**
CEM II 42,5 / A-LL	3620	9,40	55,50	24,60	10,50

3. Description of crystallization admixtures tested

The description and basic peculiarities of the admixtures tested is given in Table 3. Their dosage rates are in accordance of the respective manufacturers.

KRYSTALINE Add1 has the advantage of being dosed in all cases in constant quantities (1,0 kg/m^3) regardless of the concrete formulation of the concrete. The only requirement is cement content above 300 kg/m^3.

Krystol Internal Membrane (KIM®), SIKA WT-200P, MAPEI Indrocrete KR1000 and ADING Hydrofob Crystal are dosed depending on the type and amount of cement used in the concrete mix design, which determines the need for specific calculations and non-constant costs in different projects.

Table 3 *Product description and dosage rates*

Product	**Description**	**Dosage rates (accordance producer's recommend-dations)**
KRYSTALINE Add1 Krystaline Technologies SA, Spain	Crystallizing waterproofing admixture with catalytic action to increase the water resistance and durability of concrete. Slightly slows down the concrete setting and hardening times and decreases exothermic. Self-healing cracks up to 0.5 mm wide.	1,00 kg/m^3 (permanent, regardless of the cement content)
Krystol Internal Membrane (KIM®)	Krystol Internal Membrane (KIM®) is a chemical admixture in dry powdered form, effective in creating waterproof concrete. It enhances the hydration process by intensifying and prolonging the hydration of the cementitious materials in concrete. The admixture delays the setting time of concrete. Self-healing cracks up to 0,5 mm wide.	6,60 kg/m^3 (2% by weight of cement, max 8 kg/m^3 concrete)
SIKA WT-200P, SIKA Limited, U.K.	SIKA WT-200P consists of mixture of cements, amino alcohols and fillers to increase the water resistance and concrete durability. Some specific conditions can affect the setting time. Self-healing cracks enhancement.	3,50 kg/m^3 (for concrete with min cement content 350 kg/m^3 and max water-cement ratio 0,45)
MAPEI Indrocrete KR1000, Italy	Indrocrete KR1000 is a mixture of active components which, in presence of water, transform the by-products of cement hydration into crystals reducing concrete porosity and micro-cracks. Self-healing cracks up to 0,4 mm wide.	6,6 kg/m^3 (1-3 kg/100 kg cementitious materials)
ADING Hydrofob Crystal, North Macedonia	Crystallizing waterproofing admixture with hydrophobic effect. Self-healing – no data available.	3,50 kg/m^3 (3-4 kg/m^3 concrete, min compressive class C25/30)

4. Results and discussion

The focus of this paper is to emphasize the significant differences in respective mechanical and micro-structural characteristics at 28-days of age. The first range of testing are performed in accordance of all respective Bulgarian and EN standards. The second one - by using of advanced direct physics methods - low-temperature gas absorption (BET method), differential thermal analysis (DTA), X-ray phase analysis (RFA) and scanning electron microscopy (SEM).

4.1. Mechanical tests

All results are presented in Table 4. The characteristics of the hardened concrete with equal workability of the fresh concrete show significant advantages of crystallization admixtures KRYSTALINE Add1 over Krystol Internal Membrane (KIM®), SIKA WT-200P, Indrocrete KR1000 and Hydrofob Crystal - compressive, tensile splitting strength and modulus of elastic deformation increasing, a reduced depth of water penetration under pressure and significantly higher frost resistance.

Table 4 *Mechanical characteristics*

CHARAC-TERISTICS	**COMPOSITIONS TESTED (at equal workability)**					
	Ref. concrete without admixture	**KRYS-TALINE Add1 1,0 kg/m^3**	**KIM®, Kryton 6,6 kg/m^3**	**SIKA WT–200 P 3,5 kg/m^3**	**Indrocrete 6,6 kg/m^3**	**Hydro-fob Crystal 3,5kg/m^3**
Volume density (mean), kg/m^3	2330	2320	2330	2320	2330	2310
Compressive strength, (mean), MPa compared to reference concrete, %	27,30 0	38,10 +39,56	32,00 +17,21	32,30 +18,32	32,70 +9,78	30,80 +12,82
Tensile splitting strength, (mean), MPa Compared to reference concrete, **%**	2,28 0	2,78 +21,93	2,69 +17,98	2,61 +14,47	2,71 +18,96	2,58 +13,16
Static elastic modulus,GPa compared to reference concrete, %	27,6 0	30,1 +9,1	29,0 +4,7	29,1 +5,4	29,4 +6,1	28,3 +2,2
Depth of water penetration under pressure, mm compared to reference concrete, %	36 0	10 -360	20 -180	21 -171	16 -225	17 -212
Freeze-thaw resistance, weight lost up to 2%: - %, after 2 cycles, (C_{frost} 75); - %, after 3 cycles (C_{frost}100); - %, after 4 cycles (C_{frost}150); - %, after 5 cycles (C_{frost}200)	1,82 (passed) 2,5	0,42 (passed) 0,92 (passed) 1,79 (passed) 2,03	1,03 (passed) 1,60 (passed) 2,13	1,08 (passed) 1,56 (passed) 2,19	0,77 (passed) 1,13 (passed) 2,04	1,03 (passed) 1,94 (passed) 2,46

4.2. Low temperature gas absorption (BET- method)

Gas adsorption is a modern method of characterizing porous materials. In the case of physical gas adsorption, inert gas (most commonly nitrogen) is adsorbed on the surface of a solid material. Based on the amount of adsorbed gas and the corresponding gas pressure, so-called an Arizona thermal adsorption curve from which basic parameters of the pore structure of materials can be determined.

The results are presented in Table 5 and Figures 1-6.

Table 5 *Micro-pore structure characteristics*

CONCRETE TESTED	STRUCTURE CHARACTERISTICS		
	Specific surface of pore structure, S_{BET}, m^2/g	**Total pore volume, Vt, cm^3/g**	**Pore size distribution by diameter, D_{av}, nm**
Reference concrete – without admixture	61	0,13	8,8
KRYSTALINE Add1	35	0,07	7,5
Krystol Internal Membrane (KIM®)	44	0,09	8,3
SIKA WT-200P	50	0,11	9,1
MAPEI Indrocrete KR1000	55	0,09	6,3
ADING Hydrofob Crystal	54	0,10	7,4

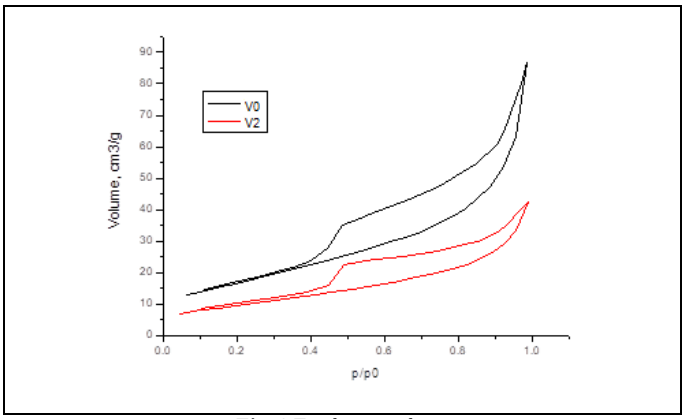

Fig. 1 *Total pore volume - Reference concrete (V0) vs. KRYSTALINE Add1 (V2)*

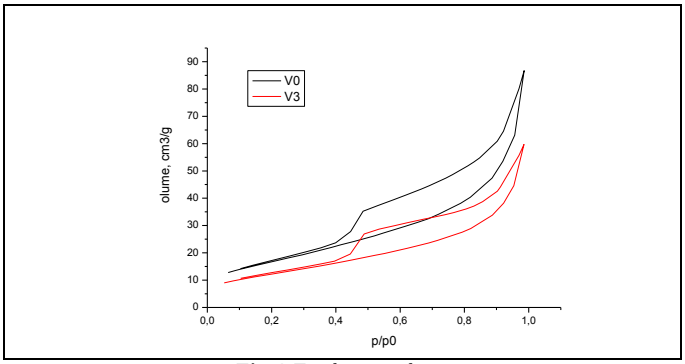

Fig. 2 *Total pore volume - Reference concrete (V0) vs.* Krystol Internal Membrane (KIM®) *(V3)*

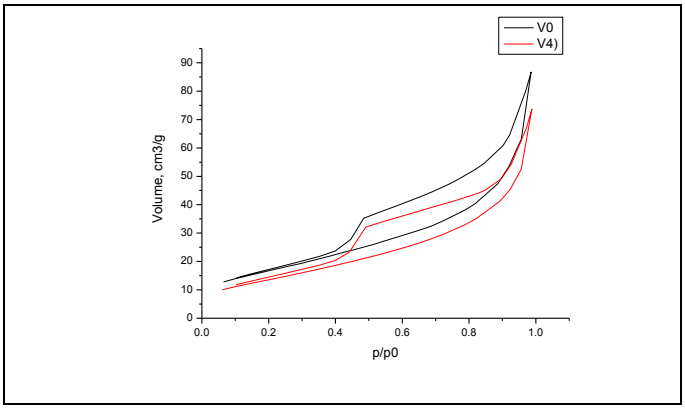

Fig. 3 *Total pore volume - Reference concrete (V0) vs. SIKA WT – 200P (V4)*

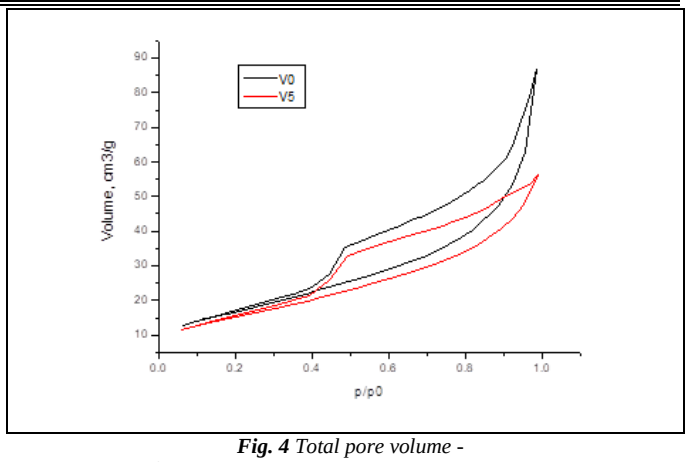

Fig. 4 *Total pore volume - Reference concrete (V0) vs. MAPEI Indrocrete (V5)*

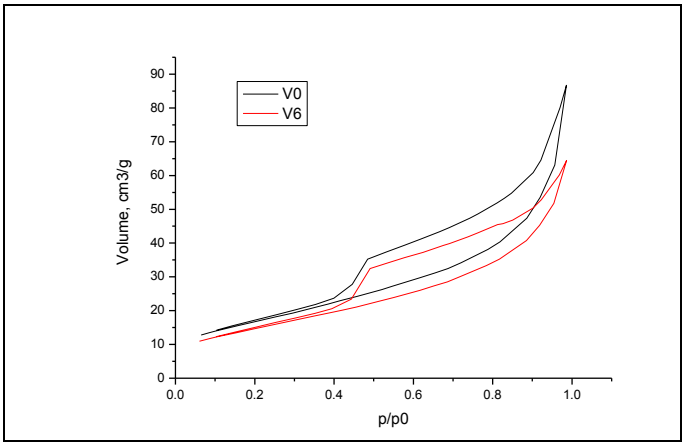

Fig. 5 *Total pore volume - Reference concrete (V0) vs Hydrofob Crystal (V6)*

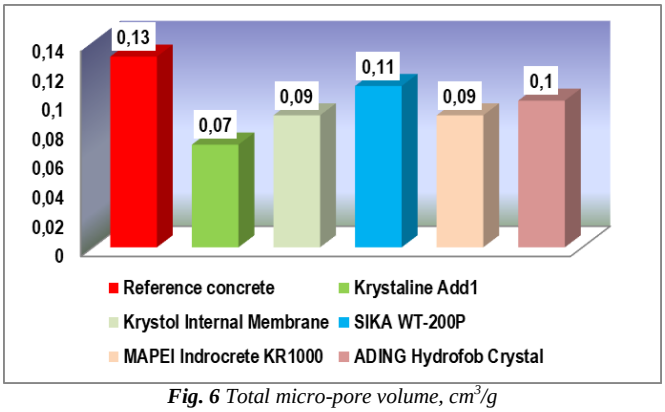

Fig. 6 *Total micro-pore volume, cm^3/g*

With the same workability of the fresh concrete, the crystallization admixture KRYSTALINE Add1 form a fine-dispersed cement stone structure in the concrete with a significantly reduced total micro pore volume, compared to the concrete with the participation of Krystol Internal Membrane (KIM®), SIKA WT-200P, Indrocrete KR1000 and Hydrofob Crystal.

4.2. Differential-thermal analysis (DTA)

The results are presented in Table 6 and Figures 7-12.

Differential thermal analysis (DTA) is a method that belongs to the set of direct physical methods for the study of crystalline structure in silicate composites. It is based on the characteristic feature of the hydrated formations in the cement stone to dehydrate in a precisely defined temperature range. The corresponding dehydration is accompanied by a characteristic thermal effect that alters the heat balance of the system. The monitoring of the respective endo- and exo-effects allows one to judge the phase transformations identified by the release of chemically bound water. Knowing the reference for the individual silicate formations and

temperatures of the phase transition, one can directly judge the presence and the indicative amount of the corresponding compound.

Table 6 *Structure characteristics*

CONCRETE TESTED	BASIC STRUCTURE COMPOSITIONS	
	Portlandite $Ca(OH)_2$, rel.%	**Crystals C-S-H, Calcite $CaCO_3$, rel.%**
Reference concrete (K "0") without admixture	2,311	9,108
KRYSTALINE Add1	1,600	11,089
Krystol Internal Membrane (KIM®)	1,939	9,866
SIKA WT-200P	2,183	9,391
MAPEI Indrocrete KR1000	2,016	10,953
ADING Hydrofob Crystal	2,238	9,403

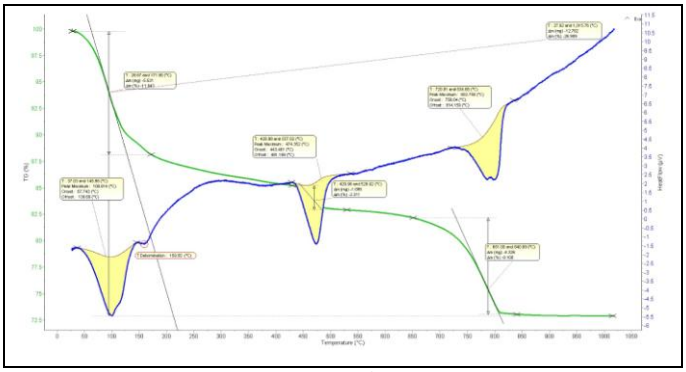

Fig. *7 DTA - Reference concrete*

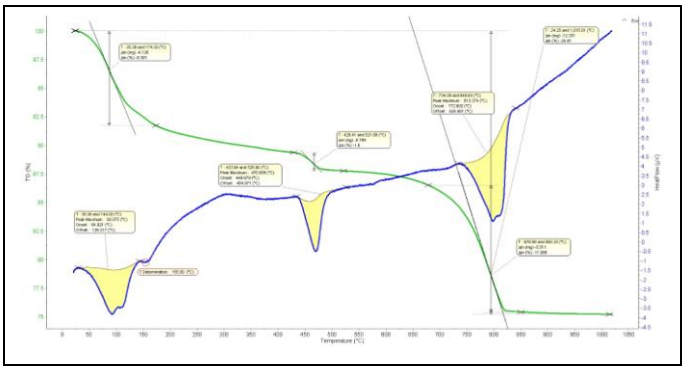

Fig. 8 *DTA - KRYSTALINE Add1*

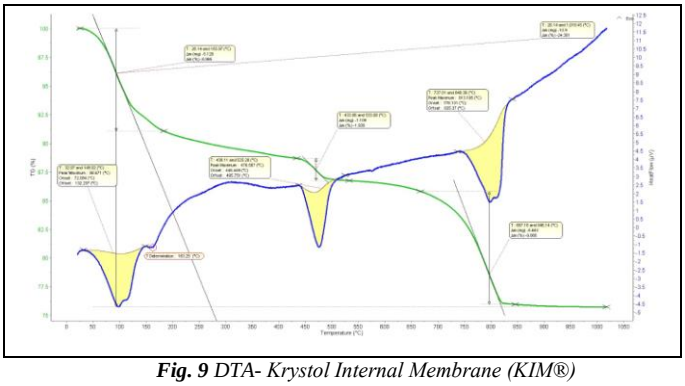

Fig. 9 *DTA- Krystol Internal Membrane (KIM®)*

With the same workability of the fresh concrete, the crystallization admixtures KRYSTALINE Add1 form a waterproof crystalline structure with a predominant involvement of CSH-type high-alkalinity hydrate formations (main carriers of high mechanical properties of the composite), compared to concrete with Krystol Internal Membrane (KIM®), SIKA WT-200P, Indrocrete KR1000 and Hydrofob Crystal.

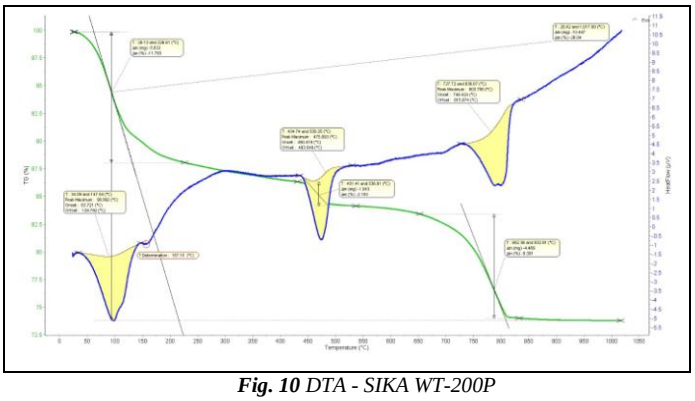

Fig. 10 *DTA - SIKA WT-200P*

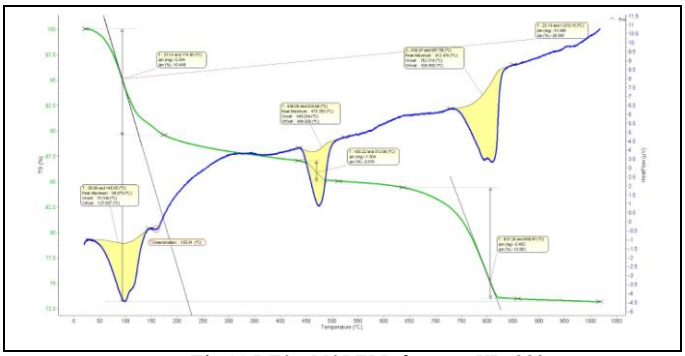

Fig.11 *DTA - MAPEI Indrocrete KR1000*

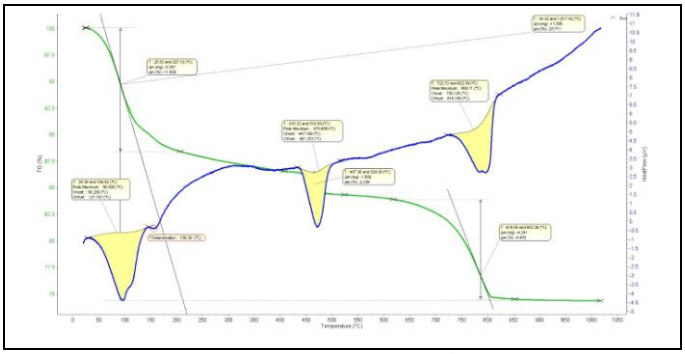

Fig. 12 *DTA - ADING Hydrofob Crystal*

4.3. Scanning Electron Microscopy (SEM)

The results are presented in Photos 1-6.

Scanning electron microscopy (SEM) is performed using a high magnification electron microscope (up to 10,000 times), resulting in visual data on the shape and size of individual sub-microscopic crystals, their growth, decomposition and destruction processes, and this base passed is sued for past chemical interactions in solution and solid phase, incl. to seal the structure.

In support of the demonstrated significant advantages with respect to the basic physics-mechanical properties of the crystallization additive KRYSTALINE Add1 over Krystol Internal Membrane (KIM®), SIKA WT-200P, Indrocrete KR1000 and Hydrofob Crystal, are the results obtained by using modern direct physics-chemical methods. They show that the concrete with KRYSTALINE Add1 form a denser waterproof crystalline structure with a dominant participation of high-alkalinity C-S-H hydrate formations, bearing high mechanical performance of the composite.

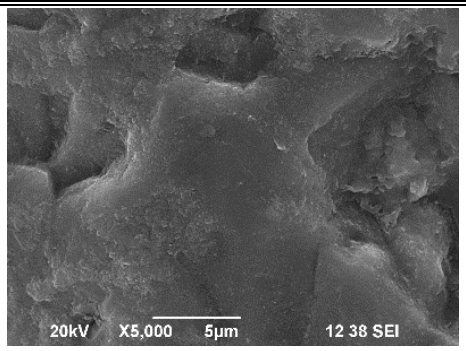

Photo 1 *Reference concrete*

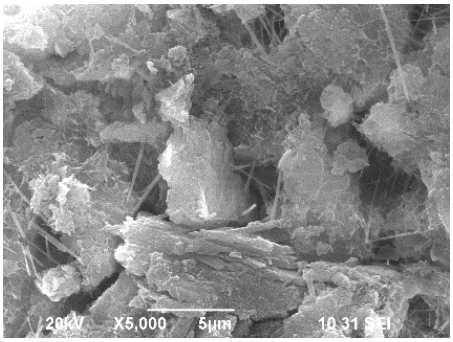

Photo 2 *KRYSTALINE Add1*

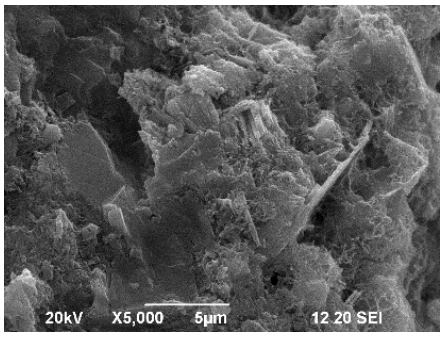

Photo 3 *Krystol Internal Membrane (KIM®)*

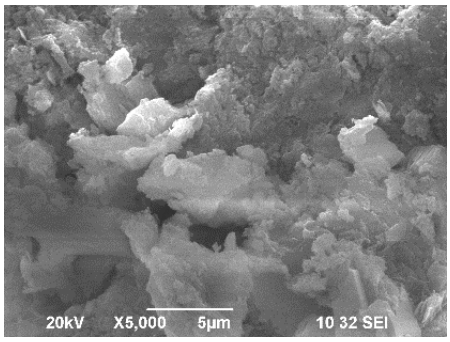

Photo 4 *SIKA WT-200P*

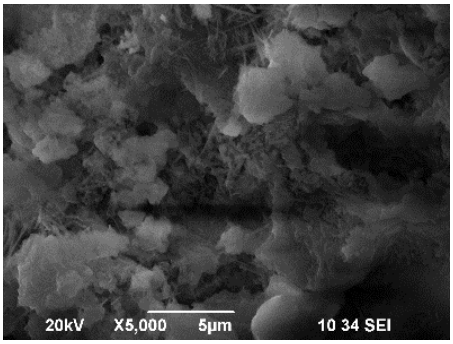

Photo 5 *MAPEI Indrocrete KR1000*

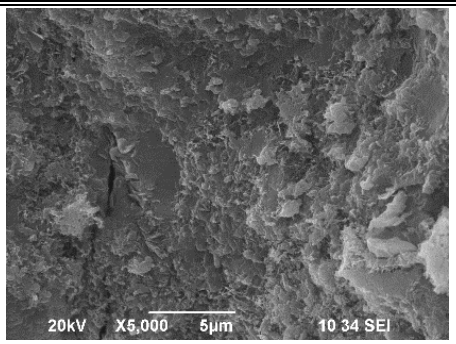

Photo 6 *ADING Hydrofob Crystal*

5.Conclusions

The above comprehensive comparative analysis for the evaluation of the basic physical-mechanical and structural characteristics of the fresh and hardened concrete with 5 types of internal crystallization chemical admixtures entering the Bulgarian construction market, objectively presents the characteristics of the compared products.

In accordance with the stated goal, this report is able to assist the participants in the investment construction process (investors, designers, contractors, project managers and supervisors), in situation of an informed choice, to evaluate the complex advantages of KRYSTALINE Add1 vs. Krystol Internal Membrane (KIM®), SIKA WT-200P, Indrocrete KR1000 and Hydrofob Crystal.

Concretes with the participation of KRYSTALINE Add1 (with a constant dosage rate of 1,0 kg/m^3), ensure the impermeability and safe water-tightness of the concrete cross section, even under water pressure, without the need for additional waterproofing activities of various types - brushed and sprayed coatings, coiled and membrane conventional systems. At the same time, such concrete has increased frost-resistance and durability without the need for accompanying repair and restoration work.

By all tested parameters, concrete with KRYSTALINE Add1 outperformed with Krystol Internal Membrane (KIM®), SIKA WT-200P, Indrocrete KR1000 and Hydrofob Crystal.

6. References

1. Maher Al-Jabari, Integral waterproofing of concrete structures – Advanced protection technologies of concrete by pore blocking and lining, Elsevier Ltd., 2022, ISBN: 978-0-12-824355-8, USA.

2. V. Naidenov, M. Mironova, I. Rostovsky, Investigation on the efficiency of internal crystallization chemical admixtures for cement concrete - mechanical characteristics, *International Conference Materials, Methods & Technologies, 22-26 June 2020 in Burgas, Bulgaria, ISSN 1314-7269, Volume 14, (25-31).*

3. V. Naidenov., M. Mironova, Investigation on the efficiency of internal crystallization chemical admixtures for cement concrete – structural characteristics, International Scientific Journal "MACHINES. TECHNOLOGIES. MATERIALS", Issue 3/2020, Year XIV, ISSN print 1313-30226, ISSN web 1314-507X (114-128).

Processing and properties of polymer - mineral compositions

Tomasz Garbacz[1,*], Aneta Tor-Swiątek[1], Lukasz Garbacz[2]
Lublin University of Technology, Lublin, Poland[1]
Doctoral School at the Lublin University of Technology, Lublin, Poland[2]
t.garbacz@pollub.pl

Abstract: *Recycled plastics find more and more applications. In addition to recycled bulky products, the number and type of products also being used in polymer -mineral composites based on recycled PE and PP. One of the paving products sought by investors are traditional concrete blocks. However, they have their drawbacks, they are heavy, so their transport, logistics must meet stricter requirements, are products that are not very resistant to cracking as a result of impact, are fragile. Mineral-polymer products are the solution to such problems. Innovative compositions for their processing are a polymer - mineral mixture, containing mainly recycled material and mineral fillers (sand, ceramic waste dust). They are therefore products made of waste materials from recycling, recyclates and flakes of polymer materials.*

The technology for producing the polymer - mineral composition is based on the extrusion and compression molding technology of the compositions obtained. Polymer compositions are secondary materials, after recycling in the form of recyclates, flakes, and waste plastics, mineral fillers, that is waste ceramic dust, sand as well as activating substances (dyes, plasticizers, adhesion compatibilizers, polymer-mineral wetting agents). As a result, plastic waste and ceramic waste that cannot be recycled will be effectively processed. The sprinklers were made of various polymer materials (PP, HDPE) as well as characterized by different shape of working elements and a variable degree of contamination with mineral sludge. The research on the structure of manufactured materials and melt flow rate are presented. The influence of the type of material and mineral deposits on the process ability of the tested polymer-mineral compositions was determined.

Keywords*: RECYCLED PLASTICS, POLYMER SANDS COMPOSITES, POLYMER PROCESSING, PROPERTİES OF COMPOSİTES*

1. Introduction

Material recycling of polymeric plastics makes it possible to achieve measurable savings, as well as their management, this applies to more and more plastic waste that otherwise must be landfilled. There is a need to produce compositions and products that have the performance characteristics of porous polymeric materials and the performance characteristics of mineral material products [1-5], which will be characterized by the visual effect of a porous structure, high mechanical strength, impact strength and hardness, low abrasiveness, high weather resistance and low manufacturing cost [1, 4-6]. In addition, for environmental reasons, there is a need to use post-production and post-consumer waste of polymer plastics, mineral post-production waste such as fly ash and ceramic waste, which occurs in large quantities [5, 6-12]. The mineral filler in the produced composition is, for example, silica fly ash which is a by-product of coal combustion, shredded ceramic waste which is post-production waste, construction quartz sand.

Fig. 1 *Main components of polymer - mineral composition; recycled polymer plastic and mineral waste, example*

A product that can be made from plastic waste with a few tens of % addition of mineral compounds are polymer-mineral compositions, which, when processed by extrusion, can be used to produce garden architectural elements (bench slats, balcony panels, outdoor floor profiles), replacing concrete, ceramic, cast and vibro-pressed products [13-20]. Polymer compositions can be made from recycled plastic, after recycling in the form of recyclates, flakes, and waste plastics, mineral fillers, that is, waste industrial dust, ceramic waste or sand. As a result, plastic waste and mineral, ceramic waste, which so far cannot be reused, will be efficiently processed to create new products [14, 20, 21-25].

The expected performance characteristics of the polymer-mineral composition products are as follows:

- manufactured from recycled waste plastics,
- shape, dimensions do not differ from concrete products,
- have a smooth or textured surface,
- are not subject to mechanical damage, do not break, do not crack,
- are as much as about 30% lighter than traditional products,
- are characterized by very low hygroscopicity, ease of cleaning,
- are resistant to oils, greases, acid compounds,
- are characterized by complete frost resistance, up to -70°C,
- have a variety of colors, uniform color throughout the mass of the product [4, 6, 10, 13, 22].

The essence of the material produced is a polymer-mineral composition for the manufacture of building and garden architecture products by extrusion and pressing, mainly sections such as bench slats, balcony panels, outdoor floor panels, paving blocks, paving slabs and others [23-31].

The purpose of the work is to determine the possibility of recycling and reuse of plastic waste containing several tens of percent mineral waste. The scope of work includes the study of the recyclability of polymer recyclate, using the Melt Flow Rate (MFR) method and the processing of polymer-mineral recyclate in the extrusion process. The scope of work also includes structural studies of the morphology of the produced polymer-mineral composites [30-37].

2. Materials and methods

Recycled plastics find more and more applications. In addition to recycled bulky products, the number and type of products also being used in polymer sands composites based on recycled PE and PP. One of the paving products sought by investors are traditional concrete blocks. However, they have their drawbacks, they are heavy, so their transport, logistics must meet stricter requirements, are products that are not very resistant to cracking as a result of impact, are fragile. Polymer - mineral products are the solution to such problems. Innovative compositions for their processing are a mineral-polymer mixture, containing mainly recycled material and mineral fillers (sand, ceramic waste dust). They are therefore products made of waste materials from recycling, recyclates and flakes of polymer materials.

The process water cooling sprinklers found in this type of cooling equipment have very large dimensions of 300x300x2400 mm. They are mainly made of PP, HDPE and PVC, and so far have not undergone any recovery and recycling processes leading to the manufacture of products from these materials. The waste panels are composed of about 5-20% plastics, and strongly associated sludge, primarily mineral, in amounts ranging from about 80 to 95% by weight. So far, in practice, used sprinkler parts are a huge amount of about 50 thousand tons per year, and in Poland alone, are not subjected to any recovery and recycling processes. This means that every year thousands of tons of plastic waste from the overhaul of cooling towers and fan coolers end up in landfills or are deposited in disused mines and will decompose emitting CO_2 and other toxic substances into the atmosphere for the next 100 years.

Fig. 2 *View of used cooling tower sprinklers used in processability studies of polymer - mineral composites.*

Four types of cooling tower sprinklers were used in the conducted research immediately after disassembly from cooling towers. These are sprinklers made of HDPE and PP. The sprinkler samples used differ primarily in the degree of mineral contamination, resulting from the use of the sprinkler in question. This includes the way it is used, the cooling conditions, the type and quality of the cooling medium. This translates, in effect, into the amount and type of organic contamination in the tested sprinklers.

3. Results and Discussion

The technology for producing the polymer - mineral composition is based on the extrusion and compression molding technology of the compositions obtained. Polymer compositions are secondary materials, after recycling in the form of recyclates, flakes, and waste plastics, mineral fillers, that is waste ceramic dust, sand as well as activating substances (dyes, plasticizers, adhesion compatibilizers, polymer-mineral wetting agents). As a result, plastic waste and ceramic waste that cannot be recycled will be effectively processed.

Fig. 3 *The appearance of the shredder blades and the made polymer-mineral recyclate.*

The samples were subjected to a knife grinding process in a single shaft XC-GP 230 from Xiencheng, with a drive power of 4.0 kW. A sieve with a hole size of 5.95 mm was used.
Fig. 3 shows an example of the samples to be subjected to grinding. The sprinklers were made of various polymer materials (PP, HDPE) as well as characterized by different shape of working elements and a variable degree of contamination with mineral sludge.

Fig. 4 *Appearance of particulate refresher plates and mineral sludge for the production of polymer - mineral composites.*

The polymer processing was carried out with the use of a single-screw extruder, type W-25 with the screw diameter of D=25 mm. The plasticizing unit was equipped with four heating zones. The process line was composed of the extrusion coating head, vacuum calibrator, the cooling bath and the remaining process line components.

The extrusion head used in the conducted research, is used for extruding a section in the form of a strip has a width - 15.5 mm, while the height of the nozzle is 2.0 mm. The extrusion head has two heating zones and corresponding two ring heaters mounted on the head body. The laboratory extrusion line for poring sections also includes a cooling bath, with a length of 1740 mm, a width of 220 mm and a depth of 200 mm. A belt extraction system was also used in the study, designed to transport the extrudate using a 100 mm wide, 2000 mm long belt.

Fig. 5 *Experimental investigations of the possibilities of effective production, by plasticizing with extrusion, of new polymer - mineral compositions.*

The process of extrusion of HDPE and PP recyclates was realized with the developed and set conditions, set in the extrusion process line. They are as follows: the temperature of the heating zones of the plasticizing system, respectively: 160, 170, 180 and 190 ^{o}C; head temperature in the heating zones 190 ^{o}C. The set screw speed was changed in the range of 0.83÷1.66 s-1 (50÷100 rpm). The temperature of the coolant in the cooling bath, determined by a temperature sensor, was in the range of 16÷19 ^{o}C.

The Melt Flow Rate (MFR) is a measure of the ease of flow of the melt of a thermoplastic polymer. It is defined as the mass of polymer, in grams, flowing in ten minutes through a capillary of a specific diameter and length by a pressure applied via prescribed alternative gravimetric weights for alternative prescribed temperatures. The method is described in the similar standards ASTM D1238 and ISO 1133. MFI tests were carried out on the test stand equipped with a Ceast weight plastometer type 6542.00 with additional equipment and a laboratory balance.

Fig. 6 *View of MFI instrument, Ceast 6542.0 and selected measurement samples.*

The results of tests of the melt flow rate of recyclates, produced from cooling tower sprinklers, are characterized by MFR values ranging from 0.10 to 1.69 g/10 min. Such a wide range of MFR is mainly due to the content of mineral deposits deposited on the plastic.

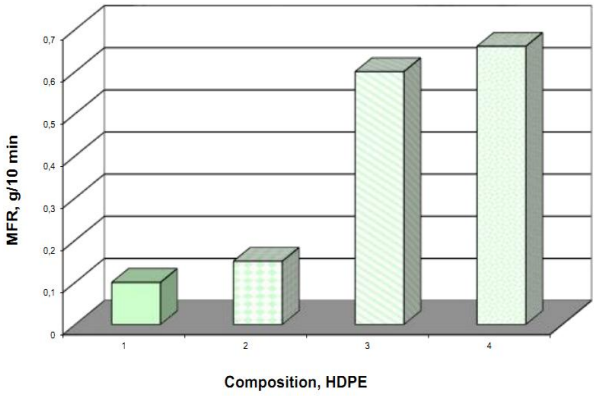

Fig. 7 *Block diagrams illustrating the dependence of MFI on contents of polymer compositions with HDPE.*

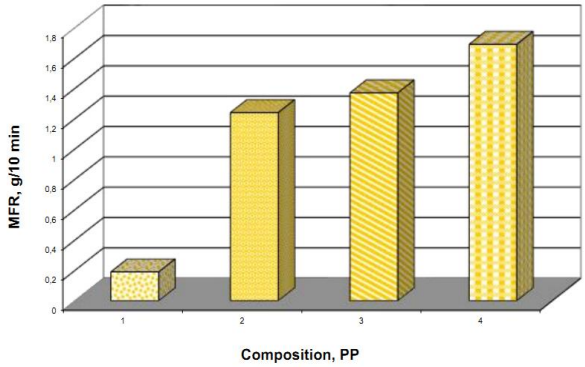

Fig. 8 *Block diagrams illustrating the dependence of MFI on contents of polymer compositions with PP.*

Samples of untreated recyclate, had in their composition a significant amount of crushed sludge, bound to flakes and in loose form, which affected their lower processability. The determined values of the melt flow rate indicate the possibility of their further processing by extrusion and injection molding.

The investigation and analysis of the porous structure of the produced parts were conducted using an confocal microscope, type Nikon Eclipse LV100ND and copyright position of image analysis of structure. The morphology shows that the plastic-mineral structure is present throughout the cross-section. No solid outer layer is visible, with no mineral filler content. The resulting structure is characterized by the variable position of the mineral filler in the polymeric material. This is due to the type and amount of mineral waste in the shredded sprinklers.

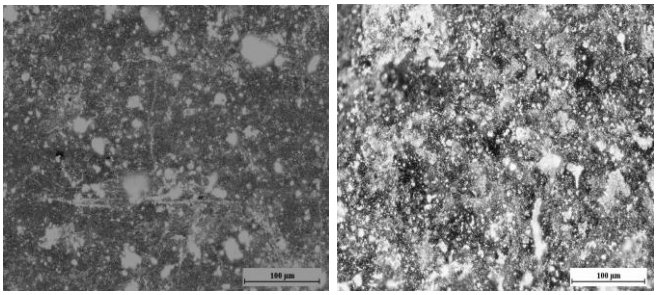

Fig. 9 *Fragment of the cross section of the polymer compositions with HDPE, test samples 1 and 2.*

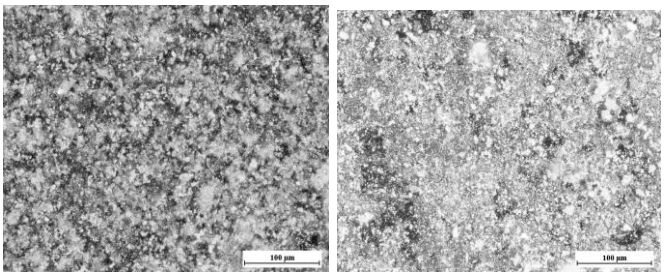

Fig. 10 *Fragment of the cross section of the polymer compositions with with HDPE, test samples 3 and 4.*

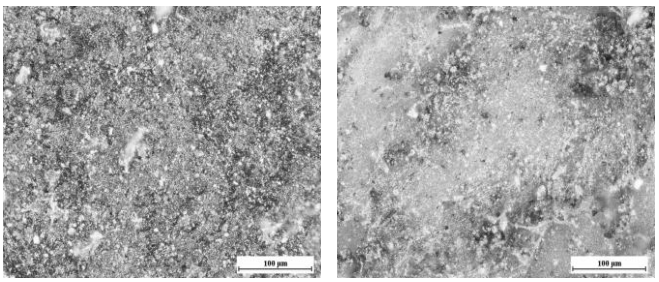

Fig. 11 *Fragment of the cross section of the polymer compositions with PP, test samples 1 and 2.*

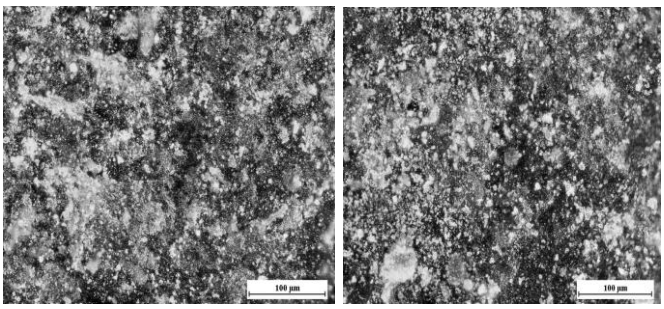

Fig. 12 *Fragment of the cross section of the polymer compositions with PP, test samples 3 and 4.*

Microscopic examination of the morphology showed a significant difference in the structure of the different compositions. The precipitate visible on the surface of the sprinklers has a significantly lighter hue. Compositions 3-4 have a visible yellow glow, which is the residue of the precipitate. . All compositions were characterized by heterogeneity in the distribution of sediments and irregularity in their dimensions. In addition, in the studied compositions, mineral sediments form agglomerative clusters distributed irregularly on the surface.

4. Conclusions

The packaged design of shredders, in which thin-walled, interconnected plastic elements are separated by voids containing air or varying amounts of solidified mineral sludge, causes difficulties in the shredding process and requires the development of both the appropriate geometry of the working elements of the shredding system and the selection of tool materials and their surface treatment. The heterogeneity of the shredded waste and the variable content of impurities can adversely affect the stability of the shredding and purification processes and result in difficulties in selecting appropriate process parameters.

The trials and tests carried out will enable the preparation of a prototype sample batch of recyclates purified and with different contents of mineral fraction derived from sprinkler sludge, bound to plastic and obtained during separation of shredding and waste treatment products, to be scheduled for subsequent stages of testing.

The results of tests of the melt flow rate of recyclates, produced from cooling tower sprinklers, are characterized by MFR values ranging from 0.10 to 1.69 g/10 min. Such a wide range of MFR is mainly due to the content of mineral deposits deposited on the plastic.

Microscopic examination of the morphology showed a significant difference in the structure of the polymer compositions. The precipitate visible on the surface of the sprinklers has a significantly lighter hue. Above that, the amount of type and amount of mineral precipitate is different in each case. All compositions were characterized by inhomogeneity of distributed precipitates and irregularity of their dimensions, especially visible in composition 1. In addition, in the case of composition 4, the precipitates form agglomerative clusters distributed irregularly on the surface of the produced test samples.

5. References

1. T. Garbacz, L. Dulebova, V. Krasinsky, Adv. Sci. Technol. Res. J., 18, 74-80 (2013)
2. T. Standau, C. Zhao, S. Murillo Castellón, C. Bonten, V. Altstädt, Polymers, 11, 306-315 (2019)
3. M. Mahdavi, O. Yousefzade, H. Garmabi, Adv.Polymer Tech., 37, 3017-3026 (2018)
4. D. Sykutera, M. Bieliński, Polimery-W, 59, 602-605 (2014)
5. J-M. Pin, A. Tuccitto, M.E. Shivokhin, P.C. Lee, Polymer, https://doi.org10.1016/j.polymer.2020.123123 (2020)
6. T. Garbacz, Polimery-W, 57, 91-94 (2012)
7. Z. Han, Y.Zhang, W. Yang, P. Xie, Key Engineering Materials, 717, 68-72 (2016)
8. J. Guo, Ch. Zhang, Sh. Liang, W. Zou, Polym. Eng. Sci., https://doi.org10.1002/pen.25499 (2020)
9. D. Chandramohan, International Journal of Advanced Engineering Sciences and Technologies, 6, 97-104 (2011)
10. K. Głogowska, J. Sikora, B. Duleba, Journal of Polymer Engineering, 7, 36, 705-712 (2016)
11. J. Janik, Kompozyty, 4, 10, 205-211 (2004)
12. J. Korol, J. Lenża, D. Burchart-Korol, K. Bajer, Przemysł Chemiczny, 11, 91, 2196-2201 (2012)
13. E. Kowalska, Z. Wielgosz, M. Zubrowska, S. Pasynkiewicz, M. Choroś, Polimery -W, 49, 828-836 (2004)
14. S.T. Peters, *Handbook of Composities* (Mountain View, California, 1998)
15. M. Szostak, N. Antczak, M. Barczewski, J. Andrzejewski, T. Klepka, Przetwórstwo Tworzyw, 5, 451-457 (2014)
16. J. Kijeński, A.K. Błędzki, R. Jeziórska, *Recovery and recycling of polymeric materials* (PWN, 2011)
17. M. Goliszek, B. Podkościelna, T. Klepka, O. Sevastyanova, Polymers, 12, 1159-1177 (2020)
18. T. Klepka, R. Jeziorska, A. Szadkowska, Przemysł Chemiczny, 94, 1352–1355 (2015)
19. Ch. Rauwendaal, E.M. Pilar Noriega, *Troubleshooting the extrusion process: a systematic approach to solving plastic extrusion problems* (Hanser Publishers, 2001)
20. M. Świetlicki, D. Chocyk, T. Klepka, A. Prószyński, A. Kwaśniewska, J. Borc, G. Gładyszewski, Materials, 13, 698-711 (2020)
21. L. Dulebova, T. Garbacz, Adv. Sci. Technol. Res. J., 11, 66–71 (2017)
22. T. Klepka T., H. Dębski, H. Rydarowski, Polimery-W, 54, 668-672 (2009)
23. M. Celina M., K.T.Gillen R.A. Assink, Polymer Degradation and Stability, 90, 395-404 (2005)
24. T. Standau, C. Zhao, S. Murillo Castellón, C. Bonten, V. Altstädt, Polymers, 11, 306-315 (2019)
25. S. Ghosh, D. Khastgir, A. Bhowmick, Polymer Degradation and Stability, 67, 427-436 (2000)
26. Y. Hu, A. W. Lang, X. Li, S.R. Nutt, Polymer Degradation and Stability, 110, 464-472 (2014)
27. M. Ito, K. Nagai, Polymer Degradation and Stability, 93, 1723-1735 (2008)
28. J. Korol, J. Lenża, D. Burchart-Korol, K. Bajer, Przemysł Chemiczny, 91, 2196-2201 (2012)
29. E. Kowalska, Z. Wielgosz, M. Zubrowska, S. Pasynkiewicz, M. Choroś, Polimery -W, 49, 828-836 (2004)
30. P. Palutkiewicz, P. Postawa, Journal of Cellular Plastics, 52, 399-418 (2016)
31. A.Woszuk, W. Franus, Logistyka, 4, 6819-6827 (2015)
32. M. Xanthos, *Functional fillers for plastics* (Wiley-VCH Verlag GmbH & Co. KGaA, Weinhaim, 2010)
33. Y. Zhao, B. Choi, A. Chudnovsky, International Journal of Fatique, 51, 26-35 (2013)
34. S. Zha, H. Lan, International Journal of Pressure Vessels and Piping, 189, 104270-104282 (2021)
35. D. Chandramohan, International Journal of Advanced Engineering Sciences and Technologies, 6, 97-104 (2011)
36. H. Leda, *Polymer composites with continuous fibers* (Wydawnictwo Politechniki Poznańskiej, Poznań 2006)
37. X. Zhang, R. Ma, J. Liu, W. Wu, Journal of Polymer Engineering, doi.org/10.1515/polyeng-2019-0024 (2019)

CeO_2-ZrO_2 Multi-layer Cubic Coatings Obtained by Sol-Gel Technology

Vladimir Petkov, Mihaela Aleksandrova, Bojidar Jivov, Marieta Gacheva

Bulgarian Academy of Sciences, Institute of Metal Science, Equipment, and Technologies with Center for Hydro- and Aerodynamics "Acad. A. Balevski ", Shipchenski Prohod Blvd. 67, 1574 Sofia, Bulgaria, vladimir2pe@yahoo.com

Abstract: *A solution was synthesized in a system* ZrO_2-CeO_2 *by sol-gel synthesis and deposited by the immersion method. The pretreated Nb substrate was treated with sulfuric acid and absolute alcohol solutions. Layering was in three stages. The sample was heat treated at 500°C. The obtained results are characterized by XRD, XPS, CEM analyzes.*

Key words: *SOL-GEL, DIP-COATING,* ZRO_2-CEO_2*, XRD, CEM*

1. Introduction

In the last few decades, intensive work has been done on the synthesis of layers and bulk materials (hybrid, composite) from ZrO_2-Al_2O_3 by the sol-gel method. A number of valuable qualities of the obtained compounds and materials have been established, such as: very good mechanical properties including resistance to wear, high chemical and thermal resistance, inertness to various corrosive environments, very good adhesion to various supports and sub-layers - inorganic, organic and composite inorganic - organic. [1-11]. The use of sol-gel technology allows to obtain uniform homogeneous thin films (at the molecular level) at much lower temperatures and in a shorter time than conventional solid-phase methods. Through this method, compounds with very good optical properties are also obtained. The sol-gel method allows the effective combination with other methods such as hydrothermal production, co-precipitation, combustion, etc. [6,10]. The mentioned qualities make it possible for the ZrO_2-Al_2O_3 samples obtained by sol-gel technology to be used on an industrial scale as well. It should be emphasized that the ZrO_2-Al_2O_3 system is effectively studied both from an applied and from a scientific point of view regarding the production of layers, as well as for composite bulk materials. For the synthesis of the thin films, the following were used: inorganic, organic and mixed inorganic - organic starting substances such as organic precursors predominate [1-11]. Vitanov and al. pay special attention to the formation of amorphous phases in zirconium oxide - aluminum oxide under the influence of the promoting effect of Al_2O_3. The authors synthesized thin films by the sol-gel method using the dipping technique. Combined organic-inorganic precursors were successfully used to deposit the layers of ZrO_2-Al_2O_3, which have very good dielectric properties and allow them to be used at relatively high temperatures [1,2]. Of particular interest are the results obtained by Malkai et al. for new composite materials in the ZrO_2-Al_2O_3 system – The authors synthesized tetragonal ZrO_2 stabilized as a result of the promoting effect of Al_2O_3. The obtained zirconium dioxide is stable even after annealing at 1450°C [3]. Asl obtains ZrO_2 and ZrO_2 – Al_2O_3 thin layers which it deposits on aluminum alloy AA 2024. It uses inorganic and organic precursors establishing the very good anti-corrosion properties of the layers[4]. Hao used a sol-gel method to obtain composite membranes based on ZrO_2–Al2O3 at a zirconium dioxide molar content of 50%. The authors found that upon tempering in the range 700-1100°C, tetragonal ZrO_2 is formed without the presence of other phases. Both inorganic and organic precursors have been used [5]. Nouri synthesized ZrO_2 – Al_2O_3 composite nano powders from organic starting materials without using stabilizing substances, finding that at 20% molar content of Al_2O_3 and annealing at 1100°C, only a tetragonal phase of ZrO_2 is obtained in the absence of a monoclinic phase. Annealing from 500°C Leads to the formation of an intermediate amorphous phase [6]. Wasim obtained bio-nano-structured composites by annealing at 1000°C by stabilizing ZrO_2 by adding 4%YCl_3. The resulting composite is 15 – 25 nm in size. The influence of heating was investigated and it was found that even at 1000°C the obtained tetragonal zirconium dioxide does not undergo phase changes [7]. X.Zhang synthesizes crack-free ZrO_2-Al_2O_3 materials by sol-gel method and immersion technique. The authors used isothermal and cyclic oxidation of coated and uncoated TiAl-based alloy samples (annealed at 1000°C). Coatings have been found to reduce the oxidation rate of alloys and increase their resistance to applied cyclic oxidation.[8] Kikkawa synthesized by burning ZrO_2 – Al_2O_3 material using inorganic precursors and found that at temperatures below 1000°C tetragonal ZrO_2 with dimensions of 17nm is formed [9]. W.Zhang obtained from inorganic precursors an amorphous sol using 1 day aging at 20°C [10].

Current research is aimed at the synthesis and deposition of thin films of the ZrO_2-CeO_2 system on a pure niobium substrate and the characterization of the obtained results.

2. Experimental part.

Zirconium oxochloride $ZrOCl_2.8H_2O$ was dissolved in absolute alcohol used to prepare a 0.1M solution by the sol-gel method. It is dissolved in HNO_3 in a certain stoichiometric ratio. $Ce(NO_3)_3.6H_2O$ dissolved in isopropanol to a 0.4M solution was also used as a precursor. The Nb substrate was previously cleaned in H_2SO_4 and absolute alcohol. Dip into the solution and withdraw at a constant speed of 3 cm/min. Immersion takes place in three stages. The first stage is the deposition of seven layers in the $ZrOCl_2.8H_2O$ solution. The second stage is the deposition of 3 layers in a solution of $Ce(NO_3)_3.6H_2O$. The third stage is mixing the two solutions into one common and again depositing three layers. After each deposition, the sample is dried at 120°C. Thermal treatment is at 500°C with a delay of 2 hours.

3. Results and discussions

X-ray analysis was performed with CuKa-radiation (Philips PW 1050 apparatus). XPS analysis was used to characterize the electronic structure of the films and SEM analysis (Philips 515 apparatus used) was used to determine the morphology of the sample.

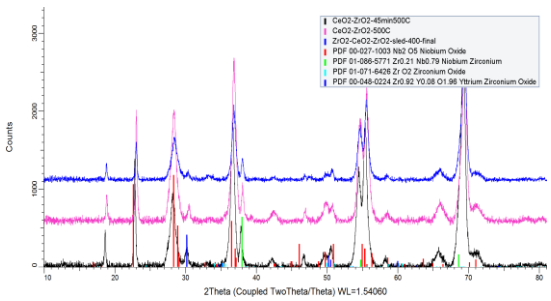

Fig. 1 X-ray analysis of the specimen

X-ray phase analysis data (Fig. 1) show that nanocrystalline phases are formed after isothermal heating. Figure 1 shows the oxides of ZrO_2, Nb_2O_5, a mixture of CeO_2-ZrO_2, and also the intermetallic $Zr_{0.21}$ $Nb_{0.79}$. At 18.5°, 19° 2θ a cubic ZrO_2 phase is observed. No monoclinic zirconium oxochloride phase is contained

XPS analysis

XPS (fig.2) measurements were performed with an electron spectrometerAXIS Supra (Kratos Analytical Ltd.),using a monochromatic AlKα X-ray source with a photon energy of 1486.6 eV and a surface charge neutralization system. The binding energy (BE) was determined with an accuracy of ±0.1 eV using the C1s line at 284.6 eV (of adsorbed hydrocarbons) as a reference. The chemical composition of the films was determined based on the areas and binding energies of the photoelectron peaks.Kthe concentrations of the various chemical elements (in atomic %) were calculated by normalizing the areas of the photoelectron peaks to their relative sensitivity factors.

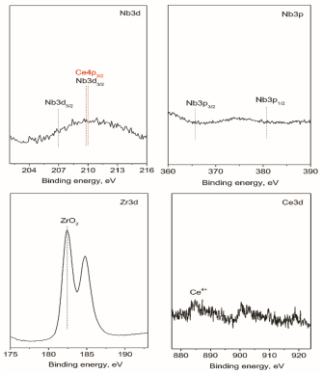

Fig. 2 XPS analysis of the sample

XPS analysis of the sample confirmed the result of the X-ray analysis. CeO_2 and ZrO_2 peaks were found. Binding energies for Zr 3d – 182.2 and 184.5 eV are characteristic of ZrO_2 and of Ce3d – about 885 eV characteristic of CeO_2. The obtained niobium spectra are from the substrate (sample) on which the sol-gel films were deposited.

CEM analysis

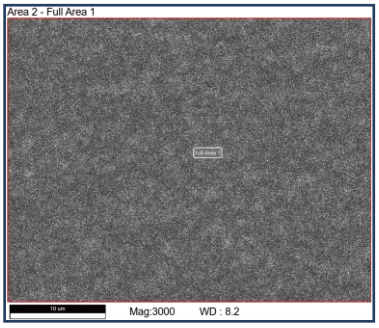

Fig. 3. SEM image of the surface of the deposited sol-gel layer

Figure 3 shows the morphology of the coated sample from a layer with a fine-grained structure. This fine layer is uniform and dense over the entire surface of the sample.

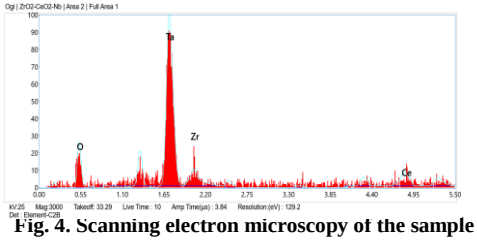

Fig. 4. Scanning electron microscopy of the sample

SEM images of ZrO_2-CeO_2 thin films are shown in Figure 4. The Zr-Ce atomic ratio is determined to be 5.79:3.50. The main spectra of the individual elements of the layer (O, Zr, Ce and Ta) are observed, and the last spectrum is very likely to be of Nb overlapping the spectrum of tantalum, since the starting sample is only of niobium.

4. Conclusion:

The sol-gel method has been successfully used both for obtaining layers and for synthesizing bulk materials from ZrO_2 – CeO_3. 3 steps were used to apply the layers by dipping. Successful application to the substrate and sub-layers depends on the appropriate concentration. The results were characterized by XRD XPS and CEM analyses. The presence of a Zr-Ce layer was established by X-ray analysis. XPS and CEM analyzes confirm these results. ZrO_2 – CeO_3 samples are also very promising for applications at high temperatures, as they have high corrosion resistance, wear resistance and high fire resistance.

Acknowledgement

The authors are grateful for the financial support of the Bulgarian National Science Fund at the Ministry of Education and Science, Contract No КП-06-Russian/18/15.12.2020.

References

1.P.Vitanov, A.Harizanova, T.Ivanova,Ch.Trapalis,N.Todorova, Sol –Gel ZrO_2 and nanocrystalline ZrO_2 – Al_2O_3 thin films on Si as high – k dielectrics, Materials Science and Engineering B, 165 [2009] ,p. 178 -181.

2.P. Vitanov, A. Harizanova, T. Ivanova, Characterization of ZrO_2 and (ZrO_2) $x(Al_2O_3)_{1-x}$ thin films on Si substrates: effect of the Al_2O_3 component, Journal of Physics: Conference Series, 514 [2014]012011.

3.I.E.Malka, A.Danelska,G.Kimmel, The influence of Al_2O_3 content on ZrO_2 – Al_2O_3 nanocomposite formation – the comparison between sol – gel and microwave hydrothermal methods, Materials Today Processings, 3 [2016] p.2713 -2724.

4.RMAsl,,M.Yousefpour, A.Shanaghi, The investigation of corrosion behavior of ZrO_2 – Al_2O_3 inhibitor / AA 2024 nanocomposite thin films using sol –gel and AHP-TOPSIS method, Material Chemistry and Physics, 262[2021]124220.

5.Y.Hao, J.Li, X.Yang, X.Wang, L.Li, Preparation of ZrO_2 – Al_2O_3 composite membranes by sol –gel process and their characterization, Material Science and Engineering A, 367 {2004], p .243-247.

6.E.Nouri, M.Shahmiri, HRRezaie, F.Talay, The effect of alumina content on the structural properties of ZrO_2 – Al_2O_3 unstabilized composite nanopowders, Journal of Industrial Chemistry, [2012],3:17.

7.MFWasim, S.Ali, MWAshraf, A.Rafigue,Dr.S.Tayyaba, M.Jawad, M.Akhlaq, Z.Ahmad, G.Sarmar, N.Tariq, J.Ahmad, Synthesis and characterization of ZrO_2 – Al_2O_3 bio-nanostructures with sintering effect, residual and thermally stable analysis, Digest Journal of Nanomaterials and Biostructures, 16[2021]p.1163-1171.

8.X.Zhang, J.Wang, C.Gao, Q.Li et al., Preparation of Al_2O_3/ZrO_2 coatings by sol-gel method and its effect on high temperature oxidation behavior of -TiAl based alloys, Rare Materials and Engineering , 39 [2010]p.367 – 271.

9. S. Kikkawa, A. Kiyama, K. Hirota, O. Yamaguchi, Soft solution preparation method in a ZrO_2 – Al_2O_3 binary system, Solid State Ionics, 151 [2002], p.359-364.

10.W.Zhang, FPGlasser, The preparation of Al_2O_3 – ZrO_2 sol-gels from inorganic precursors, Journal of the European Ceramic Society, 11[1993]p.143-147.

.

Investigation of an appropriate marl raw material for the production of innovative ceramic beehives

Todorka Lepkova*, Lyuben Lakov, Bojidar Jivov, Gergana Mutafchieva, Marieta Gacheva,

Bulgarian Academy of Sciences, Institute of Metal Science, Equipment and Technologies with Hydro- and Aerodynamics Centre "Acad. Angel Balevski", 67 "Shipchenski prohod" Blvd., 1574 Sofia, Bulgaria,
e-mail: rosbul@abv.bg

Abstract: *An observation of the current state of the beekeeping industry and the prevailing main problems was carried out. The prospects for increasing the efficiency and functional capabilities of the bee farms were analyzed. According to the long-term research activity, a technological regulation was contrived for producing innovative ceramic hives. The development is superior to the existing standard beehives made of other materials, in terms of complex operational indicators. The phase composition and technical characteristics of obtained samples of marl raw material (from Bulgarian deposits) were investigated, potentially applicable for the production of various modifications of ceramic collapsible hives.*
Keywords: *MARL RAW MATERIAL, CERAMIC BEEHIVE*

1. Introduction

The existing standard collapsible hives (wooden, plastic, polystyrene, polyurethane) are characterized by a relatively limited shelf life, depreciation and aging of the material during operation and practically complete unreliability in fire conditions. On the other hand, collapsible (frame) hives allow the application of highly productive methods for obtaining quality bee products [1-3].

At the same time, in rarer cases, the limited use of primitive indestructible hives made of flammable and combustible organic materials (mainly of plant origin) and untreated thermally natural clays continues [1,3]. Immovably fixed honeycombs and the limited functionality of the hive structure do not allow effective control of the life cycle of the bee family, and when extracting the apian product, it is impossible to apply centrifugation, and there is a risk to the integrity of the bee colony. Relatively low yields, limited purity of bee products [4], unreliability in prolonged contact with water environment, and fires are characteristic of non-sortable hives.

The individual types of beehives that have become widespread represent, at varying degrees, a potential environment for the development of mites, fungi, and other biologically active crops with adverse effects [2,4].

An opportunity to overcome some essential problems and increase the efficiency of beekeeping is the creation of new hive models [5-10] with improved functionality. The comparison of the research carried out in different thematic aspects allows the achievement of an adequate technological solution [11-22].

Based on a conducted study, a conceptual model and construction documentation of an innovative collapsible hive consisting of ceramic construction elements with air thermal insulation chambers have been prepared. A technological regulation suitable for the production of experimental prototypes from technical ceramics under laboratory and semi-industrial conditions is developed [5]. The application of the technological capabilities of ceramic production allows the production of non-flammable and non-combustible waterproof products with a long service life in the conditions of cyclical daily and seasonal climatic factors [5,10].

At the same time, the used classic collapsible structure of the hives [10] allows active control of the development of bee families, the application of modern economic methods to obtain high yields of bee products, and the use of standard equipment (centrifuges, etc.).

The development provides a favorable living environment for the natural growth of bee families and reduces the risk of the development of fungal and other potentially dangerous microbiological cultures [5,10].

The high resistance of ceramic materials allows the implementation of varied sanitary treatments [10]. For instance, if a hive has to be decontamination and settles with new bee families, it is possible to apply heat treatment. Such processing is inadmissible and destructive for other hive types (wooden, plastic, etc.).

The produced prototypes possess superior complex functional characteristics compared to the existing traditional beehives and represent a competitive alternative [6-9].

During the task development, a need for suitable raw materials (from accessible deposits on the territory of the country) appeared to organize a profitable production activity.

The present report aims to investigate the characteristics of obtained samples of marl raw material, potentially applicable for the development of compositions and the preparation of molding slurries for the production of various modifications of ceramic beehives. The technological approach used for the preparation of the experimental prototypes is fully considered with the silicate industry conditions. The technology could be applied to the realization of a production process in enterprises of the branch based on available standard equipment and additional equipment of a separate specialized production section.

2. Experimental procedures

The direction of the conducted research corresponds with the specific technological regime for the production of a complete set of ceramic structural elements (planes and profiles). A necessary prerequisite for further development, according to a detailed technological regulation, is the selection of suitable raw materials, allowing the implementation of a productive production process with standard available equipment through the possibilities of classical ceramic technology.

In manufacturing, marl raw materials have been used for a limited range of construction-ceramic products (such as tiles, bricks, etc.) for many years. Occasionally, marl clay is considered an alternative to replacing certain traditional materials of faience and porcelain production.

For the study purposes, samples of marl raw material from a batch mined from a random local section of the Polski Trambesh deposit, Veliko Tarnovo district, Bulgaria, were provided.

The preparation of the experimental samples was carried out using standard laboratory equipment: precision scale "KERN" RSV 200-2, standard scale up to 10 kg, porcelain ball mill with a working volume of 50 L (rotational speed about 260 rev/min), agate mortar, set of standard sieves, spatula, laboratory dryer "Astel", programmable muffle kiln "LM-312.11" (Veb Electro bad Frankenhausen), programmable periodic chamber furnace with support of a homogeneous temperature field and the working area of 900x600x250 mm, etc.

The laboratory analysis used a Bruker D8 Advance diffractometer (Cu K-alpha radiation, CynxEye solid-state detector), STA PT1600 TG-DTA/DSC apparatus (in an inert gas environment, temperature range 20÷1300°C, heating rate 10°C/min., crucibles type S (Pt10%/Pt-Rh), multipurpose transmission electron microscope JEOL JEM 2100 (fig. 1), modernized machine for carrying out tensile, compressive, and bending strength tests "Amsler" (at a loading rate of 0.2 up to 0.8 mm/s).

***Fig. 1**. Multipurpose transmission electron microscope JEOL JEM 2100.*

In the interpretation of part of the obtained results, the existing available information arrays of the Crystallography Open Database and specialized Digital Micrograph software were used.

3. Results and Discussion

The presence of vaterite, quartz, calcite, feldspar, illite, and kaolinite was recorded during the X-ray phase analysis (XRD) of a powdered sample of the provided raw material (marl). The presence of the mineral vaterite, a natural polymorphic modification of calcium carbonate $CaCO_3$, also designated as μ-$CaCO_3$, can be considered a specific characteristic of the studied batch of marl. The chemical and grain-metric composition of the marl raw material was investigated (tables 1 and 2).

***Table 1**. Chemical composition of the marl raw material.*

Composition	Quantity, mass.%
SiO_2	39,26
CaO	18,93
Al_2O_3	12,14
Fe_2O_3	4,36
MgO	2,23
K_2O	1,7
Na_2O	1,2
TiO_2	0,36
MnO	0,14
P_2O_5	0,12
3H	19,56

***Table 2.** Established grain-metric composition of the studied specimen.*

Grain size distribution	wt.%
Fraction under 0,005	43
Fraction between 0,005 - 0,05	46
Fraction over 0,05	11

Indexing of the obtained diffraction pattern (fig. 2) of a powdered nano-sized sample, after the drying process, from the initial composition of the studied raw material was performed.

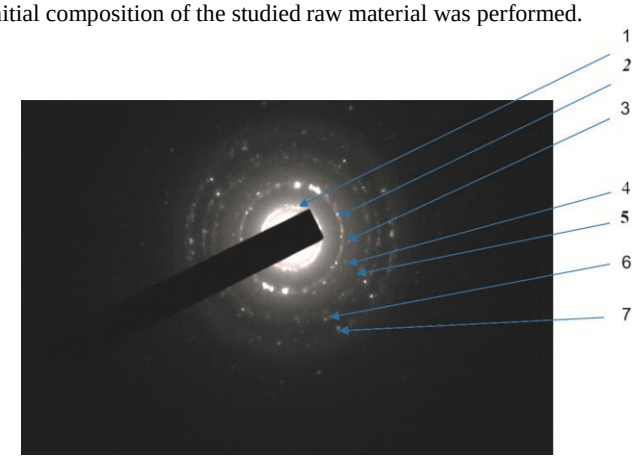

***Fig. 2.** Selected area electron diffraction (SAED) of the raw material.*

The composition and characteristics of the marl raw material vary according to the specifics of the specific local area of the deposit. The experimental results obtained through various research methods present the characteristics of the specific sample, which is only a part of the total amount of raw material provided.

Powdered samples of the initial raw material were given for investigation by thermochemical methods. DTA curve revealed a characteristic end effect determined by the thermal decomposition of the carbonate phases, mainly calcium carbonate $CaCO_3$ to CaO and CO_2.

The registered mass loss of the raw material is comparable to the results obtained from the chemical analysis. The melting interval was found to start with the formation of small amounts of liquid phase at about 1000°C. Figure 3 presents the experimental results of the laboratory DSC-TG analysis of the starting material.

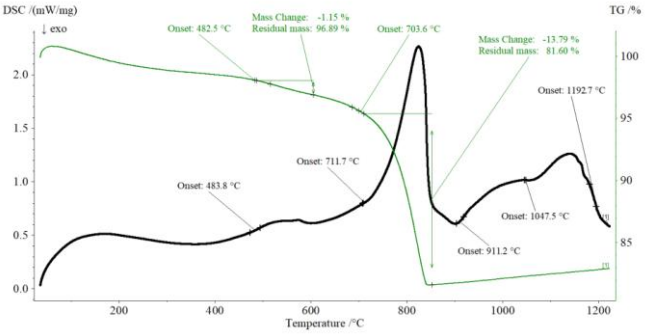

***Fig. 3.** DSC-TG analysis of the studied raw material (marl) originating from the Polski Trambesh deposit.*

The stated properties characterize the studied raw material as potentially applicable for the production of ceramic products by using classic silicate production methods. At the same time, due to the specificity of the marl raw materials and the specific requirements for the properties of the synthesized materials, there is a need to introduce additional components and modifiers when preparing the compositions intended for production purposes. This allows for the correction of the technical indicators of the masses and an increase in the performance characteristics of the final products. The introduction of appropriate additional components lowers the tendency of patterns to deform, affects the firing interval, increases the fire resistance of the products, and changes the ratio of oxides in the compositions. However, with the addition of the modifiers, it is a need to change the heat treatment mode.

Based on the studied marl raw material, compositions were developed that are applicable for molding experimental samples (table 3).

***Table 3.** Prescription compositions of molding masses.*

Raw materials	Composition, wt.%			
	S1	S2	S3	S4
Marl, Polski Trambesh deposit	60	50	40	35
Shamotte from the marl, fraction < 200 μm	20	25	30	35
Washed kaolin	20	15	20	5
Powder fraction quartz glass (<50 μm)	-	10	10	-
Powder fraction waste glass (<50 μm)	-	-	-	25

During previous laboratory investigations for the production of preliminary experimental samples by applying different technological approaches, it was determined that for development purposes, the most expedient method for molding the structural details is slip casting. This approach allows for complex-shaped hollow specimen production and provides high productivity through high-speed casting methods in manufacturing conditions (e.g., through the stand and conveyor casting). Measuring of the individual raw materials (according to the formula composition) and joint wet grinding and homogenization were carried out. Aqueous colloid-dispersed systems (casting masses / shlickers) with moisture content of about 60% were prepared (table 4.).

Table 4. *Characteristics of the prepared casting masses (shlickers).*

Properties	S1	S2	S3	S4
Liter weight [g/l]	1486	1483	1484	1496
Viscosity [Pa.s]	2,23	2,21	2,25	2,27
Dry matter in the slurry [kg/l]	0,72	0,74	0,77	0,81
Sieve residue in the sieve 0,063 mm [g/l]	0,07	0,11	0,14	0,27

During the research, it was found that the viscosity of the prepared shlickers was similar, and the dry matter content varied within certain limits. The most significant sieve residue on a sieve of 0.063 mm was obtained in composition S4, which is determined by the content of the powder fraction of waste glass (household glass waste).

According to the achieved DTA data of the marl raw material and the specifics of the added components, an adequate mode of heat treatment of the molded samples was reached.

The prepared semi-finished products are subjected to free drying for 3 to 5 days and in a dryer in a temperature range from 100 to 130^{o}C for 24 hours to a residual humidity of 7-8%. The obtained samples were subjected to further heat treatment (in an oxidizing environment at a homogeneous temperature field in a programmable chamber kiln) at a set speed of increasing the temperature values of 5^{o}C/min and applied isothermal retention at 200^{o}C (40 min), 600^{o}C (30 min), 700^{o}C (30 min), 830^{o}C (30 min) and maximum firing temperatures (for individual experiments) 1000, 1100, 1150^{o}C±5^{o}C (for 50 min). When cooling the test bodies, a rate of decrease in temperature values of 5^{o}C/min and isothermal retention at 700 and 600^{o}C (for 30 min) were applied. The characteristics (table 5) of the experimental samples obtained at different values of heat treatment were investigated.

The higher content of calcium carbonate $CaCO_3$ lowers the viscosity of the mass during sintering vitrified and reduces the high-temperature synthesis interval. At the same time, the increased $CaCO_3$ content contributes to a higher porosity of the patterns due to the release of carbon dioxide during the thermal decomposition of the carbonate. Due to a larger quantity of melt formation, the briefest time interval and the lowest sintering temperature values were found for samples obtained from composition S1.

Table 5. *Established experimental results in the study of experimental samples prepared from different compositions and subjected to heat treatment up to 1150^{o}C.*

M	T max, ^{o}C Heat treatment	Firing shrinkage, %	Water absorption, %	Apparent density
S1	1000	6,7	12,4	1,73
	1100	7,4	3,0	1,81
	1150	8,2	0,3	1,92
S2	1000	5,9	10,6	1,71
	1100	6,4	1,8	1,83
	1150	7,6	0,2	1,94
S3	1000	3,4	7,3	1,75
	1100	4,6	0,05	1,83
	1150	5,3	0,02	1,96
S4	1000	4,2	9,7	1,78
	1100	5,3	0,06	1,86
	1150	6,1	0,03	1,95

The presence of anorthite, wollastonite, diopside, and quartz was recorded during the X-ray phase analysis (XRD) of the obtained experimental samples after high-temperature thermal treatment.

In terms of studying the mechanical properties of the obtained materials, experimental specimens from the developed compositions were produced. The determined strength indicators (table 6) of pressure and bending increase with an increase in the heat treatment temperature of the experimental samples.

Table 6. *Values of compressive and bending strength of the samples obtained from different compositions and subjected to heat treatment up to 1150^{o}C.*

Indicators	S1	S2	S3	S4	T max, ^{o}C Heat treatment
Compressive strength, MPa	95	110	150	130	1000
	120	140	180	170	1100
	140	165	240	190	1150
Bending strength, MPa	30	40	45	40	1000
	40	55	65	60	1100
	55	65	80	75	1150

The experimentally observed optimum composition S3 (developed based on the studied raw material) was applied in the laboratory conditions during the implementation of the entire process for the production of the structural details. According to the technological characteristics of the used casting masses (shlickers), an original set of experimental gypsum molds was used for molding the samples. The shrinkage values of the samples during drying, heating, and high-temperature heat treatment were determined. The prepared slurry was cast into the assembled molds, and after the required time of about 50-60 min, the residual liquid phase was removed by pouring. After an additional continuance (from 2 to 3 hours), the obtained patterns are removed from the casting forms by dissembling. The samples are subjected to drying, heating, and high-temperature heat treatment according to the developed technological regime. The presence of technological flaws is not optical observed in the finished structural items. The designed tolerances (of the molding equipment) allow the unobstructed mount of the separate ceramic elements during the assembly of the prototype.

4. Conclusions

The possibilities for effectively increasing the production resources of bee farms have been analyzed. An original ceramic collapsible beehive was designed with improved complex functional indicators.

The main innovative contribution of the development is the application of long-lasting, highly resistant ceramic structural elements with the presence of heat-insulating air cavities. A technological regulation is developed for the production of an entire set of structural items made of technical ceramics. Slip casting as a forming process is used, and a special mode of high-temperature treatment is implemented.

The provision of accessible raw materials with appropriate technological properties is of significant interest to the cost-effective production of ceramic hives.

According to study purposes, samples of marl raw material from a random local section of the Polski Trambesh deposit were provided.

On the basis of the provided marl raw material and other components, a series of compositions were developed and casting masses (shlickers) with different technological characteristics were prepared.

The phase composition and physicomechanical characteristics of experimental samples prepared under different technological conditions were investigated. In terms of the obtained experimental data, an accurate heat treatment mode was developed.

With the use of the selected molding slip in laboratory conditions, a complete technological cycle was carried out for the production of a set of structural details and the assembly of an experimental prototype.

During the laboratory analysis, it was established that the technical characteristics of the studied marl raw material correspond to the set goals of the development.

5. References

1. D. M. Caron, L. J. Connor, "Honey Bee Biology and Beekeeping", Book, Publisher Wicwas Press, Revised Edition, Eds R. G. Muir, A. Harman, 2013.
2. M. L. Winston, "The Biology of the Honey Bee", Book, Revised Edition, Publisher Harvard University Press, 1991.
3. J. Tautz, "The Buzz about Bees: Biology of a Superorganism", Book, Springer-Verlag, 2008.
4. R. M. Johnson, "Honey Bee Toxicology", Annual Review of Entomology, 60(1), 2015, pp. 415–434.
5. T. Lepkova, I. Martinova, G. Martinova, I. Marinova, B. Pincheva, "Ceramic Beehive - Conceptual Paper", International Scientific Journal "Science. Business. Society", Year IV, Issue 2, 2019, pp. 52–55.
6. T. Lepkova, L. Lakov, I. Martinova, G. Martinova, K. Toncheva, "Thermal conductivity of the ceramic beehives", International Scientific Conference Machines. Technologies. Materials, 11-14.03.2020, Borovets, Bulgaria, Proceedings, Year III, Issue 1 (16), Volume I, 2020, pp. 109-111.
7. L. Lakov, N. Stoimenov, M. Aleksandrova, T. Lepkova, G. Mutafchieva, "Study of temperature changes in ceramic cavity walls of beehives", International Scientific Journal Innovations, Year IX, Issue 2/2021, pp. 78-82.
8. Lakov L., N. Stoimenov, M. Aleksandrova, "Investigation of hollow ceramic structures by contactless computer-tomographic nondestructive method", International Scientific Journal "Industry 4.0", year VI, issue 1, 2021, pp. 21- 24.
9. L. Lakov , Y. Ivanova, T. Partalin , M. Aleksandrova, T. Lepkova, G. Mutafchieva, "Study of the thermal and sound insulation properties of ceramic plates with cavities designed for beehives", International Scientific Journal Mathematical Modeling 2/2021, pp. 59-61.
10. L. Lakov, B. Jivov, T. Lepkova, K. Toncheva, S. Yordanov, "Comparison of innovative collapsible ceramic hive and traditional non-separable hives made on the basis of natural plastic raw materials", International Scientific Journal "Machines. Technologies. Materials", Year XVI, Issue 10/2022, pp. 340-343.
11. R. Dehghannasiri, D. Xue, P. V. Balachandran, M. R. Yousefi, L. A. Dalton, T. Lookman, E. R. Dougherty, "Optimal experimental design for materials discovery". Comput. Mater. Sci. 129, 2017, pp. 311–322.
12. A. Bachvarova-Nedelcheva, R. Iordanova, K. L. Kostov, S. Yordanov, V. Ganev, "Structure and Properties of a Non-traditional Glass Containing TeO_2, SeO_2 and MoO_3", Optical Materials, 34, 11, 2012, 1781-1787.
13. S. I. Yordanov, A. D. Bachvarova-Nedelcheva, R. S. Iordanova, I. D. Stambolova, "Sol-gel Synthesis and Properties of Sm Modified TiO_2 Nanopowders", Bulgarian Chemical Communications 50, 2018, pp. 42-48.
14. A. Bachvarova-Nedelcheva, R. Iordanova, K. L. Kostov, V. Ganev, St. Yordanov, Y. Dimitriev, "Synthesis and Structural Characterization of a Glass in the Ag_2O-SeO_2-MoO_3 System", Journal of Non-Crystalline Solids 481, 2018, pp. 138-147.
15. T. Satyanarayana, S. Sudhakar Reddy, "A Review on Chemical and Physical Synthesis Methods of Nanomaterials", International Journal for Research in Applied Science & Engineering Technology (IJRASET), Vol. 6 Issue I, 2018, pp. 2885-2889.
16. M. Frigione, J. L. Barroso de Aguiar, "Innovative Materials for Construction", Materials 2020, 13, 5448.
17. V. Petkov, M. Aleksandrova, R. Valov, "Partial oxidation of biocompatible titanium alloy Ti6Al4V during deposition of glassy carbon coating", International Journal "NDT Days", Vol. III, Issue 4, Year 2020, pp. 225-230.
18. M. Aleksandrova M., V. Petkov**,** V. P. Korzhov, I. S. Zheltyakova. "Study the influence of immersion in the synthesis of thin layers on a composite substrate". International Scientific Journal INDUSTRY 4.0, VII, 6, Scientific technical union of mechanical engieneering "INDUSTRY 4.0" Bulgaria, 2022, pp. 226-228.
19. V. Petkov, M. Aleksandrova, V. Blaskov, "Deposition of ZrO_2 thin films obtained by sol-gel method on monolithic composite with layered structure of Nb_30Ti/Al", International Scientific Journal "Machines. Technologies. Materials", Year XVI, Issue 2/2022, pp. 58-61.
20. V. Petkov, M. Aleksandrova, V. Petkov, D. Teodosiev, A. Bouzekova-Penkova, „Investigation of the glassy carbon coating deposited on the titanium alloys, microstructure and mechanical properties", Journal of Theoretical and Applied Mechanics, Vol. 52, No 4, (2022), p. 381-392, ISSN: print 0861-6663, online 1314-8710, https://jtambg.eu/issues.php
21. L. Lakov, B. Jivov, M. Aleksandrova, S. Yordanov, K. Toncheva, "Synthesis, phase composition and microstructure of colored ceramic materials based on diopside". International Scientific Journal Materials Science. Non-Equilibrium Phase Transformations, Year VI, Issue 3/2020, Scienticic Technical Union of Mechanical Engineering, Industry 4.0, 2020, pp. 77-79.
22. L. Lakov, B. Jivov, Y. Ivanova, S. Yordanov, K. Toncheva, "Alternative possibilities for application of foamed silicate materials", International Scientific Journal "Machines, Technologies, Materials", XV, Issue 1, 2021, pp. 25-27.

On Transfer Functions Limitations to Active Vehicle Suspension

Katerina Hyniova
Faculty of Information Technology
Czech Technical University in Prague, Prague, Czech Republic
hyniova@fit.cvut.cz

Abstract: *It is often assumed that if practical difficulties are neglected, active suspension systems could produce in principle arbitrary ideal behavior. This paper presents the factorization approach that is taken to derive limitations of achievable frequency responses to active vehicle suspension systems in terms of invariant frequency points and restricted rate of decay at high frequencies. The factorization approach enables the determination of complete sets of such constraints on various transfer functions from the load and road disturbances for typical choices of measured outputs and then chooses the optimal vector of the measurements from the point of view of the widest class of the achievable frequency responses. Using a simple linear two-degree-of-freedom car suspension model, it will be shown that even using complete state feedback and in the case in which the system is controllable in the control theory sense, there are still limitations to suspension performance in the fully active state.*
Keywords: *VEHICLE, ACTIVE SUSPENSION, CONTROL, LIMITATIONS, PARAMETRIZATION*

1. Introduction

Two major performance requirements of suspension are to improve ride and handling quality when random road and load disturbances from the environment act upon running vehicles. Automotive suspensions are designed to provide good vibration insulation of the passengers and to maintain adequate adherence of the wheel for braking, accelerating, and handling i.e., the purpose of active suspensions in terms of performance is to improve both these conflicting requirements.

In this paper the factorization approach taken to derive limitations of achievable frequency responses for active vehicle suspension systems is discussed. It is shown that limitations derived for a traditional one-quarter-car model (Fig.1) in the frequency domain arise in the form of invariant frequency points and restricted rate of decay at zero and infinite frequencies.

Youla-Kucera factorization approach to feedback system stability is shown in [2], [3] to derive achievable dynamic responses for active suspension systems of vehicles. Complete sets of constraints on various transfer functions from the road and load disturbance inputs were derived for typical choices of measured outputs [3].

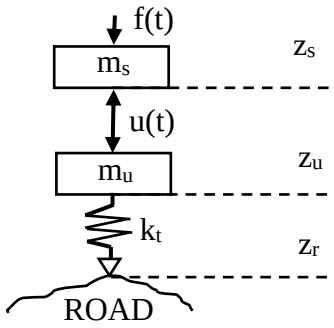

Fig. 1 *One-quarter-car model*

The approach was illustrated for the one-quarter-car model shown in Fig.1, where:

- *u(t)* control input (active suspension force) [N]
- m_u weight of the unsprung mass (wheel) [kg]
- m_s weight of the sprung mass supported by each wheel and taken as equal to a quarter of the total body mass [kg]
- k_t stiffness of the tyre [N/m]
- $z_r(t)$ road displacement (road disturbance) [m]
- $z_s(t)$ displacement of the sprung mass [m]
- $z_u(t)$ displacement of the unsprung mass [m]
- *f(t)* load disturbance [N]

Note, that if the one-quarter-car model contains also a traditional passive suspension system then the active suspension force *u(t)* involves also an adequate force generated by a spring and a damper of the passive suspension system.

On the base of the Youla-Kucera parametrization [2], [3], complete sets of limitations were derived for transfer functions from the road disturbance input only (load *f(t)* is absent i.e. *f(t)=0*):

$$H_{zw}^{1}(s) = \left[\frac{Z_s(s)}{Z_r(s)}\right]_{f=0} \quad \text{(to the sprung mass position)} \tag{1}$$

$$H_{zw}^{2}(s) = \left[\frac{Z_s(s)-Z_u(s)}{Z_r(s)}\right]_{f=0} \quad \text{(to the suspension deflection)} \tag{2}$$

$$H_{zw}^{3}(s) = \left[\frac{Z_u(s)-Z_r(s)}{Z_r(s)}\right]_{f=0} \quad \text{(to the tyre deflection)} \tag{3}$$

and analogically, for the load disturbance input *f(t)* transfer functions can be derived for various choices of measured outputs even for full state feedback.

2. Comprime Factorization

Consider the standard feedback configuration shown in Fig.2,

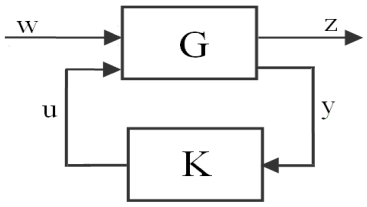

Fig. 2 *Standard feedback configuration*

where *w* is the exogenous input, typically consisting of disturbances and sensor noises, *u* is control signal, *z* represents output to be controlled, and *y* is measured output. In general, *u*, *w*, *y*, and *z* are vector-valued signals.

Assume, the transfer matrices *G(s)* and *K(s)* are real-rational and proper: *G* represents a generalized plant, the fixed part of the system, and *K* is the controller [4]. Partition *G(s)* as:

$$G(s) = \begin{bmatrix} G_{11}(s) & G_{12}(s) \\ G_{21}(s) & G_{22}(s) \end{bmatrix} \tag{4}$$

Then Fig.2 stands for the following algebraic equations:

$$Z(s) = G_{11}(s)W(s) + G_{12}(s)U(s) \tag{5}$$

$$Y(s) = G_{21}(s)W(s) + G_{22}(s)U(s) \tag{6}$$

$$U(s) = K(s)Y(s) \tag{7}$$

Manipulating the equations listed above, the following transfer function $T_{zw}(s)$ from w to z as a linear-fractional transformation of $K(s)$ can be derived:

$$T_{zw}(s) = G_{11}(s) + G_{12}(s)K(s)[I - G_{22}(s)K(s)]^{-1}G_{21}(s) = \\ = G_{11}(s) + G_{12}(s)[I - K(s)G_{22}(s)]^{-1}K(s)G_{21}(s) \quad (8)$$

It is shown in [1] that the set of all proper real-rational matrices $K(s)$ stabilizing $G(s)$ is parametrized by a free parameter $Q(s) \in RH_\infty$ as follows:

$$K(s) = [Y(s) - M(s)Q(s)][X(s) - N(s)Q(s)]^{-1} = \\ = \left[\tilde{X}(s) - Q(s)\tilde{N}(s)\right]^{-1}\left[\tilde{Y}(s) - Q(s)\tilde{M}(s)\right] \quad (9)$$

where:

$$\mathrm{M}(s), N(s), X(s), Y(s) \in RH_\infty,$$

and $\tilde{M}(s), \tilde{N}(s), \tilde{X}(s), \tilde{Y}(s) \in RH_\infty$ can be found by comprime factorization approach of $G_{22}(s)$:

$$G_{22}(s) = N(s)M^{-1}(s) = \tilde{M}^{-1}(s)\tilde{N}(s) \quad (10)$$

$$\begin{bmatrix} \tilde{X}(s) & -\tilde{Y}(s) \\ -\tilde{N}(s) & \tilde{M}(s) \end{bmatrix}\begin{bmatrix} M(s) & Y(s) \\ N(s) & X(s) \end{bmatrix} = I \quad (11)$$

Substituting the equation (9) into (8) we obtain the transfer matrix $T_{zw}(s)$ from w to z in terms of the free parameter $Q(s) \in RH_\infty$:

$$T_{zw}(s) = \\ = G_{11}(s) + G_{12}(s)M(s)\left[\tilde{Y}(s) - Q(s)\tilde{M}(s)\right]G_{21}(s) = \\ = G_{11}(s) + G_{12}(s)[Y(s) - M(s)Q(s)]\tilde{M}(s)G_{21}(s) \quad (12)$$

As the parameter $Q(s)$ varies over the set of all stable proper functions, the equation (12) parametrizes all achievable transfer functions $T_{zw}(s)$.

If it is assumed that the tyre does not leave the ground, for the one-quarter car model (Fig.1), the linear differential equations of motion are:

$$m_s\ddot{z}_s = u - f \quad (13)$$

$$m_u\ddot{z}_u = -u + k_t(z_r - z_u) \quad (14)$$

where z_u and z_s are measured from the static equilibrium position.

First, let the load disturbance is absent ($f=0$). Adding equations (13) and (14), we obtain the invariant eq. (15):

$$m_s\ddot{z}_s + m_u\ddot{z}_u = k_t(z_r - z_u) \quad (15)$$

that is independent on the suspension force u. The following transfer functions from road disturbances will be investigated:

sprung mass position $H_{SP}(s) = Z_s(s)/Z_r(s)$ (16)

suspension deflection $H_{SD}(s) = [Z_s(s) - Z_u(s)]/Z_r(s)$ (17)

tyre deflection $H_{TD}(s) = [Z_u(s) - Z_r(s)]/Z_r(s)$ (18)

3. Invariant Properties

Manipulating the equation (15), the following invariant identities can be derived:

$$[(m_u + m_s)s^2 + k_t]H_{SP}(s) - [m_us^2 + k_t]H_{SD}(s) = k_t \quad (19)$$

$$m_ss^2H_{SP}(s) + [m_us^2 + k_t]H_{TD}(s) = -m_us^2 \quad (20)$$

$$[(m_u + m_s)s^2 + k_t]H_{TD}(s) + m_ss^2H_{SD}(s) = \\ = -(m_u + m_s)s^2 \quad (21)$$

It is obvious from (19) and (20) that the sprung mass position transfer function $H_{SP}(s)$ has an invariant "tyre-hop" frequency at $\omega_1 = \sqrt{k_t/m_u}$, where:

$$H_{SP}(s)/_{s=j\omega_1} = -m_u/m_s \quad (22)$$

Similarly, from (16) and (18), the suspension deflection transfer function $H_{SD}(s)$ has an invariant "rattle-space" frequency at $\omega_2 = \sqrt{k_t/(m_u + m_s)}$ and:

$$H_{SD}(s)/_{s=j\omega_2} = -(1 + m_u/m_s) \quad (23)$$

Finally, from (20) and (21), the tyre deflection transfer function $H_{TD}(s)$ does not have any invariant frequency point except $\omega_3 = 0$, where:

$$H_{TD}(s)/_{s=j\omega_3} = 0 \quad (24)$$

At invariant frequencies ω_1, ω_2, and ω_3 the values of the corresponding transfer functions are fixed and cannot be influenced by the free parameter $Q(s) \in RH_\infty$ (eq. (1)) of the stabilizing controller K(s).

4. Transfer Functions Limitations

In the next, consider the standard block diagram shown in Fig.2. As an example, consider:

$w=z_r$, $z=z_s$ $\quad \underline{y} = [\dot{z}_u, z_s - z_u, z_u - z_r]^T$.

Then:

$$G(s) = \begin{bmatrix} G_{11}(s) & G_{12}(s) \\ G_{21}(s) & G_{22}(s) \end{bmatrix} = \\ = \begin{bmatrix} 0 & \frac{1}{m_ss^2} \\ \begin{bmatrix} \frac{sk_t}{m_us^2+k_t} \\ \frac{-k_t}{m_us^2+k_t} \\ \frac{-m_us^2}{m_us^2+k_t} \end{bmatrix} & \begin{bmatrix} \frac{-s}{m_us^2+k_t} \\ \frac{(m_u+m_s)s^2+k_t}{m_ss^2(m_us^2+k_t)} \\ \frac{-1}{m_us^2+k_t} \end{bmatrix} \end{bmatrix} \quad (25)$$

The limitations of all achievable closed-loop transfer functions $T_{zw}(s) = H_{SP}(s)$ are derived from the right and left comprime factorization of $G_{22}(s)$, i.e.:

$$G_{22} = \underbrace{\begin{bmatrix} \frac{-m_ss^3}{p_4(s)} \\ \frac{(m_u + m_s)s^2 + k_t}{p_4(s)} \\ \frac{-m_ss^2}{p_4(s)} \end{bmatrix}}_{N(s)}\underbrace{\left[\frac{m_ss^2(m_us^2 + k_t)}{p_4(s)}\right]^{-1}}_{M^{-1}(s)} = \\ = \underbrace{\begin{bmatrix} \frac{m_ss}{p_2(s)} & \frac{m_ss^2}{p_2(s)} & 0 \\ 0 & \frac{m_um_ss^2}{p_2(s)} & \frac{-m_sk_t}{p_2(s)} \\ \frac{-1}{p_2(s)} & 0 & \frac{s}{p_2(s)} \end{bmatrix}^{-1}}_{\tilde{M}^{-1}}\underbrace{\begin{bmatrix} \frac{1}{p_2(s)} \\ \frac{m_u+m_s}{p_2(s)} \\ 0 \end{bmatrix}}_{\tilde{N}(s)} \quad (26)$$

where $p_2(s)$ and $p_4(s)$ are Hurwitz polynomials of degree 2 and 4, respectively. Then:

$$H_{SP}(s) = \\ = G_{11}(s) + G_{12}(s)M(s)\left[\tilde{Y}(s) - Q(s)\tilde{M}(s)\right]G_{21}(s) = \\ = -\frac{1}{p_4(s)}\tilde{Y}(s)\begin{bmatrix} -sk_t \\ k_t \\ m_us^2 \end{bmatrix} + \frac{s(m_us^2+k_t)}{p_4(s)}Q^*(s) \quad (27)$$

where $Q^*(s) = \left[\frac{Q_3(s)}{p_2(s)}\right]$, $Q(s) = [Q_1(s)\ Q_2(s)\ Q_3(s)]$.

It follows from (27) that thanks to the term $s^2H_{SP}(s)$ bounded for large s:

$$\lim_{s\to\infty} s^2H_{SP}(s) < \infty \quad (28)$$

the resulting rate of decay is of second degree:

$$H_{SP}(s)/_{s\to\infty} = O(s^{-2}) \quad (29)$$

It is obvious from (27) that the term $\frac{s(m_u s^2+k_t)}{p_4(s)}$ has two imaginary axis zeros - at s=0 and $s = j\omega_1 = j\sqrt{k_t/m_u}$- which can not be canceled by the denominator of $Q^*(s) \in RH_\infty$. With respect to (27) and the Bezout identity (11) it follows, that:

$$H_{SP}(s)/_{s=0} = -\frac{1}{p_4(s)}\tilde{Y}(s)\begin{bmatrix}-sk_t\\ k_t\\ m_u s^2\end{bmatrix}/_{s=0} =$$

$$= -\frac{k_t}{p_4(s)}\tilde{Y}_2(s)/_{s=0} = 1 \quad (30)$$

and similarly:

$$H_{SP}(s)/_{s=j\omega_1} = -\frac{1}{p_4(s)}\tilde{Y}(s)\begin{bmatrix}-sk_t\\ k_t\\ m_u s^2\end{bmatrix}/_{s=j\omega_1} =$$

$$= -m_u/m_s \quad (31)$$

This result endorses (25).

Thanks to the first order of the imaginary axis zero at s=0, the first derivative of the transfer function $H_{SP}(s)$ does not have any similar restrictions at this point. Expressions (29), (30) and (31) create the complete set of limitations which any admissible transfer function $H_{SP}(s) \in RH_\infty$ must satisfy. Another words, if any complex transfer function satisfies the mentioned limitations, there exists a stabilizing controller $K(s)$ so that $T_{zw}(s) = H_{SP}(s)$. It does not depend on what variables are chosen as the measured output - the limitations always arise in the form of invariant frequency points as was shown in paragraph 3 and in the form of restricted rate of decay at infinite frequencies as shown in (29).

Complete sets of limitations for the transfer functions $H_{SD}(s)$ and $H_{TD}(s)$ can be similarly carried out from the corresponding transfer functions $G(s)$ or using (26), (27), (28) and the corresponding invariant equation stated above (19), (20), and (21). This way the following complete sets of limitations can be derived:

$$H_{SD}(s)/_{s\to\infty} = O(s^{-2}) \quad (32)$$

$$H_{SD}(s)/_{s=0} = 0, \qquad H_{SD}(s)/_{s\to 0} = O(s) \quad (33)$$

$$H_{SD}(s)/_{s=j\omega_2} = -\left(1+\frac{m_u}{m_s}\right), \text{ where}$$

$$\omega_2 = \sqrt{k_t/(m_u+m_s)} \quad (34)$$

$$H_{TD}(s)/_{s\to\infty} = -1 + O(s^{-2}) \quad (35)$$

$$H_{TD}(s)/_{s=0} = 0,$$

$$H_{TD}(s)/_{s\to 0} = -(m_u+m_s)s^2/k_t + O(s^3) \quad (36)$$

Note, that even though it is desirable to prevent amplitudes of the frequency responses $H_{SP}(s)$, $H_{SD}(s)$, and $H_{TD}(s)$ being too large in any frequency domain, a brief analysis of the expressions (29) - (36) enables to find out that the investigated transfer functions must have modulus strictly grater that one at some frequencies what indicates the fact that the road disturbance signal is amplified at these mentioned frequencies.

The same approach can be used to derive limitations for other transfer functions and various choices of the measured outputs.

It has been shown that the limitations always arise in the form of invariant frequency points (for example $\omega_1 = \sqrt{\frac{k_t}{m_u}}$ for $H^1_{zw}(j\omega_1)$, $\omega_2 = \sqrt{\frac{k_t}{m_u+m_s}}$ for $H^2_{zw}(j\omega_2)$ and $\omega_3 = 0$ for $H^3_{zw}(j\omega_3)$) and in the form of restricted rate of decay at frequencies tending to zero and infinity.

As an example, the complete sets of constraints for transfer functions $H^1_{zw}(s)$, $H^2_{zw}(s)$ and $H^3_{zw}(s)$, when suspension deflection and suspension deflection velocity are measured, is as follows [2],[3]:

$H^1_{zw}(s)/_{s\to\infty} = O(s^{-3})$ (infinite frequency constraint),

$H^1_{zw}(s)/_{s\to 0} = 1 + O(s^2)$ (zero frequency constraint),

$H^1_{zw}(j\omega_1) = -\frac{m_u}{m_s}$ for $\omega_1 = \sqrt{\frac{k_t}{m_u}}$,

and analogically:

$H^2_{zw}(s)/_{s\to\infty} = -\frac{k_t}{m_u}s^{-2} + O(s^{-3})$ (infinity frequency constraint),

$H^2_{zw}(s)/_{s\to 0} = O(s^2)$ (zero frequency constraint),

$H^2_{zw}(j\omega_2) = -(1+\frac{m_u}{m_s})$ for $\omega_2 = \sqrt{\frac{k_t}{m_u+m_s}}$,

and:

$H^3_{zw}(s)/_{s\to\infty} = -1 + \frac{k_t}{m_u}s^{-2} + O(s^{-3})$ (infinity freq. constraint),

$H^3_{zw}(s)/_{s\to 0} = -\frac{(m_u+m_s)}{k_t}s^2 + O(s^4)$ (zero freq. constraint),

$H^3_{zw}(j\omega_3) = 0$ for $\omega_3 = 0$.

It is often assumed that if practical difficulties are neglected, active systems can in principle produce arbitrary ideal behavior. This paper presents the factorization approach that is taken to derive limitations of achievable frequency responses for active vehicle suspension systems in terms of invariant frequency points and restricted rate of decay at high frequencies.

In control law design for active suspension system of vehicles it is demanded to prevent magnitudes of the road and load frequency responses from being too large. There are some frequency points and frequency ranges where the transfer functions have modulus strictly greater than one i.e., where road and load disturbance amplification occur. On the base of the Bode integral, it can be shown that the transfer functions must be greater in modulus to at least the same extend that it is less than one, when measured in terms of the area on a Bode magnitude plot [1], [2] [3]. In such a case, there is a possibility to shift frequency ranges where disturbance amplification occurs to a more proper frequency range or to make magnitudes lower spreading the frequency range.

5. Bode Integral Theorem

To analyze results given above , it is useful to make a short review of some relevant ideas and definitions of sensitivity theory.

It is well known that the Bode sensitivity theory can formally be extended to the characterization of the transfer function $F(s)$ with respect to the transfer function $G(s)$, called the variable component. Suppose that $G(s)$ is a transfer function of the controlled plant and $K(s)$ is a transfer function of the feedback controller. Then the Bode sensitivity function of the closed loop with the transfer function:

$$F(s) = \frac{G(s)}{1+G(s)K(s)} \quad (37)$$

is defined as

$$S(s) = \frac{\partial logF(s,G(s))}{\partial logG(s)} = \frac{1}{1+G(s)K(s)} = \frac{1}{1+L(s)} \quad (38)$$

Where $L(s)=G(s)K(s)$ is open-loop transfer function. As the open-loop (i.e., the control chain) sensitivity function $S_o(s)$is equal to one in the whole frequency range, the sensitivity function $S(s)$ can serve as a criterion for comparison of the sensitivity of the control loop with any control chain containing the same plant. For frequencies ω, at which $|S(j\omega)|<1$, the parameter sensitivity of the control loop is larger than that of the open control chain i.e., the parameter sensitivity is increased by introducing feedback. To show this in terms of the Nyquist locus suppose the Nyquist locus of the open loop $L(j\omega)$ as shown in Fig. 3.

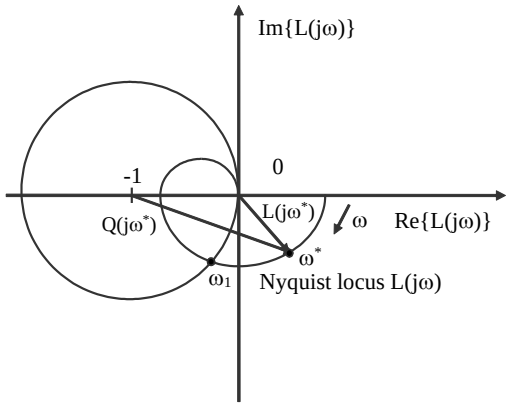

Fig. 2 *Sensitivity evaluation from Nyquist diagram*

The vector from point *(-1, 0j)* to point ω^* represents the denominator of the closed loop sensitivity function $S(j\omega^*)$.

Thus:

$$Q(j\omega^* = 1 + L(j\omega^*) \tag{39}$$

This implies:

$$|S(j\omega^*)| = |Q(j\omega^*)|^{-1} \tag{40}$$

From Fig. 3, we can therefore make the following observations. For those frequencies at which the locus $L(j\omega)$ cuts the unit circle centered at -1, the sensitivities of the closed-loop and open-loop systems are the same. For all frequencies $\omega<\omega_1$ at which the locus $L(j\omega)$ lies outside the unit circle, $|S((j\omega)| <1$ holds and the closed-loop system is less sensitive than the open-loop system. For all frequencies $\omega>\omega_1$ at which the locus $L(j\omega)$ lies inside the unit circle, $|S((j\omega)| >1$ holds and the closed-loop system is more sensitive than the open-loop system. For a control system $L(j\omega)$ which has at least two more poles than zeros, there always exists a frequency ω_1 such that:

$$|S((j\omega)| >1 \text{ for } \omega>\omega_1 \tag{41}$$

i.e. , there exist frequencies at which the feedback control system is more sensitive than the uncontrolled one- The frequency range $\omega<\omega_1$ for which $|S((j\omega)| <1$ holds, can be influenced in a wide range by a proper choice of the transfer function $K(j\omega)$. This fact has been already recognized by Bode and expressed by the following theorem.

Theorem 1. (Bode integral theorem): If the transfer function $L(s)$ of the open loop does not contain poles and $1+L(s)$ does not contain zeros in the right half of the *s*-plane and if the number of poles of $L(s)$ exceeds the number of zeros at least by *2* then the following equality holds:

$$\int_0^\infty log|1 + L(j\omega)|d\omega = -\int_0^\infty log|S(j\omega)|d\omega = 0 \tag{42}$$

In words: For a stable control system with a pole excess of at least 2 , the logarithm of the magnitude of the sensitivity function is on average equal to zero. This means that if the logarithmic Bode diagram $S(j\omega)$ is drawn, the area enclosed with 0 dB line for the region $|S((j\omega)| > 1$ is exactly the same as that for the region $|S((j\omega)|<1$. For frequency ω_1 at which $|S(j\omega)| =1$ can be specified by a suitably chosen transfer function $K(s)$ of the controller.

Bode original result was valid only for open-loop stable systems and was generalized by Freudenberg and Looze [1] for systems with unstable open loops as:

Theorem 2. (Generalized Bode integral theorem): Assume that the open-loop transfer function $L(s)$ possesses finitely many open right half-plane poles $\{p_i: i = 1,\dots,n \quad n \in N\}$, $Re(p_i)>0$ including multiplicities. In addition, assume that:

$$\lim_{R\to 0} \sup_{|s|\geq R, Re(s)\geq 0} R|L(s)| = 0 \tag{43}$$

Then, if the closed loop is stable the sensitivity function must satisfy:

$$\int_0^\infty log|S(j\omega)|\, d\omega = \pi \sum_{i=1}^n Re(p_i) \tag{44}$$

The proof of this theorem is given by Freudenberg and Looze in [1].

6. Analysis of the Complete Sets of Limitations

In context with transfer functions $H(s)$ of the one-quarter-car model given in Section 1, the generalized Bode integral theorem can be modified as follows:

Theorem 3. Let RH_∞ is a set of rational transfer functions that are stable (their poles lie in the open right half-plane) and proper (the numerator polynomial degree of these functions is less than or equal to the denominator polynomial degree). Let $H(s)$ belongs to RH_∞ and satisfies $H(s)/_{s\to\infty}= -1 + O(s^{-2})$. Let $\{z_i, i = 1,..,n \quad n \in N\}$ are zeros of $H(s)$ with $Re(z_i) > 0$. Then:

$$\int_0^\infty log|H(j\omega)|\, d\omega = \pi \sum_{i=1}^n Re(z_i) \tag{45}$$

In control law design, it is desirable to prevent amplitudes of the dynamic responses $H^1_{zw}(s)$, $H^2_{zw}(s)$ and $H^3_{zw}(s)$ from being too large.

A brief examination of the results stated in Section 1 shows that the suspension deflection transfer function $H^2_{zw}(s)$ has modulus strictly grater than one for $\omega_2 = \sqrt{\frac{k_t}{m_u+m_s}}$ ($H^2_{zw}(j\omega_2) = -\left(1+\frac{m_u}{m_s}\right)$), i.e. an amplification greater than one occurs at frequency ω_2. This amplification can be made less only and only by adjusting the ratio of the unsprung and sprung masses. From the result:

$$H^3_{zw}(s)/_{s\to\infty}= -1 + \frac{k_t}{m_u}s^{-2} + O(s^{-3}) \tag{46}$$

it is evident, that $|H^3_{zw}(j\omega)|$ must tend to one from above as ω tends to ∞ and it turns out that $|H^3_{zw}(j\omega)|$cannot be made less than or equal to one at all frequencies. Since the right-hand side of (45) is non-negative then it is not possible for $|H^3_{zw}(j\omega)|$ to be less than or equal to one at all frequencies since that would make the left-hand side of the eq. (34) negative. It has been shown in [3], that no matter what signals are used for feedback, the tyre deflection transfer function must amplify road disturbances at some frequencies. As shown in [3], this fact is valid even for full state feedback used in the control loop.

A similar theorem is valid for transfer functions where $H(s)_{-\atop s\to 0} = 1 + O(s^2)$.

Theorem 2. Let $H(s)$ belongs to RH_∞ and satisfies $H(s)/_{s\to 0}= = 1 + O(s^2)$. Let $\{z_i, i = 1,..,n \quad n \in N\}$ are zeros of $H(s)$ with $Re(z_i) > 0$. Then:

$$\int_0^\infty log|H(j\omega)|\frac{d\omega}{\omega^2} = \pi \sum_{i=1}^n \frac{Re(z_i)}{|z_i|^2} \tag{47}$$

Similarly to the consequences of Theorem 1, the result $H^1_{zw}(s)/_{s\to 0}= 1 + O(s^2)$ from Section 1 is the case when $|H^1_{zw}(j\omega)|$ cannot be less than or equal to one at all frequencies since that would make the left-hand side of (47) negative. Again, this fact is valid even when full state feedback is introduced in the control loop [3].

In such cases that were mentioned above, designers have the only possibility to shift the frequencies where amplifications occur to more proper frequency ranges or to spread the ranges where amplifications occur making the amplification lower. The positive area of the Bode magnitude plot i.e., the area where $|H(j\omega)|$ is greater than one (is grater to at least the same extent as the negative area where $|H(j\omega)|$ is less than one) by choosing a proper feedback

controller. Analogically, similar results can be derived for arbitrarily chosen measurements and for any load disturbances.

7. Results

Using a simple linear two-degree of freedom car suspension model in Fig.1, it was shown that there are still some limitations to suspension performance even in the fully active state. It has been shown in the paper that there are some frequency points and frequency ranges where the transfer functions have modulus strictly greater than one i.e., where road and load disturbance amplification occur. On the base of the Bode integral theorems, it has been shown that the transfer functions must be greater in modulus to at least the same extent that is less than one when measured in terms of the area on a Bode magnitude plot. In such a case, there is a possibility to shift frequency ranges where disturbance amplification occurs to a more proper frequency range or to make magnitudes lower spreading the frequency range. A survey of transfer function limitations for all possible measured outputs in the active automotive suspension system are explained in [3].

Acknowledgment

This research has been supported by MSMT project INTER-VECTOR 17019.

References

[1] Freudenberg, J. S., Looze, D. P., “Right-half Plane Poles and Zeros and Design Tradeoffs in Feedback Systems”, IEEE Transactions on Automatic Control, 30/6, 1985

[2] Hyniova, K., “Frequency Response Limitations for Active Suspension of Vehicles”, Micro-CAD 99 – International Computer Science Conference, Miskolc, pp. 209-217, 2006

[3] Hyniova, K., Achievable Dynamic Responses for Active Suspension System of Vehicles, Habilitation thesis, Prague, 2000

[4] Zhou, K., Doyle, J.C., Essentials of Robust Control, Prentice Hall, London, 1998

Analysis of the influence of internal forces and moments on the nozzle of the main downcomer of a steam boiler drum

Pejo Konjatić[1], Ana Konjatić[2], Dajana Bičanić[3], Ivan Dunđer[4]
University of Slavonski Brod, Croatia[1], Industrial and Trade School Slavonski Brod, Croatia[2]
Đuro Đaković TEP d.o.o, Croatia[3], University of Slavonski Brod, Croatia[4]
pkonjatic@unisb.hr, ana.konjatic@gmail.com, dajana.bicanic@ddtep.hr, idundjer@unisb.hr

Abstract: *The present work deals with the analysis of the influence of internal forces and moments on the nozzle of the main boiler of a steam boiler used in the waste incineration industry. The analysis is carried out analytically by performing calculations using standards, and later numerically using finite element method software. As results of the analyses, equivalent von Mises stresses, displacements and buckling eigenvalues are obtained and compared with analytical solutions.*
Keywords*: STEAM BOILER, DOWNCOMER, NOZZLE, FINITE ELEMENT ANALYSIS*

1. Introduction

A steam boiler is an object in which the heat energy obtained by the combustion of organic fuels is transferred by means of heating surfaces to the liquid that evaporates in it and whose vapor is superheated to a certain temperature. [1]

Steam boilers are an integral part of many plants, including waste-to-energy (WTE) plants. Boilers for waste-to-energy plants are usually water tube boilers and usually have four passes: three vertical radiant passes and one convective pass. The first of the radiant passes is integrated into the furnace as an afterburner chamber. The convective pass, which houses the evaporators, superheaters, and economizers, can be vertical or horizontal. [2]

Boilers for waste systems are drum boilers, characterized by a drum. The drum is a large high-pressure cylinder of water located in the upper part of the boiler that physically separates the evaporation of the water from the superheating of the steam. The water circulates naturally over the downcomers and up through the evaporator tubes because the evaporated water (steam) has a lower density than the water in the downcomers. [3]

It is very important to ensure the safe operation of steam boilers, and standard calculations and inspections of all parts of the boiler object are required to verify and confirm safety. This also applies to the downcomers of the WTE boiler under consideration, the structure of which is shown in Figure 1.

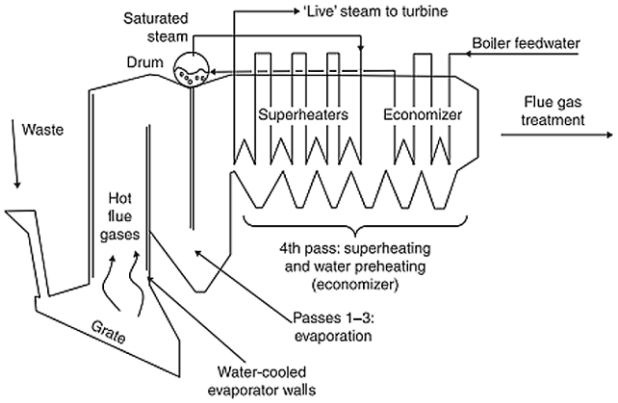

Fig. 1 *Four-pass WTE boiler [3]*

2. Problem description

To ensure safe operation of the steam boiler, the parts of the steam boiler and its supporting structure must be designed and tested using existing standards, and other means, including finite element analysis where required and applicable. Steam boiler downcomers are common and important parts of steam boilers used in the waste incineration industry, and they are connected to the drum of the steam boiler through nozzles. Therefore, safe operation of the above parts must be ensured.

The main focus was on the study of the influence of internal forces and moments on the nozzle of the main downcomer (Figure 2), which together with other loads and boundary conditions act on the mentioned component, in order to analyze its stability. This influence was analyzed analytically using the European standards. A 3D model of the structural part was created and the numerical calculation was also performed in Abaqus CAE. [4]

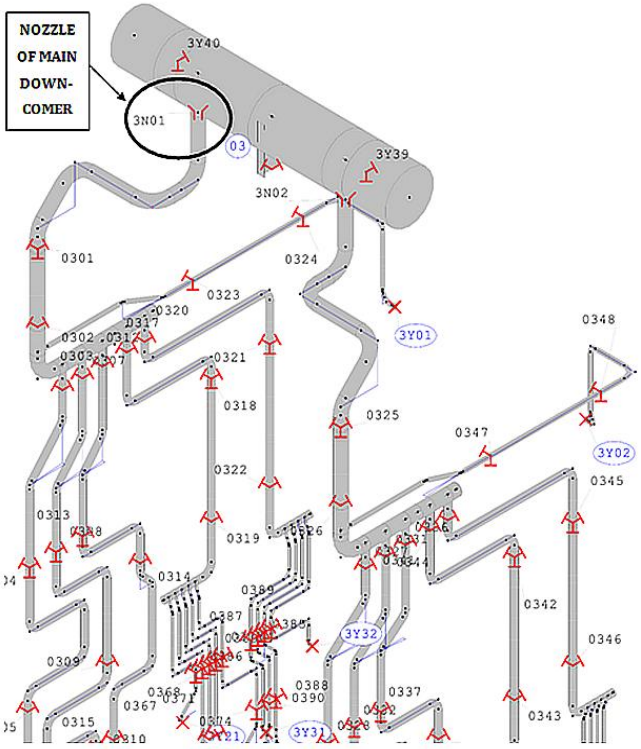

Fig. 2 *Downcomers of a steam boiler drum [5]*

3. Analytical calculation using EN 13445-3

In general, the standard EN 12952-3 [6]: 'Water-tube boilers and auxiliary installations - Part 3: Design and calculation for pressure parts of the boiler" is used for water-tube steam boilers, i.e. also for drums. However, this standard assumes in its chapter 8.3.2.1, which considers openings, including nozzles of downpipes, that external forces and moments acting on the nozzle are insignificant. If this is not the case, EN 13445 should be used to calculate and evaluate the resulting stresses.

Therefore, the third part of this standard, EN 13445-3 [7]: 'Unfired pressure vessels - Part 3: Design', is used for this calculation.

In addition to this standard, the following standards are also used: EN 10028-2 [8]: 'Flat products made of steels for pressure vessels - Part 2: Unalloyed and alloyed steels with specified properties at elevated temperatures" and EN 10216-2 [9]: 'Seamless

steel tubes for pressure vessels - Technical delivery conditions - Part 2: Unalloyed and alloyed steel tubes with specified properties at elevated temperatures".

Figure 2 shows the boiler drum with all its downcomers. As shown in the figure, the main downcomer bears the designation 3N01. The input data were determined in accordance with EN 13480 [10] and presented in the form of calculation results of the internal forces and moments at the nozzle of the main downcomer (Table 1).

Table 1 *Calculation results of downcomers according to the EN 13480*

Node	Displacement, mm			Force, kN			Moment, kN·m		
	w_x	w_y	w_z	Q_x	Q_y	Q_z	M_x	M_y	M_z
3N01	-	12,6	-9,6	-20,4	-2,1	-29,4	50,4	103,6	52,3
3N02	-	-12,6	-9,6	-20,4	2,1	-29,4	-50,4	103,6	52,3

Section 16.5 of EN 13445-3 provides a method for the design of a cylindrical shell with a nozzle subjected to local loads and internal pressure. In this calculation, the standard has been worked through its subsections. The sequence is as follows:

1. Calculation of allowable stresses of shell material and nozzle material,
2. Calculation of the conditions of applicability,
3. Calculation of maximum allowable individual loads (allowable pressure, allowable axial nozzle load, allowable circumferential and longitudinal moments),
4. Calculation of the combination of external loads and internal pressure (individual load ratios, interaction of all loads),
5. Calculation of stress ranges and their combination and
6. Calculation of nozzle longitudinal stresses (maximum longitudinal tensile stress, longitudinal stability of the nozzle). [7]

All calculations meet the conditions from the standard and are presented in related investigation [11] and due to the scope of the analytical calculation are not shown here.

4. Numerical analysis

For finite element method (FEM) analysis, a 3D model of the considered part of construction of a steam boiler was modelled in Abaqus CAE. Dimensions of model are obtained from technical documentation as well as loads, constraints and boundary conditions from previous investigation. [5]

Due to symmetry only one half of the drum shell geometry has been modelled: half of cylindrical shell with diameter of 2130 mm, one support (with saddle) and one nozzle of main downcomer. Model of geometry has been modelled as a 3D-shell model (Figure 3).

The material properties of the steels 15NiCuMoNb5-6-4 and 16Mo3 required for the finite element analysis are determined for the calculation temperature of 303°C according to EN 10216-2, for the required wall thickness by means of linear interpolation and fed into the material model. The material properties for 15NiCuMoNb5-6-4 are: E = 182,98 GPa, $R_{p0,2}$ = 354,2 MPa, ν = 0,3 and for 16Mo3 the material properties are: E = 182,98 GPa, $R_{p0.2}$ = 172,2 MPa and ν = 0,3.

Analyzed part of construction of a steam boiler drum consists not only of material of shell and nozzle, but also of material of pipelines inside the drum. Inner pipelines and isolation material are omitted in this analysis to simplify to the model, but an added material has been introduced in order to take into account influence of the additional materials as well as water inside the structure.

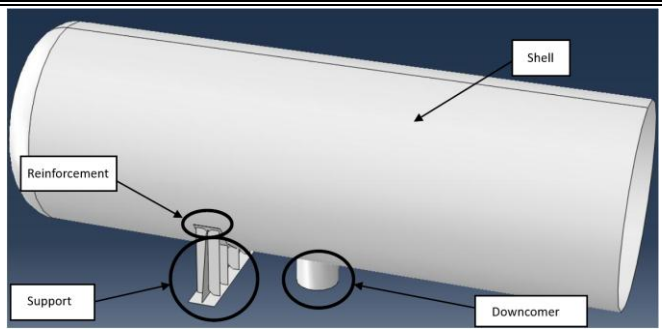

Fig. 3 *3D-shell model used for finite element analysis*

Beside material, in this modulus, sections of supporting construction have been defined as well as section thickness. Along with defining general step, a linear perturbation step was required in order to perform buckling analysis. Using interaction modulus contacts and constraints were defined as well (Tie Constraint, Rigid Body constraint). Construction was loaded with provided load (forces and moments, friction forces, acceleration of gravity, pressure) and boundary conditions (movement restriction in x and z direction, symmetry). Model is meshed with coarse mesh with size of elements of 25 mm. Finer mesh is defined on the nozzle where shell meets the downcomer (Figure 4).

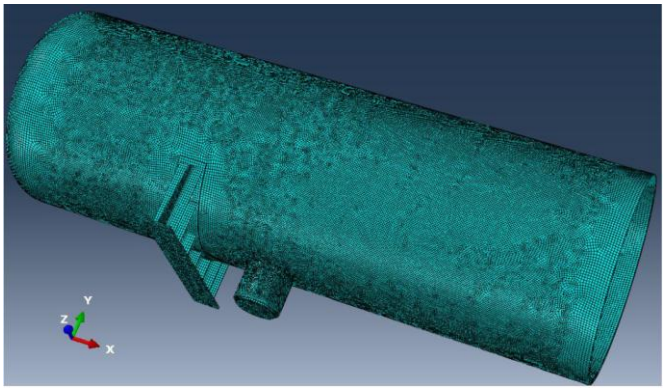

Fig. 4 *3D-shell model used for finite element analysis*

Shell element type has been used for whole construction. Results convergence has been conducted in order to check proper sizing of defined mesh to meet required accuracy. At the end, results in form of stresses, displacements and buckling eigenvalues have been obtained.

5. Results and discussion

An analysis of the influence of forces and moments on the connection of the main downcomer also considers dealing with the main drum parts under pressure.

After conducted finite element analysis described in previous chapter, equivalent von Mises stress distribution is obtained (Figure 5). It can be noted that the maximum stress occurs on the drum, i.e. exactly on the connection of the main downcomer with its value of 498,73 MPa.

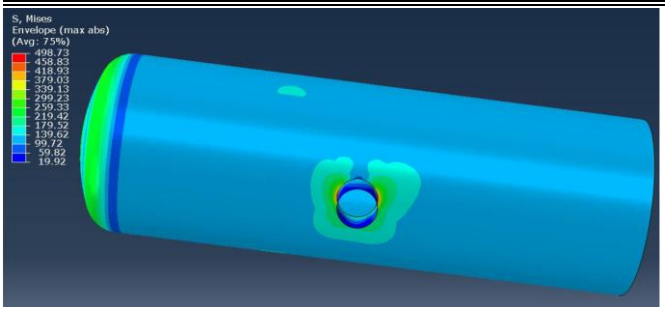

Fig. 5 *Distribution of equivalent von Mises stress on pressure parts of drum construction in MPa*

According to EN 13445-3, ANNEX 3, part C.7.3, the maximum stress is the range of equivalent stresses resulting from the changes in primary and secondary stresses $(\Delta\sigma eq)_{P+Q}$. By definition, primary stresses are those stresses that satisfy the equilibrium laws of the given loads (pressure, forces and moments). Thus, they are caused by internal forces and moments required to balance external forces and moments.

Secondary stresses are stresses that are a consequence of constraints due to geometric discontinuities, the use of materials with different modulus of elasticity under the action of external loads, or constraints due to different thermal expansions. Therefore, they cause internal forces and moments required to satisfy the specified constraints.

The range of equivalent stresses resulting from the primary and secondary stresses, i.e., those that balance the external forces and moments and those that satisfy the specified limitations, is the maximum stress determined by the finite element analysis. This combination of stresses gives $(\Delta\sigma_{eq})_{P+Q}$ stress defined in [7] with value of $(\Delta\sigma_{eq})_{P+Q}$ = 498,73 MPa. According to [7] this stress cannot exceed triple value of allowable stress obtained by reducing yield load with safety factor, which is fulfilled in this situation.

Distribution of equivalent von Mises stress on the support is shown on Figure 6. It can be noted that maximum equivalent stress is lower than allowable stress of (116,47 MPa). Allowed von Mises equivalent stress on the support is obtained via yield strength and safety factor 1,5.

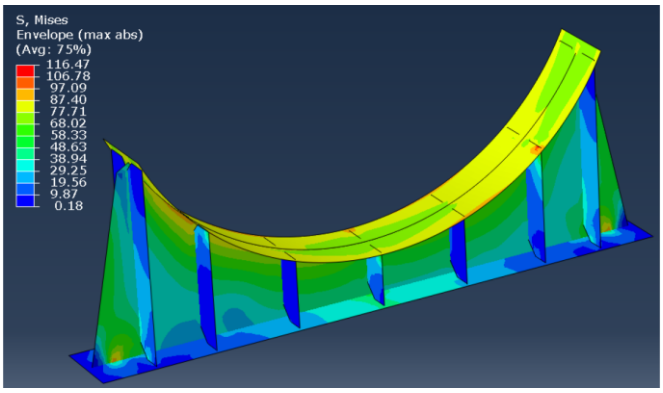

Fig. 6 *Distribution of equivalent von Mises stress in drum support in MPa*

Total displacements due to load, self-weight and pressure are presented on Figure 7 where can be noted that maximum value of displacement is under 4 mm.

As result of the buckling analysis obtained using finite elements so-called eigenvalue ("Eigen Value") is obtained. It represents the buckling factor. This factor is a value that indicates by how many times the load must be increased to cause buckling. In this case, this value is -1,79 (Figure 8). Therefore, the condition that absolute value of buckling factor must be greater than one is fulfilled.

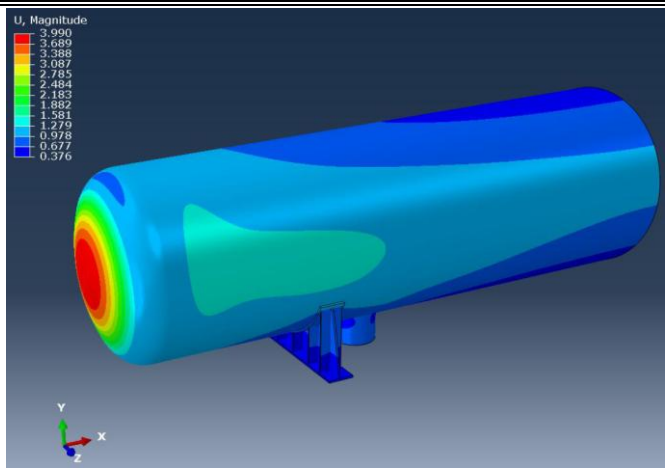

Fig. 7 *Distribution of total displacement in mm*

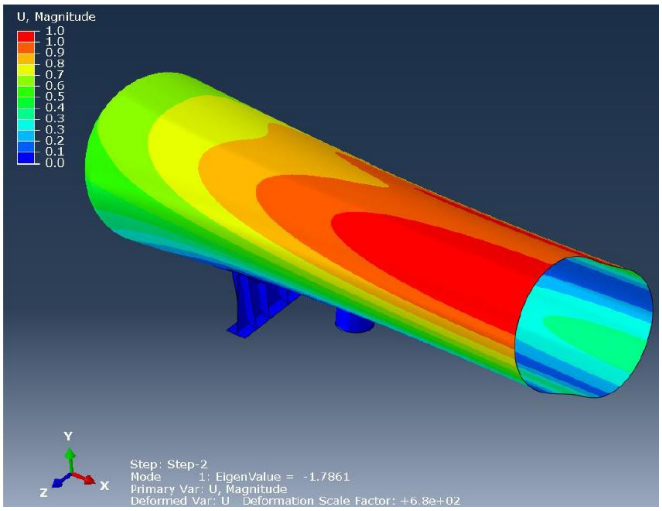

Fig. 8 *Distribution of Eigenvalue in buckling analysis*

This means that there is no risk of buckling due to the action of the internal forces and moments, gravity and pressure load on the connection of the main downcomer pipes. Buckling would only occur if the load were increased by 1,79 times. A negative value occurs for vessels under pressure and indicates that buckling would occur if the pressure acted in the opposite direction, i.e., if the vessel was subjected to excessive external pressure, i.e., vacuum.

6. Conclusion

After the analytical and numerical analysis of the critical parts in steam boiler construction, the connection of the steam boiler drum with the main downcomer is analyzed analytically using the existing standards and numerically using the finite element method.

Using the whole finite element model of the steam boiler, loads, internal forces and moments are determined and later used as boundary conditions and loads for the shell 3D finite element model of the connection between the drum and the main downcomer.

According to the performed analysis, it can be concluded that the stresses occurring in the expected operation of the critical parts of the steam boiler structure are within the allowable values for the steam boiler drum and the supporting structure.

A local stress concentration occurred at the connection between the drum and the downcomer. This stress intensity does not exceed the maximum stress defined in the standard EN 13445-3, ANNEX 3, part C.7.3.

Finally, a buckling analysis of the shell model of the drum-downcomer connection with support was performed. This analysis

has shown that there is no risk of buckling due to the action of internal forces and moments, gravity and compressive load on the connection of the main pipes of the downcomer.

7. References

[1] M. Gulić, Lj. Brkić, P. Perunović, *Steam boilers*, Faculty of Engineering, Beograd, (1988)

[2] L. Branchini, *Waste-to-energy Advanced cycles and new design concepts for efficient power plants*, Springer International Publishing, Bologna (2015), pp. 34

[3] N. Klinghoffer; M. Castaldi, *Waste to energy conversion technology*, *Woodhead Publishing Limited*, Cambridge (2013), pp. 125-126

[4] Abaqus/CAE 2016, Dassault Systemes Simulia Corp.

[5] ĐĐ TEP, Technical Report, *Strength calculation of a boiler drum*

[6] BS EN 12952-3: 2001: BSI British Standards, *Water-tube boilers and auxiliary installations – Part 3: Design and calculation for pressure parts of the boiler*

[7] BS EN 13445-3: 2009: BSI British Standards, *Unfired pressure vessels – Part 3: Design*

[8] BS EN 10028-2: 2003: BSI British Standards, *Flat products made of steels for pressure purposes – Part 2: Non-alloy and alloy steels with specified elevated temperature properties*

[9] EN 10216-2: 2002/prA2 2007: European Standard, *Final Draft, Seamless steel tubes for pressure purposes – Technical delivery conditions – Part 2: Non-alloy and alloy steel tubes with specified elevated temperature properties*

[10] BS EN 13480: BSI British Standards, Metallic industrial piping

[11] D. Bičanić: *Analysis of influence of inner forces and moments on the nozzle of main downcomer of a steam boiler drum*, graduation thesis, Mechanical Engineering Faculty in Slavonski Brod, University of Slavonski Brod, Croatia (2018)

Stress and stability calculation of the third pass module of the steam boiler during lifting

Pejo Konjatić[1], Sara Radojičić[1], Marko Katinić[1], Meri Rendulić[1]
University of Slavonski Brod, Croatia[1]
pkonjatic@unisb.hr, sradojicic@unisb.hr, mkatinic@unisb.hr, rendulicmeri@gmail.com

Abstract: *This paper presents the calculation of the stress and stability of a third-cycle module of a steam boiler during the lifting process. A steam boiler is a key element of a cogeneration plant, so all calculations are performed according to prescribed standards. Before the numerical analysis of the steam boiler, the characteristics, components and function of the boiler are described, as well as the required standards. The 3D model of the boiler was created using the Abaqus/CAE 2016 program package according to the manufacturer's technical documentation. Using the finite element method, the stresses and stability during lifting of the boiler from the horizontal and vertical positions were calculated and presented. It was found that when lifting from a horizontal position, the structural stress values of the main elements do not exceed the allowable values. On the other hand, when lifting from a vertical position, the stresses exceed the allowable values. In this case, the connection point between the lug and the profile was checked and analytically dimensioned. The obtained values of the stability analysis of the boiler module are satisfactorily defined and there is no risk of buckling in both cases of lifting. The boiler conforms with the standard and fulfils the requirements handed over to the engineer.*
Keywords*: STEAM BOILER, STRESS, STABILITY, FINITE ELEMENT METHOD*

1. Introduction

In a conventional context, a steam boiler is a closed vessel and it allows the transfer of combustion heat to the working medium until it is boiling and becomes steam. It could be stated that a steam boiler is an exchanger of heat between water and fire. It is the part of a steam generated power plant process that and as a result produces the heat. That generated steam can then be utilized to pass the heat to a process that and transforms it to work [1].

The main components of a cogeneration plant are: Steam Boiler, Steam Turbine and Electricity Generator. Fuel and air are supplied to the steam boiler to produce high pressure steam through the combustion process. The high-pressure steam is fed into the steam turbine, where the expansion of the steam converts some of the heat energy into mechanical energy of rotor rotation. The rotor of the electric generator is attached to the steam turbine rotor, and the mechanical energy is converted into electricity. Depending on the needs, the steam exiting the turbine is used for technological processes or for heating. If the thermal energy of the output steam is not fully used, it is directed to the condenser and released to the ambient air or water. The energy efficiency of this type of equipment ranges from 0,7 to 0,8 [2].

A cogeneration plant that uses biomass as a fuel source becomes more environmentally friendly by using waste materials from the wood industry and more competitive in the marketplace by having a more acceptable price and locally available fuel sourcing [3-7]. In the following chapters, the characteristics, components, and functions of combined heat and power plants and steam boilers are described in more detail. The calculation of the stresses and stability of the module of the third pass of the steam boiler during lifting is performed using the Abaqus/CAE 2016 program package. The cases of lifting from the horizontal and vertical position are considered, all stages of the analysis are described in detail. It is essential for a designer to engineer and calculate a steam boiler that provides security, durability and usability to the customer. Completing that task requires a great understanding of the design specifications, especially geometry of the pressure vessel, which has to be reviewed to abide with the standards for the design [8]. For that reason, various studies have been conducted and performed to describe the design and calculations of steam boilers [9-12].

This paper presents the results of the stress and stability calculation of the third pass module of the boiler during the lift. The 3D model of the steam boiler was designed using the Abaqus/CAE 2016 program package [13] based on the technical documentation of company Đuro Đaković Termoenergetska Postrojenja d.o.o. [14]. Using the finite element method, the stresses and stability in the course of lifting the boiler from the horizontal and vertical positions were calculated and described.

2. Problem description

The lifting and positioning of the boiler to a certain height is done with an overhead crane using trusses, pulleys and ropes. A truck with a trailer is positioned under the lifted boiler, which is lowered onto the trailer and transported to the cogeneration plant construction site. The process is shown in Figure 1.

Fig. 1 *Steam boiler module transport*

At the construction site, the boiler module must be lifted from the trailer and installed in a supporting steel structure (Figure 2). The boiler is lifted by two cranes, and its rotation is performed in the air. The supporting steel structure is a spatial metal structure used for fastening, supporting and suspending heating surfaces, walls, smoke ducts, piping and other elements belonging to the boiler. Due to significant thermal expansions, the structure is a very responsible part of the boiler. The design of the steel structure depends on the steam boiler, because the design solutions of boilers can be very different.

Fig. 2 *Supporting steel structure*

The steel support structure consists of the main columns mounted on concrete foundations and steel feet. The main columns are connected by cross beams, and the areas between them are filled with auxiliary frames and struts. They are most commonly used for supporting brackets for studs and sheet metal boiler formwork. In this paper, two cases of lifting are considered: from a horizontal and a vertical position.

Lifting from a horizontal position is done in such a way that the first crane is connected to the first lifting beam, lifting beam 1 is attached with ropes to the auxiliary lifting beam, which is connected to lugs no. 1 and 2. The second crane is connected to the second lifting beam, two pulleys are connected to beam 2, a rope is passed through them and attached to lugs no. 3 and 5 and no. 4 and 6 respectively. In this way, the load is evenly distributed to all four lugs, as can be seen in Figure 3. The first and the second crane simultaneously lift the boiler module to the required height in relation to the trailer. After that, the first crane maintains the position reached, while the second crane continues its rotation to the final vertical position.

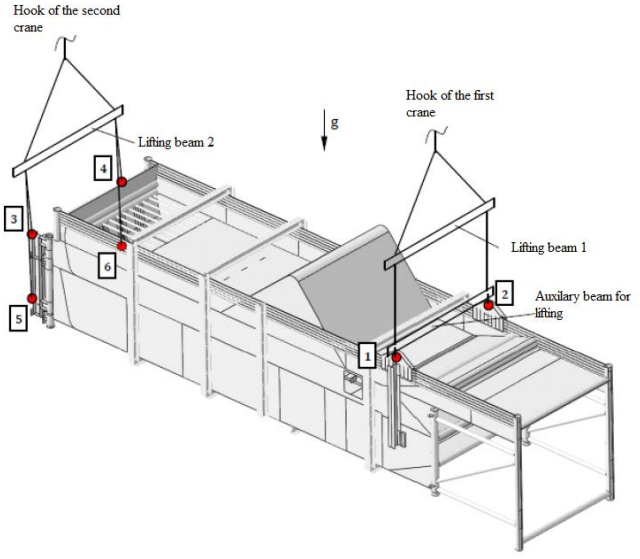

Fig. 3 *The display of lifting the module from the horizontal position*

After the boiler module is rotated to the vertical position, it is lifted and inserted into the supporting structure. Figure 4 shows the process of fixing the boiler module to the cranes, its lifting, rotation and insertion into the supporting steel structure.

Fig. 4 *Attaching the boiler module to cranes, its lifting, rotation and placement in the load-bearing steel structure.*

3. Numerical analysis of the boiler module

The boiler module is bounded by the back and side walls of the first, second, and third boiler passages. The 3D model shown in Figure 5 was created using Abaqus software [13]. The geometric model is discretized mainly with finite shell elements. Around the walls of the boiler module, there are bandages enclosed in a support ring, which help to stiffen the membrane walls (defined as an orthotropic plates) to maintain stability during lifting and placement of the module. Supporting profiles and bandages are defined by beam elements to which the required properties are assigned. The 3D model was created according to the technical documentation [14].

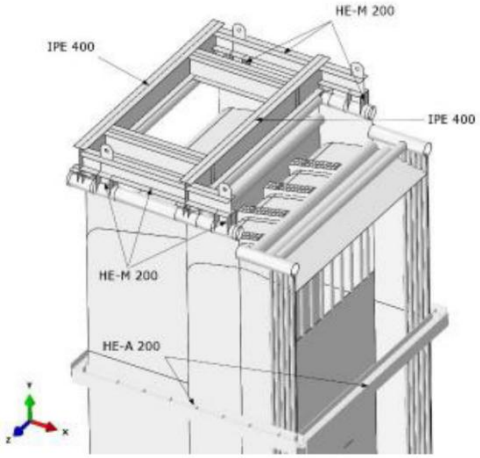

Fig. 5 *Display of loading profiles and bandages*

The numerical calculation of the boiler module is performed for the cases of lifting from horizontal and from vertical position. The first step is to create and define the properties of all materials used. The material 16Mo3 is applied to the side and rear walls of the passage, bandages, supporting profiles and chamber. The material S235JR+N / S355J2+N is defined for lugs and reinforcements, the

yield strengths of the mentioned materials are defined by standards [15-17], as shown in Table 1.

Table 1 *Properties of defined materials [15-17]*

Material	Thickness, t, mm	Yield strength, $R_{p0,2}$, MPa	Norm
16Mo3	$t \leq 16$	280	EN 10216
	$16 < t \leq 40$	270	
16Mo3	$t \leq 16$	275	EN 10028-2
	$16 < t \leq 40$	270	
S235JR+N	$t \leq 16$	235	EN 10025-2
	$16 < t \leq 40$	225	
S355J2+N	$t \leq 16$	335	EN 10025-2
	$16 < t \leq 40$	345	

The membrane wall of a steam boiler can be approximated by an equivalent orthotropic plate that has the same elastic properties as a true membrane wall. Using Kirchhoff-Love shell theory, the constitutive equation of an equivalent orthotropic plate can be written:

$$\sigma = D \cdot \epsilon \tag{1}$$

Where σ is the vector of internal forces, D is the elasticity matrix, ε is the deformation vector. The matrix expression (1) represents the six constitutive equations of the membrane wall as a structurally orthotropic plate or an equivalent orthotropic plate, which connect the internal forces with the corresponding deformations. The next step of the numerical calculation is to define the stiffness matrix for each wall (back wall and side walls of the first, second and third pass).

To obtain the desired results, the model is assigned the material properties of the above-mentioned materials. For lifting from the horizontal position, a global model is created using a coarse mesh with a finite element mesh size of 40 mm, and an element size of 5 mm is specified at the locations of the structural elements that are important for the lifting conditions. Four boundary conditions are applied. The first boundary condition is located on lug no. 1, with restricted x-direction. The second boundary condition applies to the lug No. 2, with restricted x-direction. The third boundary condition is on lug no.3, with both the x and y directions constrained. The fourth boundary condition is applied to lug no. 4, with both the x and y directions constrained. For lifting from the vertical position, a global model is also created with a coarse mesh, but with a finite element mesh size of 50 mm. An element size of 5 mm is specified at the locations of the structural elements that are important for the lifting conditions. The same boundary conditions apply as for lifting from the horizontal position. Figure 6 shows the model with a fine mesh of the lug.

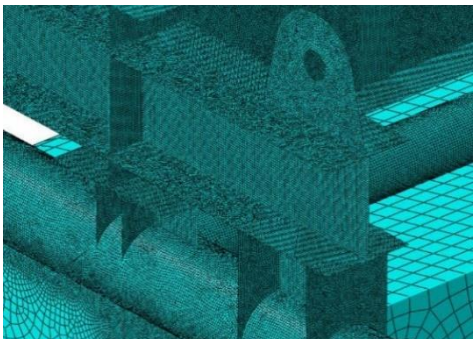

Fig. 6 *Model with fine mesh of the lug*

4. Results analysis

All material and test pressure data previously given were used to obtain results for lifting from horizontal and vertical positions. The stresses that occur at the top of the module when lifted from a horizontal position are shown in Figure 7. The maximum stress according to von Mises is 98 MPa.

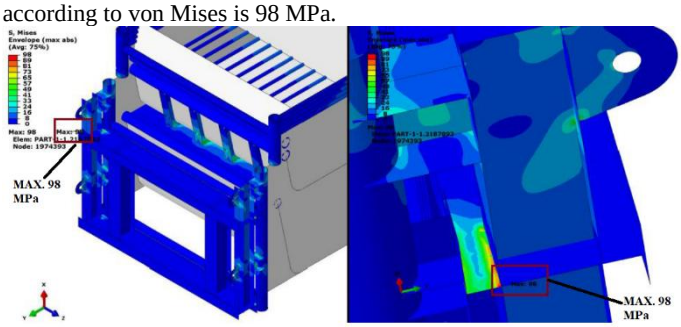

Fig. 7 *Distribution of the equivalent von Mises stress in conditions of lifting from a horizontal position*

The stresses occurring in the lower part of the boiler module are highest in the area of lugs 1 and 2, more precisely near lug 2, where the maximum stress according to von Mises is 125 MPa (Figure 8). The highest stress according to von Mises is at lugs 1 and 2, it is 43 MPa and is shown in Figure 9.

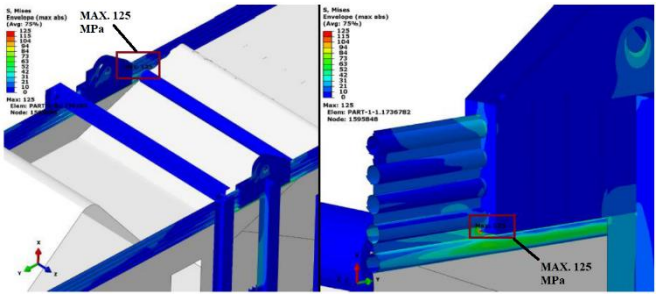

Fig. 8 *Distribution of the equivalent von Mises stress of the lower part of the module*

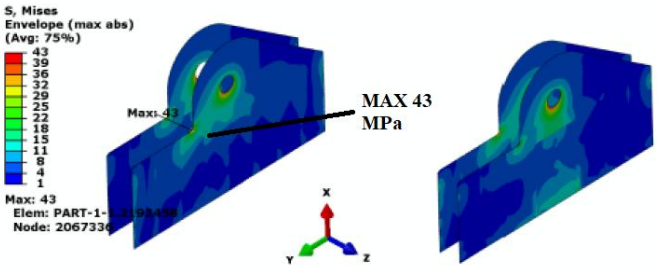

Fig. 9 *Distribution of the equivalent von Mises stress of the lugs 1 and 2*

The calculation of the stress on the structure in the conditions of lifting from a horizontal position was carried out under the load of its own weight. The yield strength of the lug material is $R_{p0,2}$ = 225 MPa [17], the safety factor is equal to S_F = 1,35 and the dynamic factor is equal to S_{din} = 1,2 [18]. According to the given data, the allowable stress is:

$$\sigma_{all} = \frac{R_{p0,2}}{S_F \cdot S_{din}} = \frac{225}{1{,}35 \cdot 1{,}2} = 138{,}8 \text{ MPa} \tag{2}$$

Since the maximum stress is 125 MPa, it does not exceed the allowable values, and it is not necessary to analytically check the joint between the lug and the profile HEM 200.

The stresses that occur on the upper part of the module when it is lifted from a vertical position are shown in Figure 10. The maximum stress according to von Mises is 217 MPa at the junction of the lug no. 6 and the profile HEM 200. The highest stress according to von Mises is at the lugs 1 and 2, it is 43 MPa and is shown in Figure 11.

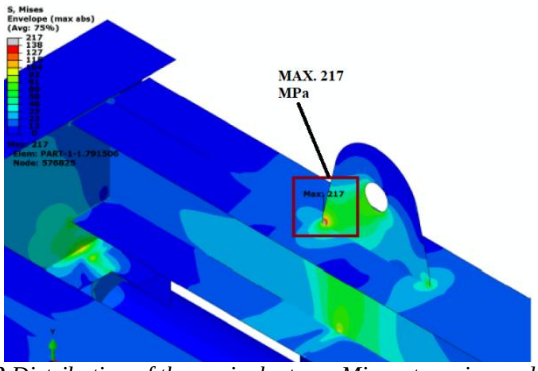

Fig. 10 *Distribution of the equivalent von Mises stress in conditions of lifting from a vertical position*

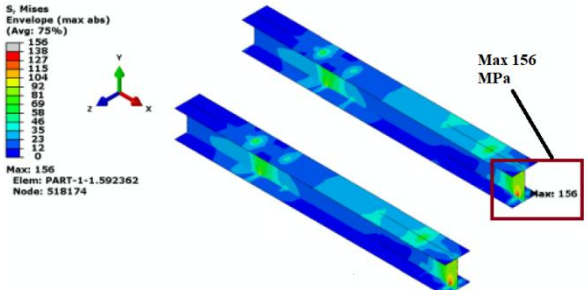

Fig. 11 *Distribution of the equivalent von Mises stress of the HEM profile*

The stress calculation of the structure under the conditions of lifting from a vertical position was carried out under the load of its own weight. Yield strength, safety factor and dynamic factor have the same values as in the case of lifting from a horizontal position. Since the highest stress occurs in the lugs, which are made of the same material, the allowable stress is equal to 138,8 MPa like in expression 2. Since the highest stress is 217 MPa, which exceeds the allowable values, it is necessary to check the connection point between the lug and the profile and dimension the lug. With this analytical calculation, the link plate, whose maximum stress is 105 MPa, is sized so that it does not exceed the allowable value and meets the prescribed condition.

4. Conclusions

This paper presents the results of stress and stability calculation of the third pass module of the steam boiler during the lift. The cases of lifting from a horizontal and vertical position are considered, and the work was carried out according to the technical documentation of the company ĐĐ TEP. In the work, the module is tested as described in the standard. Based on the obtained results of the numerical analysis, an analytical calculation of the lug was performed. The numerical analysis of the problem was performed using the Abaqus/CAE 2016 program package. The stress and stability results during lifting of the boiler module in two cases are presented.

It was found that when lifting from a horizontal position, the stress values of the structurally important elements do not exceed the allowable values and it is not necessary to analytically check the location of the connection of the lug and the profile. On the other hand, when lifting from a vertical position, the stresses occur in the upper part of the module, i.e. at the point of connection of lug no. 6 and the profile HE -M 200, exceed the permissible values. In this case, the position of the connection between the lug and the profile was checked and the required lug was analytically dimensioned. The boiler module conforms with the standard and fulfils the requirements handed over to the engineer in the construction of steam boilers.

5. References

1. Teir, S. *Steam Boiler Technology.* Scope 11 in Energy Engineering and Environmental Protection publications, Helsinki University of Technology, Department of Mechanical Engineering, Helsinki University of Technology, (2002)
2. Stojkov, M., Hnatko, E., Kljajin, M., Živić, M., Hornung, K. *CHP and CCHP Systems Today*, International journal of electrical and computer engineering systems, Vol 2. No.2, (2011), pp. 75.-79.,
3. Dong, Z. *Dynamical modeling and coordinated control design of a multimodular nuclear power-hydrogen cogeneration plant*, Energy Conversion and Management, 272, (2022), 116369. https://doi.org/10.1016/j.enconman.2022.116369
4. Sadeghi, M. M., Mahmoudi, S. R., & Rosen, M. A. *Thermoeconomic analysis of two solid oxide fuel cell based cogeneration plants integrated with simple or modified supercritical CO2 Brayton cycles: A comparative study*, Energy, 259, (2022) 125038. https://doi.org/10.1016/j.energy.2022.125038
5. Asadzadeh, S. M., & Andersen, N. A. *Model-based fault diagnosis of selective catalytic reduction for a smart cogeneration plant running on fast pyrolysis bio-oil*, IFAC-PapersOnLine, 55(6), (2022) pp. 427–432. https://doi.org/10.1016/j.ifacol.2022.07.166
6. Desai, N. B., Mondejar, M. E., & Haglind, F. *Techno-economic analysis of two-tank and packed-bed rock thermal energy storages for foil-based concentrating solar collector driven cogeneration plants*, Renewable Energy, 186, (2022), pp. 814–830. https://doi.org/10.1016/j.renene.2022.01.043
7. Abdel-Dayem, A., & Hawsawi, Y. M. *Feasibility study using TRANSYS modelling of integrating solar heated feed water to a cogeneration steam power plant*, Case Studies in Thermal Engineering, 39, (2022), 102396. https://doi.org/10.1016/j.csite.2022.102396
8. EN 12952-1:2015, *Water-tube boilers and auxiliary installations -- Part 1: General* (2015.)
9. Abdel-Dayem, A., & Hawsawi, Y. M. *Feasibility study using TRANSYS modelling of integrating solar heated feed water to a cogeneration steam power plant*, Case Studies in Thermal Engineering, 39, (2022), 102396. https://doi.org/10.1016/j.csite.2022.102396
10. Pástor, M., Lengvarský, P., Trebuňa, F., & Čarák, P. *Prediction of failures in steam boiler using quantification of residual stresses*, Engineering Failure Analysis, 118, (2020), 104808. https://doi.org/10.1016/j.engfailanal.2020.104808
11. Taler, J., Dzierwa, P., Jaremkiewicz, M., Taler, D., Kaczmarski, K., Trojan, M., & Sobota, T. *Thermal stress monitoring in thick walled pressure components of steam boilers*, Energy, 175, (2019), pp. 645–666. https://doi.org/10.1016/j.energy.2019.03.087
12. Lazić, V., Arsić, D., Nikolić, R. R., Rakić, D., Aleksandrović, S., Djordjević, M., & Hadzima, B. *Selection and Analysis of Material for Boiler Pipes in a Steam Plant*, Procedia Engineering, 149, (2016), pp. 216–223. https://doi.org/10.1016/j.proeng.2016.06.659
13. Abaqus CAE, Abaqus/CAE 2016., Dassault Systemes Simulia, 2015.
14. ĐĐ TEP, Technical Report
15. EN 10216:2014, *Seamless steel tubes for pressure purposes – Technical delivery conditions*, (2014.)
16. EN 10028-2:2017, *Flat products made of steels for pressure purposes – Part 2: Non-alloy and alloy steels with specified elevated temperature properties*, 31, (2008.)
17. EN 10025-2: 2004: *European standard for hot-rolled structural steel. Part 2 – Technical delivery conditions for non-alloy structural steels*, (2004.)
18. EN 1993-1-7:2008/NA, *Eurocode 3: Design of steel structures -- Part 1-7: Plated structures subject to out of plane loading*, 5, (2008.)

ИССЛЕДОВАНИЕ ВЛИЯНИЯ РЕЖИМОВ КОМБИНИРОВАННОЙ ТЕРМОМЕХАНИЧЕСКОЙ ОБРАБОТКИ НА МИКРОСТРУКТУРУ ЭКОНОМНОЛЕГИРОВАННОЙ СТАЛИ 5ХВ2С

INVESTIGATION OF THE EFFECT OF COMBINED THERMOMECHANICAL PROCESSING MODES ON THE MICROSTRUCTURE OF ECONOMY-ALLOYED STEEL 5KHV2S

Sergey Lezhnev[1], Abdrakhman Naizabekov[1], Dmitry Kuis[2], Igor Stepankin[3], Evgeniy Panin[4], Andrey Tolkushkin[1]

[1] Rudny industrial Institute, 50 let Oktyabrya str. 38, Rudny, 115000, Kazakhstan
[2] Belarusian State Technological University, Sverdlova str. 13a, Minsk, 220006, Belarus
[3] Belorusneft, 9 Rogachevskaya Street, Gomel, 246003, Belarus
[4] Karaganda Industrial University, Republic av. 30, Temirtau, 101400, Kazakhstan
e-mail: sergey_legnev@mail.ru

Abstract: *Until now, an urgent task for the machine-building industry is to replace expensive high-alloy steel grades with cheaper economically alloyed grades, but not inferior to high-alloy ones in mechanical and operational properties. This work is devoted to the study of the influence of various modes of combined thermomechanical processing technology, including forging in a tool that implements alternating deformations in metal, as well as thermal or thermochemical processing, on the evolution of the microstructure of economically alloyed steel grade 5KHV2S. The conducted studies allowed us to prove that the proposed modes of combined thermomechanical processing contributed to a qualitative improvement of the microstructure compared to samples not subjected to pre-forging in a new forging tool that implements alternating deformations in metal. And first of all, this was expressed in obtaining a finer-grained and uniform structure, both in the surface layer and in the base. At the same time, the thickness of the modified layers was up to 1.5 mm after cementation, up to 0.6 mm after nitrocementation.*

Keywords: *THERMOMECHANICAL PROCESSING, FORGING, HARDENING, CEMENTATION, NITROCEMENTATION, MICROSTRUCTURE, ECONOMICALLY ALLOYED STEEL.*

1. Введение

Термомеханическая обработка легированных сталей является обязательной технологической операцией обработки различных заготовок при формировании структуры в металлоизделиях. Измельчение и текстурирование зерен твердого раствора в совокупности с направленным формоизменением позволяет существенно улучшить механические и эксплуатационные показатели различных деталей машин. Как правило, ковка, обеспечивает подготовку микроструктуры к последующей термической обработке хромистых и других сталей, содержащих карбидообразующие элементы. Интенсивность проработки структуры при ковке, а также обработка поковки и заготовок в состоянии аустенитной структуры, предоставляет возможность для комбинированного использования собственно горячей обработки давлением в совокупности с термической обработкой для получения структуры металла с улучшенными характеристиками. Поэтому разработка новых технологий комбинированной термомеханической обработки заготовок из экономнолегированных сталей, является актуальной научно-технической задачей.

Основной целью данных исследований является изучение влияния разработанной комбинированной технологии термомеханической обработки, включающей ковку в инструменте, реализующем в металле знакопеременные деформации, а также термическую или же термохимическую обработку, на эволюцию микроструктуры экономнолегированной марки стали 5ХВ2С.

На первом этапе данных исследований была разработана новая технология ковки заготовок в инструменте, реализующем в металле знакопеременные деформации [1] и исследовано влияния данной технологии на эволюцию микроструктуры и изменение механических свойств стали марки 5ХВ2С [2-4].

На втором этапе были предложены следующие режимы термической и термохимической обработки стали 5ХВ2С, ранее подвергнутой ковке в инструменте, реализующем в металле знакопеременные деформации.

1) Термическая обработка: закалка от температуры 880°С в масле с последующим отпуском при температуре 200°С (1-й режим) и 500°С (2-й режим).

2) Термохимическая обработка:

2.1) цементация в твердом карбюризаторе (920°С, 8 и 12 часов) + закалка от температуры 880°С в масле с последующим отпуском при температуре 200°С и 500°С;

2.2) нитроцементация в твердом карбюризаторе модифицированном карбамидом (880°С, 6 и 8 часов) + закалка от температуры 880°С в масле с последующим отпуском при температуре 200°С и 500°С.

Именно второму этапу исследований и посвящена данная работа. Хочется отметить, что для проведения сравнительного анализа параллельно с проведением термической и термохимической обработки стали 5ХВ2С, ранее подвергнутой ковке в инструменте, реализующем в металле знакопеременные деформации, по аналогичным режимам была проведена термическая и термохимическая обработка стали 5ХВ2С, подвергнутой отжигу при температуре 700°С с выдержкой 40 минут [5].

2. Экспериментальная часть

Экспериментальные исследования проводили на лабораторной базе Рудненского индустриального института (Казахстан) и Белорусского государственного технологического университета (Беларусь). Для нагрева образцов использовали муфельные печи SNOL 30/1300 LSF01. Нагрев не подвергаемых упрочнению образцов, осуществляли в контейнерах с чугунной стружкой и герметичным затвором между крышкой и корпусом. Замок засыпали мелкозернистым кварцевым песком. При проведении закалки контейнер извлекали из печи и сразу после открытия образцы на подвеске извлекали из стружки и помещали в закалочное масло. При проведении упрочняющей обработки, осуществляемой до закалки, реализовали два варианта. По первому проводили науглероживание в контейнерах с модифицированным углекислым барием древесным углем. После его окончания контейнеры охлаждали вместе с печью, а затем проводили нагрев под закалку в контейнере с чугунной стружкой. По второму варианту высокотемпературную нитроцементацию

проводили в контейнере с древесным углем, модифицированным мочевиной. Поскольку температура насыщения совпадала с температурой нагрева под закалку, то ее проведение осуществляли путем непосредственного извлечения подвески с образцами из контейнера с углем и погружения в закалочное масло. Во всех случаях в качестве закалочной среды использовали полимерную композицию «ТЕРМОВИТ-М». Таким образом, для проведения металлографических исследований стали 5ХВ2С была получена серия образцов, подвергнутых термической и термохимической обработке на различных режимах.

Для изучения микроструктуры из всех образцов на отрезном станке для влажной абразивной резки BRILLANT 230 ATM были вырезаны темплеты и подготовлены микрошлифы на полировально-шлифовальном станке SAPFIR 520. Для выявления микроструктуры использовался универсальный для железоуглеродистых сплавов травитель: 4 % HNO3 в этиловом спирте.

3. Результаты и обсуждение

Анализ эволюции микроструктуры был проведен с применением металлографического комплекса, включающего световой микроскоп МИ-1, цифровую камеру Nikon Colorpix-4300 с фотоадаптером. Результаты исследования микроструктуры исследуемых образцов представлены на рисунках 1–4.

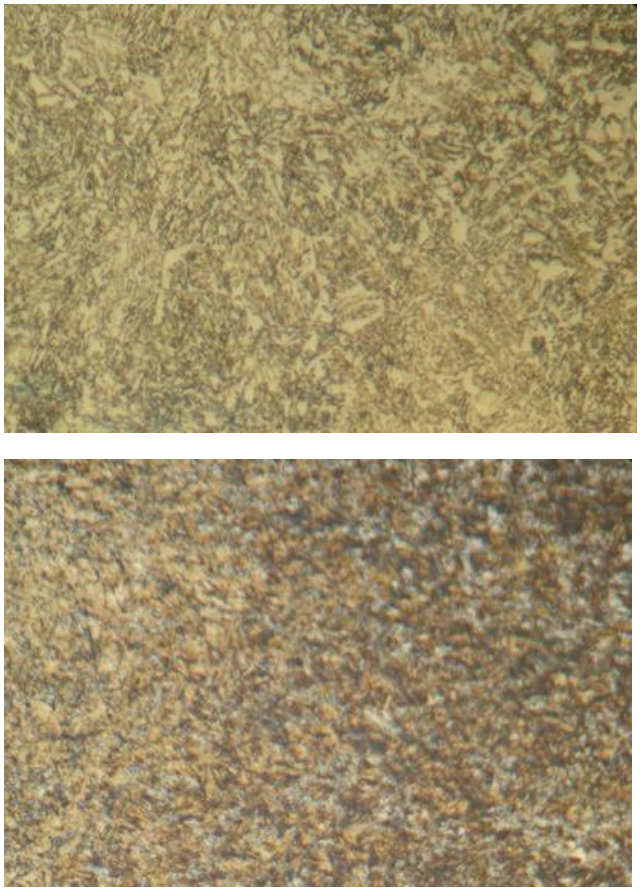

а

б

Рис. 1. *Микроструктура стали 5ХВ2С после отжига (а), и ковки (б); ×1000*

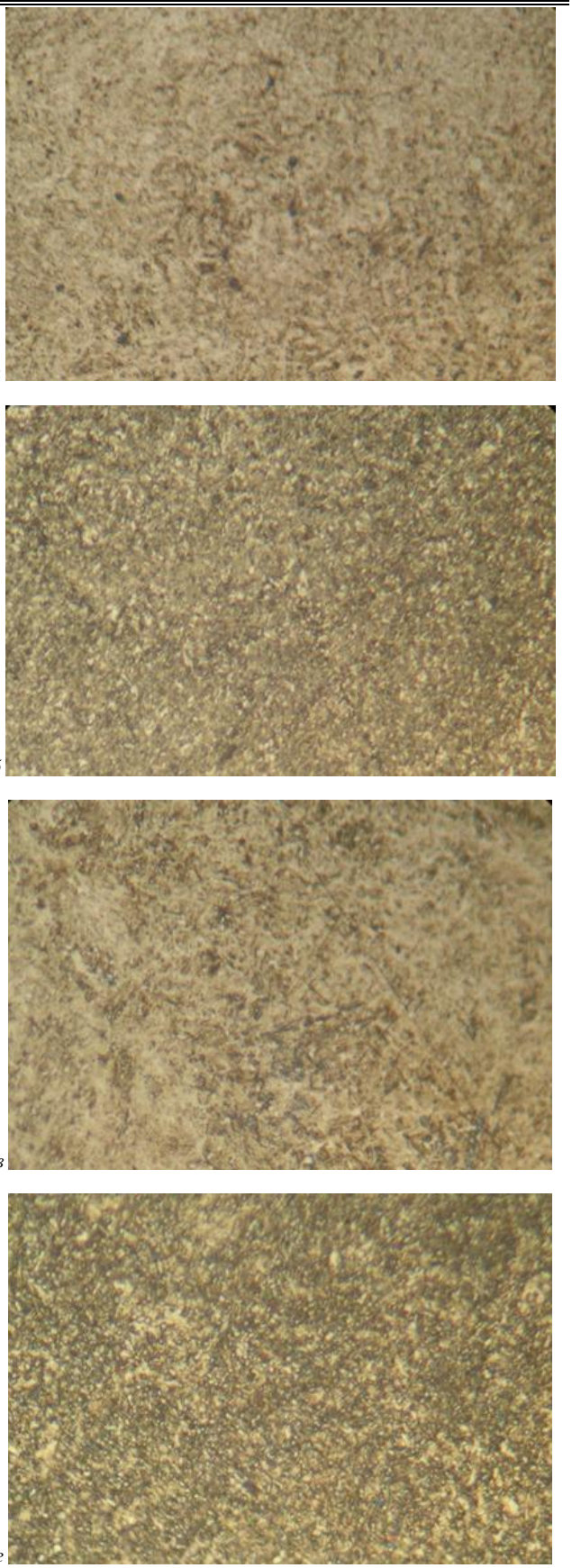

а

б

в

г

а - ковка, закалка 880 ℃ + отпуск 200 ℃; б -ковка, закалка 880 ℃ + отпуск 500 ℃; в -отжиг, закалка 880 ℃ + отпуск 200 ℃; г - отжиг, закалка 880 ℃ + отпуск 500 ℃

Рис. 2. *Микроструктура стали 5ХВ2С после термической обработки; ×1000*

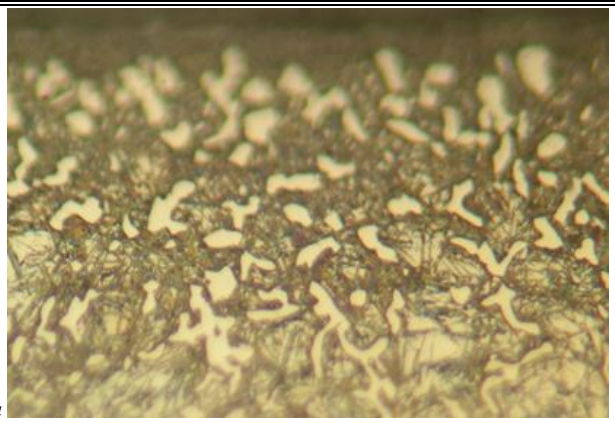

а

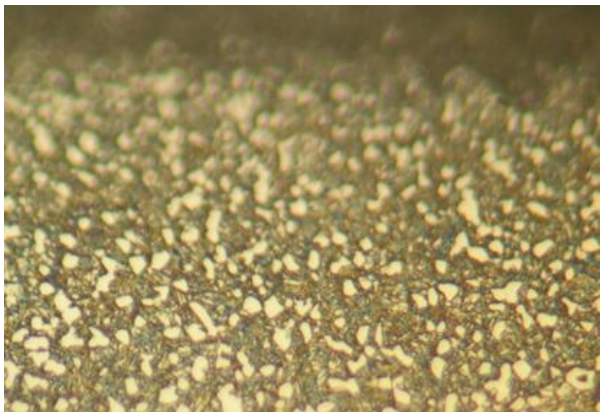

б

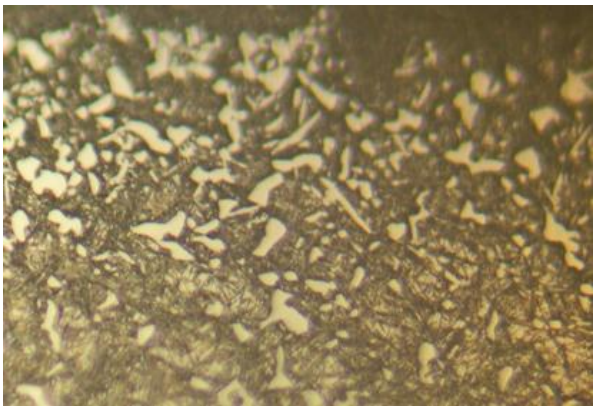

в

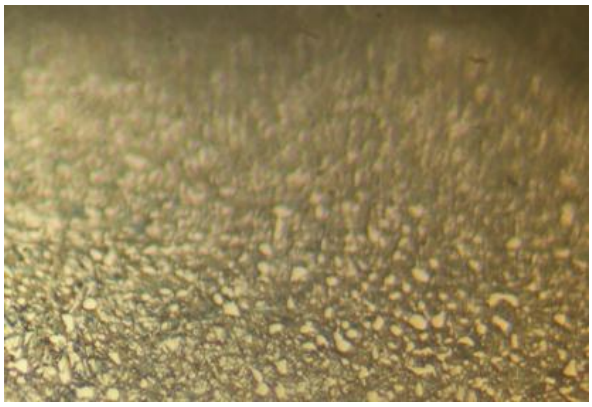

г

а - ковка, цементация 8 часов + отпуск 200 ºС; б - ковка, цементация 12 часов + отпуск 200 ºС; в - отжиг, цементация 8 часов + отпуск 200 ºС; г - отжиг,
цементация 12 часов + отпуск 200 ºС

Рис. 3. *Микроструктура стали 5ХВ2С после термохимической обработки 1; ×1000*

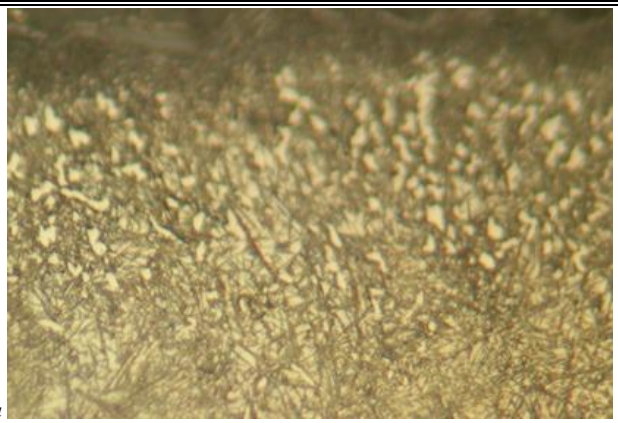

а

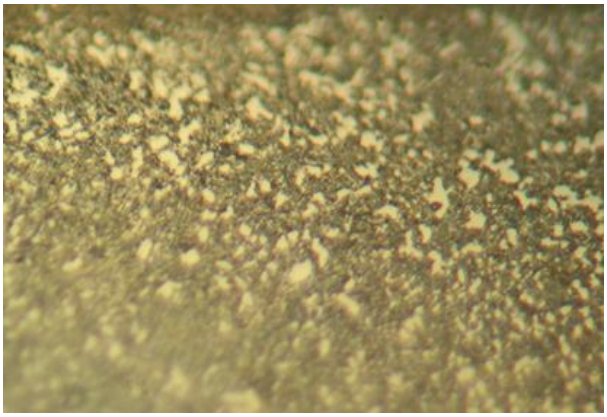

б

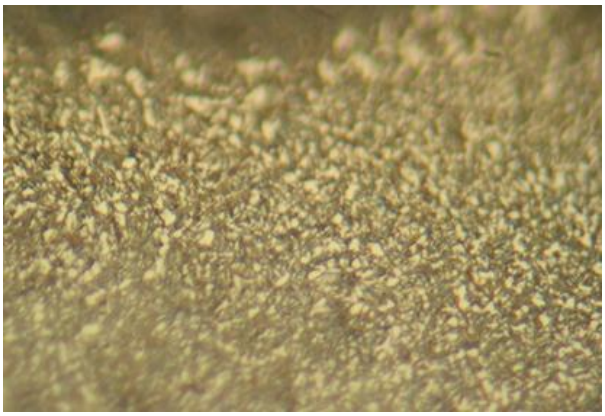

в

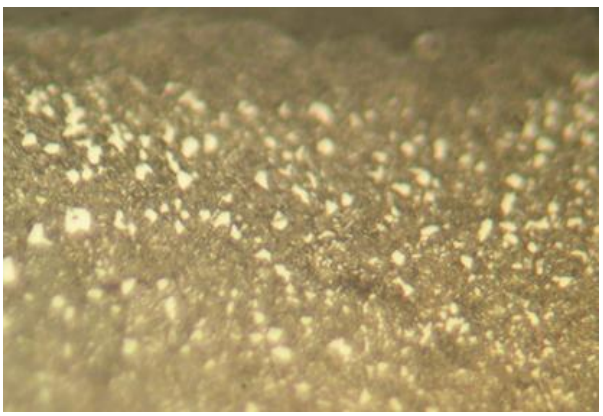

г

а - ковка, нитроцементация 6 часов, закалка 880 ºС + отпуск 200 ºС;
б- ковка, нитроцементация 8 часов, закалка 880 ºС + отпуск 200 ºС;
в - отжиг, нитроцементация 6 часов, закалка 880 ºС + отпуск 200 ºС;
г - отжиг, нитроцементация 8 часов, закалка 880 ºС + отпуск 200 ºС

Рис. 4. *Микроструктура стали 5ХВ2С после термохимической обработки 2; ×1000*

Результаты исследования микроструктуры исходных образцов полученных ковкой в инструменте, реализующем в металле знакопеременные деформации (рисунок 1, б)

показывают доэвтектоидную структуру с присутствием текстурированности в направлении протяжки заготовки, выраженной наличием вытянутых светлых зон на поверхности микрошлифа. В то время как образцы, не подвергнутые ковке (рисунок 1, а) направленности структуры не имеют.

Сравнительный анализ микроструктуры исходных образцов (рисунок 1) показал положительное влияние ковке в инструменте, реализующем в металле знакопеременные деформации, которое выразилось в измельчении и большей равномерности структурных составляющих, что таким же образом отразилось и на структурном состоянии образцов, подвергнутых упрочняющей термической (рисунок 2) и термохимической обработке (рисунки 3-4), что в свою очередь должно положительно сказаться и на комплексе их механических свойств. Это обусловлено тем, что измельчение и более равномерное распределение структурных составляющих по сечению кованой заготовки улучшает динамику фазовых превращений при последующей термической обработке.

Анализ результатов исследования микроструктуры образцов стали 5ХВ2С после термохимического упрочнения показывает, что на поверхности образуются диффузионные слои, состоящие из заэвтектоидной зоны постепенно переходящей к основе.

Исследованиями установлено, что длительность термодиффузионного насыщения незначительно повлияла на общую глубину модифицированного слоя. При этом цементация обеспечила диффузию на несколько большую глубину чем нитроцементация. Толщина модифицированных слоев составила до 1,5 мм после цементации, до 0,6 мм после нитроцементации.

Отдельного внимания заслуживают морфологические признаки перераспределения имплантируемых атомов углерода в образцах, цементация которых длилась 8 часов. Для обеих партий образцов как для отожжённых, так и для подвергнутых ковке, заметно выраженная локализация карбидных включений по границам зерен (рисунки 3, а и 3, в). При этом структура карбидной фазы сохраняет обособленную разрозненность отдельных зерен, редко отличающихся от глобулярной формы. Сплошная сетка практически не образуется. Похожая морфология выявляется и после проведения высокотемпературной нитроцементации в течение 8-ми часов. При этом увеличение выдержки при цементации до 12-ти часов снижает уровень погранично-зеренной ликвации. Объем карбидной фазы распределен более равномерно на одном и том же расстоянии от поверхности и убывает по мере углубления. В образцах подвергнутых нитроцементации обратная ситуация – более равномерную структуру имеет слой, сформированный при 6-ти часовом упрочнении. При этом основные структурные составляющие – зерна твердого раствора, отличаются признаками, которые присущи предварительной обработке.

Выводы

Сравнительный анализ микроструктуры образцов, подвергнутых новым режимам комбинированной термомеханической обработки, показал, что разработанные технологии способствовали качественному улучшению микроструктуры по сравнению с образцами, не подвергнутыми предварительной ковке в новом кузнечном инструменте, реализующем в металле знакопеременные деформации. Это выразилось в получении более мелкозернистой и равномерной структуры, как в поверхностном слое, так и в основе материала (центральная часть и промежуточная). При этом толщина модифицированных слоев составила до 1,5 мм после цементации, до 0,6 мм после нитроцементации.

Данное исследование финансировалось Комитетом науки Министерства науки и высшего образования Республики Казахстан (Грант № AP09259236).

Литература

1. Патент на полезную модель Республики Казахстан №5700. Инструмент для протяжки заготовок. Найзабеков А.Б., Лежнев С.Н., Волокитина И.Е., Панин Е.А., Волокитин А.В., 2020. Бюл.52.

2. Лежнев С.Н., Найзабеков А.Б., Волокитина И.Е., Панин Е.А., Куис Д.В. Влияние ковки в бойках новой конструкции, реализующих знакопеременные деформации, на структуру и механические свойства стали 5ХВ2С./ Машиностроение: сетевой электронный научный журнал. 2022. Том 9, №1. - С. 9-13

3. Лежнев С.Н., Найзабеков А.Б., Панин Е.А., Куис Д.В. Эволюция микроструктуры стали 5ХВ2С при ковке поковок в бойках, реализующих знакопеременные деформации./ Материалы Всероссийской научной конференции с международным участием «IV Байкальский материаловедческий форум», Улан-Удэ, 2022. – С. 527-529.

4. Волокитина И.Е., Панин Е.А., Куис Д.В., Лежнев С.Н. Исследование новой инновационной технологии ковки поковок и заготовок круглого поперечного сечения./ Материалы международной научно-технической конференции молодых ученых «Инновационные материалы и технологии – 2022», Минск, 2022. – С. 228 – 230.

5. Лахтин Ю.М., Рахштадт А.Г. Термическая обработка в машиностроении. Справочник. - М.: Машиностроение, 1980 - 783 с.

A new high-quality dynamic identification structure for im parameters

Daniela Perdukova[1,*], Pavol Fedor[1], Marek Fedor[1]
Technical University of Kosice, Slovakia[1]
[*]daniela.perdukova@tuke.sk

Abstract: *In the presented work a new identification method of difficult measured internal quantities of IM, such as components of magnetic flux vector and electromagnetic torque, is proposed. Commonly measurable quantities of IM like stator currents, stator voltage frequency and mechanical angular speed are used for identification to determine a feedback effect of the rotor flux vector on vector of stator currents of IM. Stability of the identification structure is guaranteed by position of roots of characteristic equation of its linear transfer function. Results obtained from simulation in MATLAB measurements confirm quality, effectivity, feasibility, and robustness of the proposed identification method.*

Keywords*: INDUCTION MOTOR, MOTOR TORQUE, MAGNETIC FLUX, IDENTIFICATION METHOD, MOTION CONTROL*

1. Introduction

In industrial practice, induction motors (IMs) are used both for conventional and high-performance applications. From the control point of view, the control of IMs brings difficulties, because it requires more complicated actuators and generally more complex control algorithms like field orientation control (FOC) [1], direct torque control (DTC) [2], model predictive control (MPC) [3] and model reference adaptive control (MRAC) [4]. For high quality control algorithms, it is necessary to identify motor parameters and internal quantities that are changed during operation of the electric drive system, for example due to temperature fluctuations or magnetic flux saturation.

For the high-quality dynamic control of IM, it is necessary to know the motor basic static parameters during its operation. Additionally, it is important to identify the basic internal quantities of the machine, such as the rotor magnetic fluxes and motor internal electrical torque on the rotor shaft. As the direct measurement of these quantities is rather difficult and often impossible, the instantaneous values of these quantities can be obtained indirectly, using various more or less complex identification methods.

The identification of the parameters, magnetic fluxes and torque of IM is often applied to a specific type of motor control in order to improve drive dynamics, or to eliminate the angular speed sensor. Improving the identification of IM magnetic fluxes based on a neural network, and thus improving the control at DTC (direct torque control), is described in [5]. Accurate identification of the IM parameters and magnetic fluxes for subsequent control by genetic algorithms using a reduced-order robust observer can be found in the [6].

This paper proposes a new high-quality dynamic identification structure for IM based on its mathematical model and allowing to identify rotor magnetic fluxes and IM electromagnetic torque simultaneously with an on-line adaptation of the rotor resistance. There is an identification method based on determining a feedback effect of the rotor flux vector on the vector of stator currents. The method requires only the knowledge of measurable quantities of IM, such as its stator currents and mechanical angular speed. The identification structure for identifying the rotor feedback influence on the stator of IM is simple and linear. Its stability is guaranteed by position of roots of the characteristic equation of its transfer function. It preserves the same properties within the whole range of angular of IM speeds. It also withstands any changes of rotor resistance. Achieved results confirming the efficiency and the quality of the proposed identification method were verified by the simulation measurements.

2. Mathematical Model of Induction Motor

Generally, an IM model consists of a system of five nonlinear first-order differential equations that cannot be solved analytically. When selecting the stator current and rotor flux for the model state variables one can describe the induction motor by the following equations:

$$\begin{bmatrix} \frac{di_{1x}}{dt} \\ \frac{di_{1y}}{dt} \\ \frac{d\psi_{2x}}{dt} \\ \frac{d\psi_{2y}}{dt} \end{bmatrix} = \begin{bmatrix} -\omega_0 & \omega_1 & -K_{12}\omega_g & -K_{12}\omega_m n_p \\ -\omega_1 & \omega_0 & K_{12}\omega_m n_p & -K_{12}\omega_g \\ M\omega_g & 0 & -\omega_g & \omega_2 \\ 0 & M\omega_g & -\omega_2 & \omega_g \end{bmatrix} \begin{bmatrix} i_{1x} \\ i_{1y} \\ \psi_{2x} \\ \psi_{2y} \end{bmatrix} + \begin{bmatrix} K_{11} & 0 \\ 0 & K_{12} \\ 0 & 0 \\ 0 & 0 \end{bmatrix} \begin{bmatrix} u_{1x} \\ u_{1y} \end{bmatrix} \quad (1)$$

$$n_p \frac{M}{L_2}\left(\psi_{2x} i_{1y} - \psi_{2y} i_{1x}\right) - T_{load} = J\frac{d\omega_m}{dt} \quad (2)$$

In this model, the particular motor quantities (the stator current vector $\mathbf{i_1}$ and the rotor flux vector $\boldsymbol{\psi}_2$) are expressed by their components in the reference frame *x-y* rotating synchronously with the stator field vector by the angular frequency ω_1.

The notation of the IM parameters motor and their values used for simulation are given in the Table 1 in the Appendix. The parameters in (1) and (2) can be determined from the motor parameters by simple recalculation according to the following formulas:

$$K_{11} = \frac{3}{2}\left(L_{s1} + \frac{L_{s2}L_m}{L_{s2}+L_m}\right)^{-1} \quad (3)$$

$$K_{12} = -\frac{3}{2}\left(L_{s1} + L_{s2} + \frac{L_{s1}L_{s2}}{L_m}\right)^{-1} \quad (4)$$

$$\omega_0 = K_{11}\left[R_1 + \left(\frac{M}{L_2}\right)^2 R_2\right] \quad (5)$$

$$M = \frac{2}{3}L_m \quad (6)$$

$$\omega_g = \frac{R_2}{L_2} \quad (7)$$

$$L_2 = \frac{2}{3}(L_{s2} + L_m) \quad (8)$$

The block diagram of the IM corresponding to equations (1) - (2) with the parameters adjusted according to the above equations (3) – (8) is shown in Fig. 1.

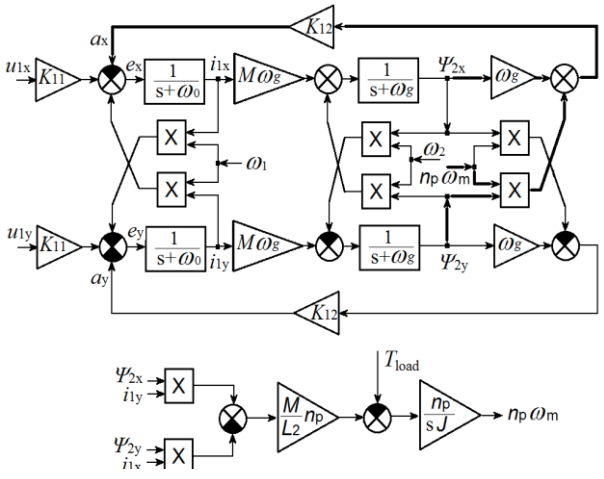

Fig. 1 *Block diagram of IM*

The dynamics of motor quantities (components of stator currents and rotor fluxes, and angular speed) after motor connection to the stator voltage $U_1 = 40$ V with the angular frequency $\omega_1 = 28.03$ rad/s., obtained by digital simulation in MATLAB/Simulink program is shown in Fig. 2.

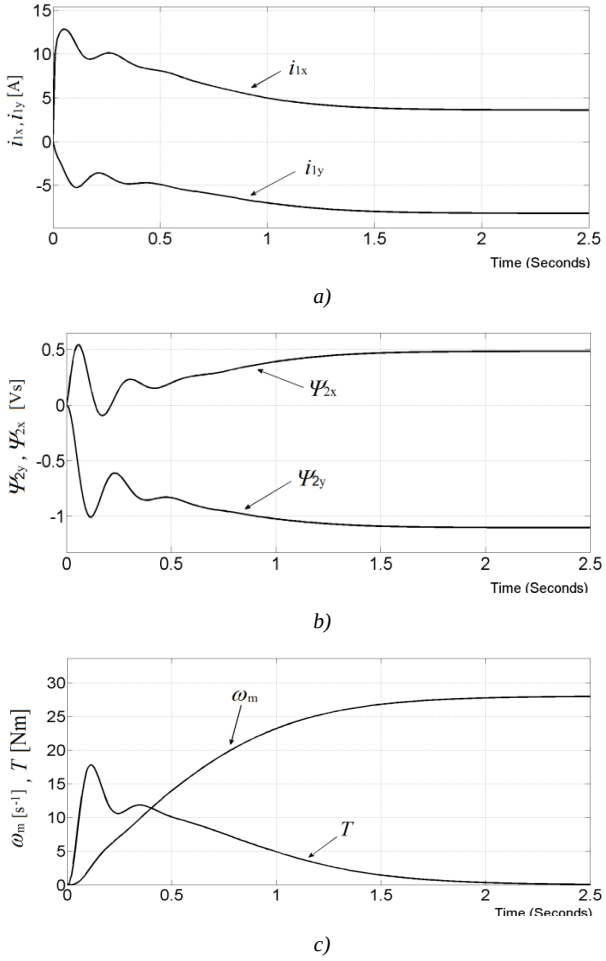

Fig. 2 *Dynamic responses of the induction motor:*
a) stator currents; b) rotor fluxes; c) mechanical angular speed and torque

At verification of properties by numerical simulation it is assumed, that the IM operates under scalar control and for the supply voltage U_1 and frequency ω_1 the known ratio U_1/ω_1 = const. is kept. In this case, the x-component of the voltage u_{1x} can be considered identical to the magnitude of the stator voltage U_1, i.e. $U_1 = u_{1x}$.

3. Identification Structure Design

The presented idea of the identification of difficult measurable internal quantities of the IM (the rotor flux vector components and electromagnetic torque) is based on the identification of the feedback effect of the rotor flux vector on the stator current vector. The identification of the feedback effect of the rotor flux is commonly completed based on the induced voltage, which is either equal to zero at zero speed or is insignificant at low speeds [7]. However, the considered feedback effect of the rotor flux also reflects itself on the stator current components equally within the entire speed range of IM. This fact was used in the design of the presented identification method. This influence upon the variable a_x is shown in the block diagram (Fig. 1), indicated by a thicker line starting from the quantities ψ_{2x}, ψ_{2y} and ω_m.

The same is valid for the variable a_y. For a clarity, the corresponding block diagrams are shown separately in Fig. 3.

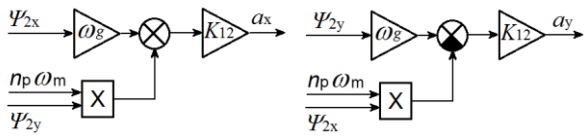

Fig. 3 *Block diagrams for determining variables a_x and a_y*

Let's suppose that for the induction motor with known instantaneous values of the stator input quantities U_1 a ω_1, the stator current components i_{1x}, i_{1y} and the mechanical angular speed ω_m can be measured. The instantaneous feedback value of the stator current component i_{1x} from the first line of equation (1) is:

$$a_x = K_{12}(\omega_g \psi_{2x} + \omega_m n_p \psi_{2y}) \tag{9}$$

and similarly, for the stator current component i_{1y} it is:

$$a_y = K_{12}(\omega_g \psi_{2y} - \omega_m n_p \psi_{2x}) \tag{10}$$

For a high-quality dynamic identification of the variables a_x and a_y, the following identification structures have been designed (Fig. 4).

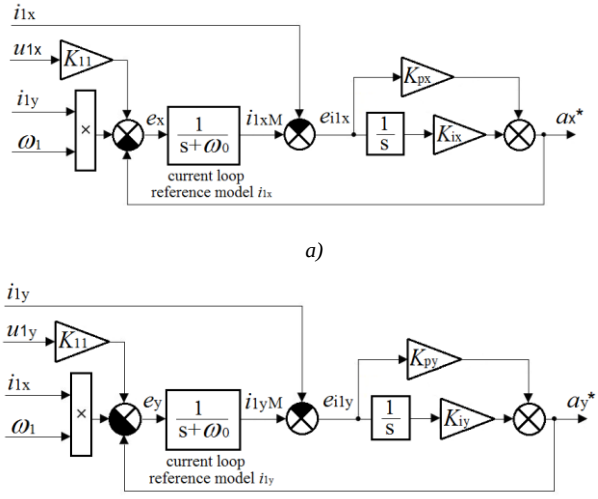

Fig. 4 *The identification structures of the rotor feedback influence on stator, for the variables: a) a_x*; b) a_y**

Fig. 4a shows the identification structure for identification of the component a_x (the identified value is denoted by an asterisk) which presents a structure with the reference model for the stator current circuit. In this reference model the same input signal is fed, like the one affecting the stator current component i_{1x}. The feedback effect of the rotor flux on this stator current component is identified from deviation of the measured current i_{1x} and its predicted value i_{1xM} obtained from the reference model. This deviation is processed by a PI controller whose output a_x* is set (identified) to the a_x value of the motor. The Laplace transfer function of the linear circuit is:

$$F(s) = \frac{a_x^*(s)}{i_{1x}(s)} = \frac{\frac{K_{px}\, s + K_{ix}}{s}}{1 + \frac{K_{px}\, s + K_{ix}}{s} \frac{1}{s+\omega_0}} = \tag{11}$$

$$= \frac{K_{px}\, s^2 + (K_{px}\, \omega_0 + K_{ix}) s + K_{ix}\, \omega_0}{s^2 + (K_{px} + \omega_0) s + K_{ix}}$$

The circuit stability and its dynamics can be easily adjusted by suitable choice of the proportional component gain where we have chosen the values $K_{px} = K_{py} = 10$ and the integration component gain $K_{ix} = K_{iy} = 11870$ based on required position of poles of the transfer function (11). The identification structure in Fig. 4a is a linear one and therefore its stability is guaranteed by negative real parts of the transfer function poles in the equation (11). This is

obviously ensured, because all terms of the characteristic polynomial are positive.

Analogically, an identification structure for identification of the component a_y has also been designed (Fig. 4b) with analogical considerations and similar results like in the previous case. The properties of the designed identification structures were verified by digital simulation (Fig. 5).

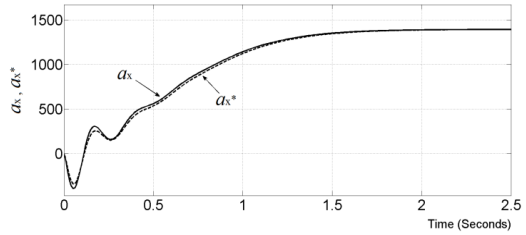

a)

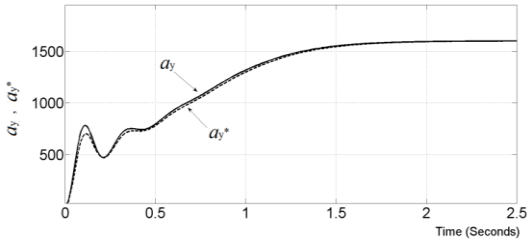

b)

Fig. 5 *Quality of identification of the variables: a) a_x*; b) a_y**

The figure shows time waveforms of the actual internal variables a_x and a_y obtained from the IM model, as well as their identified time courses a_x* and a_y*. From the courses it is clear that the proposed identification structures have excellent dynamic properties while being principally stable. Due to accuracy of sensed currents and voltages, which usually are sized percentually, the deviations between real and identified values can be considered to be negligible especially in dynamic states, because in the steady state these deviations (a_x - a_x* and a_y - a_y*) are zero.

4. Identification of Rotor Fluxes and Torque of IM

If the signals a_x* and a_y* at the output of the identification scheme in Fig. 4 are already known, then the rotor flux components can be estimated using the following equations:

$$\psi_{2x}^* = \frac{1}{K_{12}}\left(\frac{\omega_g a_x^* - \omega_m a_y^*}{\omega_g^2 + \omega_m^2}\right) \quad (12)$$

$$\psi_{2y}^* = \frac{1}{K_{12}}\left(\frac{\omega_g a_y^* + \omega_m a_x^*}{\omega_g^2 + \omega_m^2}\right) \quad (13)$$

The quality of the rotor flux components identification in comparison with their actual values obtained by simulation follows up from the time courses shown in Fig. 6.

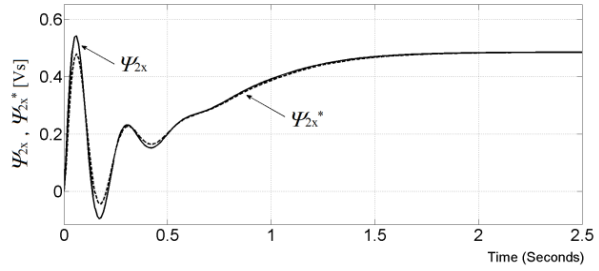

a)

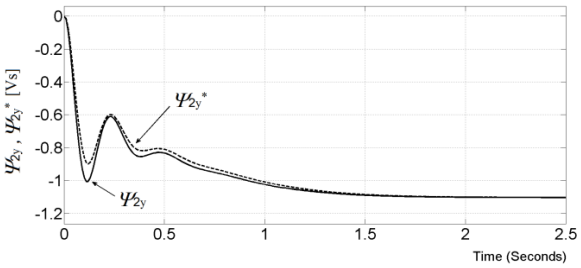

b)

Fig. 6 *Comparison of identified and actual components of IM rotor fluxes a) Ψ_{2x}; b) Ψ_{2y}*

From the figure there follows that the course of the measured rotor flux vector components almost coincide with their identified time courses. The largest deviation in the dynamic state occurs approximately at time t = 0.15 s, and its value is less than 4%. This precision is fully satisfactory for use in any practical control applications. In the steady state, the deviation between measured and identified components of the flux vector is zero, which corresponds to the zero identification deviation of the variables (a_x - a_x*) and (a_y - a_y*) in Fig. 5.

If the individual components of the rotor flux are identified, the motor electromagnetic torque can be determined on the basis of equation (2) as follows:

$$T^* = \frac{M\, n_p}{L_2}\left(\psi_{2x}^* i_{1y} - \psi_{2y}^* i_{1x}\right) \quad (14)$$

The identified electromagnetic torque waveform obtained by numerical simulation based on equation (14) is shown in Fig. 7. Its time course confirms the quality of identification both in steady and dynamic states. In the steady state, the identification deviation of the torque ($T - T^*$) is equal to zero again. The largest identification error in the dynamic state occurs in time t = 0.15 s and it represents approximately 3% of the maximum waveform range of the electromagnetic torque of IM. What concerns the maximum torque, three times nominal torque is considered here (equal to 60 Nm in the analyzed case).

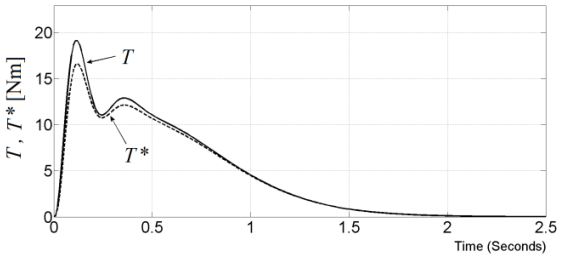

Fig. 7 *Comparison of the identified electromagnetic torque T* and the actual torque T of the induction motor*

5. Verification Results for Various Operating States

In following the properties of the rotor flux and torque identification method are verified by simulation for various operating states.

Let's suppose that IM operating under scalar control is supplied by the voltage U_1 (where $U_1 = u_{1x}$) and is loaded stepwise by the load torque T_{load}. For this reason, quasi random step changes of the input voltage U_1 on the stator of the motor and a step change of its load torque T_{load} were simulated as is illustrated in Fig. 8.

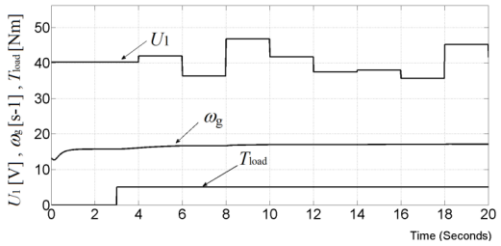

Fig. 8 *Waveforms of the motor input quantities: voltage U_1, and load torque T_{load} together with the course of parameter ω_g*

In time t = 3 s, a torque jump of T_{load} = 5 Nm is applied to the motor. The stator voltage U_1 and supply frequency jumps ω_1 are generated randomly in two-second time intervals, under maintaining the relationship $U_1/\omega_1 = const.$ This operation can be considered as the worst case for identifying the rotor resistance, as the in praxis, its step change is not realistic one.

Figure 8 shows the gradual improvement of the identification of the quality of the rotor flux components and motor electromagnetic torque identification, when taking into account the adaptation of the parameter ω_g (presenting the inverse value of the rotor resistance R_2).

The induction motor starts its operation from non-excited state and at starting, during the magnetic flux generation the identification error is the largest one. After the motor has been excited the error lies practically within the range ± 1% of the actual value both in static and dynamic states of the identified quantities, like it follows from the time courses in Fig. 9.

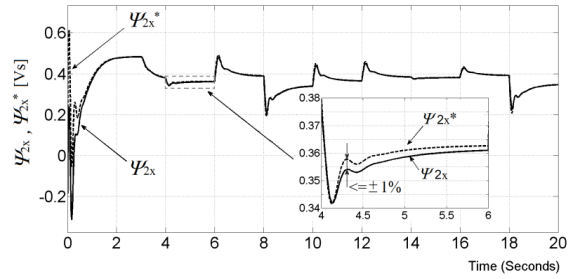

a)

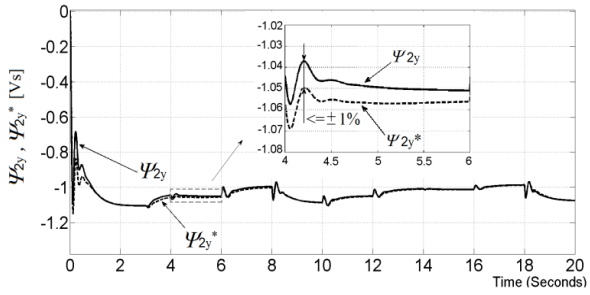

b)

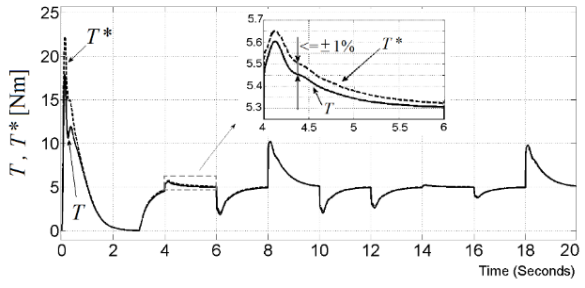

c)

Fig. 9 *Identification of the rotor flux vector components a) Ψ_{2x}; b) Ψ_{2y} and c) motor torque T*

6 Conclusion

In this paper, we have proposed an original method of a high quality identification of rotor fluxes and electromagnetic torque of induction motor (IM). It is based on identification of rotor feedback influence on stator currents with adaptation of rotor resistance. For its operation the method utilizes commonly available measurable quantities of IM: stator currents and mechanical angular rotor speed. The identification structure for identifying the rotor feedback influence on the stator IM is linear and its stability is guaranteed by position of roots of the characteristic equation of its transfer function.

The quality and efficiency of the proposed identification method was firstly verified by digital simulation in the MATLAB / Simulink program. The results from numerical simulation (Fig. 5 – Fig. 7) show that the proposed method identifies at sufficient accuracy the feedback effect of the rotor flux vector on the stator current vector of the motor in steady and dynamic states. Based on these identified variables it is further possible to calculate components of internal rotor magnetic flux and electromagnetic torque. The accuracy of identification of these quantities depends on value of the IM rotor resistance expressed by the parameter ω_g, which is generally not known precisely and varies during operation (e.g. due to temperature change).

The identified internal quantities of the motor, such as the individual components of its rotor flux and the electromagnetic torque can be used for various commonly used methods of dynamic drive control like scalar control, different types of vector control and direct torque control of the induction motor.

Acknowledgement
The paper was published with the support of the APVV-19-0210 project and APVV-16-0206.

8. References

[1] BOSE, B. K.: *Modern Power Electronics and AC Drives*, Prentice-Hall: Englewood Cliffs, NJ, USA, 2002.

[2] BRANDSTETTER, P. – KUCHAR, M. – VO, H. H. – DONG, C.S.T.: Induction motor drive with PWM direct torque control, in *Proc. 2017 18th Int. Scientific Conf. on Electric Power Eng., EPE 2017*, Kouty nad Desnou, Czech Republic, pp. 1–5, 2017.

[3] ZHANG, Y. – BAI, Y. – YANG, H.: A universal multiple-vector-based model predictive control of induction motor drives, *IEEE Trans. Power Electron.*, vol. 33, pp. 6957–6969, 2018.

[4] FEDOR, P. – PERDUKOVÁ, D. - KYSLAN, K. – FEDÁK, V.: Stable and robust controller for induction motor drive, *IEEE 18th Int. Conf. on Power Electronics and Motion Control, PEMC 2018*, Budapest, pp. 764-769, 2018.

[5] WALLSCHEID, O. – SCHENKE, M. – BÖCKER, J.: Improving torque and speed estimation accuracy by conjoint parameter identification and unscented Kalman filter design for induction machines, in *21st Int. Conf. on Electrical Machines and Systems, ICEMS-2018*, Jeju, South Korea, 2018.

[6] VENKADESAN, A. – HIMAVATHI, S. – MUTHURAMALINGAM, A.: Performance comparison of neural architectures for on-line flux estimation in sensor-less vector-controlled IM drives, *Neural Comput. & App.*, vol. 22, pp. 1735–1744, 2013.

[7] CHEN, K.Y. – YANG, W.H. – FUNG, R.F.: System identification by using RGA with a reduced-order robust observer for an induction motor, *Mechatronics*, vol. 54, pp. 1-15, 2018.

Experimental setup for studying the behavior of sheet blanks during cyclic alternating bending for roller levelling application

Tamila V.[1], Klubovich V.[2], Liaukovich V.[3]
Belarusian National Technical University [1,2], The Physical-Technical Institute of the NAS of Belarus [3], Belarus
levkovich@phti.by

Abstract: *Roller levelling is a technological process of metal forming, used to minimize the flatness of sheet blanks and reduce the level of residual stresses. When levelling, the workpiece is subjected to cyclic alternating bending with decreasing amplitude. The report presents an experimental testing set-up designed and used to determine the mechanical response of sheet steel blanks under different loading modes. The equipment is described and the first results are presented.*
Keywords*: LEVELLING PROCESS, LEVELLING FORCE, BENDING TEST*

1. Introduction

Sheet blanks are widely used in industrial production. For their cutting, laser and plasma cutting is often used. After that, sheet blanks often have insufficient geometric accuracy (flatness). To improve the geometric accuracy of sheet blanks various methods can be used, including roller levelling.

Roller levelling is a technological process of metal forming, used to minimize the flatness of sheet blanks and reduce the level of residual stresses. When levelling, the workpiece is subjected to cyclic alternating bending with decreasing amplitude. In this case, the penetration depth of deformation should be at least 0.7 of the thickness of the workpiece [1].

When levelling due to the presence of cyclic loading, there are conditions in the process that both hinder the levelling process (hardening) and facilitate it (the Bauschinger effect). All this can give rather large differences in the results of calculations performed by different methods. To obtain reliable results it is necessary to know the dependance of stress on the degree of deformation for a given material.

The existing experience of the world's leading manufacturers of process equipment (ARKU, KOHLER, etc.) shows the feasibility of using multi-roll levelers both for straightening piece sheet parts and for integrating levelers into existing and planned automated lines for the production of piece sheet blanks of a wide range for machine-building, petrochemical, aerospace and other branches of industrial production.

Multi-roll levelers are used for cold straightening of steel sheet blanks and blanks of non-ferrous alloys up to 50 mm thick and up to 5000 mm wide. Hot straightening of steel sheet blanks is carried out at temperatures of 500-700 °C, mainly immediately after leaving the working stand of the rolling mill. Sheets with a thickness of over 40 - 50 mm are usually straightened in a cold state under presses.

2. Experimental set-up

Three point bending test is a convenient experiment for determining the parameters for sheet metals under conditions of complex alternating loading. The test-up is illustrated in Fig. 1.

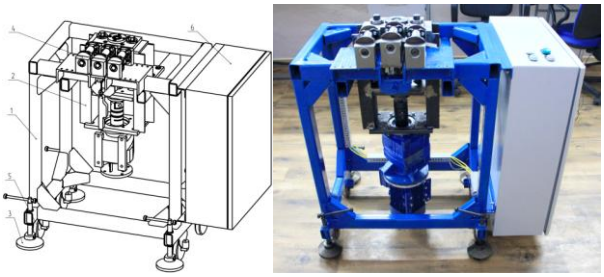

Fig. 1 *Experimental set-up used in the three point bending test.*

Especially the design of the end support should be noticed (Fig. 2).

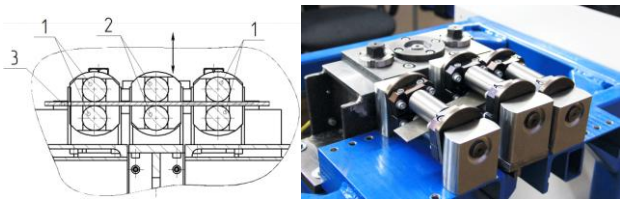

Fig. 2 *Arrangement of the end support and the punch.*

These provide a moment-free support, while the sheet strip 3 is allowed to slip freely in the axial direction. The punch 2 in the middle was moved with a prescribed displacement. The distance between the end supports 1 was 150 mm, and the width of the sheet strip was 10 to 60 mm. During the test the punch force and punch displacement were recorded.

Technical parameters are shown in table 1.

Table 1: *Experimental equipment technical parameters.*

Power supply	220 V, 50 Hz
Power of installed engines, kW	1,1
Maximum sample length, mm	200
Minimum sample length, mm	160
Maximum sample width, mm	60
Minimum sample width, mm	10
Maximum sample thickness, mm	8
Minimum sample thickness, mm	1

The bending test of the material is carried out as follows. The metal sheet strip 3 to be tested is placed between the rolls. After that, the movable punch 2 perform successive vertical movements (according to the arrow in Fig. 2) of a given amplitude with registration of the speed and force.

Force measurements were carried out using a bridge circuit (Fig. 3).

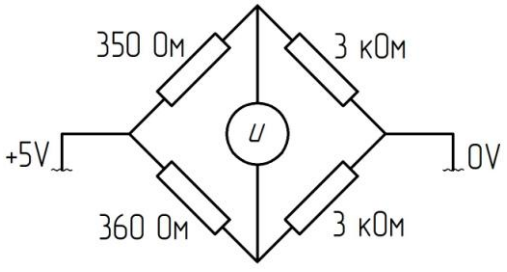

Fig. 3 *Bridge circuit.*

Strain gauges BA350-100AA(11)-BX30 with a nominal resistance of 350 ± 0.2 Ohm and a gain of 2.11 ± 1% were used. Standard 360 Ohm and 3 kOhm resistors were used.

To convert electrical quantities into force values, a preliminary calibration of the bridge circuit was carried out at two points. For calibration, an HBM RTNC3/15T sensor with a HBM WE2108M meter was used. The accuracy of the HBM RTNC3/15T sensor is within 17.5 N.

3. Conclusion

The article presents the design of an experimental testing set-up for obtaining the dependence of stress on the degree of deformation under various loading conditions, in particular, under alternating cyclic loading. This is necessary to obtain accurate results in calculations or computer simulations.

4. References

1. Korolev A.A., *Konstrukciya i raschet mashin i mekhanizmov prokatnyh stanov* [*Design and calculation of machines and mechanisms of rolling mills*] (Metallurgiya Publ., Moscow, 1985). 376 p. [in Russian]

Determining the quality of renovation layers using laser technology

Janette Brezinová[1], Ján Viňáš[1*], Miroslav Džupon[2], Marek Vojtko[2], Jakub Brezina[1]
Technical University of Košice, Slovakia[1]
Slovak Academy of Sciences, Institute of Materials Research, Košice, Slovakia[2]
jan.vinas@tuke.sk[1]

Abstract: *The paper presents the results of research aimed at determining the quality of renovation layers using laser technology. In order to repair and renovate shaped parts of molds for casting aluminum alloys under high pressure, samples of experimental welds were prepared on the base material quality 1.2343 (Dievar). The renovation layers were created using additional materials Dievar, UTP A 7002 and NIFIL NiCu7 res. NiCu7 with Dievar combination. The microstructures on the cross-sections of the deposits were checked using the light microscopy technique. The technique of scanning electron microscopy and semi-quantitative EDX microanalyses were analyzed distribution of alloys in deposits. The microhardness of the deposits was determined.*
Keywords*: RENOVATION LAYERS, LASER TECHNOLOGY, MICROSTRUCTURE, QUALITY*

1. Introduction

Renovation of functional parts of unheated aluminum alloy injection molds is a subject of many researches [1]–[4]. Possibilities of extending the lifetime of forms, as well as saving financial resources reaching several hundred thousands of Euros is their primary goal [5]–[8]. Aluminum alloy injection technology is most widely used in the automotive industry. It is a serial or mass production of components that are subject to high quality requirements. Any damage to the functional surface of the mold is reflected in the final product, the quality of which is constantly monitored. High Pressure Die Casting (HPDC) is a technological process widely used for casting complex of aluminum castings, mainly associated with the automotive industry. In this process, molten metal with a temperature of 670 – 710 °C is forced into the cavities of the molds at filling speeds of 30 – 100 m.s-1, under pressures ranging from 40 – 80 MPa [9]. This loading, in combination with the corrosive properties of liquid aluminum, leads to aluminization or oxidation of the mold surface, which results in thermal fatigue of the surfaces followed by cracking, soldering and erosive wear. The service life of die matrices made of steel alloys is approximately 100000 cycles and can be increased either by heat treatment, thin coating or cladding [10]–[12] The paper presents the results of research into the possibility of applying additional materials based on the base material or high-alloy maraging steel. The cladding layers were made using laser welding.

2. Materials and Methods

Medium alloy tool steel marked Dievar (W. Nr. 1.2344; 48 HRC) from Uddeholm Boehlers was used as the base material to produce test hardfacing layers. It is characterized by high heat strength and resistance to tempering, as well as very good toughness and plastic properties at both normal and elevated temperatures. Furthermore, the steel shows very good resistance to thermal fatigue cracking and low sensitivity to sudden thermal shocks. It is well malleable when hot and well machinable in the soft annealed condition. The chemical composition of the base tool steel and its mechanical properties are presented in Table 1.

Table 1: *Chemical composition of the base material Dievar (wt. %).*

C	Mn	Si	Cr	Mo	V	P	S	Fe
0,36	0,42	0,16	5,09	2,31	0,64	0,001	0,009	Bal.

As part of the experiments, 3 types of additional materials were used and 4 test coatings were made. Their chemical composition is in Table 2. Wire Uddeholm Dievar 1.2344 was used as additive material with a diameter of ø 1.0 mm, hardness of 46-48 HRC. The coating for the test sample was made in two layers. Cladding wire UTP A 702 is used for repair, preventive maintenance and production of highly stessed cold and hot working tools, such as punching dies, cold and hot cutting knives, Al-die cast moulds, cold forging dies, drawing-, stamping- and chamfering tools. UTP A 702 was with a diameter of ø 1,0 mm and hardness of 32-35 HRC. . The coating for the test sample was made in two layers. Cladding wire Nifil NiCu7 is a solid wire with Good bead appearance with excellent corrosion resistance in saline solutions. Suitable for desalination plant construction applications and joining MONEL type. Used was wire a diameter of ø 1,0 mm and hardness of 150 – 170 HV. The test sample was made as a single layer. As the fourth layer, a two-layer test sample was made from a combination of additional materials. The base layer was made with additional material Dievar and the cover layer using NiCu7.

Table 2: *Chemical composition of the used filler material (wt. %).*

Filler mat.	C	Mn	Si	Cr	Mo	Co	Ni	Ti	V	Cu	Fe
Dievar	0,35	0,5	0,2	5,0	2,3	-	-	-	0,6	-	Bal.
UTP A 702	0,02	-	-	-	4,0	12,0	18,0	1,6	-	-	Bal.
NiCu7	0,10	3,0	1,0				Bal.			30,0	1,0

The welding of the test samples was carried out using a disc laser TruDisk 4002. Cladding parameters used in the experiment are listed in Table 3.

Table 3: *Used cladding parameters*

Cladding parameters	Dievar	UTP A 702	DRATEC DT-SG 6356	NiCu7 + Dievar
Laser power P [W]	1500	1500	1600	1500
Wire feed speed v [mm/s]	6	6	6	6
Cladding speed v [mm/s]	10	10	10	5
Focusing [mm]	0	0	0	0
Shielding gas flow rate Ar 4.6 [l]	7	7	10	12

The quality of the coating layers was evaluated using macrostructural and microstructural analysis using an Olympus XX microscope. Transverse metallographic sections were etched using aqua regia for samples with a coating made with Ni 18% and more. An etchant (1g picric acid+5ml HCl, 97 ml ethylalcohol; HNO_3:HCl (3:1)) was used to make the structure of the base and additional material visible.

Vickers hardness was evaluated on metallographic grindings according to EN ISO 9015-1. The measurement was carried out in lines, from the surface of the coating layer towards the base material. Shimadzu HMV2 hardness tester, Vickers indentes and 2940N load were used.

3. Results

The quality of the cladded layers was assessed using non-destructive and destructive methods. A visual inspection confirmed the significant fragmentation of the surface of the deposits. The segmentation corresponded to the used diameter of additional

materials and their mutual mixing. On the surface of the weld (the presence of cracks was noted in the covering layer made with NiCu7 additional material). In practice, when renovating functional surfaces, several cladded layers are applied in order to eliminate the mixing of the weld with the base material and also because of the allowance for chip machining to the required final dimensions and tolerances.

The results of the evaluation of the macrostructures are recorded in Fig. 1 to 4. Fig.1 shows the macrostructure of the coating made with the additional material Diavar. The coating was made as two-layered. A relatively substantial fragmentation of the surface is recorded. The presence of pores in the base cladded layer was observed on the metallographic cuttings. Figure 2 shows a coating made with the additional material UTP A 702. The coating was two-layered. On the macrostructure, the powering of the base and second so-called cover layer of the coating is clearly notable. The presence of internal defects on the cuttings was not recorded. The macrostructure of the weld made with Nifil NiCu7 additional material is shown in Fig. 3. The coating was made as a single layer. The presence of pores was noted at the interface between the base material and the coating. On Fig.4 there is a two-layer coating made by a combination of two additioal materials. On the base layer of the coating made with the additional material Dievar, the covering layer was welded using additional material NiCu7. This cover layer contained cracks extending from the surface to the underlying layer. In the base layer the cracks did not reach the base material. Cracks were classified as hot. Their likely cause was an inappropriately chosen heat mode during welding. The heat-affected area of the base material was narrow, similar to the previously welded samples. The parameters of the area correspond to the welding technology used and heat input.

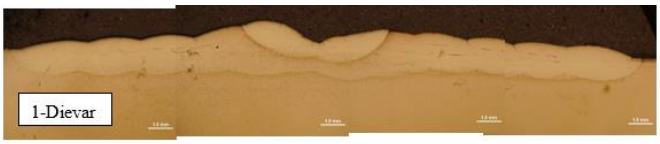

Fig. 1 *Cladd made of Diavar*

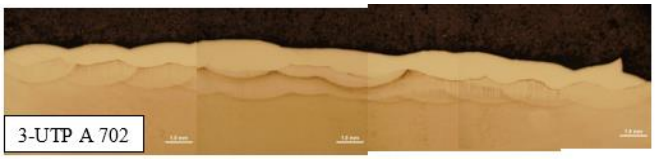

Fig. 2 *Cladd made of UTP A 702*

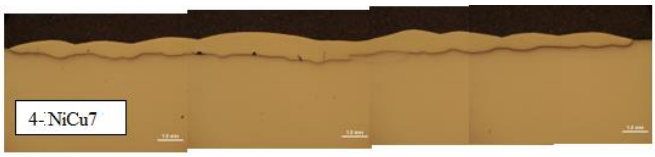

Fig. 3 *Cladd made of Nifil NiCu7*

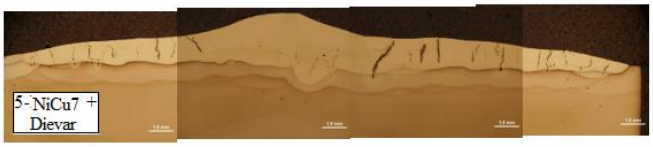

Fig. 4 *Cladd made of Nifil + Diavar*

The microstructures of the evaluated samples are documented in Fig. 5 to 10. Figure 5 shows the microstructure of the base material Dievar. It is a structure of tempered martensite. The transitional heat-affected area of the base material is also documented in Fig. 6. The structure is formed by loosened coarse-grained martensite. Figure 7 shows a structure of tempered martensite without significant grain boundaries, which was located in the base weld layer made with the additional material Dievar. A similar structure was also found in the second coating layer. The structure of the cladding metal of sample No.2 made using additional material UTP A 702 is shown in Fig. 8. This is a characteristic martensitic low-carbon structure with a columnar arrangement of grains. The structure of the cladding metal made using NiCu7 additional material is shown in Fig. 9. This is a casting structure characteristic for Monel.

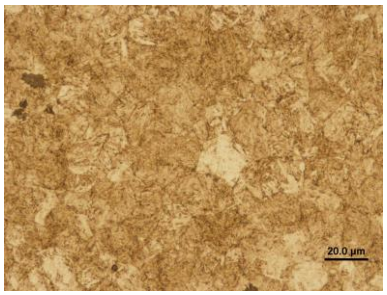

Fig. 5 Microstructure of base material (BM) Dievar

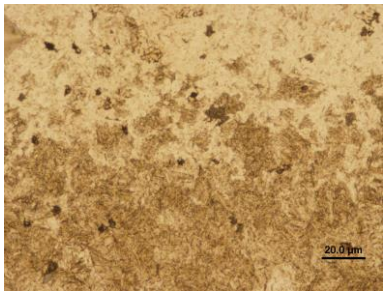

Fig. 6 Microstructure of HAZ in BM Dievar

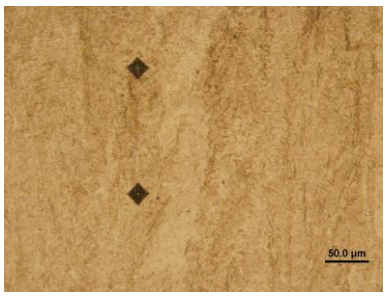

Fig. 7 Microstructure of fist cladded layer with Dievar

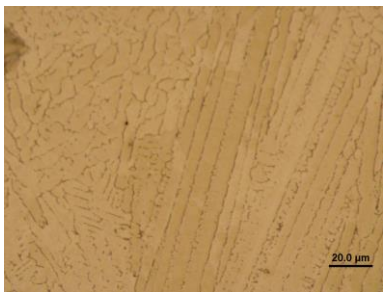

Fig. 8 Microstructure of cover layer cladded with UTP A 702

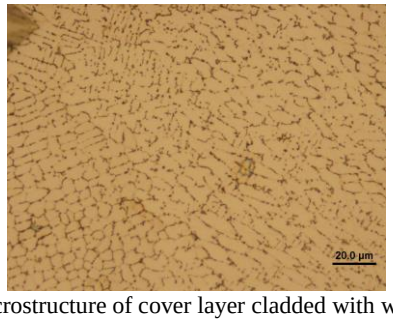

Fig. 9 Microstructure of cover layer cladded with wire NiCu7

The microstructure in the area of mixing of the cladding metal made with additional material Dievar and NiCu7 on the fourth sample is shown in Fig.10. Based on the macroscopic analysis, numerous cracks were identified in the test sample. This is an unacceptable

error. Their likely cause was an incorrectly selected thermal mode when welding individual layers. Cracks were classified as hot. They were initiated on the surface of the deposit and spread towards the underlying deposit layer. This base layer made with additional material Dievar stopped their spread. Pores not exceeding 0,2 mm were only rarely found in the undercoat layer made with the additional material Dievar.

Fig. 10 Microstructure in the area of mixing the cladding metal Dievar and NiCu7

In addition to metallographic analyses, the hardness values in individual areas were determined on the transverse cuttings. The measured results of average hardness from 5 measurements in each area are shown in Table 4.

Table 4. Average hardness values HV0,3 measured in individual areas of test samples

Area of measurement	Cover layer	First layer	HAZ	Base material
Dievar	605	620	530	483
UTP A 702	350	360	511	476
NiCu7	-	165	630	482
Nifil + Diavar	182	530	460	475

The measured hardness values correspond to the chemical composition of the additional materials and changes in the structures due to the heat introduced during welding. The maximum hardness values were manifested by heat-unprocessed welds made with the additional material Dievar, with a hardness in the range of 605-620 HV0,3. In practice, the heat treatment by temepering must follow the welding for the purpose of removing residual stresses after welding and reducing the hardness due to improving the toughness of functional surfaces. The lowest average value of 165 HV0,3 was recorded in a single-layered weld made with NiCu7 additional material. This is a nickel alloy which, as it turned out in later experiments, is not a suitable material concept even for short-term interaction with the molten metal of the Al alloy.

4. Conclusions

The paper presents the results of research focused on the area of restoration of functional surfaces of components. The possibilities of applying progressive high-alloy types of additional materials in the form of wires during laser welding were analyzed. The quality of newly created layers was evaluated by means of non-destructive inspection of the surfaces and also by means of destructive tests. The quality of the proposed welding parameters was evaluated primarily on metallographic cuttings. These revealed several imperfections and the need for further and more thorough optimization of the welding parameters. The aim of the comprehensive research was to recommend a suitable type of additional material for renovating the funcional surfaces of injection molds to manufacturers of aluminum components. From the types of additional materials presented, it is possible to recommend the additional material Dievar for renovation of functional surfaces. The quality criteria is also met by the additional material based on the progressive maraging steel UTP A 702. This one however requires heat treatment by annealing in order to remove internal stresses, but especially to achieve the required hardness of the funcional parts of the molds, which is 44-48HRC. Similarly, heat treatment by tempering is also required for coatings made with Dievar additional material. Additional material based on Monel can be marked as unsuitable for renovation. In addition to the high sensitivity to the amount of the heat introduced into the deposit, its solubility in interaction with the Al alloy is also problematic, as further research has shown. With the appropriate chemical composition of additional materials using progressive methods of production of functional layers, it is possible to restore damaged surfaces to a significant extent, extend the service life of components and thus save considerable financial resources.

Acknowledge

This research was funded by the Scientific Grant Agency, " Possibilities of application of laser additive technologies in restoration of functional surfaces" (1/0597/23); the Cultural and Educational Grant Agency KEGA 046TUKEs/2022 "Innovation of the educational process by implementing adaptive hypermedia systems in the teaching of subjects in the field of coating technology and welding of materials"; the Slovak Research and Development Agency APVV-20-0303 "Innovative approaches to the restoration of functional surfaces by laser weld overlaying".

5. References

[1] C. M. Grohol, Y. C. Shin, and A. Frank, *Surf. Coatings Technol.*, 11(10), 1633, (2021)
[2] A. M. Mikhaltsov, A. A. Skaskevich, and Y. I. Tsishkova, *Litiyo i Metall. (FOUNDRY Prod. Metall.*, 2020)
[3] B. Burlaga, A. Kroma, P. Poszwa, R. Kłosowiak, P. Popielarski, and T. Stręk, "*Materials (Basel).*, 15(19), 6545, (2022)
[4] J. Brezinová *et al.*, *Metals (Basel).*, 11(1), 134, (2021)
[5] P. Šarga, J. Brezinová, J. Viňáš, M. Pástor, and J. Brezina, "*Metals (Basel).*, 12(3), 388, (2022)
[6] I. Najbolj *et al.*, "*6th Int. Tool. Conf.*, (2013)
[7] F. De Ciencias and U. N. De Lisboa, *https://fenix.tecnico.ulisboa.pt/downloadFile/3779571902294/Congresso%20Luso-Mocambicano%20.pdf*, 2013.
[8] J. Y. Chen, K. Conlon, L. Xue, and R. Rogge, *Mater. Sci. Eng. A*, 527, 27-28, (2010)
[9] K. Bobzin, T. Brögelmann, R. H. Brugnara, and N. C. Kruppe, *Surf. Coatings Technol.*, (2015)
[10] C. Chen, Y. Wang, H. Ou, and Y. J. Lin, *Int. J. Fatigue*, (2016)
[11] J. Lin *et al.*, *Surf. Coatings Technol.*, 201, (2006)
[12] K. Domkin, J. H. Hattel, and J. Thorborg, *J. Mater. Process. Technol.*, 209, (2009)

Tribological properties of PVD nanocoatings

Janette Brezinová[1*], Miroslav Džupon[2], Viktor Puchý[2], Ján Hašul[1], Jakub Brezina[1]
Technical University of Košice, Faculty of Mechanical Engineering, Slovakia[1]
Slovak Academy of Sciences, Institute of Materials Research of SAS, Slovakia[2]
janette.brezinova@tuke.sk

Abstract: *The paper presents the results of research aimed at determining selected tribological properties of PVD nanocoatings. PVD nanocoating of the 4th generation duplex nACRo[4] was applied to the surface of shaped parts of molds and cores for high-pressure aluminium casting. The surfaces were laser textured with a random texture. The tribological properties of the coating were determined by measuring the friction coefficient using the Pin on Disc method at a temperature of 300 °C. Confocal microscopy was used to determine the parameters of the microgeometry of surfaces with random texture topography. The aim of this surface treatment was to analyse the adhesion effect of commercially used ones of lubricants in the technology of treatment of shaped parts of molds when casting aluminium alloys under high pressure on machines with a cold filling chamber. By checking the integrity of textured surfaces with deposited with the duplex PVD coating of the 4th generation nACRo[4], no damage to the integrity of the deposited material was detected PVD coating. Elements forming the PVD coating were detected on the surface by semiquantitative EDX microanalysis.*
KEYWORDS*: PVD NANOCOATINGS, TRIBOLOGY, FRICTION COEFFICIENT, TEXTURING SURFACES*

1. Introduction

One of the most fundamental findings of the physics of solids is that most of the properties of solids depend on their microstructure. In particular, the arrangement and size of the atoms that make up a solid in one, two, or three-dimensional space are key factors that determine the functional properties of materials. Currently, many researchers are making enormous efforts to prepare materials with specific properties through new unique structures. Surface treatment technologies are attracting a lot of attention these days, as non-equilibrium processes for the preparation of coatings make it possible to create structures based on nanocrystalline materials. In addition, by simply changing the deposition, or process conditions, a wide range of coatings with different unique structures can be created, which in practice provide significantly better material properties compared to conventionally used coatings. Nanocrystalline and nanocomposite materials are among those that in most cases replace conventional coarse-grained materials in many engineering applications, and thus also in the field of surface engineering, replace available conventional types of coatings used in industrial applications [1,2]. Nanocrystalline materials used in the formation of PVD nanostructured coatings exhibit various properties that are significantly different from the properties of commonly available coarse-grained polycrystalline materials. The main reason is their very small material grain size. It is known that this factor influences the properties of nanocrystalline materials, mainly on the mechanical properties. It is also the reason for reduced density, increased diffusion, higher electrical resistance, increased specific heat and coefficient of thermal expansion, lower thermal conductivity, and specific magnetic properties of nanocrystalline materials. The properties of these materials are also strongly influenced by the interfaces between individual nanocrystals [3,4]. A very high number of atoms at the grain boundaries and a high-volume fraction is enormous, especially for materials composed of very small grains with a size of less than 10 nm. The explanation for the improved material properties of nanocrystalline materials can be found in the developed microstructure and phase type of which the given material is composed. However, the most significant effect of grain size reduction can be found in the increase in hardness and toughness of nanocrystalline materials [5]. The hardness of materials represents their resistance to plastic deformation, which is mainly due to the ability of the material to prevent the movement of line faults (dislocation). The structural arrangement of individual phases in nanocrystalline materials ensures that dislocations are effectively stopped in their movement due to the existence of a high volume of grain boundaries. Therefore, nanocrystalline structures are suitable for the development of materials and coatings that provide us with high hardness, reduced Young's modulus and improved toughness [6]. In Fig.1 is a comparison of the hardness of materials depending on the size of the grains in the material [7]:

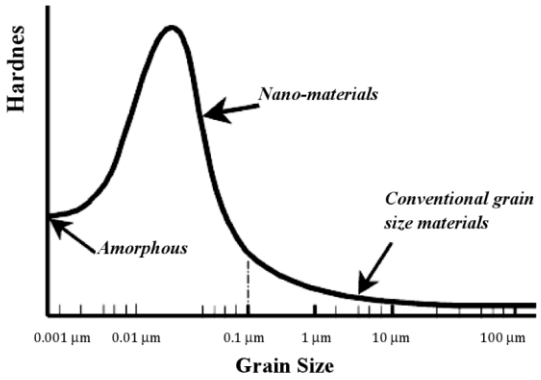

Fig. 1 The hardness of materials is depended on the size of the grains in the material [7]

Surface texturing is one of the important branches of surface engineering. The principle of texturing is the formation of ordered patterns of various shapes on the surface of materials, which greatly improves the properties of materials, whether it is tribological properties (reducing COF) or improving the adhesion of the surface of the underlying material during the coating process. The structure of the textured surface is given as a 3-dimensional topography of the given surface. We know 2 types of surface texturing technology. The first of them is the laser beam texturing technology (LBT), which is used most often in practice. The second type of surface texturing technology is Electron Beam Texturing (EBT) technology [8]. In laser beam texturing, a focused pulsed laser beam creates surface depressions surrounded by a smooth rim of solidified melt. Most of the material in contact with the laser beam is vaporized and ejected by the vapor pressure, creating a texturing pattern (pit or groove). Repeated pulses on spatial and temporal gauges create a surface texture. Texturing can also be applied to molds intended for high-pressure casting of aluminum and its alloys. The textured surface of the mold provides increased traction, resistance to oxidation at high temperature and many other improved properties that increase the life of the mold and its molded parts [9]. Fig.2 shows a process of the surface texturing process with a laser beam [10].

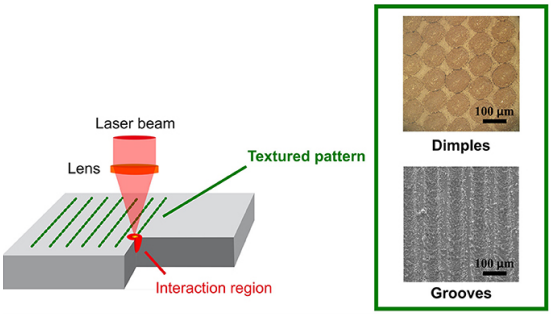

Fig. 2 *The process of the surface texturing process with a laser beam [10]*

2. Materials and methods

Aim of the contribution was to increase the lifetime of the mold used for high-pressure casting of aluminum and its alloys by applying a PVD nanostructured coating in combination with laser texturing of the surface. The research was carried out on the base material used by the foundry for the production of shaped parts of the mold for high-pressure casting of aluminum and its alloys. It is a tool steel called Uddeholm Dievar, which is alloyed with chromium, molybdenum, vanadium and other alloying elements. It is intended for work at high temperatures. Molds for high-pressure aluminum castings and their shaped parts are most often made from this material. This type of material is produced by powder metallurgy technology. The chemical composition of the material is indicated in Table 1.

Table 1: *Chemical composition of Uddeholm Dievar*

Element	C	Si	Mn	Cr	Mo	V
Weight. [%]	0.38	0.2	0.5	5	2.3	0.6

A PVD duplex nACRo^4 coating was deposited on the non-textured as well as the textured surface of the base material. Nanocomposite coating nACRo^4 belongs to the group of 4th generation nanocomposite coatings. It has high toughness and is resistant to abrasion and suitable for working at high temperatures. PLATIT LARC technology® (lateral arc cathode) was used to deposit the coating.

Table 2: *PVD duplex coating deposition parameters*

Deposition parameters									
PVD	Equipment	Deposition	I (A)	I (A)	I (A)	I (A)	Bias (V)	Temperature (°C)	Pressure (mbar)
nACRo^4	Pi 1511	Layer 1	Cr	AlSi	AlCr 65/35	AlCr 65/35	30	470	0.035
			200	160	155	155			
		Layer 2	Cr	AlSi	AlCr 65/35	AlCr 65/35	60	470	0.032
			250	200	135	135			

In the next stage of the research, a microscopic and EDX analysis of the PVD coating was carried out and its mechanical and tribological properties were determined.

The microgeometry of the surface with PVD nanostructured coating as well as the analysis of pit textures with PVD nanostructured coating was captured by a ZEISS LSM 700 laser confocal microscope. Surface roughness profiles were defined according to the EN ISO 4287 standard.

The adhesion of PVD nanostructured coatings was measured by the Scratch test method on a BRUKER device. The ball was made of SiC silicon carbide with a diameter of Φ 6 mm and traveled a distance of 500 m. The load on the ball was 5 N with a linear speed of 0.10 m/s.

The tribological properties of the PVD coating were evaluated under dry friction conditions by the Pin on Ball method at a temperature of 300 °C according to the ASTM G99-17 standard. The coefficient of friction of the non-textured and textured surface, on which the separating agent Safety Lube 7815 was applied, was determined. The agent is used to separate the melt from the mold during casting.

3. Results and discussion

The coating thickness was 2.75 µm. No pores and cracks in the structure were identified. The EDX line analysis of the nACRo^4 coating (see Fig. 3) identified the main elements contained in the coating (aluminum, chromium) and the proportion of nitrogen present in the layer. The proportion of iron and molybdenum in the area of the base material was also determined.

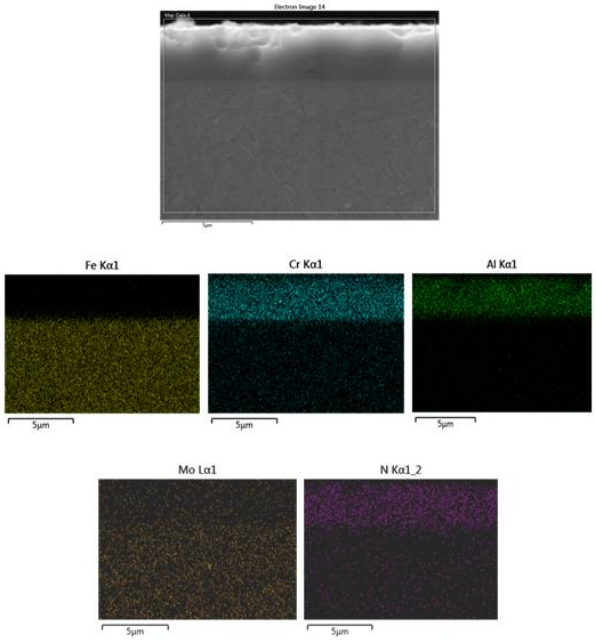

Fig. 3 *EDX elemental analysis of nACRo^4 coating*

The scratch after the Scratch test of the nACRo^4 duplex coating was documented by a scanning electron microscope, Fig.3. From the mentioned nature of the scratch and the course of the Scratch test (see Fig. 4), it is clear that there was no cohesive failure. However, the adhesive failure of the coating is visible in the form of separated particles of the coating material and their transport towards the edges of the track. The first failure occurred at a value of 4.8 N. The adhesive failure occurred at a value of 14.7 N at the end of the test. This violation was correlated with the AE acoustic emissions signal. Fluctuations in the course of the coefficient of friction COF are small, the indenter did not overcome high resistance due to the fact that there was no significant roughening of the surface of the tested coating.

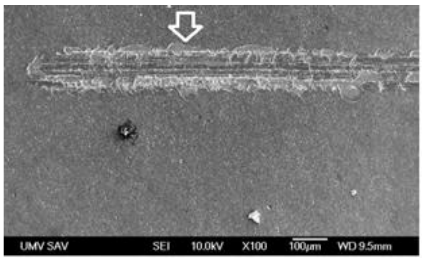

Fig. 4 *SEM image of the scratch after the Scratch test - nACRo^4*

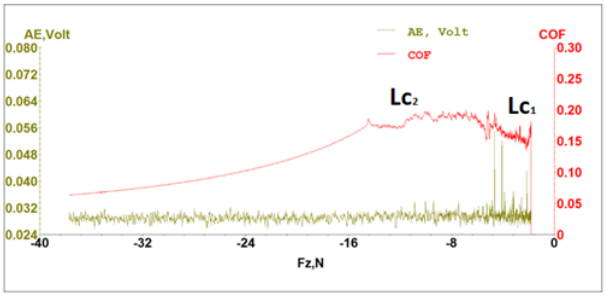

Fig. 5 *Course of wear of nACRo^4 coating*

When evaluating the nACRo^4 coating by the "Pin on Ball" test deposited on a non-textured surface, the nature of the abrasive wear was identified. In the first run-in phase, an interface was formed between the materials that were in contact, and changes at the interface gradually occurred. These changes also resulted in an increase in friction from zero COF to 0.57 at 50 m, which was related to microplastic deformation of the surface. The average COF value was 0.53.

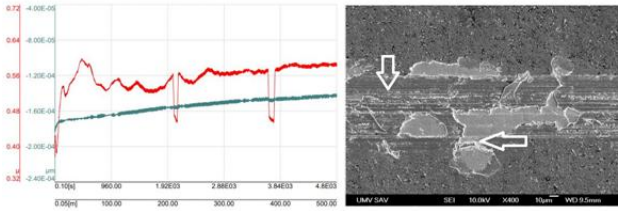

Fig. 6 *Course of wear of nACRo[4] coating*

Another series of samples was prepared with pretreatment of the surface of the base material by laser texturing. Stochastic pit textures were created on the ZM surface, which were created randomly on the surface of the samples (laser random). The depth of pit textures in the case of random texturing was different along the entire measured length of 575 µm, Fig. 6.

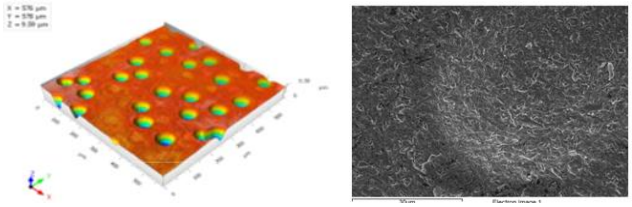

a) *b)*

Fig. 7 *a) Textured surface appearance, b) hole detail*

The tribological properties of the samples treated were evaluated using the Pin on Ball method. Fig.6 and Fig.7 show the course of wear of the textured coating. During the test, a lower COF was noted compared to the coating deposited on the non-textured surface. EDX analysis confirmed that the pits created by texturing serve as a reservoir of a separating agent to ensure the necessary adhesion.

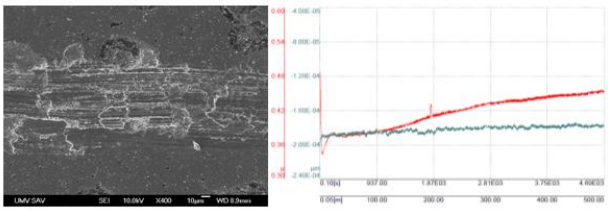

Fig. 8 *Wear course with a textured surface*

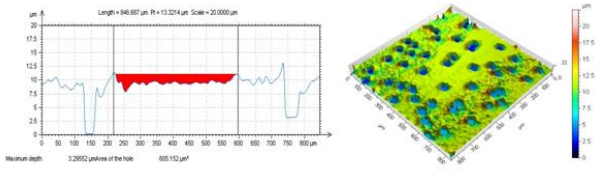

Fig. 9 *3D trace map of the Pin on Ball test of a laser-textured nACRo[4] coating*

4. Conclusions

The paper presents the results of research aimed at increasing the technological life of molds for high-pressure casting of Al alloys. A duplex nACRo[4] coating was applied to the surface of the forms. The adhesion of the coating was determined by the Scratch test. The results confirmed the very good quality of the evaluated coating. Tribological properties were evaluated on the untextured coating as well as on the textured surface. Stochastic pit textures (laser random) were created. the experimental work carried out confirmed that the COF was reduced by the application of surface texturing and that the created wells serve to improve the effect of the separation agent.

5. References

1. F. Jasempoor et. al.: Improving the mechanical, tribological and eletrochemical behavior of AISI 304 stainless steel by applying CrN single layer and Cr/CrN multilayer coatings. In: Wear, Vol. 504-505, 2022, pp. 204425, https://doi.org/10.1016/j.wear.2022.204425

2 J. K. Katiyar et.al.: Tribology and Sutainability, First Edition, CRC Press by 2 Park Square, Milton Park, Abingdon, Oxon, c. 2022. ISBN 978-0-367-55146-9

3. R. Khuengpukheiw et.al.: Wear behaviors of HVOF-sprayed NiSiCrFeB, WC-Co/NiSiCrFeB and WC-Co coatings evaluated using a pin-on-disc tester with C45 steel pins. In: Wear, Vol. 484-485, 2021, pp. 203699, https://doi.org/10.1016/j.wear.2021.203699

4. S.B. Humam et.al.: Microstructure, interface and nanostructured surface modifications to improve mechanical and tribological performance of electrodeposited Ni-W-TaC composite coating. In: Surface & Coating Technology, Vol. 419, 2021, pp. 127293, https://doi.org/10.1016/j.surfcoat.2021.127293

5. A.K. Basak et.al.: Abraisve wear of nanostructured cermet coatings in dry and slurry conditions. In.: International Journal of Refractory Metals and Hard Materials, Vol. 100, 2021, pp. 105638, https://doi.org/10.1016/j.ijrmhm.2021.105638

6. C.W. Luo et.al.: Structure, mechanical and tribological properties of thich CrNx coatings deposited by HiPIMS. In: Vacuum, Vol. 203, 2022, 111253, https://doi.org/10.1016/j.vacuum.2022.111253

7. R. Daniel, J. Musil: Novel nanocomposite coatings, CRC Press Taylor & Francis Group, c. 2013, ISBN 978-981-4411-17-2

8. Z. Wang, et.al: The performance of textured surface in friction reducing: A review. In: Tribology International, Vol. 177, 2023, pp.108010, https://doi.org/10.1016/j.triboint.2022.108010

9. Q. Huang, et.al: Recent progress on surface texturing and solid lubricants in tribology: Designs, properties, and mechanisms. In: Materials Today Communications, Vol. 35, 2023, pp. 105854, https://doi.org/10.1016/j.mtcomm.2023.105854

10. Laser texturing & Wettability modification. [online] [cit. 2023-28-05].Available on internet: http://laser4mat.webs.uvigo.es/wettability-modification/

Acknowledge

This paper is the result of the project implementation: „Innovative approaches to the restoration of functional surfaces by laser weld overlaying“ (APVV-20-0303) supported by the Slovak Research and Development Agency; Scien-tific Grant Agency „Possibilities of application of laser additive technologies in restoration of functional surfaces“ (VEGA 1/0597/23) and Cultural and educational Grant Agency „Modernization of teaching in the field of technologies for joining construction materials” (046TUKE-4/2022).

Application of innovative procedures for modification of surface topography

Janette Brezinová[1*], Miroslav Džupon[2], Marek Vojtko[2], Ján Hašuľ[1], Jakub Brezina[1]
Technical University of Košice, Faculty of mechanical engineering, Slovakia[1]
Slovak Academy of Sciences, Institute of Materials Research of SAS, Slovakia[2]
janette.brezinova@tuke.sk

Abstract: *The paper presents the results of research focused on the application of innovative procedures for surface topography modification. The experimental work was aimed at adjusting the microgeometry and surface topography of new and renovated shaped parts of molds for casting aluminium alloys under high pressure. In the phase of experimental verification of suitable surface topography, a group of samples from Dievar material was prepared. A multilayer nanostructured PVD coating of the 4th generation duplex nACRo[4] was deposited on part of the experimental samples. The surface of the samples was ground and polished. The microgeometry of the surface of the samples was modified by low-energy laser radiation - microtexturing. The maximum interval was chosen to create a stochastic texture, also called a random texture crater distance up to 200 µm. The aim of this surface treatment was to analyze the adhesion effect of commercially used ones of lubricants in the technology of treatment of shaped parts of molds when casting aluminium alloys under high pressure on machines with a cold filling chamber. In the run-in of the mold, after the first cycles of spraying with a separating agent, a compact layer was created to increase the technological life of the shaped parts of the molds.*
Keywords*: nanostructured PVD coating, microgeometry of the surface, microtexturing*

1. Introduction

Nanostructured coatings represent a new generation of coatings, or they are composed of at least two separate phases with a nanocrystalline or amorphous structure. The formation of the nanostructured coating is attributed to the segregation of one phase to the grain boundary of the second stage. This effect is responsible for preventing grain growth and structure formation at the nanoscale. The new functional properties of nanostructured coatings result from this microstructure, where the dominant role is played by the boundary regions that surround the individual grains. Due to the very small grains of less than or equal to 10 nanometers separated by a second phase (predominantly amorphous), nanostructured coatings are managed differently compared to conventional coatings that have grains larger than 100 nanometers [1,2].

The optimal thickness of the phase that separates the nanocrystals from each other is 1-3 nm, which corresponds to only a few monolayers. The optimal size of the grains forming the nanocrystalline structure is given in the range of 3-10 nm. The various borides, nitrides, carbides, or oxides forming the nanocrystalline structure together with the ceramic, metal or carbon amorphous matrix provide unique properties for each combination of materials. Such diversity of composition and properties of nanostructured coatings enables their wide use in various areas of engineering applications. The formation of coatings with a nanocrystal structure requires optimization of the deposition conditions to reduce the grain size and at the same time ensure the development of the segregation phase. Among the basic process parameters that affect the size and crystallographic orientation of the grains are the current, the temperature of the base material, the bias on the sample, the low current density of the base material and the partial pressure of the reactive gas used [3-5].

Grain growth can be effectively controlled through the kinetic energy of impact particles that are transferred to a very small surface area. Ion bombardment contributes to the minimal surface mobility of atoms, which is necessary for the formation of a crystalline phase and to sufficient diffusion in the segregation system. However, it is also necessary to regulate the temperature of the process, because exceeding the critical temperature value no longer prevents grain growth and segregation of grain boundaries. Like low-energy bombardment, the addition of one or more alloying elements to the base material has the same effect on the formation of the nanostructured phase. The Fig.1 shows a typical structure of a nanostructured coating [6,7].

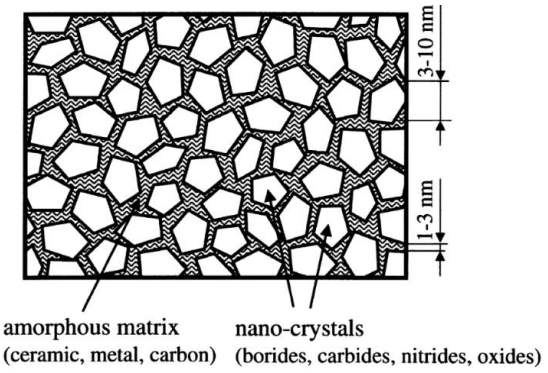

Fig. 1 *Typical structure of a nanostructured coating [8]*

Surface texturing refers to a series of regular micro-structures machined on the surface of a sample through process technology. The textures with suitable size can act as micro-bearing to increase the dynamic pressure between friction pairs, store lubricants, and capture debris produced during the friction process. The structure of the textured surface is given as a 3-dimensional topography of the given surface [9]. We know 2 types of surface texturing technology. The first of them is the laser beam texturing technology (LBT), which is used most often in practice. The second type of surface texturing technology is Electron Beam Texturing (EBT) technology. It is confirmed that the shapes are confirmed further reduction of friction and properties. On the surface shapes of the textures, simulations and experiments were carried out during individual studies, including a typical number of rectangular, circular, elliptical, triangular, and V-shaped textures as shown in Fig.2 [10]:

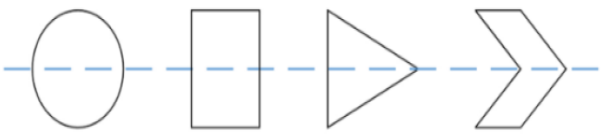

Fig. 2 *Shapes of textures created on the surface of materials [10]*

2. Materials and methods

For the experimental work carried out in the dissertation, a base material identical to the material of the mold was used. It is a tool steel called Uddeholm Dievar, which is alloyed with chromium, molybdenum, vanadium, and other alloying elements. It is intended for work at high temperatures. Molds for high-pressure aluminium casting and their shaped parts are most often made from it. This

type of material is produced by powder metallurgy technology. The chemical composition of the material is shown in Table 1:

Table 2: *Chemical composition of Uddeholm Dievar*

Element	C	Si	Mn	Cr	Mo	V
Weight. [%]	0.38	0.2	0.5	5	2.3	0.6

The surface texturing of the samples was performed by the LBT (laser beam texturing) method. The Yb fiber laser type Piranha II Multi FL205 with a power of 20 W was used. The creation of dimple textures was used, which serves as a reservoir for the separating agent in the process of high-pressure casting of Al and its alloys. Before the coating and texturing process, the surface of the base material was pretreated with wet sandblasting and polishing technologies. Two types of dimple textures were created, random and large. Three types of PVD duplex coatings AlTiN G, $AlXN_3$ and $nACRo^4$ were deposited on the surfaces prepared in this way using PLATIT LARC technology. $AlXN_3$ is a duplex coating composed of: X=Cr; CrN layer + Al/CrN nanomultilayer + AlN layer. The $nACRo^4$ nanocomposite coating consists of layers of layers: the first adhesive layer is formed by chromium nitride, on which a gradient AlCrN layer is subsequently deposited. Very thin AlCrN nanolayers are applied to the thus prepared gradient layer. The final top layer of $nACRo^4$ is formed by a nanocomposite coating of nc-AlCrN/a-Si_3N_4. AlTiN is a hard coating that solves many tribological problems with components that can be coated at temperatures of 450°C - 475°C. PLATIT LARC technology® (lateral arc cathode), which is patented and unique worldwide, was used to deposit the coatings. PLATIT Pi411 equipment was used for AlTiN G coatings and AlXN3 coating. A PLATIT Pi1511 device was used for the $nACRo^4$ coating. The roughness recommended by the manufacturer was 0.3 µm. The AlTiN G coating is gradient where 2 stages are given: gradient 1 - where the deposition starts and gradient 2 - the deposition ends. The other coatings are multi-layered, where the parameters of Layer 1 and Layer 2 alternate during deposition. Microscopic analysis of the coatings was performed.

The microgeometry of the textured surface without and with PVD nanostructured coatings was captured by a ZEISS LSM 700 laser confocal microscope. The roughness profiles of the textured surface were defined according to EN ISO 4287.

Release agent Safety Lube 7815 is used in the high-pressure casting process. Safety Lube separators are based on an organic base and contain the basic element silicon in their composition. They are manufactured by ChemTrend. These release agents are sprayed onto the mold surface before each casting process to ensure easier removal of the castings from the mold and to create a thermal barrier between the melt and the steel surface of the mold. The standard separation agent used in practice is Safety Lube 7815.

The coefficient of friction of the non-textured and textured surface with PVD nanostructured coatings was determined by the Pin on ball method according to the ASTM G99-17 standard when dry and using the release agent Safety Lube 7815. A 6 mm ball traveled 500 m and the load on the ball was 5 N with a linear velocity of 0.10 m/s.

3. Results and discussion

Microscopic analysis of coatings

In Fig.3 a cross section of the AlTiN G coating is shown. The coating thickness was 1.55 µm. It is clear from the cross section that the coating was continuous over the entire surface without any pores or cracks.

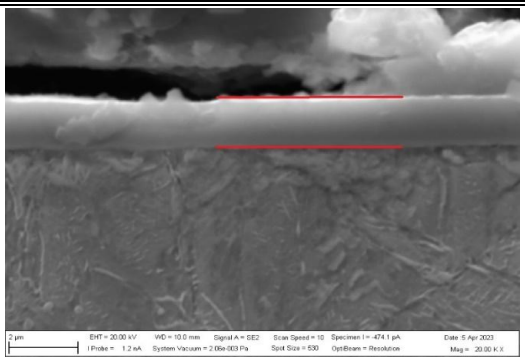

Fig. 3 *Cross section of the AlTiN G coating*

In Fig.4 an EDX surface elemental analysis is shown, which shows us the distribution of the coating element, i.e. titanium, aluminium, nitrogen, as well as the base material on the analyzed sample:

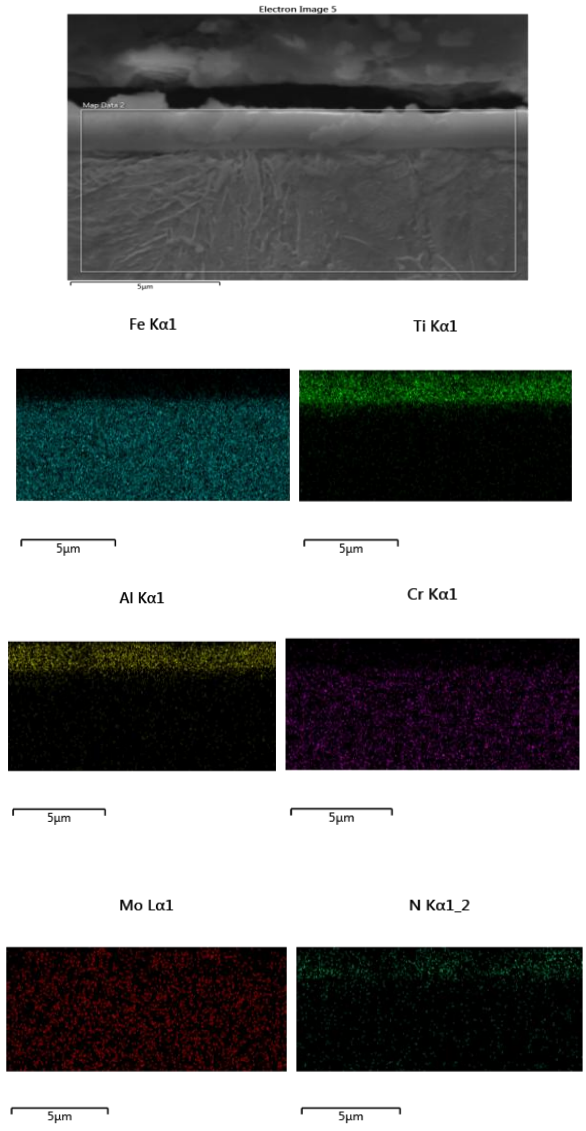

Fig. 4 *EDX surface elemental analysis of the AlTiN G coating*

During the microscopic analysis of the surface morphology of the AlTiN G coating, cracks in the form of drops, slimes and pores were detected. This heterogeneity is provided by the delivery of the coating after the deposition process. The mentioned phenomenon is typical for the coating on AlTiN and this phenomenon does not occur in the deposition process. The value of the Ra parameter reached a value of 0.142 µm. It is clear from the roughness profile

that the AlTiN G coating showed the highest roughness along the entire measured length of the analyzed coatings.

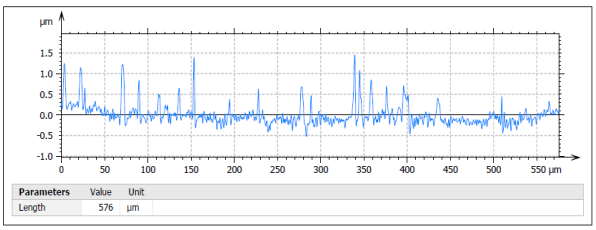

Fig. 5 *Roughness profile of AlTiN G coating*

The thickness of the $AlXN_3$ coating marked in red was 1.12 µm. From the cross-section the coating is not continuous, where cracks and pores are present in the layer.

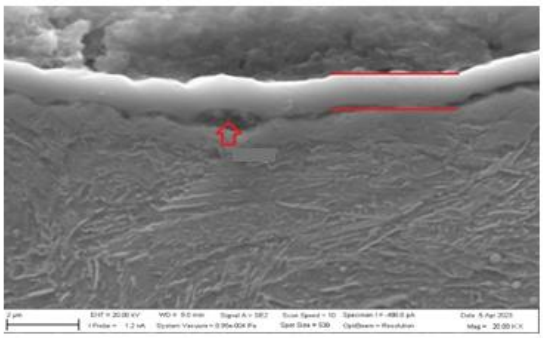

Fig. 6 *Cross section of the $AlXN_3$ coating*

EDX elemental analysis of the $AlXN_3$ duplex coating shows the distribution of the individual elements of the coating (chromium, aluminum, nitrogen) and the base material (iron, molybdenum) in the analyzed part.

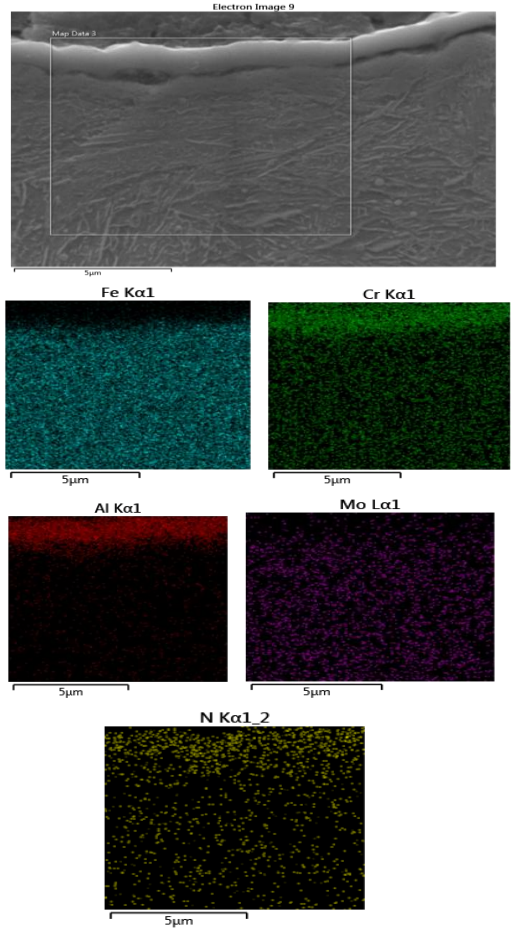

Fig. 7 *EDX surface elemental analysis of the $AlXN_3$ coating*

Inherent droplets and holes were also observed in the surface morphology of the deposited $AlXN_3$ coating. Equiaxial AlN grains were observed in the upper part of the coating. Under the upper zone there were multilayers of AlCr grains. An adhesion layer of CrN was identified, which was closest to the base material in the lower part and ensures better adhesion of the coating to the base material. The value of the parameter Ra reached a value of 0.126 µm. Compared to the AlTiN G duplex coating, it can be concluded that the surface of the $AlXN_3$ coating is less roughened along the entire measured length.

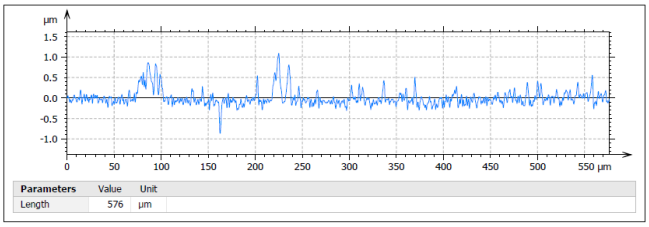

Fig. 8 *Roughness profile of AlTiN G coating*

The coating thickness of $nACRo^4$ marked in red was 2.75 µm. This coating showed the greatest thickness compared to the previous two coatings. No pores and cracks in the structure were identified.

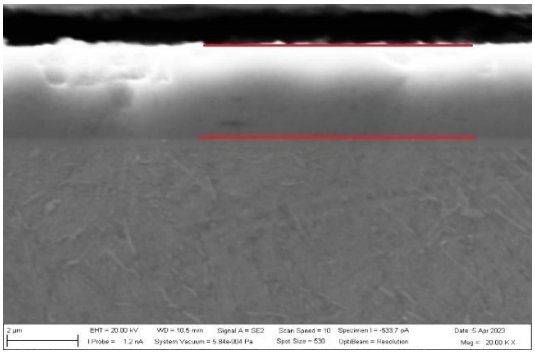

Fig. 9 *Cross section of the $nACRo^4$ coating*

EDX elemental analysis of the nanostructured $nACRo^4$ coating revealed the distribution of the basic elements contained in the coating (chromium, aluminium, nitrogen) as well as the elements contained in the basic material (iron, molybdenum).

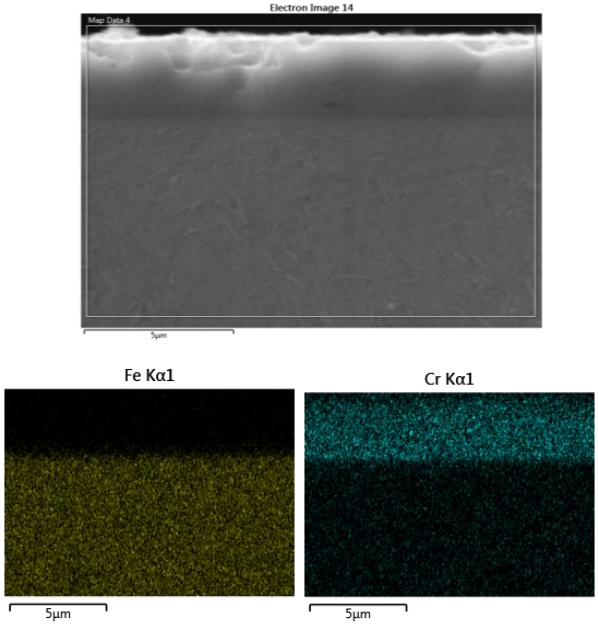

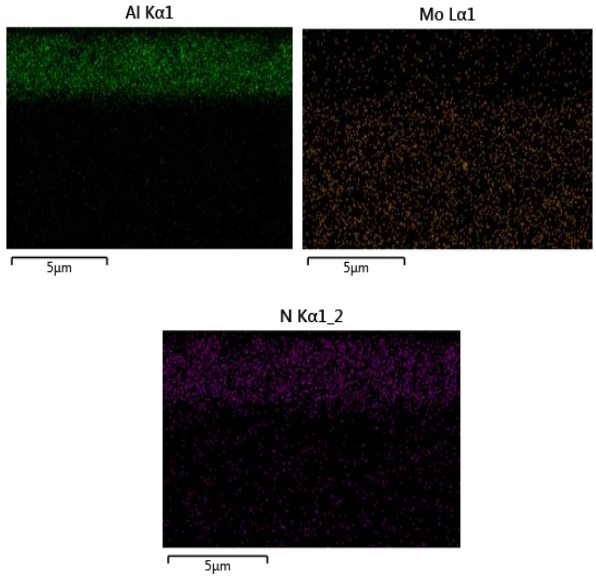

Fig. 10 *EDX surface elemental analysis of the nACRo[4] coating*

Many microparticles were observed on the surface, which are inherent in cathodic arc deposition and originate from excess ions from the target during deposition. Si content was observed, resulting in the support and formation of the nc/Si_3N_4 nanostructured phase in the coating. The value of the Ra parameter reached a value of 0.0984 µm. From the given value, it can be concluded that the nACRo[4] nanostructured coating showed the lowest surface roughness compared to the previous duplex coatings.

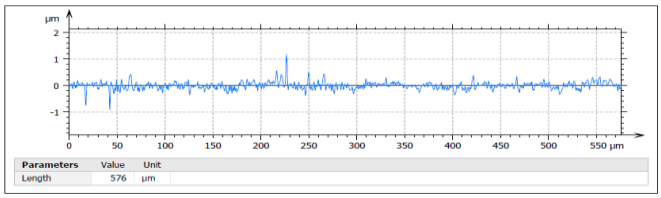

Fig. 11 *Roughness profile of nACRo[4] coating*

EDX analysis of release agent Safety Lube 7815

A "dry" of Safety Lube 7815 release agent was prepared at 250°C in which silicon was detected by EDX microanalysis as evidence that the release agent remained on the surface with dimpled texture.

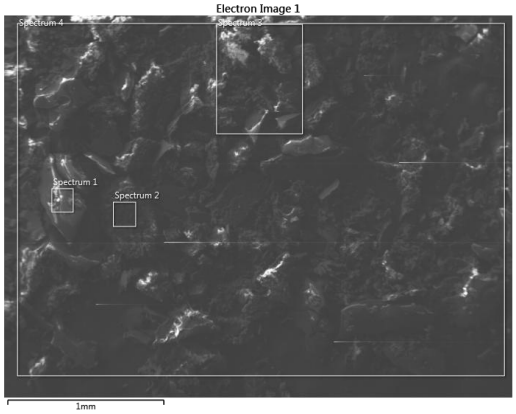

Fig. 12 *Analyzed parts of Safety Lube 7815 release agent*

In Fig.13 is the EDX analysis of the separating agent Safety Lube 7815 itself is shown, where the proportion of the main silicon component was detected, namely 9.8 wt.%. Carbon, oxygen, and sodium were also present.

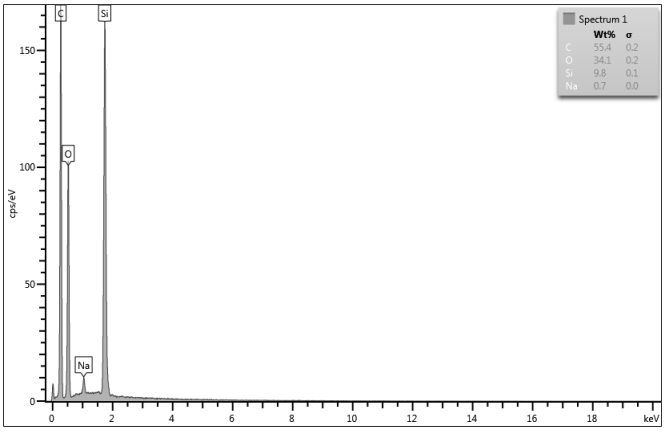

Fig. 13 *EDX analysis of Safety Lube 7815*

The percentage of Si in dimpled textures together with PVD duplex coatings is shown in Table 2:

Table 2: *Si percentage in dimpled textures with PVD duplex coatings*

Share of Si in dimpled textures [wt.%]			
Coating	**AlTiN G**	**$AlXN_3$**	**nACRo[4]**
10x	0.3	1.1	4.8
20x	1.1	1.2	5.1

From the table it is this, that with cyclic storage of the separating agent 10x and 20x the base element Si was present as a result of the residue of the release agent on the surface of the PVD duplex coatings. Increased values are detected in the nACRo[4] coating because the coating itself contains the Si element in its microstructure, which provides us with a nanostructure embedded in the $S_{i3}N_4$ matrix.

Texturing of surface

In the case of random texturing, the depth of dimpled textures was different along the entire measured length of 575 µm (Fig.). The randomness of the process can be observed at a length of 100 µm, where the depth of the dimpled texture reaches a value of 3.5 µm. At lengths of 400 or 500 µm are dimpled texture depths of approximately 5 µm and 6 µm. From the depth profile of the stochastic textures, it can be said that during random texturing, the depth of dimpled textures varied depending on the measured length of the surface. Since the dimpled textures were created randomly, it can be assumed that the profile was measured in different parts of the dimples:

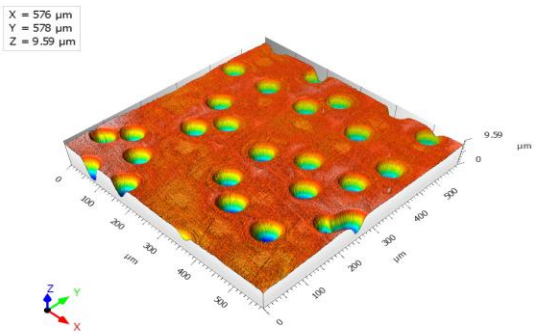

Fig. 14 *AFM image of stochastic surface texturing*

With ordered texturing, the depth of dimpled textures was found to be the same over the entire measured length of 576 µm, in contrast to random laser texturing. The depth of the dimpled

textures during ordered laser texturing was 5 µm. The analysis found that there was no degradation of the base material during the texturing of the dimple textures.

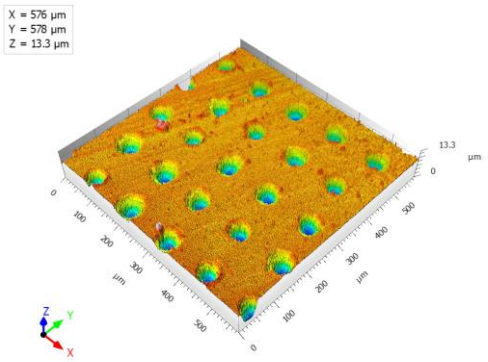

Fig. 15 *AFM image of ordered surface texturing*

Because the molds itself and its parts are complex in shape and construction, have sharp transitions, various roundings and bevels, it was found within the experiment that it is appropriate to perform random texturing of the surface by applying stochastic pit textures to the form's complex surface. The depth of the stochastic well textures was 5 µm. If the textures had more depth, they would also affect the surface quality of the castings. The texture imprint would remain on the surface of the casting, reducing the surface quality.

Coefficient of friction

Average COF values of PVD duplex coatings without and with laser texturing were measured:

Table 3 Average COF values without and with laser-textured PVD duplex coatings

COF	AlTiN G	$AlXN_3$	$nACRo^4$
Without texture	0.45	0.42	0.53
With texture	0.43	0.39	0.42

It was found that a pitted surface with Safety Lube 7815 release agent applied resulted in a lower coefficient of friction value compared to an untextured surface for all three PVD coatings. The largest reduction in COF value was observed for the $nACRo^4$ coating, where a value of 0.53 was measured in untextured measurements. By applying pitting textures and Safety Lube 7815 release agent, the COF of the $nACRo^4$ coating was reduced to 0.42. The wear rate was also the lowest for the $nACRo^4$ coating, which corresponded to its hardness value of 40 GPa.

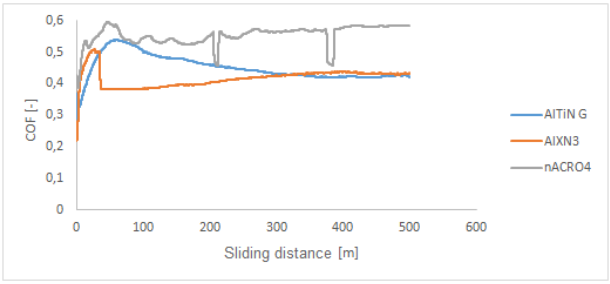

Fig.16 *COF curves of duplex coatings without surface texturing*

The course of friction coefficients of coatings without texturing is shown in Fig.16. Coatings with texturing achieved similar trends, but with a lower value of the coefficient of friction (Table 3).

4. Conclusions

The aim of the contribution was to propose a methodology for increasing the technological life of molds for high-pressure Al casting. Three types of PVD duplex coatings were designed to increase the technological service life. The surface of the base material before depositing the coatings was modified by laser texturing using LBT technology (Laser Beam Technology). The tribological properties of the coatings were evaluated by the Pin-on-ball method. A hypothesis was put forward about ensuring the supply of the separating agent in critical parts of the mold by applying pit textures on the surface of the material. The mentioned hypothesis was confirmed by tribological tests. The measured COF on textured coatings reached lower values.

Acknowledge
This research was funded by the Scientific Grant Agency VEGA 1/0597/23; Cultural and educational grant agency KEGA 046TUKE-4/2022; Agency for research and development APVV-20-0303.

5. References

1. H. Zhen et.al.: Discontinuous oxidation in wet air of T91 with a novel Al2O3-forming NiCrAl nanocomposite coating in as-desposited and pre-oxidized states. In: Surface & Coating Technology, Vol.449, 2022, pp. 128937, https://doi.org/10.1016/j.surfcoat.2022.128937

2. A. Ostlind et.al.: Scalable synthesis of a bulk nanocrystalline material with a multitude of divergent properties through a traditional manufacturing process. In: Materials Today Communications, Vol. 33, 2022, pp. 104390, https://doi.org/10.1016/j.mtcomm.2022.104390

3. A.D. Pogrebnjak, O.Bondar: Microstructure and Properties of Micro- and Nanoscale Materials, Films and Coatings (NAP 2019): Selected Articles from the International Conference on Nanomaterials: Applications and Properties, Springer Nature, c2020, ISBN 978-981-15—1741-9

4. A. Krella, A. Marchiewicz: Effect of the reversla of the layers thickness ratio in the CrN/CrCN multilayer coating on cavitation induced degradation. In: Tribology International, Vol. 168, 2022, pp. 107432, https://doi.org/10.1016/j.triboint.2022.107432

5. K.S. Selivanov et.al.: Erosive wear of Ti/Ti(V, Zr)N multilayered PVD coatings for Ti-6Al-4V alloy. In: Wear, Vol. 418-419, 2019, pp. 160-166, https://doi.org/10.1016/j.wear.2018.11.016

6. M. Fangsheng et.al.: Microstructure, mechanical, tribological and oxidizing properties of AlCrSiN/AlCrVN/AlCrNbN multilayer coatings with different modulated thicknesses. In: Ceramics International, Vol. 48, 2022, pp. 32973-32985, https://doi.org/10.1016/j.ceramint.2022.07.228

7. T. Pengfei et.al.: Microstructure evolution and nanohardness of nanostructured TiAlN coating under N+ ion irradiation. In: Surface & Coating Technology, Vol. 441, 2022, pp. 128494, https://doi.org/10.1016/j.surfcoat.2022.128494

8. R. Daniel, J. Musil: Novel nanocomposite coatings, CRC Press Taylor & Francis Group, c. 2013, ISBN 978-981-4411-17-2

9. S. Fang. et.al.: Surface texturing of PECM tools and the validation. In: Procedia CIRP 2022, Vol. 95, p. 891-896, https://doi.org/10.1016/j.procir.2020.01.183

10. Z. Wang, et.al: The performance of textured surface in friction reducing: A review. In: Tribology International, Vol. 177, 2023, pp.108010, https://doi.org/10.1016/j.triboint.2022.108010

Study of the properties of the metal surface after pre-treatment by phosphating

Dagmar Draganovská[1,*], Gabriela Ižaríková[2], Róbert Moro[3]
Technical University of Košice, Slovak Republic[1,2,3]
dagmar.draganovska@tuke.sk[1], gabriela.izarikova@tuke.sk[2], robert.moro@tuke.sk[3]

Abstract: *The contribution is focused on the analysis of the roughness of metal surfaces after applying a conversion layer using phosphating. The types of basic materials is used in the experiment hot-dip galvanized microalloyed steel HX340LAD+Z. During the application of the conversion layer, changes in surface roughness were studied with respect to the phosphating time, which was 3, 5 and 10 minutes. The paper deals with the evaluation of the relationship between the individual roughnesses parameters of pre-treated surfaces using correlation analysis. Based on the measured roughness values on the surfaces, the standard of statistical significance of the correlation between the observed parameters was determined from them. The achieved results provide information for other technological operations such as the creation of adhesive joints, where the correct anchoring of the adhesive is important for load bearing capacity of joints.*
Keywords*: SURFACE, PHOSPHATE LAYER, ROUGHNESS, STATISTICAL ANALYSIS*

1. Introduction

The term conversion layers collectively refers to chemical pre-treatments of metal materials, which are created by a chemical reaction between the metal and the applied coating. Chemical conversion layers or surface passivation are one of the cost-effective methods of surface treatment of steel substrates. When a metal and an inorganic chemical solution come into contact, a chemical reaction occurs. The result of this chemical reaction is the formation of a surface layer. Phosphate layers are created by immersing a metal object in a chemical solution with or without applying an electric current to the object.

The result of the reaction between the material and the chemical solution is the growth of a layer from the surface of the substrate. The layer is an integral part of the surface of the component and not only affects the surface but also changes the subsurface layer of the material. Thus, there is no distinct mechanical interface between the layer and the underlying material. [1-4]

Phosphate layers are applied to metals to improve corrosion resistance due to their relatively high electrical resistance. Their function is also to support the adhesion of organic coatings or other adhesives. The conversion coating has the ability to adhere excellently to the treated metal and resists solubility in water or other solvents. Subsequently applied coatings are characterized by excellent adhesion to the material. They are applied in a multi-step process that involves cleaning the metal to remove impurities of organic contamination, surface oxides and surface cracks that can prevent coating formation.

The phosphate layer is applied by spraying or dipping in phosphoric acid or metal phosphates. A thin non-conductive and insoluble layer of microscopic crystals of metal phosphates forms on the surface of the metal.

There are three types of phosphating, iron, zinc and manganese. The uniqueness of these species is characterized by the crystals that form in each of them. Manganese phosphating is generally considered the most durable in corrosion protection. Iron phosphating is more stable than zinc phosphating at higher pressures and temperatures. With iron phosphating, there is an increase in coating adhesion and impact resistance, and at the same time it provides a lower degree of protection against corrosion. Zinc phosphate is suitable for cold forming with the required sliding properties, for preserving the surface and before subsequent painting. [5, 6]

In addition to increased resistance to corrosion, phosphating also increases the adhesion of the next applied layer, coatings, lubricant or adhesive for joint formation. The paper deals with the relationship between the applied phosphating time and roughness changes on the surface of the material.

2. Materials and methods

2.1 Used basic material

HX340LAD+Z steel (abbreviation designation HX) is a hot-dip galvanized microalloy steel. The chemical composition of the materials is in Table 1.

Table 1: *Chemical composition of used steel HX 340LAD+Z*

Material	C	Mn	P	Si	S	Nb	Ti
HX	0,07%	0,60%	0,02%	0,01%	0,01%	0,03%	0,00%

The tested samples were pre-treated with zinc phosphate conversion layer. During the phosphating process, small crystals form on the surface of the material, creating a phosphate layer that serves as protection against corrosion or as a base layer to improve adhesion when applying additional layers and when gluing.

A total of 8 types of samples were used for the experiment. Sample HX 0 is sample of HX type steel, the surface of which was not treated with a zinc phosphate conversion layer. The other samples used in the experiment were treated with a layer of zinc phosphate with different immersion times of the sample in the phosphating bath, namely 3, 5 and 10 minutes. In Table 2 shows the labels of the samples according to their phosphating times.

Table 2. *Designation of samples*

Sample	Steel type	Time of phosphating
HX0	HX340LAD+Z	-
HX 3	HX340LAD+Z	3 min
HX 5	HX340LAD+Z	5 min
HX 10	HX340LAD+Z	10 min

2.2 Used pre-treatment

For the phosphating of the samples, the technology of phosphating with Pragofos 1500, manufactured by Pragochema s.r.o., applied by immersion, was used. The phosphate layer has the task of protecting the material from corrosion or serves as a base layer before applying other layers. Before the phosphating process itself, the treated steel surface was degreased with an alkaline, medium-emulsifying preparation Pragolod 57 N from Pragochema s.r.o. The preparation was applied to remove preservative oils and other impurities from the surface of the steel samples. Its effectiveness is also high on modern types of biodegradable oils such as rapeseed oil or oils based on acid esters

of vegetable oils. The dispersant contained in the preparation is effective on graphite and metal particles, which are more complicated to remove from the surface. Pragolod 57 N was applied by immersing the sample in a bath.

Before applying the phosphate layer after the application of the degreaser Pragolod 57 N, the rinse in the bath was diluted with the activating rinse Pragofos 1007 at a concentration of 0.3% at room temperature with a mixing time of 3 minutes. Pragofos 1501 is a concentrate for the preparation of a phosphating bath, the main components of which are zinc phosphate and chlorate. HX340LAD+Z steel samples were phosphated in a bath mixed with Pragofos 1501 and Pragofos 1502 products from Pragochema s.r.o., used to treat hot-dip galvanized steel. The preparation Pragofos 1502 is a preparation containing fluorides. The conversion phosphate layer was applied at a temperature of 60 °C for 3, 5 and 10 min. After the phosphating process, the samples were rinsed with demineralized water and dried with hot air.

2.3 Surface roughness measurement methods

The surface roughness of the individual samples was measured by the touch measurement method with a profilometer of the type Surftest SJ-201 from the Japanese manufacturer of metrological equipment Mitutoyo. The measurement took place in accordance with the standard ISO 21920-2. For the purpose of the experiment, parameters were chosen that could accurately describe the differences in the roughness of the evaluated surfaces [7-12]:

The following parameters were selected:

Ra [μm] – mean arithmetic deviation of the surface

Rz [μm] – average value of the largest profile heights

RSm [μm] - average width of profile elements

RPc [-/cm] - number of profile elements per cm of length

2.4 Methods of statistical processing of roughness results

In order to evaluate the measured quantities, evaluating the microgeometry and the influence of the phosphating time on the change in the character of the surfaces, the obtained results were processed using statistical methods. The evaluation of the influence of the material and the phosphating time on the surface roughness represented by the parameters Ra, Rz and RPc was realized using the STATISTICA software. Specifically, graphic tools (histogram, boxplot) and statistical tests (Shapiro Wilk normality test, Levene's test, Two-sample t-test, Mann-Whithey test, ANOVA, Kruskal-Wallis test) were used.

3. Results

The resulting average values of the measurement of individual roughness parameters are shown in Table 3. It follows from the measurements that the value of the parameters does not change significantly for individual materials and surface treatments. Based on this fact, the influence of the phosphating time on the Ra parameter was statistically verified.

The zinc phosphate on the surface consists of a number of insoluble phosphate crystals that grew on the surface in the phosphating process and the density of the protrusions increased. The surfaces of the modified HX material rather just copy the original surface, so the density of the protrusions did not change significantly.

The surfaces of the HX treated material show approximately the same density of RPc protrusions. It is therefore possible to conclude that the original surface profile was copied during the phosphating of the HX material.

SEM appearance of the base material and pretreatment samples are in Fig. 1 – 4.

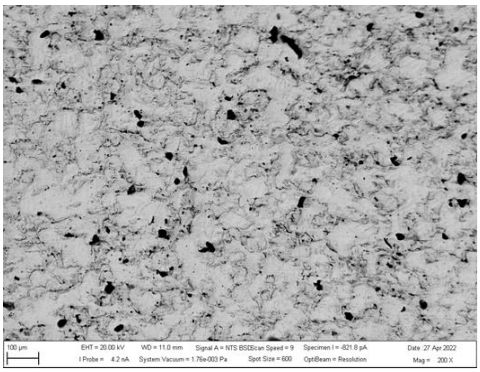

Fig. 1 *Appearance of the sample surface HX 0*

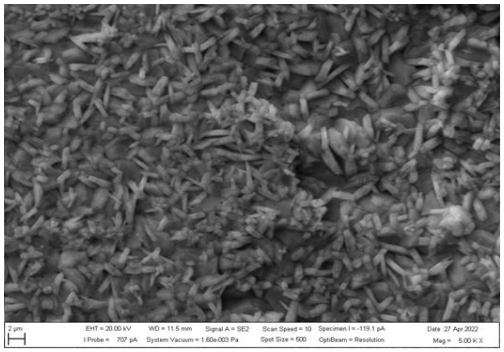

Fig. 2 *Appearance of the sample surface HX 3*

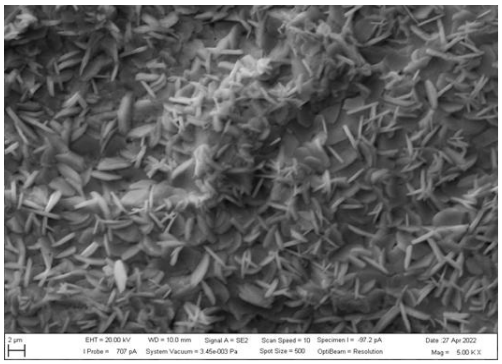

Fig. 3 *Appearance of the sample surface HX 5*

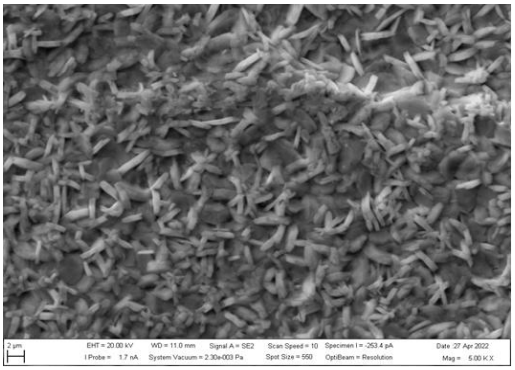

Fig. 4 *Appearance of the sample surface HX 10*

***Table 3**. Measured values of roughness parameters*

Sample	Measured values of roughness parameters			
	Ra [µm]	Rz [µm]	RPc [-/mm]	RSm [µm]
HX 0	1,05 ± 0,07	5,88 ± 0,44	111,90 ± 12,40	90 ± 10
HX 3	0,80 ± 0,08	5,13 ± 0,53	100,08 ± 17,84	104 ± 24
HX 5	1,17 ± 0,12	5,97 ± 0,96	99,86 ± 21,41	105 ± 24
HX 10	0,89 ± 0,12	5,83 ± 1,18	98,14 ± 13,21	104 ± 27

3.3 Results of statistical evaluation for parameter Ra

In order to choose a suitable method of comparison, the condition of normality of the distribution was verified, graphically and also by the Shapiro-Wilk test (Fig. 5). For all assessed groups, is p >0.05, which means that at the significance level of 0.05, the null hypothesis H_0 is not rejected, i.e. the condition of normality is met.

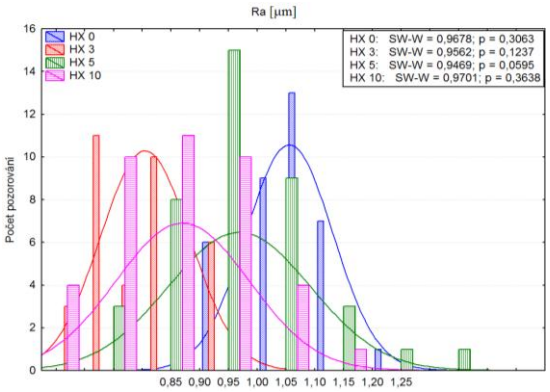

***Fig. 5** Verification of normality conditions for parameter Ra*

The homogeneity condition for the Ra parameter values at different phosphating application times was verified by Levene's test. The value of p was as follows: HX (p = 0.099 > 0.05) and this means that the null hypothesis of equality of variances is not rejected at the significance level of 0.05. The condition of homogeneity is fulfilled. A graphical comparison of the phosphating time for the parameter Ra is in Fig. 6.

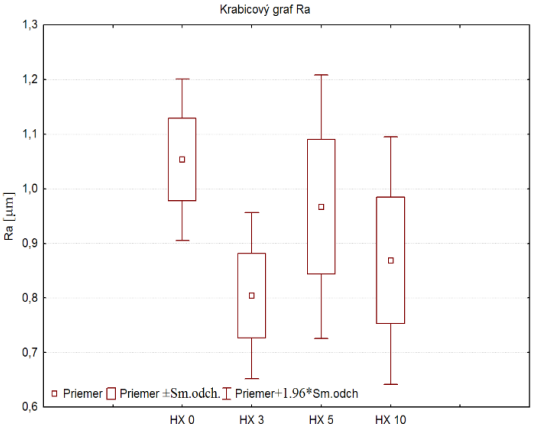

***Fig. 6** Comparison of phosphating time for parameter Ra*

The result of the one-factor variance analysis is 0.0000 < 0.05, i.e. the null hypothesis is rejected at the level of significance, i.e. there is a statistically significant difference between the individual mean values of the Ra parameter at different phosphating times. This means that the time of phosphating has an influence on the value of the Ra parameter.

Due to the fact that the null hypothesis of equality of mean values was rejected at the 0.05 significance level, post-hoc analysis subsequently identified pairs between which there is a statistically significant difference (Table 4). Statistically significant differences were noted between all observed groups.

***Table 4.** Post-hoc analysis – parameter Ra*

Ra - HX	Tukey HSD test			
	HX0	HX3	HX5	HX10
HX0	-	0,0000	0,0000	0,0000
HX3	0,0000	-	0,0000	0,0203
HX5	0,0007	0,0000	-	0,0000
HX10	0,0000	0,0203	0,0000	-

4. Conclusions

Based on the experimental measurements, the following conclusions can be made:

- When measuring the roughness, the value of the parameters Ra and Rz does not change significantly after surface treatment by phosphating, the differences were manifested in the parameters RSm and RPc. The surfaces of HX material modified by phosphating copy the original surface, the density of protrusions has not changed significantly,
- Statistical evaluation showed that the phosphating time has an effect on the value of the Ra parameter.

Acknowledgement

Authors are grateful for the support of experimental works by projects APVV-20-0303 “Innovative approaches to the restoration of functional surfaces by laser weld overlaying” and VEGA 1/0229/23 „ Research into the applicability of thermal drilling technology for the creation of multi-material joints in the automotive”.

References

1. P. Pokorný, Koroze Ochr. Mater, **4**, 115-126 (2013)
2. K. Ogle et al., Corros. Sci., **46**, 975-995 (2004)
3. L. Jiang et al., Corros. Sci., **55**, 76-89 (2012)
4. P. Szelag, J. Chocholousek, MM spectrum, **4** (2008)
5. A. Guzanová et al., J. Adhes. Sci. Technol., **11**, 1153-1175 (2022)
6. A. Guzanová et al., Metals, **4**, 1 – 23 (2022)
7. E. S. Gadelmawla et al., J.Mater.Proc. Technol., **1**, 133 – 145 (2002)
8. J. Wang et al., Col. Pol. Sci., **8**, 1107 – 1112 (2020)
9. C. Yang et al., Phys. Rev. Let., **11**, 1074 – 1077 (2008)
10. D. J. Whitehouse, Meas. Sci. Technol., **8,** 955 – 972 (1997)
11. D. Draganovská et al., Mater. Sci. Forum, **818,** 15 – 18 (2015)
12. D. Draganovská et al., Metals, **8**, 938 (2018)

Analysis of the possibilities of joining thin-walled metallic and composite materials

Nikita Veligotskyi*, Anna Guzanová, Erik Janoško
Technical University of Košice, Faculty of Mechanical Engineering, Department of Technology, Materials and Computer Supported Production, Slovakia
nikita.veligotskyi@tuke.sk

Abstract: *This paper presents an overview of technologies for joining fibre-reinforced polymer composites to thin-walled metal sheets. It covers the areas of welding, bonding with different surface texturing as well as mechanical joining. It analyses the problems arising from the different mechanical, physical properties of metals and composite materials and presents the possibilities of solving them by the application of individual and combined joining technologies.*
Keywords*: METAL TO CPOMPOSITE JOINING, DISSIMILAR MATERIALS, MECHANICAL JOINING, WELDING, FLOWDRILL, ADHESIVE BONDING, HYBRID JOINING*

1. Introduction

Today, the automotive industry is under pressure from new emission and safety standards with stricter requirements. Awareness of climate change is increasing globally, putting pressure on all sectors of the industry to minimise their emissions. One way to meet these demands in the case of the automotive industry is to reduce vehicle weight. Therefore, in recent years, multi-material vehicle structures have started to be used, where, in addition to steels and light non-ferrous metal alloys, polymer composites reinforced with different types of fibres are also featured [1, 2].

A major problem in the production of multi-material vehicle structures is the joining of heterogeneous materials. Thus, in modern car bodies, there is also the problem of joining metallic materials - steels and aluminium alloys - with fibre reinforced polymer composites (FRPC). The difference in chemical composition, material, physical and technological properties requires modification of existing technologies such as adhesive bonding, mechanical joining and fusion welding, up to the development of new bonding technologies. In addition to these methods, hybrid joining methods have also been developed, where several technologies are combined into a single process. Most commonly, bonding is used in combination with mechanical joining (bolting, riv-joining, etc.) or welding (FSW, RSW), or several welding technologies are combined into a single joint [3].

The paper presents an overview of joining technologies for thin walled materials based on polymer composites and metals.

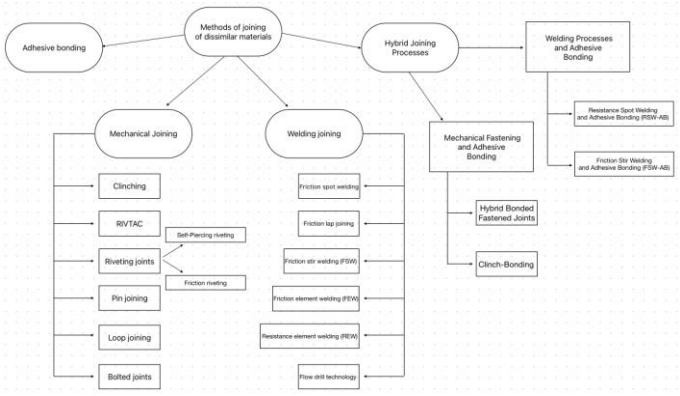

Fig. 1 *Classification of basic methods of joining dissimilar materials*

2. Adhesive joining

Adhesive bonding is the process of joining two components using an adhesive, it is suitable for joining elements made of dissimilar materials (metals, polymers or ceramics) in the aerospace, automotive and construction industries. As bonding is an irreversible process, it seals the joints and also prevents galvanic or crevice corrosion between two dissimilar materials. With adhesive bonding, lightweight structures can be produced compared to other assembly technologies [4].

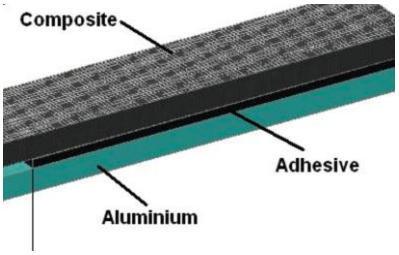

Fig. 2 *Adhesive joint of polymer composite and aluminium alloy [5]*

When bonding metals and composites, there are two ways to create an adhesive bond, either by using an adhesive and curing it with pressure, time or solvent evaporation, or by using the adhesion of the thermoplastic matrix of the composite itself, without the use of a separate adhesive. The second method uses heat to melt the thermoplastic matrix of the composite and, after compression with the metal plate and solidification, an adhesive bond is formed. This means that thermoset matrix composites cannot be bonded in this way [3].

Advantages:

- Improves stress distribution which improves fatigue properties
- No galvanic corrosion
- Temperature sensitive materials can be joined (No change in material properties due to heat)
- No thickness restrictions
- Smooth surface finish
- No added weight from bolts and rivets

Disadvantages:

- Stress concentrations at the edges of the joint
- Sensitive to peel stress
- Sensitive to mismatches in CTE (coefficient of thermal expansion), will create residual stresses
- Surface preparation often needed
- Cannot easily be dissembled for service or inspection

3. Mechanical joining

3.1 Clinching

Clinching is a mechanical joining method that is widely used in the automotive industry to produce automobile body panels and electrical appliance skeletons. It is a cold forming process.

In metal-to-composite joining, either a composite plate or a metal sheet is deformed to form a geometric connection, Fig. 3. It is preferable to place the material with the higher ductility (metal) in the upper position, on top of the composite materials with the prepared hole, because during forming, an intense plastic deformation of the upper plate occurs, filling the hole in the composite with metal, thus forming a mechanical joint. The composite plate may have a pre-drilled hole necessary to ensure interlocking, or the hole may be punched out during nailing. Pre-drilling the hole is an extra operation, but the prepared hole reduces the risk of damage to the material during joining, which often happens with joints without a prepared hole [4,6].

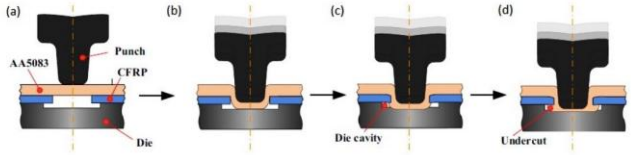

Fig. 3 *The Clinching process: a) placement of the materials to be joined, b) deformation of the top plate, c) filling the space in the die with metal to form the joint, d) Clinching joint [6]*

Advantages:

- No added weight from bolts and rivets
- Does not require pre-drilled holes nor surface preparation
- Temperature sensitive materials can be joined

Disadvantages:

- Two-sided access required
- Risk of damage from deformation and galvanic corrosion
- Brittle materials cannot be joined
- Stress concentrations

3.2 RIVTAC® (High-speed impact nailing)

The RIVTAC® method is based on the grooved rivet penetrating the materials at high speed (20 to 40 m/s), Fig. 4. During bonding, a short heat increase occurs thus achieving better formability of the metal, the material first expands and then contracts and fits into the grooves of the rivet body as it cools. The rivet head then presses and locks the composite to the metal, creating another form lock [3].

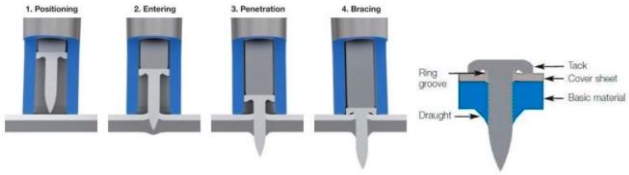

Fig. 4 *The RIVTAC process [3]*

Advantages:

- High productivity/short process times
- Does not require pre-drilled holes
- No surface preparation needed
- Temperature sensitive materials can be joined
- One sided access (depends on structural integrity)
- No emissions

Disadvantages

- Risk of galvanic corrosion
- Stress concentration
- Rivet adds weight
- Restrictions regarding maximum penetration (material strength and thickness)
- Risk of damage from hole generation
- Not user friendly (loud process)
- No smooth surface finish

3.3 Riveting joints

Conventional riveting of composite materials can lead to damage to the composite matrix around the rivet, so this method cannot be used for safe joining of metal and composite parts. However, self-piercing riveting (SPR) and friction riveting methods do not require drilling holes in composite materials and impose less mechanical assembly loads on composites.

3.3.1 Self-Piercing riveting

Self-piercing riveting process of involves joining two overlapped sheets of the same or different materials using a rivet that is pressed into materials with a punch. The rivet pierces the top material and partially penetrates the bottom material. The punch on the underside of the sheets to be joined causes the rivet to expand under the action of the force, forming a mechanical connection, Fig. 5. Both, the rivet and the bottom sheet are subjected to plastic deformation [4,6,7].

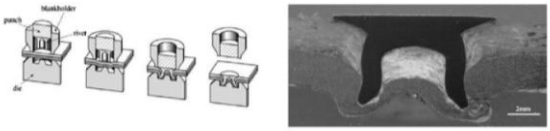

Fig. 5 *Self-piercing riveting process and cross-section of SPR joint [6]*

Advantages:

- The process does not require pre-drilled holes, it is done in one operation, saving production time and cost. However, a hole can also be drilled or cut in the top plate before riveting.
- No surface pre-treatment is required.
- The process is operator friendly and produces low noise, no fumes and is easy to automate.

One of the disadvantages of this method is that it requires double-sided access to the plates to be joined.

3.3.2 Friction Riveting

Friction riveting was first developed to form joints of metals and thermoplastic materials, but more recently several papers have looked at using this method to join fiber-reinforced polymer composites. Friction riveting involves anchoring a metal rivet inside a polymer or polymer composite base plate. The rivet passes into the composite material by frictional heat which softens the thermoplastic matrix of the composite and subsequently a high axial force causes the head to expand and wedge the rivet into the composite [6].

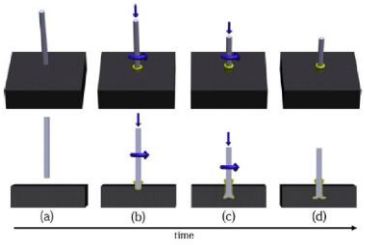

Fig. 6 *Friction riveting process steps: a) positioning of the joining, b) friction heat generates molten layer of polymer and the rivet penetrates it, c) increasing the axial force in order to widen an anchor rivet tip, d) consolidation of the joint [8]*

3.4 Pin joining

Another method of making joints between fibre-reinforced plastic composites and metal parts involves making a metal part with a set of pins, or sharp protrusions of different shapes, that protrude vertically from it. Layers of the fibre-reinforced composite in the form of weaves are placed on top of the metal plate with the pins so that, when the composite is heated, the pins pass through the weave of the reinforcing fibres without damaging them. This creates a mechanical joint without damaging the fibres in the composite. The composite then solidifies [6].

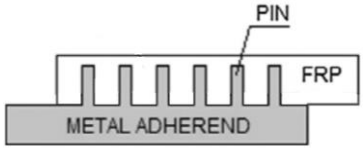

Fig. 7 *Schematic of an advanced hybrid metal/composite pin joint. The pin joints combine adhesive bonding with mechanical interlocking [6]*

3.5 Loop joining

All loop joining concepts aim to separate the carbon fibre from the aluminium alloy to prevent galvanic corrosion, which inevitably occurs when the two materials come into contact and can lead to increased corrosive degradation of the aluminium with subsequent catastrophic failure of the aluminium and carbon fibre reinforced composite joints. Corrosion is caused by the electrochemical potential difference between the carbon fibres and the aluminium alloys and can be prevented by bonding the carbon fibres to the aluminium alloy substrate using titanium transition elements, which reduce the electrochemical potential difference by approximately two-thirds. This potential difference can be further reduced by surface treatment of titanium or even by using non-conductive materials such as glass and boron fibres. The titanium wire is attached to the aluminium alloy in the form of a series of loops by welding or casting. Bundles of carbon fibre are then threaded through these loops. In the foil concept, the loops are replaced by titanium foils bonded to an aluminium substrate. The carbon fibres are sandwiched between the foils and the joint is held by frictional force. In the fibre concept, the titanium is replaced by glass or boron fibres. The joint is then formed by embedding the fibres in a polymer resin [4,6].

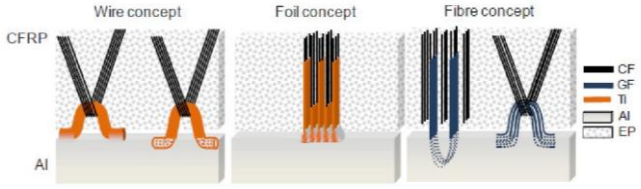

Fig. 8 *Concepts for bonding CFRP to aluminium using loops, foils and fibres [6]*

3.6 Bolted joints

Bolted joints are one of the most common joining methods in many applications. In principle, they are similar to SPR. They have a uniaxial common hole through the components to be joined, usually formed by drilling. Bolts are then inserted into the holes from one side of the joint and fastened with nuts on the other side with the correct torque. The diameter of the bolts is smaller than the diameter of the drilled holes, although the diameter of the bolt and nut heads is relatively large compared to the diameter of the holes. The bolt heads and nuts act as flanges that hold the components of the joint firmly. The bolts do not deform plastically and the diameter and material of the bolt determine the strength of the bolted joints when the other components of the joint are stronger [4].

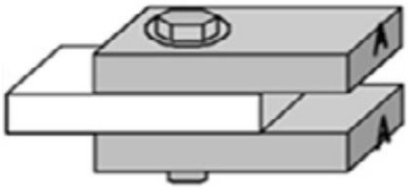

Fig. 9 *Example of bolted joint [4]*

4. Fusion joining

Conventional methods of joining FRPC to metals, such as bolting, riveting, bonding, etc., fall into the category of non-thermal processes, while welding falls into the category of thermal processes. Therefore, this method is applicable only for thermoplastic matrix composites. Local melting of thermoplastic matrices can be carried out by microwave, induction or friction heat. The principle of all these thermal processes is the partial melting of the thermoplastic matrix of the composite and the subsequent bonding to the metal surfaces.

4.1 Laser assisted welding

When welding composites and metals, a laser can be used as a heat source. The laser heats the metal in the overlapped composite-metal assembly, with the heating of the metal by the laser beam being carried out from the side of the metal or composite (if it is treansparent to the laser beam). The hot metal melts the composite thermoplastic matrix at the interface with the metal. In doing so, bubbles can form in the poymer, which pressurize the polymer against the metal and thus improve their bonding by embedding the polymer into micro-porosities on the metal surface [4].

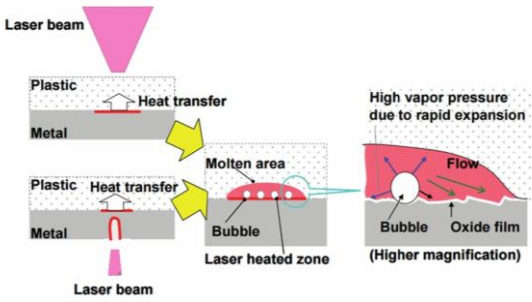

Fig. 10 *Laser assisted direct metal - polymer joining mechanism [4]*

4.2 Friction spot welding

The friction heat in friction spot welding is generated by a tool without additional materials, which consists of a clamping ring, a shoulder and a probe, which are assembled coaxially and move independently of each other. The clamping ring holds the parts to be joined. The probe and shoulder can rotate independently and generate the required heat due to friction between these parts and the workpieces. The rotating shoulder sinks into the metal plate to a predefined depth, while the probe retracts upwards. The friction

between the shoulder and the metal causes the increasing temperature to locally soften and plasticize the alloy. The plasticized alloys flow into the reservoir left after the probe was inserted. Frictional heat is also conducted into the metal alloy composite interfaces, forming a thin layer of molten polymer throughout the overlap area. The probe then extrudes the softened metal and fills the keyhole in the metal sheet. The molten layer is then consolidated under pressure, inducing adhesion and interlocking between the metals and composites [4].

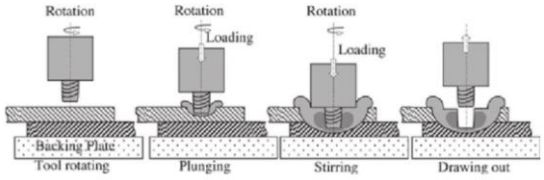

Fig. 11 *Friction spot welding method [9]*

4.3 Friction lap joining

The FLJ tool does not have a stirring pin and therefore the main function of the rotary tool is not to cause the flow of materials around the stirring pin, but to heat and squeeze the metal workpiece. Localised heating is achieved by friction between the tool and the metal workpiece. Heat is transferred by conduction from the heated metal component to the plastic component and subsequently melts the plastic materials in a narrow area at the interface. The bond between the metal and the plastic can be completed after the plastic has solidified under the pressure of the tool [4].

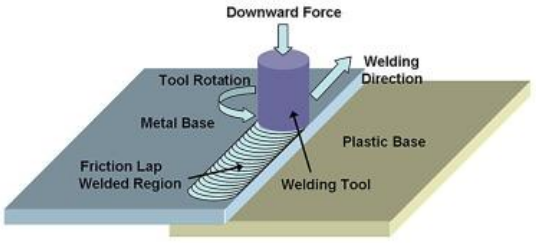

Fig. 12 *Friction lap joining process [10]*

4.4 Friction stir welding (FSW)

A rotating cylindrical tool with a pin approaches the contact point between the composite and the metal. Frictional heat is generated between the materials and the tool, which leads to softening of the materials. The tool moves forward, mixing the softened materials and pushing them towards the back of the tool where they consolidate as the temperature drops. The composite must be based on a thermoplastic resin. The disadvantage is the high risk of fibre pull-out if the reinforcement in the composite consists of woven fibre mats. When short fibres are used, the risk of damage is less [3].

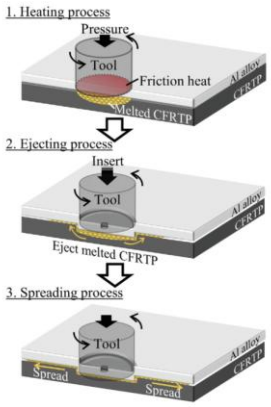

Fig. 13 *Schematic diagram of friction stir spot welding process [11]*

4.5 Friction element welding (FEW)

The theory behind FEW is that a custom rivet is welded to the bottom plate, which together with the rivet head secures the top plate in place. First, the two plates are pressed together, the friction element rotates at high speed. The rotating element contacts the surface of the top plate and the frictional heat generated causes the material to plasticize. This in turn allows the friction element to penetrate the sheet during further pressure.

When the rivet comes into contact with the bottom sheet, the frictional heat increases even further, plasticizing the rivet and activating the surfaces. The additional clamping force has a pressure welding effect that further shortens the rivet and creates a solid metallic bond between the rivet and the bottom plate. The extruded material from the cover plate collects in the groove under the friction element head, resulting in a form-fit connection, while the falling temperature of the rivet leads to axial shrinkage and a force connection between the top plate and the rivet [3].

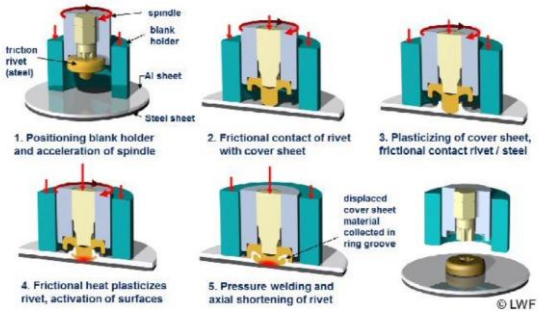

Fig. 14 *The FEW process [3]*

4.6 Resistance element welding (REW)

REW is a form of resistance spot welding developed for joining combinations of heterogeneous materials using a so-called weld rivet. This technique requires a hole to be pre-drilled into the cover sheet (which may be the composite) or a rivet to be punched in the hole before welding. Once the perforation is complete and the welding rivet is in place, electrodes are placed on top of the rivet and underneath the bottom plate, similar to the conventional resistance spot welding process. In the next stage, when pressure and electric current are applied, heat is generated due to the electrical resistance and a weld tip is formed between the bottom plate and the rivet. Subsequently, the electrodes compress the rivet and form a force connection between the cover plate and the rivet head [3].

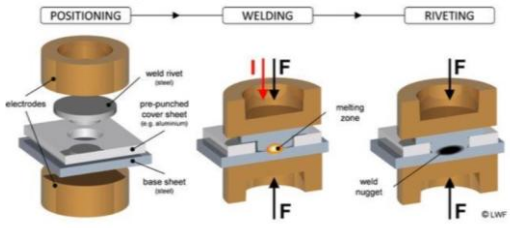

Fig. 15 *The REW process [3]*

4.7 Flow drill technology

Flow drill technology is used for joining thin-walled materials. The material is softened by frictional heat from the tool and plastically deformed by the movement of the tool. Part of the material is moved below the level of the material to be drilled as a bushing into which threads are formed for mechanical connection

with other material. The bushing is very advantageous when joining thin workpieces because it locally increases the thickness of the material. In [13], Schmerler discussed the idea of joining two or three overlapped materials using screwless thermal drilling technology, although this technology is not primarily intended for this purpose. The idea is based on the premise that if two or three thin-walled materials are overlapped and a hole is made using a flow drilling tool, coaxial bushings could be formed on the materials being joined, which would be mechanically wedged to form a shaped joint, Fig. 16. One of the materials to be joined could be a polymer composite [12,13].

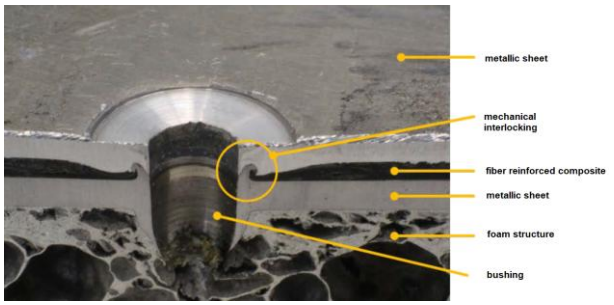

Fig. 16 *Metal-composite joints made by Flowdrill method [13]*

5. Hybrid joining

Hybrid joining processes combine basic processes to achieve some unique feature or capability of joints, often with synergistic results. These hybrid processes are generally of more recent origin and have often been developed to overcome the shortcomings of the basic processes for particularly challenging applications (e.g. advanced aerospace designs). As a result of advances in materials engineering, development work has focused on the use of thin sheets and small structural elements. There is also a growing trend to combine traditional metals with polymer composites. For example, composites are structurally more efficient in terms of strength-to-weight ratio than metals and do not suffer from galvanic corrosion, while metals have better damage resistance and failure predictability than composites and are not affected by solvents and temperatures that tend to degrade polymers.

Therefore, multi-material joints between metals and composite materials are increasingly being developed in order to optimise the benefits provided by both types of materials. Special joining techniques are required to join this type of structural elements and polymer-metal multi-material structures. Among them, hybrid processes of the main processes of mechanical fastening, bonding and welding are the most widely used.

5.1 Advanced Fastening and Bonding Processes

The main objective behind the developments in advanced fastening and adhesive bonding processes is to successfully join new advanced materials with excellent joint properties. Hybrid bonded-fastened joints and clinch bonding are produced by simultaneous actions of adhesive bonding and a mechanical fastening technique.

5.1.1. Hybrid Bonded-Fastened Joints

A hybrid bonded-fastened joining technique is developed in order to avoid individual limitations of fastening and adhesive joining for assembling of dissimilar materials, composites and metallic materials. There are two types of hybrid bonded-fastened joints, such as the joints that use bolts/rivets known as hybrid bonded-bolted (HBB) joints and the joints that use pins with adhesive, known as hybrid bonded-pinned joints.

A fastening system helps to sustain axial loads while the adhesive takes some of the load off the fasteners and redistributes the remaining load more uniformly. The fasteners, in turn, also take some load off the adhesive, particularly out of plane. Most important parameters such as type of joint configuration, type of fastener, type of adhesive, its thickness and length of bond line, loading condition, type of adherend being used and its thickness, overlap length and fastener-hole clearance of hybrid bonded-fastened joints are required to produce metallurgically satisfactory joints [14,15].

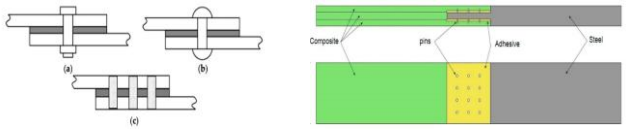

Fig. 17 *Schematic representations of a) bolted-bonded joint, b) rivet-bonded joint, c) a pin-bonded joint and example of hybrid adhesive joints with metallic pins [14,15]*

5.1.2 Clinch Bonding

It is a classic forming process, however, a suitable adhesive is applied between the workpiece sheets. It is a modern and innovative technology that allows different types of materials to be joined together to create durable and reliable lightweight structures. Compared to other mechanical joining techniques, the clinching technique has the advantage of using only adhesive as a consumable. The adhesive is applied to one of the parts to be joined and then the two parts are joined together. The parts to be joined are immediately subjected to the clinching and this process may cause some of the adhesive to be pushed out of the joint. After clinching, the adhesive is cured [14,16].

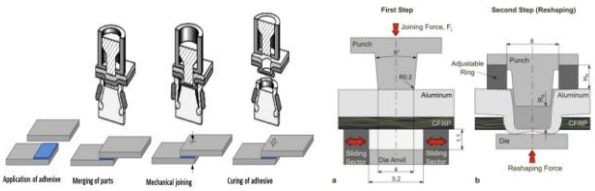

Fig. 18 *The principle of the clinch-bonding technology [14,16]*

5.2. Welding and Adhesive bonding

5.2.1 Resistance Spot Welding and Adhesive Bonding (RSW-AB)

When welding, the current is supplied to the cylindrical electrode, and closed circuit is formed between the cylinder electrode, column electrode and the metal sheet. This generates Joule heat in the metal sheet, which in turn heats the matrix of the composite at the interface. The matrix of the composite forms a molten zone in the shape of a half lens. The molten resin then wets the metal surface and chemical bonds are formed between the two sheets [11,14].

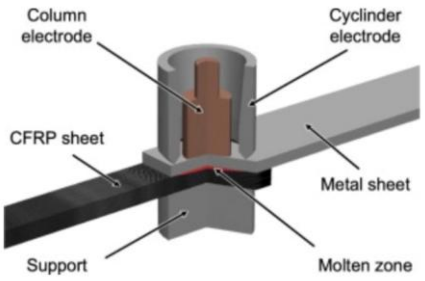

Fig. 19 *Resistance spot welding and adhesive bonding (RSW-AB) [11]*

5.2.2 Friction Stir Welding and Adhesive Bonding

As mentioned earlier, friction stir welding (FSW) is one of the most promising processes in the field of continuous joining. One of the problems posed by friction stir welding is, in the case of overlapping joints, the hook defect, which reduces the static and

fatigue strength because it acts as a crack initiator. In addition, there is a risk of galvanic corrosion. The solution to these problems could be hybrid joining - FSW and adhesive joining. FSW can produce consistent joints with high static strength, while adhesive dampens vibration, improves fatigue strength and isolates the weld from the environment [14].

The FSW-AB hybrid bonding technology also faces some challenges, for example:

- The risk of adhesive degradation in FSW, where the temperature ranges from 300 to 470°C;
- Adhesive requirements - high temperature resistance and chemical resistance in corrosive environments
- Avoid solvents or non-organic additives to reduce the environmental impact of the process.

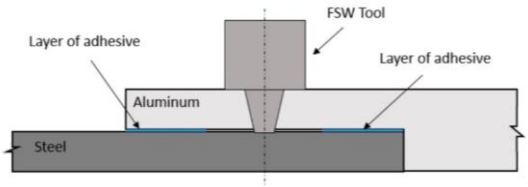

Fig. 20 *Resistance spot welding and adhesive bonding (RSW-AB) [11]*

Acknowledgements: This research was funded by the Scientific Grant Agency of the Ministry of Education, Science, Research and Sports of the Slovak Republic under project VEGA 1/0229/23: Research on the applicability of thermal drilling technology for the creation of multi-material joints in the automotive industry and Slovak Research and Development Agency under project APVV-20-0303: Innovative approaches to the restoration of functional surfaces by laser weld overlaying.

7. References

1. S.H. Hesse, D.H.-J.A. Lukaszewicz, F. Duddeck, Composite Structures, 129, 236-249 (2015). https://doi.org/10.1016/j.compstruct.2015.02.086
2. D. Chen,G. Sun, M. Meng, X. Jin, Q. Li, Thin-Walled Structures, 142, 516-531 (2019) https://doi.org/10.1016/j.tws.2019.03.056
3. E. Legdin, Joining of metal and fiber composites, 1-83 (2017)
4. A. Pramanik, A.K. Basak, Y. Dong, P.K. Sarker, M.S. Uddin, G. Littlefair, A.R. Dixit, S. Chattopadhyaya, Composites Part A: Applied Science and Manufacturing, 101, 1-29 (2017) http://dx.doi.org/10.1016/j.compositesa.2017.06.007
5. J.M. Arenas, C. Alía, R. Ocaña, J.J. Narbón, Procedia Engineering, 63, 287-295 (2013) doi:10.1016/j.proeng.2013.08.218
6. A. Galińska, C. Galiński, Polymers 2020, 12, (2020) doi:10.3390/polym12081681
7. J. Wang, G. Zhang, X. Zheng, J. Li, X. Li, W. Zhu, J. Yanagimoto, Composite Structures, 259, 113-219 (2021) https://doi.org/10.1016/j.compstruct.2020.113219
8. J. Altemeyer, J.F. dos Santos, S.T. Amancio-Filho, Materials & Design, 60, 164-176 (2014) https://doi.org/10.1016/j.matdes.2014.03.042
9. C. Yeni, S. Sami, U. Ozdemir, Materials Testing, 54, 233-239 (2012) DOI: 10.3139/120.110322
10. F.C. Liu, J. Liao, K. Nakata, Materials & Design, 54, 236-244 (2014) https://doi.org/10.1016/j.matdes.2013.08.056
11. S. Han, X. Guang, Z. Li, Y. Li, Polymer Composites, 43, (2022) DOI: 10.1002/pc.27088
12. N. Veligotskyi, E. Janoško, A. Guzanová, D. Draganovská, Acta Mechanica Slovaca, 27, 48-57 (2023) DOI: 10.21496/ams.2023.011
13. Schmerler, R.; Rothe, F.; Grunert,M. Hybrid Joining Using the Flow Drill Technology. Available online: https://www.researchgate.net/publication/341616091_Hybridfugen_durch_Fliesslochformen_Hybrid_joining_using_the_flow_drill_technology (accessed on 17 April 2023).
14. S. Maggiore, M.D. Banea, p. Stangnaro, G. Luciano, Polymers 2021, 13, 39-61 (2021) https://doi.org/10.3390/polym13223961
15. J. M. Arenas et al., Procedia Manufacturing, 41, 500–507, (2019)
16. F. Lambiase, D. Ko, Composite Structures, 164, 180-188 (2017) DOI: 10.1016/j.compstruct.2016.12.072

Analysis of interference fit joints formed by thermal drilling technology with CNC process control

Erik Janoško*, Anna Guzanová, Nikita Veligotskyi
Technical University of Košice, Faculty of Mechanical Engineering, Department of Technology, Materials and Computer Supported Production, Slovakia
erik.janosko@tuke.sk

Abstract: *The paper focuses on the evaluation of the quality of joints of thin-walled dissimilar overlapped materials, formed by thermal drilling without a screw. The shaped interference fit joint is formed by simultaneously forming both overlapped materials, preheated by the friction of a flowdrill tool, and forming a pair of embedded concentric bushings. The joints were made on a CNC milling centre, at constant speed, with tool feed being the only variable. Three tool movement strategies - three movement schemes - were tested. By evaluating the quality of the joints using metallographic sections, the optimum tool movement strategy was selected.*
Keywords*: MECHANICAL JOINING, THERMAL DRILLING, DISSIMILAR MATERIALS, LOAD-BEARING CAPACITY OF JOINTS*

1. Introduction

In many industrial applications, components made of thin plate or thin-walled profiles are widely used. The problem with such structures is the joining, especially when different materials have to be joined (uncoated and galvanized steel, steel with aluminum or composite, etc.) [1].

The Flowdrill process is characterized by the formation of an elongated bushing, which is formed by rotation and pressure of the tool without chip removal [2]. The bushing has a specific shape according to the tool used. This process is also called friction drilling, flow drilling, thermomechanical drilling, etc. The purpose of this method of hole formation is to form a bushing in thin sheets without any addition of material where a sufficient number of threads can be placed [3-6]. Subsequently, a thread can be formed in the formed bushing, thus forming a detachable joint with a connecting element. However, it is also possible to form a mechanical form fit joint of two sheets without a bolt, just by two concentric nested bushings wedged together [7]. In this process, it is necessary to ensure that the resulting bushings of the two materials to be interpenetrated adhere tightly to each other, follow each other's shape, and do not push away from each other due to the spring back effect, which could lead to "opening" of the joint. As this is an atypical application of thermal drilling for joining two overlapped dissimilar materials, there is a lack of information on suitable process parameters in the relevant literature. These vary according to the type of material to be drilled. For example, tool speeds for drilling corrosion-resistant steels are recommended to be reduced compared to those for low carbon steels by 15%, while for Al and non-ferrous alloys it is recommended to increase the speed by 50% compared to drilling carbon steels [8]. The question is what are the appropriate parameters for joining the steel-Al alloy pair, which material should be adapted to. In order to achieve repeatability of process parameters during joint formation, thermal drilling should be done on CNC machines where drilling parameters can be precisely defined and controlled during the toolpath. The heat generated affects the drilling process and depends mainly on the speed and tool feed. Regarding CNC centers, it is more efficient to vary the tool feed than the tool speed, so we decided to take this route in the experiment [8].

The aim of the paper work is to experimentally verify the possibility of using the side effect of the thermal drilling technology (flowdrill) for joining two overlapped thin plates without the use of a bolt, just by forming a pair of nested concentric bushings, while three modes of tool feed will be tested.

2. Materials and Methods

The choice of materials for the experimental program was based on materials currently used in the construction of automotive bodies so that both Fe alloys (galvanized and ungalvanized) and non-ferrous alloys were represented.

Materials selected for experimental works:

- DC04 - extra deep-drawn, uncoated, low-carbon, cold-rolled steel for bodywork. Referenced like DC.
- TL 1550-220+Z - hot-dip galvanised fine grained HSLA steel with excellent cold formability, grade VW (equivalent to CR210LA or HR210LA). Referenced like TL.
- EN AW-6082 T6 (AlSi1MgMn) - precipitation-hardened high strength Al alloy, weldable by MIG and TIG welding technologies. Referenced like Al.

The thickness of steel sheets was 0.8mm, the thickness of Al alloy was 1mm. The chemical composition of the materials used is given in Table 1.

Table 1: *Chemical composition of materials in wt.%*

Mat.	**C**	**Mn**	**Si**	**P**	**S**	**Al**	**Nb**	**Ti**	**Fe**
DC	0.040	0.25		0.009	0.008				bal.
TL	0.1	1.0	0.5	0.08	0.03	0.015	0.1	0.15	bal.
Mat.	**Si**	**Fe**	**Cu**	**Mn**	**Mg**	**Cr**	**Zn**	**Ti**	**Al**
Al	1.0	0.4	0.06	0.44	0.7	0.02	0.08	0.03	bal.

Table 2: *Mechanical properties of materials (in transversal direction)*

Mat.	**Re [MPa]**	**Rm [MPa]**	**A80 [%]**	**Zn layer [g/m^2]**	**r**	**N**
DC	197	327	39	-	1.900	0.220
TL	292	373	34	104	1.350	0.190
	Re [MPa]	**Rm [MPa]**	**A50 [%]**			
Al	295	344	14			

r - coefficient of normal anisotropy, n - strain-hardening exponent

The shape and dimensions of the test specimens as well as the geometry of the joints calculated for tool Flowdrill long ø 5.3 mm are shown in Fig. 1. The hole is always made in the centre of the overlapped area.

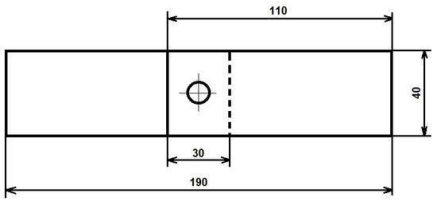

Figure 1: *Shape and dimensions of test specimens and joints designed for FD long ø5.3 mm tool*

The joints were created on a CNC milling centre DMG mori DMU 60evo. According to [8], it is recommended to set a small tool feed at the contact of the tool tip with the material, which should then increase linearly or stepwise, and then the tool feed should slow down again at the lowest reversal point of the tool movement. Based on these recommendations, three tool feed modes were selected and tested on the tool working path, Fig. 2.

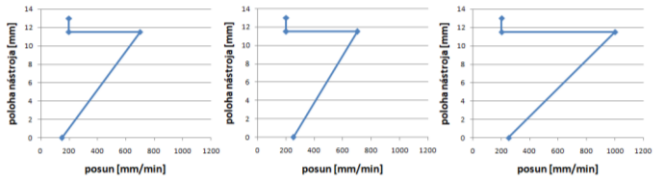

a) 150-700-200 mm/min, b) 250-700-200 mm/min, c) 250-1000-200 mm/min
Figure 2: *Selected tool feed modes*

The initial tool feed was 150 or 250 mm/min, gradually increasing to 700 or 1000 mm/min on the 11.5 mm path, finally on the 1.5 mm path the tool feed dropped to 200 mm/min and the tool stopped 0.6 mm below the flange part of the tool to prevent deformation or damage to the collar.

The geometry of the joints as a function of the tool feed mode was then examined by optical microscopy on metallographic sections along the axis of the joint.

3. Results

Table 3 shows the metallographic sections of the joints formed at the three tested tool feed modes on the CNC machining centre.

Table 3: *Metallographic cross-sections of jonts made at three tool feed modes, LM*

Mode:	Tool speed [min^{-1}], initial tool feed – maximal tool feed, tool feed in lowest reversal point [$mm.min^{-1}$]		
Joints	3800, 150-700, 200	3800, 250-700, 200	3800, 250-1000, 200
Al-Al			
DC-DC			
TL-TL	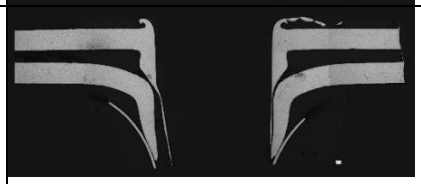	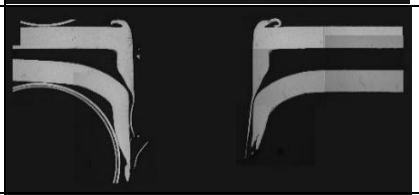	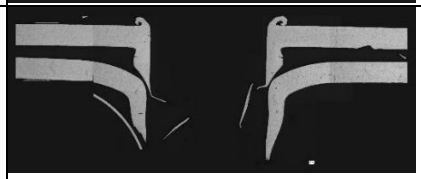
DC-TL			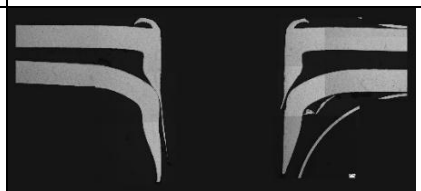
TL-DC	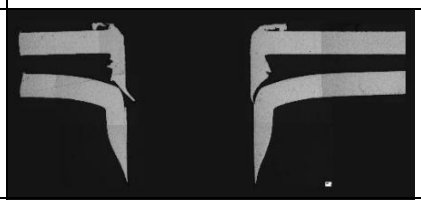		
DC-Al	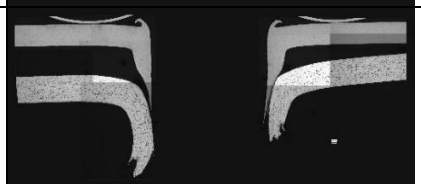	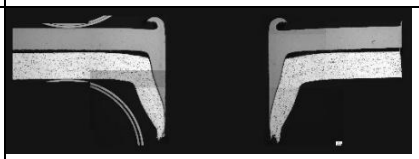	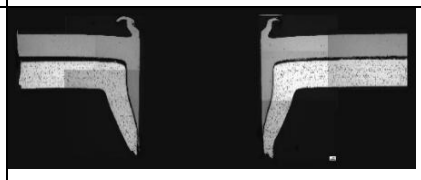
TL-Al		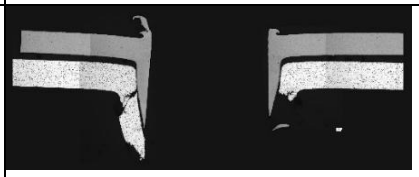	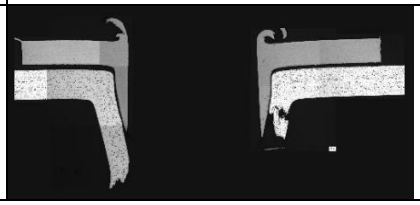

The Al-Al joints failed to establish, increasing the initial and maximum tool feed did not lead to an improvement in connection forming. The DC-DC and TL-TL joints are accompanied by a large spring back effect and too large a bending radius of the bottom plate, which makes it impossible to form nested concentric bushings of sufficient thickness. Instead, there is only an intense thinning of the heated material of inner bushing between the tool and the outer bushing, which acts as a punch and die in the process of forming the inner bushing. For the material combinations DC-TL and TL-DC the situation is similar, however, when DC is in the upper position, due to its high ductility (as an indicator of formability) it thins more intensively and therefore the inner bushing formed from it is too

thin. However, if TL steel is in the upper position, it thins less intensely. The best joints were achieved in the steel-Al combination, with minimal spring back effect and tight-fitting inner bushings. As for tool feed modes, it is the DC-Al and TL-Al joints where their effect is best seen. Too little initial tool feed caused the Al sheet to bend and the joint to open. Increasing the initial tool feed from 150 to 250 mm.min^{-1} eliminated this problem, but increasing the maximum tool feed from 700 to 1000 mm.min^{-1} did not produce any significant change in the shape of the bushings.

Fig. 3 summarizes the achieved average inner bushing height, inner bushing thickness at the expected failure location, and microhardness at the outermost part of the inner bushing for each material combination.

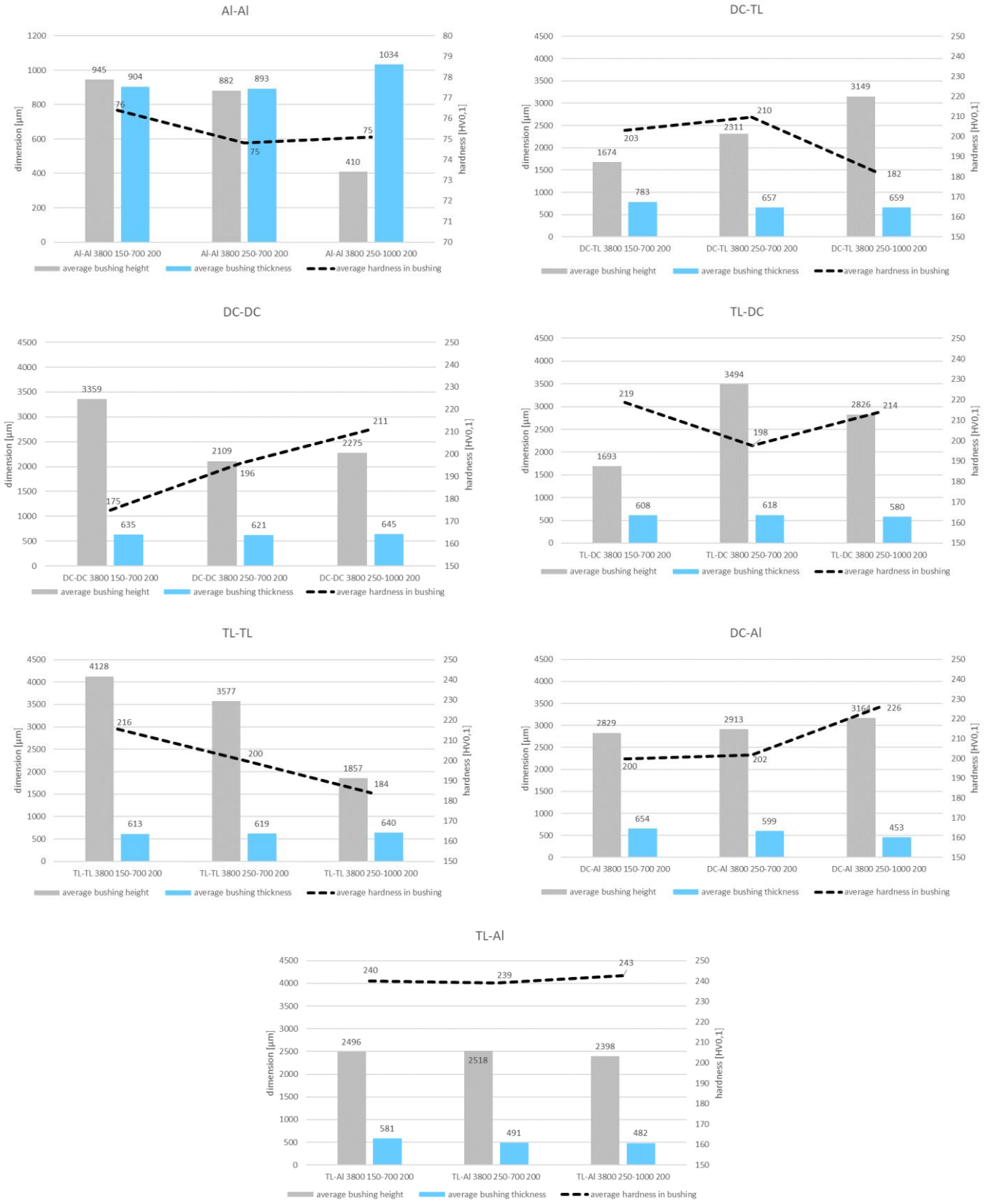

Figure 3: *Average bushing height and thickness, microhardness in the bushing for individual joints*

Fig. 3 shows that deformation hardening occurred in DC and TL steels, which was manifested by an increase in microhardness in the bushing, which represents the most overstrained region of the material in the joint. The DC steel sheet had an initial hardness of

106 HV0.1, after forming to the shape of the bushing, the hardness in the outermost part of the bushing varied between 175-226 HV0.1, depending on the tool feed used. The strain hardening of the TL steel showed an increase in hardness from 131 HV0.1 in the initial condition to values between 184 and 243 HV0.1 in the bushing.

In Al sheet material softening occured, the hardness in the bushing was around 75 HV0.1, while the initial hardness was 119 HV0.1. The Al sheet was supplied in the T6 condition, i.e. it is a solution treated and artificially aged alloy. Its structure consists of a number of Mg_2Si precipitates dispersed in an α-Al matrix. This type of alloys has limited application in terms of operating temperatures to ambient temperature. Any heating may disturb the precipitation hardening effect. At temperatures of 100-500°C, the precipitates can overage, i.e. grow, reducing their strengthening effect; bigger precipitates prevent the movement of dislocations less effectively. Heating above 500°C already leads to dissolution of the precipitates, and if followed by slow cooling, the fragile intermetallic θ phase at grain boundaries may be formed, thus weakening their cohesion. In thermal drilling, Özek et al. [9] found a maximum temperature of Al alloys 1 mm from the hole of about 245°C at comparable tool speeds but significantly smaller tool feed. It is possible to estimate the Al temperature at feed rates up to 1000 $mm.min^{-1}$ to be >300°C, which could have induced a softening of the Al alloy in the vicinity of the hole.

In thermal drilling, not only the mechanical properties determined at ambient temperature play an important role, but especially their change when heated. It is therefore necessary to know the creep curves of materials, the change in the modulus of elasticity of materials with temperature and the physical properties of materials, especially thermal conductivity. Fig. 4 shows the decrease of Young's modulus of elasticity of steel and aluminium when heated.

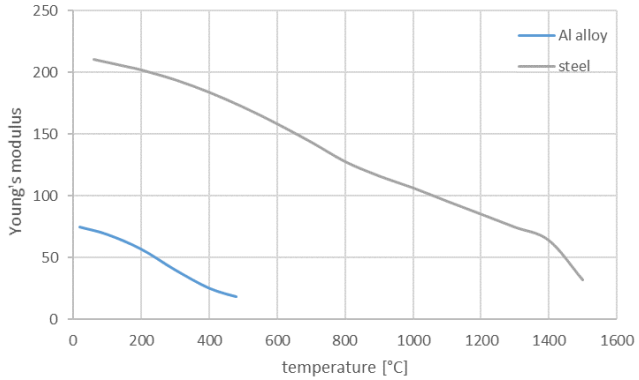

Figure 4: *Temperature-dependent change in modulus of elasticity of steel and Al alloys*

Fig. 4 shows that already at ambient temperature, it takes three times less stress to achieve some deformation of Al than to achieve the same deformation of the same cross-section made of steel. As the temperature increases, this difference increases even more, the Young's modulus of Al decreases more drastically with temperature than that of steel. This is the reason why Al sheet cannot be in the top position when joining with flowdrill technology - it is pushed sideways when heated instead of forming a bushing. Therefore, a material with a higher stiffness (Young's modulus) must be placed in the top position. In the lower position, the aluminium alloy can be placed, which will therefore only be heated indirectly, by conducting heat from the steel into the Al, and will be shaped by copying the resulting steel bushing. In this way, a joint with a suitable geometry, with tightly fitting concentric nested bushings, with certain load-bearing capacity, can be formed. Joints formed by this process can be combined with adhesive bonding.

3. Conclusions

The following main findings can be drawn:

- thermal drilling technology can be used to create a pair of nested concentric bushings capable of carrying a certain level of load
- the best joint geometry is achieved with a steel-aluminium alloy material combination, with the recommendation to place the steel in the upper position of the pair to be joined
- this technology is not suitable for joining steels of the same or unequal grades or for joining aluminium alloy pairs.
- For the most promising joints (DC-Al and TL-Al), no significant effect of the tool feed mode on the geometrical characteristics of the joints was observed, but the displacement modes 3800, 250-700, 200 and 3800, 250-1000, 200 resulted in the formation of tightly fitting concentric bushings with a minimum gap between the plates.
- From the point of view of time saving in joint formation, the following mode can be recommended for joining steels and Al alloys with the above properties and thickness: speed 3800 min^{-1}, tool feed 250-700 $mm.min^{-1}$, at the end of the movement the tool feed decreases to 200 $mm.min^{-1}$.

Acknowledgements: This research was funded by the Scientific Grant Agency of the Ministry of Education, Science, Research and Sports of the Slovak Republic under project VEGA 1/0229/23: Research on the applicability of thermal drilling technology for the creation of multi-material joints in the automotive industry and Slovak Research and Development Agency under project APVV-20-0303: Innovative approaches to the restoration of functional surfaces by laser weld overlaying.

References

1. Kaščák Ľ., Mucha J., Slota J., Spišák E. Application of modern joining methods in car production. 1. Vyd, Rzeszów: Oficyjna Wydawnicza Politechniki Rzeszowskiej, 2013. 143 p. ISBN 978-83-7199-903-8.
2. Kumar R., Rajesh Jesudoss Hynes N. Thermal drilling processing on sheet metals: A review, International Journal of Lightweight Materials and Manufacture, 2(3) 2019, 193-205, https://doi.org/10.1016/j.ijlmm.2019.08.003
3. Raju B.P., Swamy M.K. Finite element simulation of a friction drilling process using deform-3D, Int. J. Eng. Res. and App. 2(6), (2012), 716-721, https://www.ijera.com/papers/Vol2_issue6/DD26716721.pdf
4. Prabhu T., Arulmurugu A. Experimental and analysis of friction drilling on aluminium and copper, Int. J. Mech. Eng. Tech., 5 (2014), 130-139
5. El-Bahloul S.A., El-Shourbagy H.E., El-Midany T.T. Optimization of thermal friction drilling process based on Taguchi method and fuzzy logic technique, Int. J. Sci. Eng. Appl., 4 (2015), 55-59
6. Schmerler R., Rothe F. Hybridfügen durch Fließlochformen. Germany, 2020.
7. Guzanová A. et al. Investigation of Applicability Flowdrill Technology for Joining Thin-Walled Metal Sheets. Metals 12,4 (2022), 1-23, https://doi.org/10.3390/met12040540.
8. Flowdrill. User Guide. [online], 2003. Dostupné na internete: https://dts-aa.dk/pdf/User_Guide_eng.pdf
9. Ozek C., Demir Z. Investigate the Friction Drilling of Aluminium Alloys According to the Thermal Conductivity, TEM Journal, 2, 2013, 93-101, ISSN 2217-8333

Monitoring of changes in the roughness of the metal surface after the application of the conversion layer

Róbert Moro[1,*], Dagmar Draganovská[2]
Technical University of Košice, Slovak Republic[1,2,]
robert.moro@tuke.sk[1], dagmar.draganovska@tuke.sk[2]

Abstract: *The article is focused on the study of the integrity of the material that is used in the automotive industry in process of creating joints by combined technology. The article describes the study of the properties of chemically pretreated surfaces by phosphating technology. When creating new surfaces by phosphating, a new type of phosphate layer was used using modern conductive compounds of polyaniline salts. The pretreated surfaces were investigated in terms of structure, 2D and 3D microgeometry, contact angle in relation to the determination of surface wettability and surface energy. The experiment was realized in order to identify the connections between individual factors of the process and roughness characteristics.*
Keywords*: surface integrity, microgeometry, roughness, contact angle*

1. Introduction

In automotive industry, when constructing cars, they also emphasizes the use of increasingly progressive steel materials that have improved properties, in order to achieve better efficiency in the operation of cars. This fact contributes to the development and acceleration of adhesive bonding technologies, but this pace cannot be at the expense of the quality of the given joints. Therefore, constant precise testing of the joints and the quality of the surfaces that the joints create is necessary to ensure reliability at the required quality. The quality of the materials to be joined is increased by the conversion layers representing the chemical pretreatment of metal materials, which are created by the chemical reaction between the metal and the applied coating. In the final phase of a given chemical reaction, a surface layer is formed – conversion layer.

Phosphate layers are often used as conversion layers in the automotive industry. The primary advantages of phosphate layers include, for example: improved corrosion resistance, increased surface functionality and support for adhesion of organic coatings or adhesives. [1]

Usually, these phosphate layers are made of zinc or iron phosphate. Application of phosphates can be carried out by spraying or immersion. Phosphating technology is constantly evolving. The paper deals with the possibility of creating such phosphate layers by applying polyaniline salts and their influence on changes in surface properties.

2. Material and method and results

2.1 Used material

Uncoated deep-drawn steel DC04, thickness 0.8 mm (abbreviation designation DC). The chemical composition of the materials is in Table 1.

Table 1: *Chemical composition of used steel DC04*

Material	C	Mn	P	S
DC	0,04%	0,25%	0,009%	0,008%

The tested samples were pre-treated by a new approach to creating the conversion layer by chemical pre-treatment using modern conductive compounds of polyaniline salts – polyaniline phosphate and polyaniline citrate.

2.2 Used pre-treatment

a) Exclusion of polyaniline salt (PANI-H_3PO_4) by precipitation polymerization (conc. H_3PO_4 = 0.8 M) - Sample (DC_1)

Polyaniline is prepared by oxidation of aniline with ammonium peroxodisulphate in an acidic environment. The reaction takes place in air at room temperature. This is an exothermic reaction. In the practical version, 9 ml of aniline was dissolved in a beaker in 250 ml of distilled water acidified with phosphoric acid in an amount of 13.6 ml. In the second beaker, a solution of ammonium peroxidizate was prepared by dissolving 28.5 g of the substance in 750 ml of distilled water.

After complete dissolution, the prepared solutions were mixed and stirred with a glass stirrer for the entire time of polymerization due to increased diffusion of reaction substances. After mixing the solutions, panels were inserted into the beaker, on which the polyaniline salt was secreted.

The course of polymerization was accompanied by color changes. From the initially clear reaction mixture through blue to the final deep green color of polyaniline. [2, 3]

b) Exclusion of polyaniline salt (PANI-Citr) by precipitation polymerization (conc. citric acid = 1.6 M) Sample - (DC_ 4)

In this part, the pre-preparation of the phosphate was carried out as follows: in a beaker, 9 ml of aniline was dissolved in 250 ml of distilled water acidified with citric acid in the amount of 84 g.

In the second beaker, a solution of ammonium peroxidisate was prepared by dissolving 28.5 g of the substance in 750 ml of distilled water, and both were mixed throughout the polymerization.

2.3 2D surface roughness measurement method

The surface roughness of the evaluated samples was measured by the touch measurement method with a profilometer type Surftest SJ-201, Mitutoyo (Japan). The measurement was carried out in accordance with the ISO 21920-2 standard. For the purpose of the experiment, parameters were chosen that could accurately describe the differences in the roughness of the evaluated surfaces.

The following parameters were chosen:

Ra [μm] – mean arithmetic deviation of the surface

Rz [μm] – average value of the largest profile heights

RPc [-/cm] - number of profile elements per cm of length

RSm [μm] - average width of profile elements

2.4 Measured values of roughness parameters

According to the mentioned methodology, individual surface roughness parameters were evaluated, Table 2. The sample marked DC_0 presents the measured values of the unprepared surface.

Table 2: *Average values of measured roughness parameters*

Sample	Average values of measured roughness parameters			
	Ra [µm]	Rz [µm]	RPc [-/cm]	RSm [µm]
DC_0	1,08 ± 0,09	6,01 ± 0,59	56,07 ± 10,65	187,3 ± 30,27
DC _1	2,07 ± 0,56	14,44 ± 5,78	56,941 ± 12,58	172,5 ± 62,39
DC _4	2,60 ± 0,45	15,55 ± 2,12	32,95 ± 3,81	284,5 ± 39,73

On the basis of the achieved values, we can conclude that the application of phosphate layers resulted in an increase in the average values of the observed roughness parameters compared to the original surface. Sample DC_4, phosphate with polyaniline salt (PANI-Citr) by precipitation polymerization (conc. citric acid = 1.6 M) has the highest and the most appropriate values in all selected roughness parameters. [4,5] In the attached profilograms of individual surfaces of materials Fig. 1a – Fig. 1c we recorded a change in the surface roughness of tested materials and on the basis of this fact we can state that the chemical surface pretreatment has an effect on the individual roughness parameters of the monitored samples.

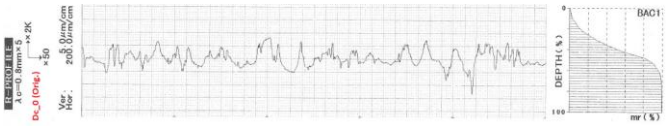

Fig. 1a *Profilogram + Firest-Abbot curve for the sample DC_0*

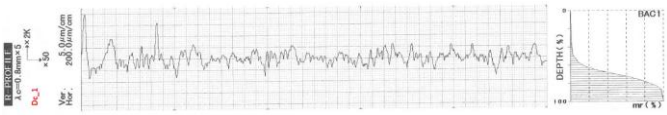

Fig. 1b *Profilogram + Firest-Abbot curve for the sample DC_1*

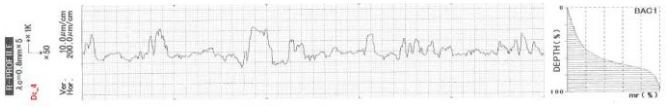

Fig. 1c *Profilogram + Firest-Abbot curve for the sample DC_4*

The geometric state of the surfaces has a decisive influence on its function. The requirements for the accuracy of the geometry of individual surfaces that are in contact with others are very high. Since it is assumed that the studied surfaces will interact with others, e.g. in the case of adhesive bonding, these were also subjected to a spatial evaluation of the surface in order to obtain a comprehensive image that tells about the character of surface. This measurement was carried out in a non-contact way using a ZEISS Smartproof 5 confocal microscope. 3D representation of the surfaces is in Fig.2a– Fig. 2c.

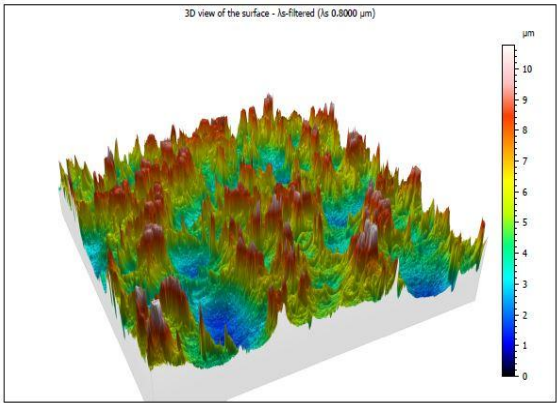

Fig. 2a *3D surface of the sample DC_0*

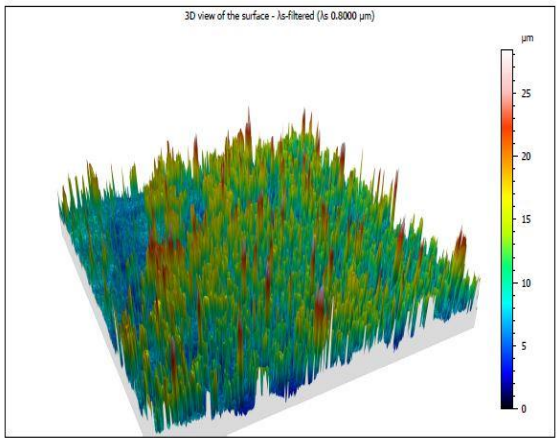

Fig. 2b *3D surface of the sample DC_1*

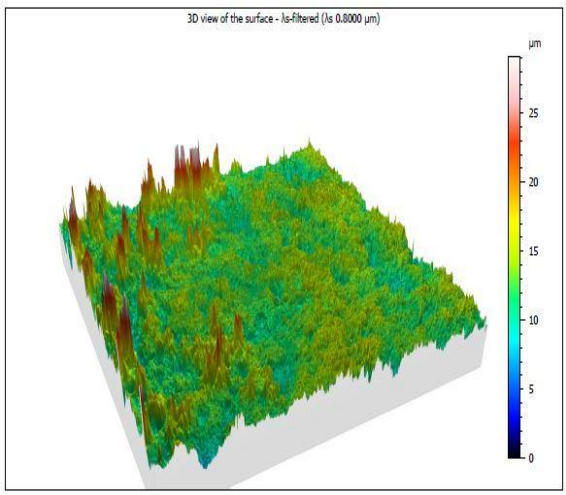

Fig. 2c *3D surface of the sample DC_4*

2.5 Measurement of the contact angle of the samples

The next step was to compare the contact angle. The contact angle of the surface of the materials was measured by a direct optical method. See System E Advex Instruments was used as the device. The method consists in placing a small drop of liquid on the measured surface, photographing it and determining the contact angle from the photograph, Fig. 3. Table 3 represents the values of the measured contact angles of the observed samples with an average value.

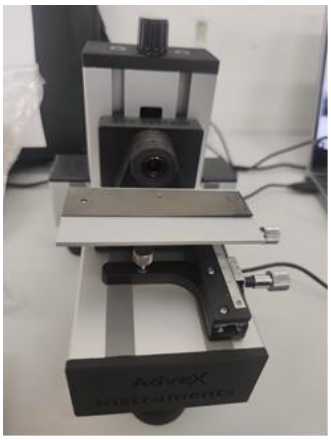

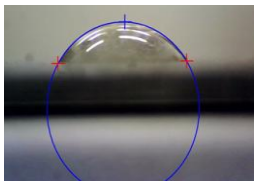

Fig. 3 *The principle of contact angle measurement*

Table 3: *Values of measured contact angle values*

Measurement number	**DC_0**	**DC_1**	**DC_4**
1.	70,2°	77,5°	75,1°
2.	68,5°	77,6°	81,3°
3.	65°	68,8°	79,2°
Average	**67,9°**	**74,6°**	**78,5°**

2.6 Morphology of films of polyaniline salts (PANI.H_3PO_4 and PANI – Citr)

The morphology of the samples with films of polyaniline salts was evaluated using the AFM method. The mean square thickness of the surface of the excluded film of polyaniline salts was measured. The root mean square thickness value provides information about the distribution of the polymer film on the material on which the film was deposited. [2]

The applied film of polyaniline salt PANI.H_3PO_4, which was formed in an environment of 0.8M phosphoric acid, reached a mean square thickness of the film surface up to 68 μm, while the film of polyaniline salt PANI – Citr, which was formed in an environment of 0.8M citric acid, reached mean square thickness of the film surface with a value of up to 0.82 μm.

Microscopic images of synthesized polyaniline salts are shown in Fig 4a and Fig. 4b.

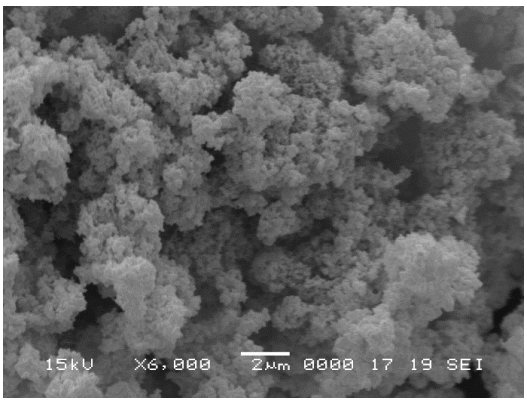

Fig. 4a *Microscopic image of synthesized polyaniline salts H_3PO_4*

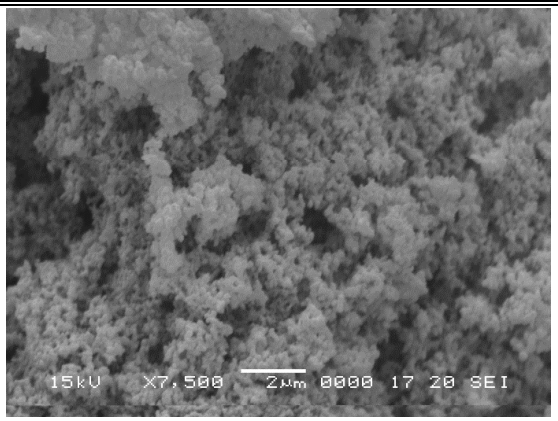

Fig. 4b *Microscopic image of synthesized polyaniline salts polyaniline citrate (PANI-Citr.)*

From the comparison of the morphology of the polyaniline salts, it is possible that there was an increase in thick layers of the applied coating film on the surface of the sample DC_04 (PANI-Citr). This means that, despite the relatively large contact angle, good anchoring of the glue is a prerequisite. Contact angle values can be improved in future research by correcting the parameters during the phosphating process.

3. Conclusions

Based on the presented results of experimental measurements, it is possible to state the following conclusions:

- when measuring and evaluating the 2D roughness parameters, it was demonstrated that the DC_4 sample has more favorable results for the further application of the adhesive coating or glue.
- the samples that were phosphated in polyaniline salts in this experiment showed satisfactory values of contact angles. It is necessary in future research to focus on the optimization of technological parameters during phosphating.

Experimental verification of the use of specific compounds of polyaniline salts in the phosphating process from the point of view of their applications for adhesive bonding is promising, but attention needs to be paid to further research from the point of view of obtaining the most optimal surface fragmentation.

Acknowledgement

This research was funded by the Scientific Grant Agency of the Ministry of Education, Science, Research and Sports of the Slovak Republic under project VEGA 1/0229/23: Research on the applicability of thermal drilling technology for the creation of multi-material joints in the automotive industry and Slovak Research and Development Agency under project APVV-20-0303: Innovative approaches to the restoration of functional surfaces by laser weld overlaying.

References

1. L. Jiang et al., Corros. Sci., **55**, 76-89 (2012)
2. A. Kalendová et al., Prog. Org. Coatings, **77**, 1465-1483 (2014)
3. A. Guzanová et al., J. Adhes. Sci. Technol., **11**, 1153-1175 (2022)
4. A. Guzanová et al., Metals, **4**, 1 – 23 (2022)
5. D.Draganovská, et al., Mater. Sci. Forum, **818**, 15-18 (2015)

Studying the composition and properties of white eco-cement

Lev Chernyak [1], Nataliia Dorogan [2], Liubov Melnyk [3], Petro Varshavets.[4], Victoria Pakhomova [5]
National Technical University of Ukraine" Igor Sikorsky Kyiv Polytechnic Institute"
Kyiv, Ukraine
lpchernyak@ukr.net

Abstract: *The possibility to produce white Eco-cement with the use of a dry method under low-temperature firing of a raw material mixture based on the CaO – SiO2 – Al_2O_3 – MgO system is shown. Computer calculations were performed and an analysis of the dependence of the characteristics of cement clinker on the quantitative ratio of raw components was carried out. A new composition of the raw material mixture with a decrease of 19 wt. % amount of the carbonate component and, accordingly, CO_2 emissions during combustion was determined. The peculiarities of phase transformations in the material during firing with a maximum temperature of 1100 °C when microtalcum was introduced into the initial mixture with the formation of pericloze, ockermanite and merwinite as a factor in the structure and properties of cement clinker were noted.*

Keywords*: ECO-CEMENT,RAW MATERIAL MIXTURE, MICROTALC, FIRING, PHASE COMPOSITION, PROPERTIES.*

1. Introduction

The production of the most common mineral binder, Portland cement, is characterized by significant energy costs by high-temperature firing (1400-1500 °C) of clinker as well as by its grinding with additives to a highly dispersed state [1-3]. At the same time, the physical and chemical transformations of rock-forming minerals into carbonate components, which make up the majority (75-80 wt. %) of the composition of the raw material mixtures, cause significant emissions of CO_2 into the atmosphere [4].

It is noted that cement clinker kilns account for about 5% of total CO_2 emissions into the atmosphere. The problem lies in cement's chemistry, which is a sort of double-whammy of CO_2 production. To turn Portland cement's key ingredient, calcium carbonate—found in limestone or chalk—into a finished product called alite, the minerals must be broken down in kilns heated to more than 1400 ºC. The heating process uses tremendous amounts of energy, which is typically generated using gas or coal, the most carbon-intensive fossil fuel. Then, the ensuing chemical process releases a second wallop of CO_2 as a byproduct of turning calcium carbonate into calcium oxide. In total, producing 1 ton of cement releases 770 kilograms of CO_2 into the atmosphere.

When solving the specified problems of resource conservation and environmental safety of cement production, considerable attention is given to the Eco-cement technology using raw material mixtures with a lower content of carbonate components [5-8] and the use of industrial waste [9,10].

The production of white Eco-cement is complicated by special requirements regarding the chemical composition of raw materials with the minimization of the content of colored oxides [11-13]. The solution of this scientific and technical problem requires the development of new compositions of raw material mixtures, the analysis of the features of phase formation and the properties of white hydraulic mineral binder under the conditions of low-temperature firing, which became the goal of the presented work.

2. Results and discussion

The selection of research objects in this work was carried out in accordance with the main goal – to obtain a white mineral binding material during low-temperature firing with a decrease in the content of the carbonate component in the initial mixture. In accordance with the above, raw materials must have:

- increased reactivity, ensuring the intensification of physical and chemical reactions in the silicate system during firing with a decrease in the maximum temperature;
- minimum content of color oxides to increase the degree of whiteness of the final product.

Materials of natural and industrial origin were used for the production of the raw material mixture:

- chalk of the Zdolbuniv deposit of the Rivne region;
- aluminum hydroxide – a product of processing bauxite into alumina;
- pyloquartz - a product of enrichment and fractionation of quartz sand;
- microtalc – a product of enrichment and fractionation of talc powder.

According to the chemical composition, among the studied raw materials, the sample of Zdolbuniv chalk is characterized by a high content of CaO, the sample of aluminum hydroxide - the largest amount of aluminum oxide, the sample of pyloquartz - the largest amount of silica, the sample of microtalc - a high content of magnesium oxide with a quantitative ratio of SiO_2:CaO:MgO = 11:1: 5 (Table 1).

The raw mixtures have been prepared by dispensing the components by mass, mixing and homogenizing in a ball mill, firing and milling of the final product in accordance with the modern dry technology of cement production.

Table 1: *Chemical composition of raw materials*

Samples	Content of oxides, wt. %									
	SiO_2	Al_2O_3	Fe_2O_3	TiO_2	CaO	MgO	SO_3	Na_2O	K_2O	LOI
chalk	0,77	0,25	0,13	-	55,0	0,25	0,08	-	-	43,49
hydrate of aluminium oxide	-	65,0	-	-	-	-	-	-	-	35,0
pyloquartz	99,16	0,16	0,06	-	-	-	-	-	-	0,12
microtalc	61,32	0,26	0,10	-	5,39	27,40	-	-	-	5,53

The samples were fired for 15 hours at a maximum temperature of 1100 °C with a holding time of 1.5 hours. All samples of the mixtures compared were fired simultaneously and together to exclude differences in the degree of heat treatment.

The properties of the binding material were determined according to standardized methods.

Methods of physical - chemical analysis of silicate raw materials and testing of properties of astringent substances which were used in this work included:

- chemical composition analysis using standardized procedures;
- X-ray diffraction analysis (powder - like preparations) using a diffractometer DRON-3M (radiation CuKα 1-2, voltage 40 kV, current 20 mA, speed 2 degrees/min);

- determination of the whiteness of materials using a leukometer Carl Zeiss JENA.

The analysis of mineralogical composition of raw material showed:

- the basic rock-forming mineral of chalk is calcite (97,6 mass.%) with the admixtures of dolomite, quartz and kaolinite;
- hydrate of aluminium oxide is characterized by the presence of hydrargillite (gibbsite), diaspore, boehmite with the insignificant admixture of ilmenite;
- the main rock-forming mineral of pyloquartz is β-quartz;
- the main rock-forming mineral of microtalc is talc with quartz impurities.

It is obvious that by the calcination of the specified raw materials during the destruction of lattices of the main rock-forming minerals, chalk and aluminum hydroxide will become a source of CaO and Al_2O_3 oxides, pyloquartz - a source of SiO_2, and microtalc - SiO_2 and MgO oxides in the process of phase formation of cement clinker [14-16].

Results and Discussion

The composition of the initial 3-component raw material mixtures basedon the chalk-aluminum hydroxide- pyloquartz and chalk-aluminum hydroxide-microtalc systems was determined according to known recommendations regarding low-temperature firing cement technology in the range of values of the hydraulic modulus HM=1.1–1.7 using a specially created program for computer calculations [17].

It was established that in the specified HM interval, the quantitative ratio of the system components changes significantly, while along with the dependence of the concentration of the components on the hydraulic modulus, a significant change in the values of the silica modulus is observed.

It was determined that at the minimum aluminum hydroxide concentration for the studied systems of 10 wt. % in the range of values of HM=1.1-1.7, the possible content of the carbonate component is 68.3-73.5 wt. % when using pyloquartz and 54.5-62.8 wt. % when using a microtad (Fig. 1). At the same time, there is a directly proportional relationship between the concentration of the carbonate component and the values of the hydraulic modulus of the binder.

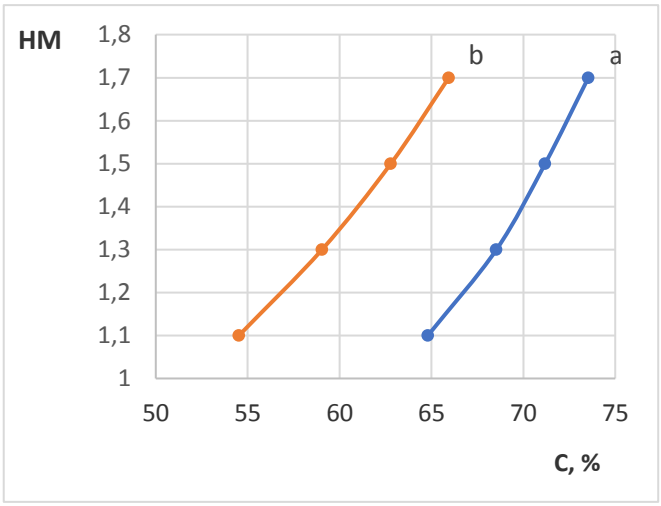

1

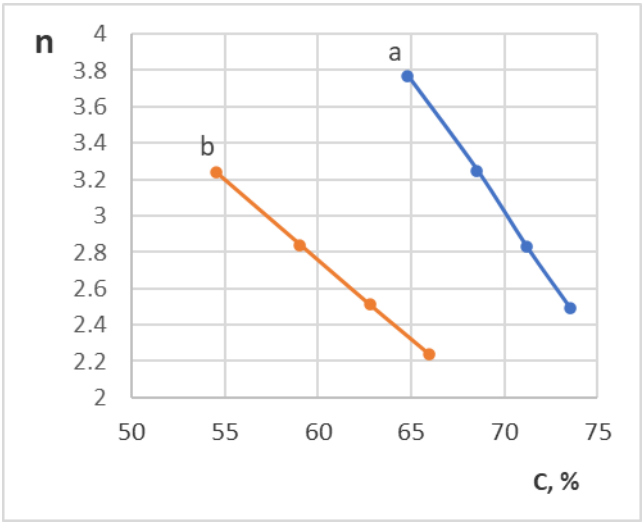

2

Fig. 1 *Dependence of the hydraulic (1) and silica (2) moduli on the concentration of the carbonate component when using pyloquartz (a) and microtalc (b)*

As for the cement modulus n of the binder, there is an inversely proportional dependence of its values on the concentration of the carbonate component: in the ranges of 2.5-3.8 for systems with pyloquartz and 2.2-3.2 for systems with microtalc.

The raw material mixtures chosen for the production of mineral binding material with the same amount of aluminum hydroxide differ significantly in the content of the carbonate component - chalk (Table 2).

Table 2**:** *Composition of raw mixtures*

Code of mixture	Quantity of components, mass %			
	chalk	hydrate of aluminium oxide	pyloquartz	microtalc
K9	73,5	10,0	16,5	-
K12	54,5	10,0	-	35,5

According to the chemical composition, the investigated raw material mixtures are characterized by the same amount of aluminum and iron oxides, but they differ significantly in the content and quantitative ratios of other oxides, which determine a potential for phase formation during firing (Table 3).

Table 3: *Chemical composition of raw mixtures*

Sample code	Content of oxides, wt. %						
	SiO_2	Al_2O_3	Fe_2O_3	CaO	MgO	SO_3	LOI.
K9	16,99	6,71	0,11	40,45	0,18	0,06	35,50
K12	22,18	6,73	0,11	31,91	9,86	0,04	29,17

Thus sample K12 differs from K9 by:

• a smaller amount of calcium oxides, a much higher content of magnesium oxide with a quantitative ratio of CaO : MgO = 3.2;

• quantitative ratios of CaO : SiO_2 = 1.4 versus 2.4 and CaO : $A_{l2}O_3$ = 4.7 versus 6.0.

The analysis of the chemical composition of cement clinker from experimental mixtures (Table 4) indicates that at low values of the saturation coefficient SF= 0.35-0.64, the formation of crystalline phases C_2S and C_3A is most likely when the amount of iron-containing compounds is minimized.

Table 4: *Chemical composition of clinker*

Sample code	Content of oxides, wt. %					
	SiO_2	Al_2O_3	Fe_2O_3	CaO	MgO	SO_3
K9	26,34	10,40	0,17	62,72	0,28	0,09
K12	31,31	9,51	0,15	45,03	13,92	0,06

The results of the X-ray phase analysis obtained in this work indicate on certain peculiarities in the physical and chemical transformations during firing of the studied mixtures with a maximum temperature of 1100 °C (Fig. 2, 3).

Thus, after firing to the maximum temperature of 1100 °C with approximately the same development of the C_2S and CA crystalline phases, sample K12 differs from sample K9 by:

- a significantly smaller amount of free CaO (1.69; 2.38 Å) and quartz (3.835; 4.25 Å);
- formation of periclase (2.10; 1.48 Å), ockermanite $2CaO•MgO•2SiO_2$ (2.87 Å) and merwinite $3CaO•MgO•2SiO_2$ (2.66 Å);
- greater development of C_2AS hellenite (2.86 Å);
- a smaller groove of the crystalline phases of wollastonite CS (2.97; 3.48 Å) and mayenite $C_{12}A_7$ (4.90 Å).

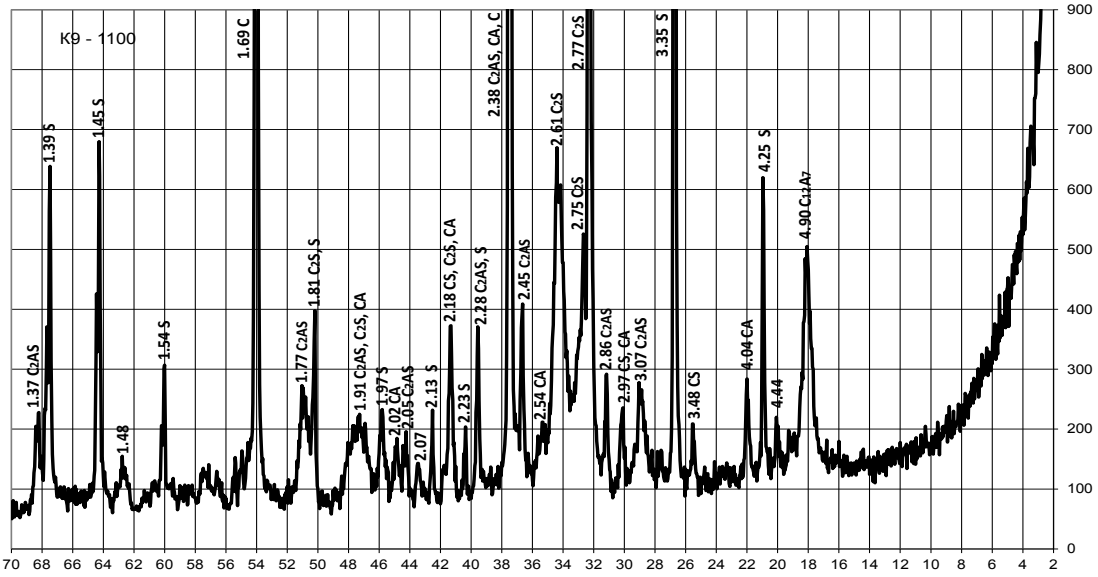

Fig. 2 *X-ray diffraction of sample K9 (1100 ºC).*

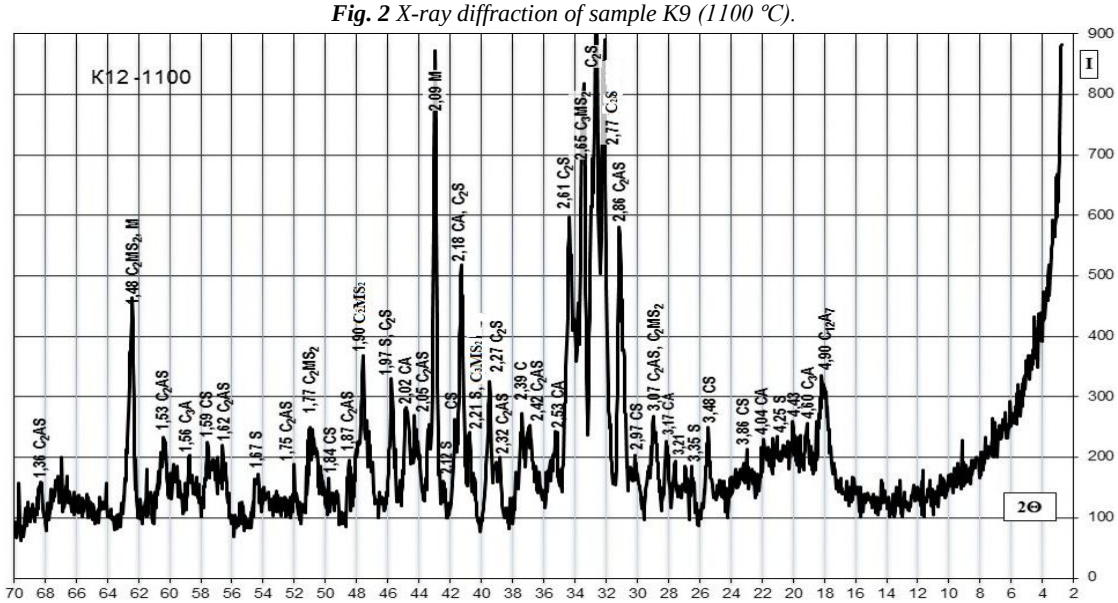

Fig. 3 *X-ray diffraction of sample K12 (1100 ºC).*

The results of the testing of the studied samples of the binder indicate differences in the influence of the composition on the property indicators (Table 5). Thus, according to the classification of DSTU B V.27-91-99 [18], when fired at a maximum temperature of 1100 °C, the binder from the K9 mixture belongs to the group of ultra-fast hardeners (starting time no later than 15 min.), which is considered typical for expanding and tensioning cement. The sample K12 belongs to a fast-hardening one (time of onset from 15 to 45 min.), which is considered typical for anhydrite and alumina cement. At the same time, the sample K12 differs from K9 in the general slowing down of the hardening process.

Table 5: *Properties of mineral astringent material*

Characteristics	Sample code	
	K9	K12
Finess of grinding, sieve residue no. 008, mass. %	7	7
Initial setting time, min	10	30
Final setting time, min	25	60
Compressive strength, MPa	32	34,5
Whiteness, %	88	90

According to the specified standard, the samples of the binder produced belong to the group of medium strength (from 30 to 50 MPa per compression). From the point of view of the purpose of this work, it is important to achieve high whiteness indicators in accordance with the requirements of the standard for white Portland cement [19,20].

Conclusions

1. The development and practical use of mineral binders of the Eco-cement type with a reduction in the content of the carbonate component of the raw material mixture contributes to the comprehensive solution of the issues of ecology, resource conservation and chemical technology for the production of silicate materials.

2. The possibility of producing white Eco-cement by a dry method at a maximum firing temperature of 1100 °C based on the chalk-aluminum hydroxide-microtalc system with a decrease in the content of the carbonate component and, accordingly, CO_2 emissions into the atmosphere by 19-20% compared to known compositions, was determined:

3. The peculiarities of phase formation during low-temperature firing of white Eco-cement clinker, manifested in the formation of crystalline phases of periclase and calcium-magnesium silicates - ockermanite $2CaO•MgO•2SiO_2$ and mervinite $3CaO•MgO•2SiO_2$, were established.

Here are some examples:

1. Duda W. Cement Data Book, Volume 3: Raw Material for Cement Production - French & European Pubns, 1988. – 188 p.
2.Ghosh S. Advances in Cement Technology: Chemistry, Manufacture and Testing / Taylor & Francis, 2003. – 828 p.
3.Anjan K. Cement Production Technology. Principles and Practice // CRC Press, 2018. – 439 p.
4. Andrew R. Research, CICERO Center for International Climate. Global CO_2 emissions from cement production // Journal of Earth Syst. Sci. Data (2017)
5. Hanehara S. ECO-CEMENT AND ECO-CONCRETE Environmentally Compatible Cement and Concrete Technology // Conference: JCI/KCI International Joint Seminar, 2001. – Vol.1.
6. Scrivener K. Eco-efficient cements: Potential economically viable solutions for a low-CO_2 cement-based materials industry // Cement and Concrete Researchl, 2018. – Vol. 114. – p. 2-26, (Scrivener K., Vanderley M., Gartner E.).
7. Schneider M. The cement industry on the way to a low-carbon future // Cement and Concrete Research, 2019. – Vol. 124(3).
8. Low Carbon Cement Production Issue Paper // https://www.climateactionreserve.org/wp-content/uploads/2022/10/Low-Carbon-Cement-Issue-Paper-05-20-2022_final.pdf
9. Uchikawa H. Eco-cement-frontier of Recycling of Urban Composite Waste, World Cement, 1995, pp. 33-36, (Uchikawa H., Obana H.).
10. Shimoda T. Eco-cement: A New Portland Cement to Solve Municipal and Industrial Waste Problems, Modern Concrete Materials, Proceedings of the International Conference 'Creating with Concrete', Dundee(UK), 1999, pp. 17-30, (Shimoda T., Yokoyama S.).
11. Zubekhin A. White Portland Cement // Rostov on/D,: Universitet, 2004. – 263 p., (Zubekhin A., Golovanova S., Kirsanov P.).
12. Moresová K. White cement - Properties, manufacture, prospects // Ceramics Silikaty, 2001. – Vol. 45(4). – pp.158-163, (Moresová K., Škvára F.).
13. Dorogan N. White Portland Cement – Kyiv: «Polytechnica», 2018. – 204 p., (Dorogan N., Sviderskyy V., Chernyak L.).
14. Taylor H. Cement Chemistry – London: Thomas Telford Publishing; 2 edition, 1997 – 459 p.
15. Bogye R. The Chemistry of Portland cement. – New York: 1995. – 326 p.
16. Kurdowski W. Chemia cement - Warzawa: PWN, 1991. – 478 s.
17. Sviderskyy V. The software for technology of low-temperature binder materials // Bulding materials and products, 2017. - № 1-2 (93). – P. 22 – 24., (Sviderskyy V., Chernyak L., Sanginova O., Dorogan N., Tsybenko M.).
18.DSTU B V.2.7-91-99. Astringent mineral. Classification.– K.: Cerzhbud of Ukraine,1999.
19.DSTU B V.2.7-257:2011. White Portland Cement. Technical Date. – K.: Minregion of Ukraine,2012.
20. ASTM C150-07. Standard Specification for Portland Cement.

Microhardness dependence of Ti-Zr alloys on time and temperature of sintering

Ljerka Slokar Benić[1*], Luka Komljenović[1], Erman Žiga[2], Magdalena Jajčinović[1]
University of Zagreb Faculty of Metallurgy, Croatia[1]
University of Ljubljana Faculty of Natural Sciences and Engineering, Slovenia [2]
slokar@simet.unizg.hr

Abstract: *Commonly used metallic biomaterials are titanium and its alloys, cobalt-based alloys and 316L stainless steel. Titanium alloys are reference materials in biomedical applications due to their desirable properties such as excellent mechanical properties and good biocompatibility. Since presence of different metals can significantly alter the properties of titanium it is usually alloyed with other metals, including the zirconium. In this work Ti-20Zr was prepared by powder metallurgy by mixing the powders in a ball mill and sintering in a tube furnace under argon atmosphere. Microscopic analysis with the light microscope showed that the porosity decreased with increasing temperature and sintering time. Scanning electron microanalysis with energy-dispersive spectrometry showed the two-phase microstructure of the sintered alloy. Microhardness was determined by Vickers method. A longer sintering time and a higher sintering temperature resulted in higher microhardness values.*

Keywords*: TITANIUM-ZIRCONIUM ALLOY, POWDER METALURGY, MICROHARDNESS, BIOMEDICAL MATERIALS*

1. Introduction

As the need for biomaterials increases over the years, their development also increases and becomes an increasingly important area from a research perspective. Titanium has been used as a construction material in the military, aerospace and aviation industries since the 1940s, and today it is used as an implant material in biomedicine[1,2]. Due to the harmful effects of some elements such as nickel and cobalt in its chemical composition, more and more commercial pure titanium (CP Ti) is being used for biomedical applications. However, since CP Ti did not have satisfactory mechanical and tribological properties, certain alloying elements were added to improve its properties. In this way, the alloy Ti-6Al-4V was created. Later scientific research showed that aluminium and vanadium have a toxic effect on the human body, and so research began into titanium alloys with new chemical compositions without toxic elements[3,4]. In biomedicine, alloys are sought that have excellent biocompatibility, wear resistance and corrosion resistance, and these alloys demonstrate this[5,6]. The reason why titanium alloys are not widely used is because of the difficulty in casting the parts and the high price of the end products. Indeed, titanium as a starting material is very expensive due to the complex and expensive manufacturing process. In this sense, the production of titanium alloys and end products using powder metallurgy has proven to be a successful alternative[7,8,9].

An important step in the powder metallurgy process is sintering. Sintering affects the final density of the sintered material, achieving densities between 25% and 85% of the reference material. The most important parameters of the sintering cycle are temperature and time[10,11,12]. The level of porosity and the distribution of pore sizes, which affect the final density, can be controlled by manipulating these parameters in order to obtain powders of satisfactory shape, sizes particles and good surface texture. By increasing the sintering temperature, a decrease in porosity is achieved, which results in an increase in diffusion due to an increase in temperature[13].

The aim of the research in this work is to produce a titanium alloy with the addition of 20 at% zirconium using the powder metallurgy process and to analyze the influence of the process parameters on the microstructural characteristics of the sintered alloy using appropriate methods.

2. Materials and methods

In this work, titanium and zirconium powders with the properties listed in Table 1 were used as starting material. Four samples with the chemical composition Ti-20Zr (at.%) were prepared.

Table 1: *Characteristics of starting powders.*

Materials	Purity (%)	Particle size (μm)	Density (g/cm^3)
Ti powder	99.8	125-250	4.51
Zr powder	99.8	150	6.49

After weighing the titanium and zirconium powders, they were mixed. The aim of mixing is to obtain a homogeneous powder mixture. Mixing of the titanium and zirconium powders was done in a ball mill for 30 minutes at room temperature. From the mixture obtained, 4 samples were taken with a mass of about 2.5 grammes each. The powders were compacted by uniaxial pressing in a hydraulic press. A pressure of 160 MPa was applied to all 4 samples and the samples obtained were in the shape of a disc. Sintering of the Ti-20Zr alloy samples was carried out after compaction in a tube furnace in an argon atmosphere with the parameters listed in Table 2.

Table 2: *Processing parameters.*

Sample No.	Temperature of sintering (°C)	Time of sintering (h)
1	1100	2
2	1350	2
3	1100	4
4	1350	4

The sintering process consisted of three phases. In the first phase, the samples were heated to the sintering temperature at a rate of 10 °C/min. In the second phase, the samples were kept at a constant temperature for 1 hour. In the third phase, the samples were cooled to room temperature in the furnace.

After metallographic preparation, which consisted of grinding and polishing, the specimens were observed with a light microscope for porosity analysis. Light micrographs were taken with the digital camera that came with the microscope. A scanning electron microscope (SEM) and energy dispersive spectrometry (EDS) were used to examine the surface of the sintered Ti-20Zr alloy samples after etching in Kroll's reagent at room temperature. Using a EDS detector, the chemical composition was determined at 5 positions and then the mean value was calculated. A line analysis was performed to gain insight into the concentration profile of the elements present and the distribution of the elements over a given area was also analysed. The microhardness of the sintered samples was determined using the Vickers method. The indentation force was 19.60 N (HV2) and the indentation time was 10 seconds. The diagonals of the impressions obtained were measured at a microscope magnification of 500 x. The microhardness was determined at 5 points on each sample and the mean value was calculated.

3. Results and discussion

The starting powders of the investigated titanium-zirconium alloy Ti-20Zr were characterised with a scanning electron microscope. Fig. 1 shows that the titanium powder particles are spherical, while the zirconium powder particles are angular and irregularly shaped.

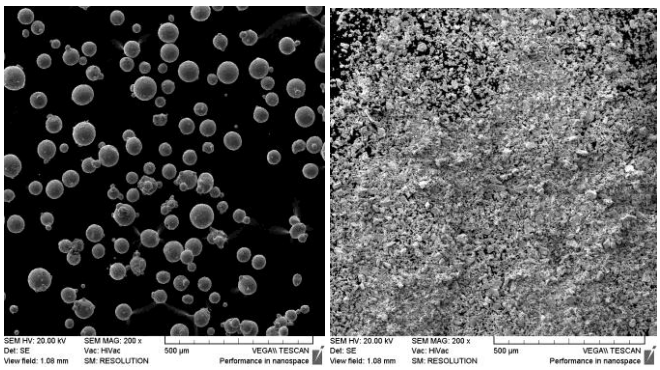

Fig. 1 *SEM images of titanium and zirconium starting powders.*

The porosity of the sintered samples after embedding in the carbon mass by hot pressing and after grinding and polishing was observed using a light microscope at 100 x magnification and recorded with a digital camera. The micrographs are shown in Fig. 2.

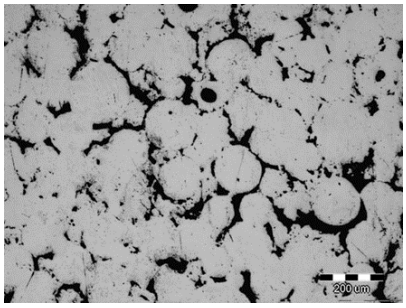

a) Sample 1, sintered at 1100°C for 2h

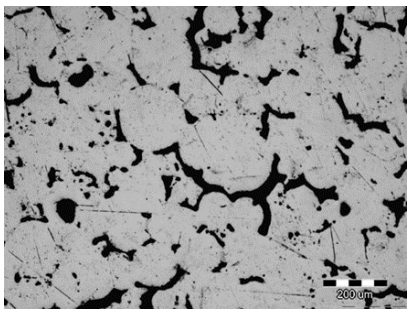

b) Sample 2, sintered at 1350°C for 2h

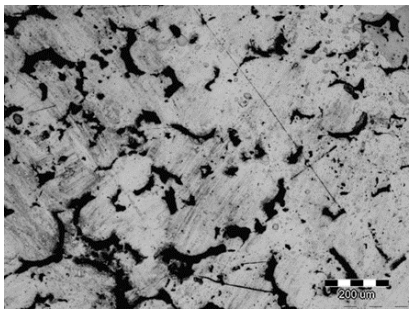

c) Sample 3, sintered at 1100°C for 4h

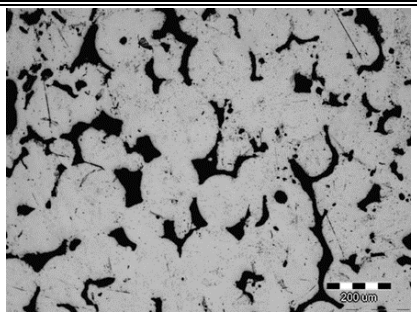

d) Sample 4, sintered at 1350°C for 4h

Fig. 2 *Light micrographs of sintered samples.*

As can be seen in Fig. 2, the pores have an irregular shape. In samples 1 and 3, which were sintered at a temperature lower than 1100 °C, the pores are interconnected, which can lead to weak densification. As a result, the boundaries between the particles are still clearly visible. This means that most of the thermodynamic energy of the system was spent on diffusion and homogenisation of the chemical composition instead of compaction. Spherical pores are present in samples 2 and 4, which were sintered at a higher temperature than 1350 °C, showing that a higher sintering temperature is favourable for achieving minimum porosity. To achieve the highest porosity density, i.e. the lowest degree of porosity, the pressure during compaction could be slightly higher.

The microstructure of all samples was examined after etching with a scanning electron microscope (SEM) at 500 x and 2000 x magnifications, as shown in Fig. 3-6.

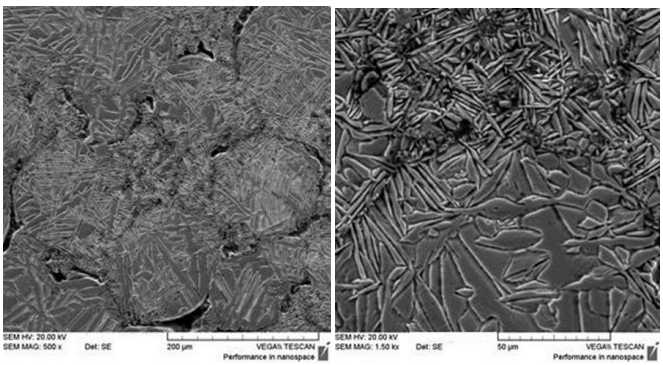

a) 500 x *b)2000 x*

Fig. 3 *Microstructure of sintered sample No. 1.*

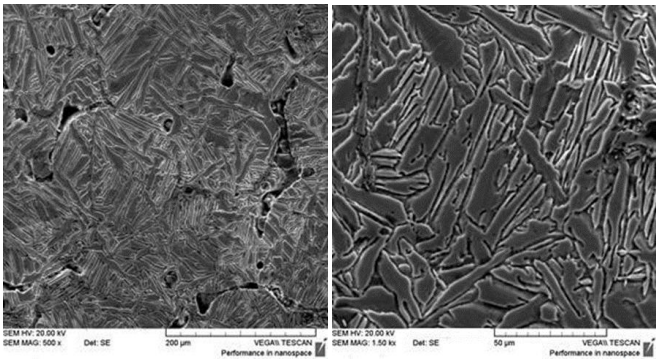

a) 500 x *b)2000 x*

Fig. 4 *Microstructure of sintered sample No. 2.*

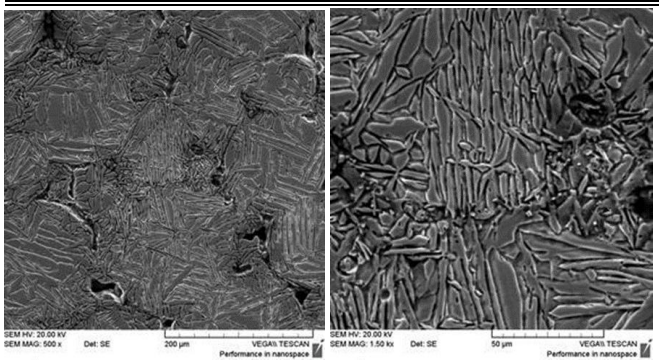

a) 500x *b)2000x*

Fig. 5 *Microstructure of sintered sample No. 3.*

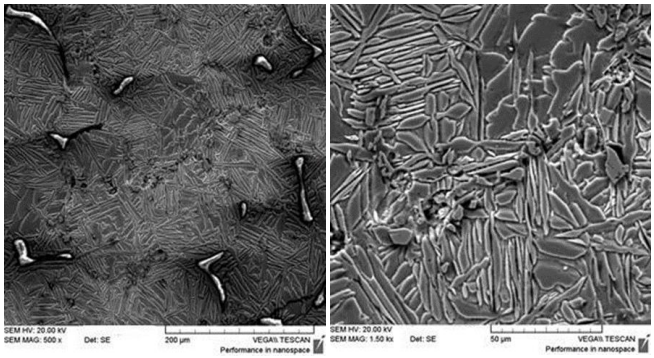

a) 500x *b)2000x*

Fig. 6 *Microstructure of sintered sample No. 4.*

It can be clearly seen that the microstructure of all observed samples after sintering is two-phase and consists of α and β-phases. This type of lamellar α + β microstructure occurs in titanium alloys where nucleation and growth of the α-phase lamellae occur at temperatures lower than the temperature of α↔β transformation.

It can also be seen that the lamellae are oriented differently, i.e. intertwined, which is characteristic of the so-called Widmanstätten structure. It can also be seen that the lamellae have different thicknesses. The reason for this could be insufficient diffusion of titanium and zirconium in the powder mixture, which could indicate that the mixing time of the starting powders was not long enough.

Energy dispersive spectrometry (EDS) was used to determine the chemical composition of the α- and β-phases in the samples after sintering. The analysis was carried out using the point analysis method, where the electron beam was focused on 5 different places in the α- and β-phase and the mean value was calculated.

The results of the averages show that the chemical compositions of all samples are very similar and that the chemical compositions of the α- and β-phases are almost identical. These phases are therefore solid solutions of zirconium in titanium whose chemical compositions are the same as the chemical composition of the alloy. Figs. 7 and 8 show the graphical result of the EDS analysis for samples no. 3 and 4, at one point the line analysis and the so-called "mapping" analysis, which shows the distribution of titanium and zirconium in a certain area.

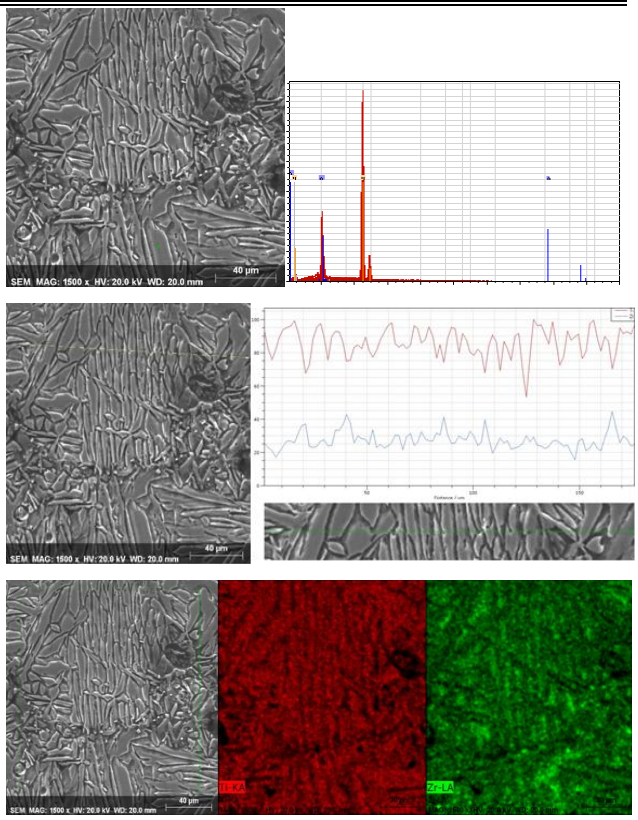

Fig. 7 *EDS spectrum, line analysis and distribution of titanium and zirconium in sintered sample No. 3*

The spectrum from EDS shows only peaks for titanium and zirconium, indicating that the preparation process, including sintering, was successful in terms of contamination.

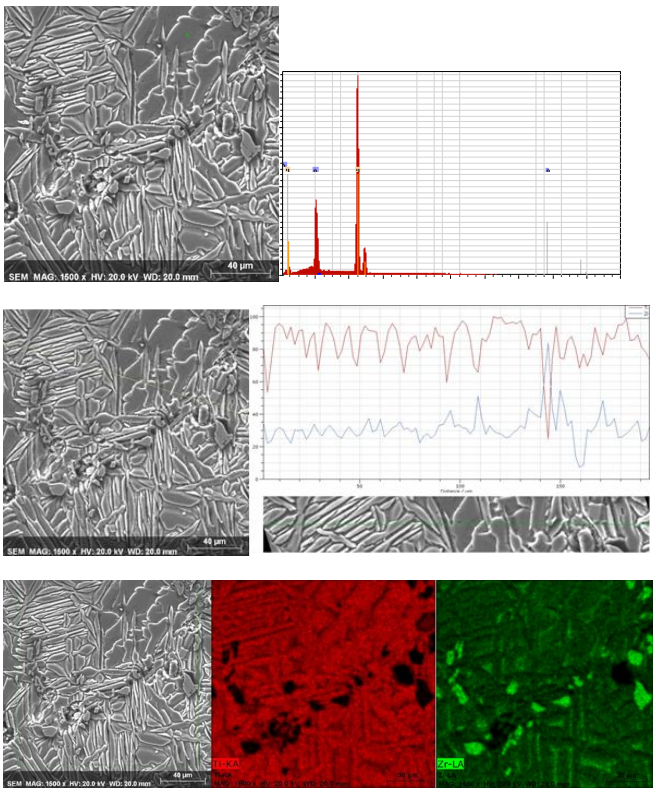

Fig. 8 *EDS spectrum, line analysis and distribution of titanium and zirconium in sample 4*

The line analysis shows the uniform concentrations of titanium and zirconium in the line EDS. The mapping analysis shows that the concentration of zirconium is increased in certain areas of the lamellae.

The same situation arises for sample 4 as far as the EDS spectrum and line analysis are concerned. Indeed, in addition to the increased concentration of zirconium on individual lamellae, the mapping analysis also shows particles of zirconium powder, which indicates that due to unsuitable process parameters, especially mixing, homogenisation of the chemical composition, did not take place and the diffusion process is not complete, even though this sample was sintered at a higher temperature. A similar result was obtained in the work of R. Karra et al[14]. This type of incomplete dissolution may be related to the fragility of zirconium particles compared to titanium particles, as the surface of the more ductile particles is usually covered with brittle particles. In view of the results of the qualitative EDS analysis, in which only titanium and zirconium were detected, contamination of the powder mixture, which could be the cause of incomplete diffusion, can be ruled out.

The microhardness of the samples after sintering was determined on polished samples using the Vickers method (HV2). The measurements were performed on each sample at 5 different points and then the mean value was calculated. The obtained data of the mean values show that the microhardness is between 379 and 462 HV2. It can also be clearly seen that the HV2 values are lower for the samples that were sintered at a lower temperature, as shown in Fig. 9. This is consistent with the fact that as the sintering temperature increases and the density or densification increases, the hardness also increases. Indeed, sintering at higher temperatures promotes additional bonding of particles and a more complete alloy due to higher diffusion and mass transfer rates.

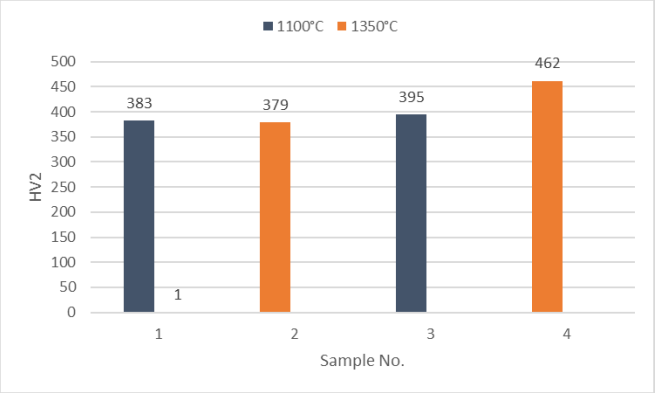

Fig. 9 *Dependence of microhardness on sintering temperature.*

The dependence of microhardness on sintering time is shown graphically in Fig. 10.

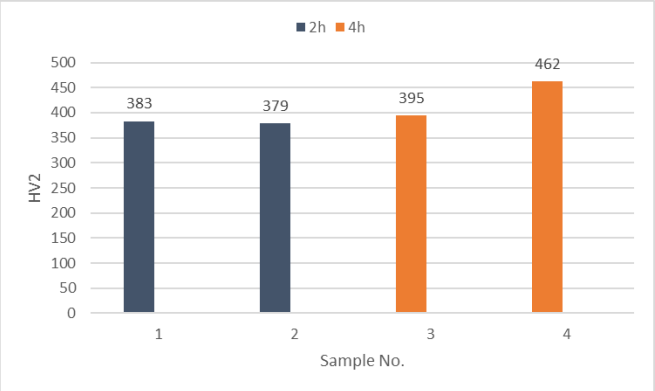

Fig. 10 *Dependence of microhardness on sintering time.*

The HV2 values of samples 1 and 3 and samples 2 and 4 were compared to evaluate the influence of sintering time on microhardness. It can be seen that samples 3 and 4, which were sintered longer than samples 1 and 2, have a higher value of microhardness. This behaviour may be related to the fact that a longer sintering time ensures a more complete bond between the particles, i.e. an alloy, which emphasises the influence of the alloying element zirconium on the base element titanium. This increase in microhardness can be explained by the formation of a solid β (Ti,Zr) solution. It is evident from the results that temperature is the dominant factor in microhardness, rather than sintering time.

4. Conclusion

From the analysis of the Ti-20Zr alloy produced by powder metallurgy, the following conclusions can be drawn:

- the porosity is lower in the samples pressed at higher pressure; it can be reduced by sintering at higher temperature for a longer time,
- the microstructure of all samples after sintering is two-phase and consists of intertwined lamellae of α- and β-phases, which are solid solutions of zirconium in titanium with a chemical composition corresponding to the chemical composition of the alloy,
- as the sintering temperature increases, so does the microhardness,
- a longer sintering time is more favourable for achieving higher microhardness values.

Finally, the powder metallurgy processing parameters applied in this work can lead to a potentially biomedical titanium-zirconium alloy.

3. References

1. L. C. Zhang, L. Y. Chen, Adv. Eng. Mater., **21**, 1–29 (2019)
2. Y. Li, C. Yang, H. Zhao, S. Qu, X. Li and Y. Li, Materials, **7**, 1709-1800 (2014)
3. F.A. Anene, C.N. Aiza Jaafar, I. Zainol, M.A. Azmah Hanim, M.T. Suraya, Mechanical Engineering Science,1–14 (2020)
4. E. L. Zhang, Rare. Met., 38, 476–494 (2019)
5. Y. Alshammari, F. Yang, L. Bolzoni, J. Mech. Behav. Biomed. Mater., **95**, 232–239 (2019)
6. A Revathi, A. Dalmau Borrásb, A. Igual Muñozb, C. Richardc, G. Manivasagamd, Materials Science and Engineering: C, **76**, 1354-1368 (2017)
7. Z. J. Wally, W. Van Grunsven, F. Claeyssens, R. Goodall, G.C. Reilly, Metals, **5,** 1902-1920 (2015)
8. M. Bönisch, M. Calin, T. Waitz, A. Panigrahi, M. Zehetbauer, A. Gebert, W. Skrotzki, J. Eckert, Science and Technology of Advanced Materials, **14**, 1-9 (2013)
9. G. Adamek, Acta Physica Polonica A, **126**, 871-874 (2014)
10. R. Mariapapan, S. Kumaran, T. Srinivasa Rao, S. B. Chandrasekar, Powder Metalurgy, **54,** 236-241 (2011)
11. A. S. Jabur, Powder Tehnology, **237**, 477-483 (2013)
12. O. Ertugrul, H.-S. Park, K. Onel, M. Willert-Porada, Powder Tehnology, **253**, 703-709, (2014)
13. C. Suryanarayana, Progress in Materials Science, **46**, 1-184 (2001)
14. R. Karre, B. K. Kodli, A. Rajendran, J. N. Pattanayak, K. Ameyama, S. R. Dev, Materials Science and Technology C, **94**, 619-627 (2019)

Analysis of the densification of a biomedical titanium alloy produced by powder metallurgy

Ljerka Slokar Benić[1*], Luka Komljenović[1], Erman Žiga[2], Magdalena Jajčinović[1]
University of Zagreb Faculty of Metallurgy, Croatia[1]
University of Ljubljana Faculty of Natural Sciences and Engineering, Slovenia [2]
slokar@simet.unizg.hr

Abstract: *Titanium as a raw material for production is very expensive due to its high price and the complex production process. One of the successful alternatives for the production of titanium alloys and final products is powder metallurgy technology. In this work, a Ti-20Zr alloy for biomedical applications was produced using the powder metallurgy process. The density values determined for the compacts depend on the compression pressure. Namely, the compressibility of the powder mixture increases with increasing compaction pressure. A higher sintering temperature as well as a longer sintering time are more favourable to obtain higher values for the sintered density. Similarly, the compression coefficient is lower for samples compacted at higher pressure, while its value increases with increasing sintering temperature. The volume change in the volume of the sample is more pronounced after sintering at higher temperature and shorter time.*
Keywords*: TITANIUM-ZIRCONIUM ALLOY, POWDER METALURGY, MICROHARDNESS, BIOMEDICAL MATERIALS*

1. Introduction

Biomedical materials are usually used to replace lost or diseased biological structures in the human body and improve the quality of life. For this reason, this type of materials has received more and more attention in the last decades. The basic requirement that such materials must meet is good biocompatibility. The most widely used group of materials is metal biomaterials[1-6].

Titanium is the most important material for biomedicine thanks to its excellent corrosion resistance both in air and in biological fluids, as well as its good mechanical properties, including a good strength-to-weight ratio, and its ease of processing. Similarly, titanium favours osseointegration with the surrounding tissues, which favours its use in orthopaedic and dental implants[7]. Titanium can be alloyed with other elements such as aluminium (Al) and vanadium (V) to increase its strength. Approximately one third of all hip and knee endoprostheses have been successfully manufactured with the alloy Ti6Al4V[8]. In addition to the above elements, alloys with zirconium (Zr), niobium (Nb), palladium (Pd) and indium (In) are also being investigated for their good mechanical properties. Both corrosion resistance and improved biocompatibility compared to Ti-6Al-4V alloy[9]. Ti alloys containing zirconium (Zr) show better tensile strength and fatigue resistance compared to cpTi[10]. Zirconium-containing alloys have high corrosion resistance in biological fluids in addition to mechanical strength[11]. Ti-Zr alloys have better biocompatibility compared to cpTi[12,13]. Because of these properties, titanium alloys are widely used in dentistry and a number of new alloys with non-toxic elements have been developed[14]. Since there are alloys that have some disadvantages, this also applies to Ti-Zr alloys. Since titanium and zirconium have the same crystal structure, they're infinitely soluble in each other. Zirconium is a stabiliser of the beta phase of titanium as a favourable phase in biomaterials, leading to satisfactory properties[15-16].

Powder metallurgy is an extremely important branch of modern industry and is developing rapidly and continuously. Powder Metallurgy is used to produce a wide range of materials[18]. It involves the production, processing and consolidation of fine metal particles that can be used in engineering components. The main feature of this technology is the reduction of costs and material, while the mechanical properties play a subordinate role[19].

In this work, the densification of a biomedical titanium alloy with 20 at% zirconium produced by powder metallurgy was analysed.

2. Materials and methods

Titanium and zirconium powders were used as starting raw materials. The purity of titanium and zirconium powder is 99.8 %. The particle size of titanium powder is 125-250 μm and of zirconia 150 μm. Eight samples with chemical composition Ti-20Zr (at.%) were prepared. After weighing the titanium and zirconium powders, they were mixed. In this research, titanium and zirconium powders were mixed in a ball mill for 30 minutes at room temperature. From the mixture obtained, 8 samples were separated, each with a mass of about 2.5 grammes. The powders were compacted by uniaxial pressing in a hydraulic press. A pressure of 80 MPa was applied to 4 samples and a pressure of 160 MPa to the remaining 4 samples. Disc-shaped specimens were produced. Sintering of the Ti-20Zr alloy samples was carried out in a tube furnace under argon atmosphere with the parameters listed in Table 1. The density of the samples was measured, a very important property of sintered materials, which depends on the proportions of the individual components.

Table 1: *Mechanical properties of selected powder materials.*

Sample No.	Compacting pressure (MPa)	Temperature of sintering (° C)	Time of sintering (h)
1	80	1100	2
2	80	1350	2
3	80	1100	4
4	80	1350	4
5	160	1100	2
6	160	1350	2
7	160	1100	4
8	160	1350	4

3. Results and discussion

To calculate the green density, the green samples were weighed after the compaction process, each of them having a mass of about 2.5 grammes. Their dimensions, diameter and height were measured.

The densities of the green compacts were calculated and are shown in Table 2. The calculated density values were compared with the theoretical density of the Ti-20Zr alloy (4.83 g/cm^3).

Table 2: *Green density values.*

Sample No.	ρg, g/cm^3	% of ρ_t
1	3.96	81.99
2	3.90	80.75
3	4.04	83.64
4	4.07	84.26
5	4.11	85.09
6	4.26	88.20
7	4.23	87.58
8	4.21	87.16

The results listed in Table 2 show high density values of all samples already after compaction. They are between 80.75 and 88.20% of the theoretical density. The density values are slightly lower for samples 1 - 4, which were compacted at a lower pressure (80 MPa), while the densities of samples 5 - 8, which were compacted at a higher pressure (160 MPa), show higher values. The dependence of the green density calculated from the dimensions of the compacts on the compaction pressure applied is shown in Fig. 1.

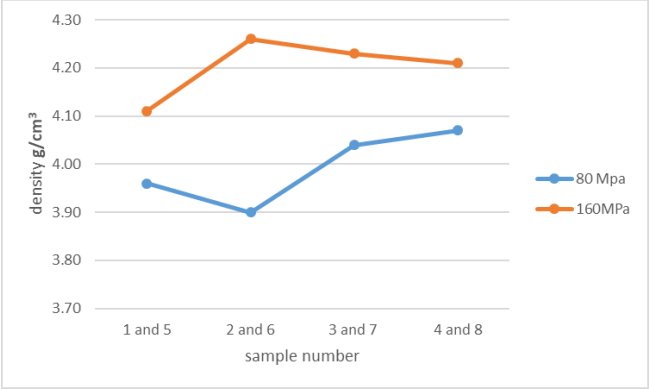

Fig. 1 *Dependence of green density on applied pressing pressure.*

From the graphical presentation it is clear that to achieve higher density values it is more advantageous to apply a higher compaction pressure. This is due to the fact that the compressibility of the powder mixture increases with increasing compacting pressure, which is to be expected with uniaxial compaction of the powder.

The sintered samples were first weighed to determine their mass and then their dimensions (diameter and height) were measured. The mass of the sintered samples was about 2.5 g. Based on the results obtained, the density values of the sintered samples were calculated. The values obtained are listed in Table 3.

Table 3: *Density values of the sintered samples.*

Sample No.	ρ_S, g/cm^3	% of ρt
1	3.84	79.50
2	34.13	85.51
3	4.06	84.06
4	4.14	85.71
5	3.97	82.19
6	3.95	81.78
7	4.15	85.92
8	4.23	87.58

The density values obtained for the sintered samples range from 3.84 g/cm^3 (sample no. 1) to 4.23 g/cm^3 (sample no. 8), which is compared with the theoretical density value of 79.50 - 87.58 %. Comparing these values with those of the samples before sintering, it can be seen that not all samples show an increase in density. This can best be seen in Fig. 2.

Fig. 2 clearly shows how the sintering process increased the density of samples 2, 3, 4 and slightly that of sample 8. Samples 2, 3 and 4 have in common that they were pressed at the same, lower pressure of 80 MPa. The density after sintering depends not only on the compaction parameters, but also on the sintering parameters, as shown in Figs. 3 and 4.

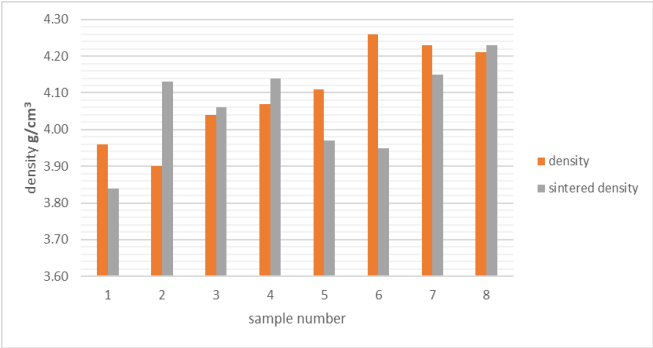

Fig. 2 *Comparison of density before and after sintering.*

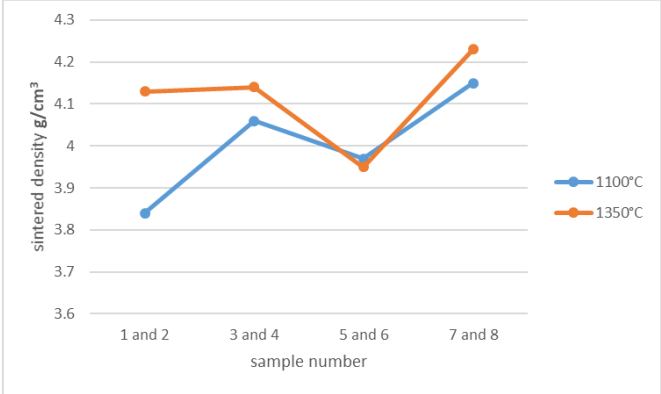

Fig. 3 *Dependence of sintered density on sintering temperature.*

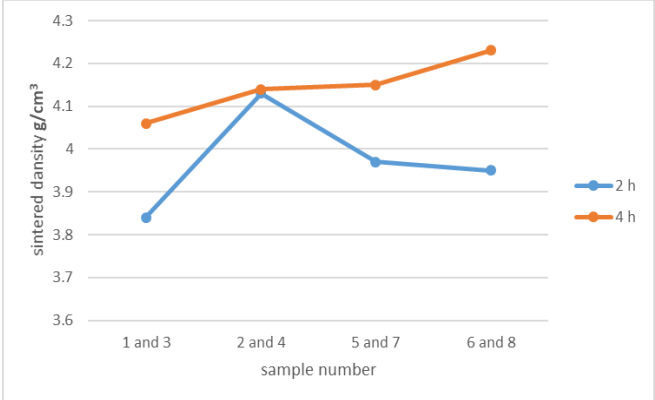

Fig. 4 *Dependence of sintered density on sintering time.*

The figures show graphically that a higher sintering temperature (1350 °C) is more favourable to achieve a higher sintering density. However, this does not apply to samples 5 and 6, which already had high density values before sintering. The achievement of higher sinter density values is also favoured by a longer sintering time (4 h) during which compaction takes place.

The densification or shrinkage of the samples is a consequence of sintering. However, during sintering there may be an increase in the dimensions of the samples, indicating that an increase in porosity rather than the desired increase in density has occurred. Figs. 5 and 6 clearly show the dimensional changes that have occurred as a result of sintering.

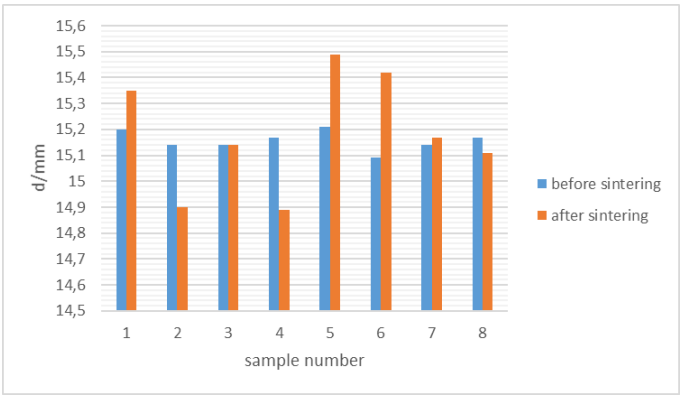

Fig. 5 *Change in the diameter of the samples due to sintering.*

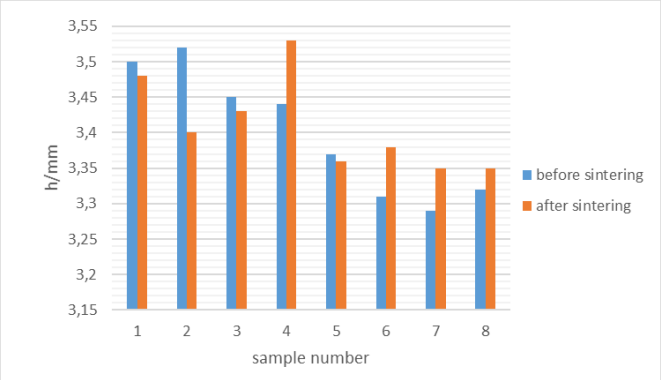

Fig. 6 *Change in the height of the samples due to sintering.*

Namely, these graphical representations show clear changes in the dimensions of all samples caused by sintering. Dimensional changes or quantification of the effect of sintering on the geometry of the samples is best expressed by the densification coefficient ϕ calculated for each sample using the formula:

$$\Phi = \frac{\rho_s - \rho_g}{\rho_t - \rho_g} \cdot 100\%. \quad (1)$$

The volume change that occurred during sintering was calculated according to the following formula:

$$\frac{\Delta V}{V} \approx \frac{\Delta h}{h} + \frac{2\Delta r}{r}. \quad (2)$$

The calculated results are shown in Table 4.

Table 4: *Compaction coefficient, changes in volume and mass of the sintered samples.*

Sample No.	Φ	ΔV/V, %	Δm, %
1	-13.79	1.51	-1.21
2	24.73	-6.75	-1.05
3	2.53	-0.58	-0.10
4	9.21	-0.94	0.43
5	-19.44	3.31	-0.14
6	-54.39	7.37	0.12
7	-13.33	2.32	0.09
8	3.22	-5.65	0.50

These results show a wide range of compaction coefficient values between -54.39 and 24.73. Negative values of the compaction coefficient indicate expansion, positive values indicate porosity[20]. The dependence of the compaction coefficient on the pressing pressure is shown in Fig. 7.

Fig. 7 *Dependence of the densification coefficient on the pressing pressure.*

From this graphical representation it can be seen that the coefficient of compaction is lower for samples that are compacted with higher pressure. This dependence was also found in the work of M. Laska at al.[20].

The dependence of the compaction coefficient on the sintering temperature is shown in Fig. 8. It is obvious that the values of the compaction coefficient increase with an increase of the sintering temperature. This means that densification becomes more pronounced at higher temperatures, indicating that diffusion of the alloying element (zirconium) is complete. An exception is sample 6, which had the highest density before sintering and whose porosity increased due to the sintering process, i.e. most of the thermodynamic energy of the system was spent on diffusion and homogenisation of the chemical composition instead of densification of the compact.

Fig. 8 *Dependence of the densification coefficient on the sintering temperature.*

From the graphical representation in Fig. 9 it can be seen that the volume change after sintering is more pronounced at higher temperature.

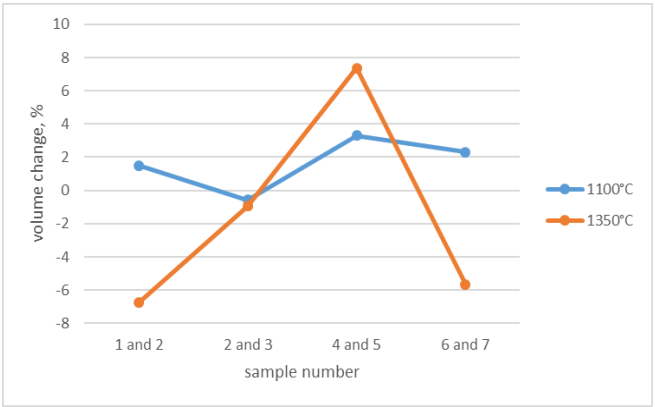

Fig. 9 *Dependence of volume change on sintering temperature.*

Looking at the dependence of the volume change on the sintering time (Fig. 10), it can be seen that the volume changes are more pronounced with shorter times.

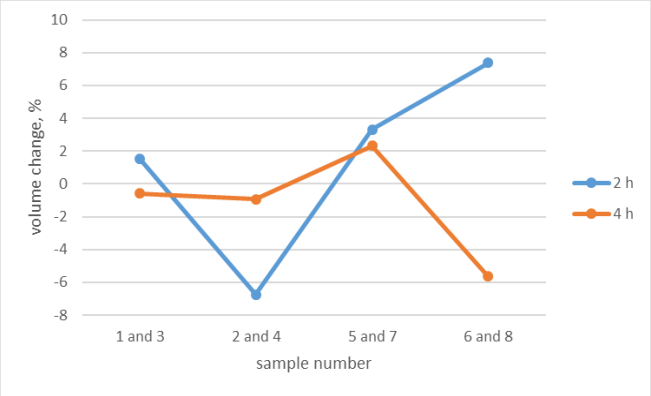

Fig. 10 *Dependence of volume change on sintering time.*

4. Conclusion

In this work, eight samples of a titanium-zirconium alloy with chemical composition Ti-20Zr were prepared by powder metallurgy technology. The results were determined and analysed using appropriate characterisation methods, from which it can be concluded that:

- the value of the density depends on the pressure at which they were compressed; the value is lower when the pressure is lower and higher when the pressure is higher,
- the compressibility of the powder mixture increases with increasing compaction pressure,
- after sintering, the density values are lower than before sintering,
- to achieve higher sintered density values, a higher sintering temperature and a longer sintering time are more advantageous,
- the compaction coefficient is lower for samples compacted at higher pressure, and its value increases with increasing sintering temperature,
- the volume change is more pronounced after sintering at higher temperature, but also at shorter time.

Finally, from the results of the densification analysis of the titanium alloy with zirconium addition, it can be concluded that with the adjustment of the process parameters, it is possible to produce an experimental alloy that has the potential for application in biomedicine.

5. References

1. S. Lascano, C. Arévalo, I. Montealegre-Melendez, S. Muñoz, J. A. Rodriguez-Ortiz, P. Trueba, Y. Torres, Appl. Sci, **9**, 982 (2019)
2. E. Zhang, X. Zhao, J. Hu, R. Wang, S. Fu, G. Qin, Bioact. Mater., **6**, 2569-2612 (2021)
3. F. Mahyudin, H. Hermawan, Biomaterials and Medical Devices, **58**, 1-249 (2016)
4. J. Enderle, J. Bronzion, Academic press series in biomedican engineering, 219-271 (2012)
5. A. W Batchelor, M. Chandrasekaran, Series on Biomaterials and Bioengineering, **3**, 1-256 (2004)
6. L. C. Zhang, L. Y. Chen, Adv. Eng. Mater., **21**, 1–29 (2019)
7. H. Michelle Grandin, S. Berner, M. Dard, Mater., **5,** 1348-1360 (2012)
8. N. Saulacic, D. D. Bosshardt, M. M. Bornstein, S. Berner, D. Buser, Eur. Cell. Mater., **10**, 273-86 (2012)
9. M.A Khan, R.L. Williams, D.F. Williams, Biomaterials, **20**, 765–772 (1999)
10. W. F. Ho, W. F. Chen, S.C. Wu, H. C. Hsu, J. Mater. Sci. Mater. Med., **19**, 3179-3186 (2008)
11. N. Bernhard, S. Berner, M. De Wild, M. Wieland, Implantol, 5, 30–39 (2009)
12. T. Naganawa, Y. Ishihara, T. Iwata, A. Koide, M. Ohguchi, Y. Ohguchi, Y. Murase, H. Kamei, N. Sato, M. Mizuno, T. Noguchi, J. Periodontol., **75**, 1701–1707 (2004)
13. Y. Ikarashi, K. Toyoda, E. Kobayashi, H. Doi, T. Yoneyama, H. Hamanaka, T. Tsuchiya, Mater. Trans., **46**, 2260–2267 (2005)
14. M. T. Mohammed, Z. A. Khan, A. N. Siddiquee, Metallurgical and Materials Engineering, **8,** 726-731 (2014)
15. H. Baker, ASM International, **3** (2006)
16. M.T. Mohammed, International Journal of Modern Science, **3,** 224-230 (2017)
17. H.–C. Hsua, S-C. Wu, Y-C. Sung, W-F. Ho, Journal of Alloys and Compounds, **488,** 279–283 (2009)
18. A. Panda, J. Dobránsky, M. Jančík, I. Pandová, M. Kačalová, Metalurgija, **57**, 353–356 (2018)
19. F. H. Froes, D. Elyon, International Materials Reviews, **35**, 162-184 (1990)
20. M. Laska, J. Kazior, Acta Polytechnica, **50**, 93 -95 (2012)

Peculiarities of sintering of porous sheet blanks from powder of tin-phosphorus bronze

Prof., Dr. Eng., Academic of NAS of Belarus Ilyushchanka A.[1, 2], PhD Eng., Doc. Kusin R.[2]
Head of the Lab., Acad. Adv. of IAE Charniak I.[2], Master of Tech. Sciences Kusin A.[2],
State research and production powder metallurgy association[1] – Minsk, Republic of Belarus
State Scientific Institution "O.V. Roman Powder Metallurgy Institute" [2] – Minsk, Republic of Belarus
alexil@mail.belpak.by, 19081877@mail.ru, irinacharniak@tut.by, 2312444@mail.ru

Abstract: *The technology for increasing the productivity of the sintering powders of tin-phosphorous bronze grade* BrSn10Ph1 *process is described. The data on technological factors influencing the implementation of the sintering process, the equipment used, product quality control and the resulting products are given.*
Keywords*: BLANKS IN THE FORM OF PLATES, TECHNOLOGY, POWDERS OF TIN-PHOSPHOROS BRONZE,* SINTERING PROCESS, PRODUCTS

1. Introduction/Введение

One of the widely used materials for the manufacture of porous filtering powder products (PPIFN) are air-sprayed powders of tin-phosphor bronze grade BrSn10Ph1: the technology for their manufacture is well mastered, molding is carried out without pressure, the sintering atmosphere can be dissociated ammonia, endogas, vacuum, argon [1-4]. The basis of the technological process is the sintering of freely poured powder into a mold. It's well known that sintering is one of the main processes in powder metallurgy, after which a powder body molded with or without application of pressure acquires the required physical and mechanical properties. The operation is carried out in vacuum, bell-type, shaft, pusher, conveyor and other furnaces under proven conditions (as a rule, the process duration is 60 minutes, the sintering temperature is 770 – 890 °C (it's selected depending on the fractional composition of the powder used, since the sintering tin-phosphorus powder grade BrO10F1 depends on the particle size) [5, 6]. batches of filter products in the form of plates or rolled long pipes with a sealed seam (for example, used for pneumatic transport of cement or filtration of liquids, respectively), it's advisable to use conveyor ovens, however, the traditional holding time in the heating zone of 60 minutes limits productivity: for a seven-hour work shift, the blanks output will be no more than eight products.

The purpose of this work is to increase the productivity of the process of sintering powders of tin-phosphor bronze.

2. Experimental results and discussion

As a starting materials for the manufacture of porous filtering powder products, we used powders of tin-phosphor bronze grade BrO10F1 of various fractional composition from (minus 100 + 40) μm to (minus 1000 + 630) μm. The powder was obtained on the developed small-sized installation for spraying the metal melt with a gas stream [7, 8].

Sintering of porous was carried out on a Formet (technology by Scame forni industriall) (Russia).

The shear strength was carried out on a universal testing machine «Tinius Olsen H150K-U» (England). The measurement error was 1%.

The surface morphology and fracture of the PPIFN were studied using a Mira scanning electron microscope ("Tescan", Czech Republic).

It's known [9] that the physical and mechanical properties of PPIFN are determined by the contact size of the necks between the powder particles, which are formed due to the occurrence of diffusion processes as a result of heating. In turn, under certain conditions, the rate of formation of contact necks can be increased by increasing the sintering temperature.

In this work, the increase in productivity was achieved due to a significant increase in the sintering temperature, which, like the speed of the conveyor belt, was selected experimentally: the criterion was the presence of shrinkage (at least 8%), sufficient shear strength (at least 40 MPa), the absence of cracks on the porous plates surface and the presence of good contact necks (approximately 0.3 particle diameters).

As a result of experimental studies on the development of technology for obtaining bronze porous blanks for the manufacture of PPIFN, the following recommendations were developed. Traditional sintering conditions can serve as guidelines for setting test temperatures during process development. Before the release of each new batch of products, as well as when changing equipment, it's necessary to sinter a test work piece, simulating the established production process using ballast equipment located on the belt before and after the equipment with powder for sintering the work piece. In this case, the main attention should be paid to the appointment of the speed of the conveyor belt and the sintering temperatures in the furnace zones, which depend on the size of the powder particles, the number and length of the heating zones, the dimensions of the work piece and equipment. At the same time, it should be taken into account that with insufficient length of the cooling zone, non-optimal speed of movement of the refrigerant in the refrigerator and when using tooling of a relatively large thickness (10 mm or more), the speed of the belt and, accordingly, the productivity of the obtaining blanks process can be limited by the time required to cool the tooling with a sintered sheet to satisfactory temperatures (about 60 – 90 °C: at lower temperatures it's difficult to apply a non-stick layer on the working side of the tooling, higher temperatures are unacceptable in order to avoid accidents in case of careless handling of the tool; the non-stick layer is applied using an aqueous suspension based on kiln clay on a hot tool immediately after removing the work piece when leaving the furnace to prevent adhesion of the powder to the tooling material during sintering). In addition, when using equipment of increased thickness, the specific load on the conveyor belt increases. The quality of sintering is determined using the methods described above, however, primary quality control for strength can be carried out immediately after the work piece has cooled down by technical personnel: the surface of the work piece, which is on weight, apply light blows with a metal object - the sound should be sonorous, metallic. Care must be taken when handling the sintered billet as it has sharp edges.

As a rule, the tooling used is stainless steel sheets 6-8 mm thick (greater thickness is possible, but, as described above, a longer cooling period in the refrigerator is required and, accordingly, belt speed and productivity are reduced). If necessary, and for research purposes, tooling made of carbon steel with preheating and applying a protective layer, as well as tooling made of corrosion-resistant steel 2 mm thick, was also used. In all cases, positive results were achieved: the resulting blanks had an equal (within tolerance) thickness and a good presentation, but the following should be noted. After sintering, the tooling undergoes thermal deformation and deviates from its original flat shape. In this regard, thin-sheet tooling is disposable: after use, it's advisable to foresee its use as a structural material.

The accumulated experience in the manufacture of PPIFN made it possible to establish that the developed technology allows the manufacture of two-layer materials in one sintering, despite the significant difference in the fractional compositions of the base material and the finely dispersed layer, provided that the latter is thin (Fig. 1); crack formation didn't occur in this case [10].

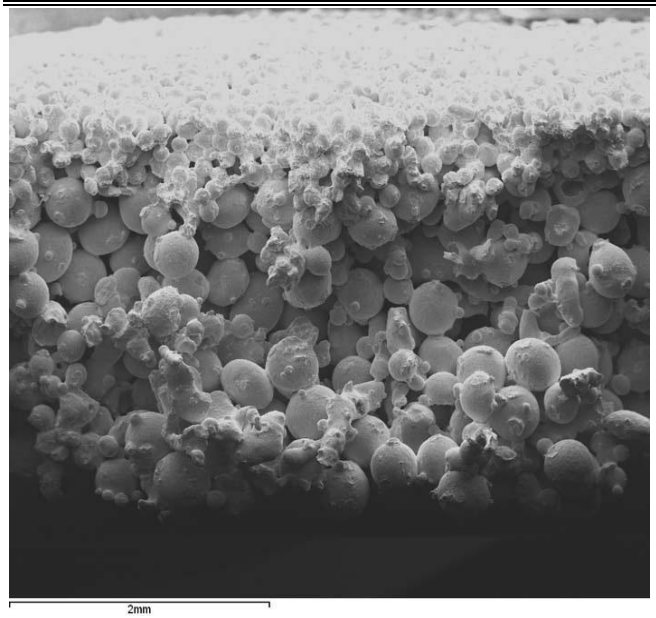

Fig. 1 The structure of a two-layer PPIFN.

When using equipment in the form of flat sheets, bevels up to 15 mm in size are observed along the edges of the work pieces, which are removed during refinement using guillotine shears. The advantage of the developed technology is its non-waste, since the resulting waste is processed at the adjacent production into the feedstock.

As noted above, in specific production conditions, technological development is necessary, aimed at determining the modes of implementation of the sintering process. As an example, we note that when sintering sheet blanks 380x600x3.5 mm on a conveyor furnace model Formet using sheet equipment with a thickness of 6 mm, the productivity in the steady state sintering was 4 blanks per hour. The temperature in the heating zone with its maximum value, depending on the fraction of the powder, was in the range from 820 to 900 °C (traditional values are in the range from 790 to 860 °C).

Figures 2 – 5 show examples of products made from blanks sintered according to the described technology [10].

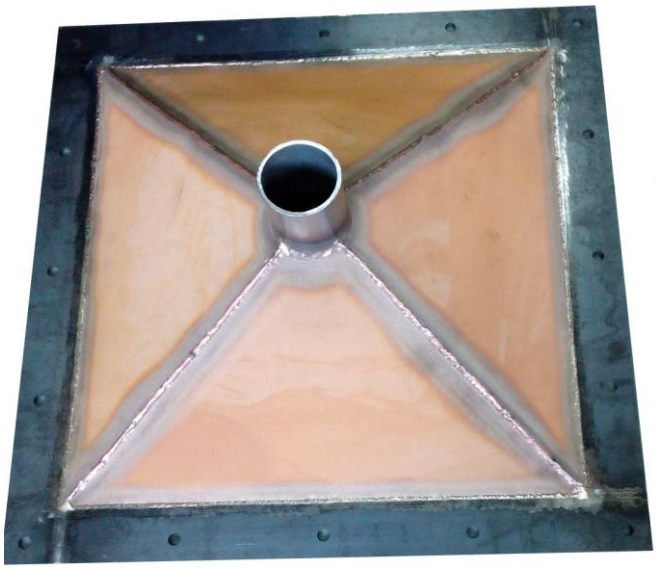

Fig. 2 Pneumobunker for backfilling sand mixture.

Fig. 3 Large-sized elements for air purification (extreme PPIFN are shown assembled with an outer coarse filtering layer made of needle-punched polypropylene fiber material).

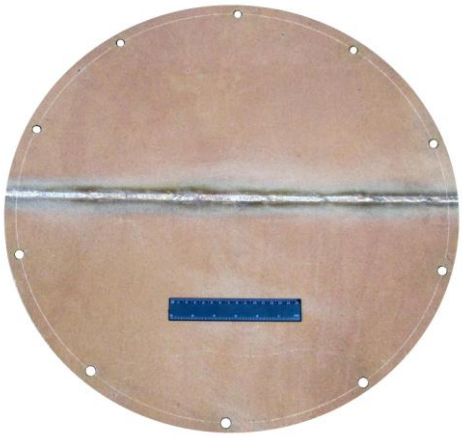

Fig. 4 Porous elements for creating a fluidized bed.

а)

б)

Fig. 5 Porous plates for mounting systems for pneumatic transport of bulk materials (cement, paint, etc.) (a) and tubular filter elements for water pre-treatment (b).

3. Conclusions

The technology for increasing the productivity of the sintering powders of tin-phosphorus bronze of the BrO10F1 grade in the manufacture of thin-sheet blanks process is described, in which the increase in productivity was achieved by experimental selection of a significantly increased sintering temperature and the speed of the conveyor belt. The criteria for determining the quality of work piece sintering are given, including for a preliminary assessment of strength immediately after removing the work piece from the tooling. The data on the technological factors influencing the implementation of the sintering process and the equipment used are given. Examples of introduced products made from blanks sintered according to the developed technology are presented.

4. Reference / Литература

1. Belov S.V. *Porous metals in mehanical engineering* (Moskow, Mehanical engineering, 1981).
2. Vityaz P.A., Kaptsevich V.M., Kostornov A.G., Sheleg V.K. *Formation of the structure and properties of porous powder materials* (Moskow, Metallurgy, 1993).
3. Fritsching U., Uhlenwinkel V. *Hybrid Gas Atomization for Powder Production. In Powder Metallurgy* (Editor Katsuyoshi Kondoh, Rijeka, In Tech, Croatia, Chapter 5, 2012).
4. Kennedy A. *Porous Metals and Metal Foams Made from Powder. In Powder Metallurgy* (Editor Katsuyoshi Kondoh, Rijeka, In Tech, Croatia, Chapter 2, 2012).
5. Andrievsky R.A. *Porous sintered materials* (Moskow, Metallurgy, 1964).
6. Shibryaev B.F. *Porous permeable materials* (Moskow, Metallurgy, 1982).
7. Ilyushchanka, A. Kusin R., Charniak I., Kusin A., Zhegzdrin D., Manoila Y., Kaptsevich V. Small-sized equipment and nozzle with a Laval design for producing sprayed powders based on copper, Powder metallurgy, Minsk, Belaruskaya Nauka, Vol. 34, pp. 37-42 (2011). (A. Ilyushchanka, R. Kusin, I. Charniak, A. Kusin, D. Zhegzdrin, Y. Manoila, V.Kaptsevich).
8. Silaev A., Fishman B. *Dispersion of liquid metals and alloys* (Moskow, Metallurgy, 1983).
9. Belov S.V., Vityaz P.A., Sheleg V.K., Kaptsevich V.M., Pavlov V.A. and et. *Porous permeable materials* (Moscow, Metallurgy, 1987).
10. Ilyushchanka A., Kusin R., Zakrevsky I., Yakimovich N., Charniak I., Kusin A., Zhegzdrin D. *Powder filter materials: structure and property management and agricultural applications* (Minsk, BSTU, 2018).